2016

Behaviour of circular concrete columns reinforced with GFRP bars and GFRP helices

Hogr Karim
University of Wollongong

UNIVERSITY OF WOLLONGONG

School of Civil, Mining and Environmental Engineering

Behaviour of Circular Concrete Columns Reinforced with GFRP Bars and GFRP Helices

A thesis submitted in fulfilment

of the requirements for the award of the degree of

DOCTOR OF PHILOSOPHY

By

Hogr KARIM

2016

THESIS DECLARATION

I, Hogr Karim, hereby declare that this thesis, submitted in fulfilment of the requirements for the award of Doctor of Philosophy, in the School of Civil, Mining and Environmental Engineering, University of Wollongong, is wholly my own work unless otherwise referenced or acknowledged. The document has not been submitted for qualification at any other academic institution.

Hogr Karim

June 2016

AKNOWLEDGMENTS

I would like to express my gratitude to Associate Professor Muhammad N. S. Hadi and Dr. M. Neaz Sheikh for their endless patience, continuous support and guidance during my study. I feel quiet lucky to have studied with them. I also want to thank Mr. Fernando Escribano, Mr. Ritchie Mclean and other technical staff for their technical help during the experimental stage.

I acknowledge the financial support from the Kurdistan Regional Government through the Human Capacity Development Program (HCDP) in Higher Education Ministry and the University of Wollongong for sponsoring my study at the University of Wollongong.

Finally, I would like to thank my wife Kizhan and my son Lawi for their love and continuous support and motivation during all stages of my PhD study.

LIST OF PUBLICATIONS

Journal papers

1. Hadi, M. N. S., **Karim, H.**, Sheikh, M. N. (2016). “Experimental investigations on circular concrete columns reinforced with GFRP bars and helices under different loading conditions." *Journal of Composites for Construction*, DOI: 10.1061/(ASCE)CC.1943-5614.0000670, 04016009.
2. **Karim, H.**, Sheikh, M. N., Hadi, M. N. S. (2016). “Axial load-axial deformation behaviour of circular concrete columns reinforced with GFRP bars and helices.” *Construction and Building Materials*, Vol. 112, 2016, 1147-1157.
3. **Karim, H.**, Sheikh, M. N., Hadi, M. N. S. (2016). “Load and moment interaction diagram for circular concrete columns reinforced with GFRP bars and GFRP helices.” *Journal of Composites for Construction*, DOI: 10.1061/(ASCE)CC.1943-5614.0000737, 04016076.
4. **Karim, H.**, Sheikh, M. N., Hadi, M. N. S. (2016). “Minimum and maximum longitudinal reinforcement ratio for FRP reinforced concrete members.” *ACI Structural journal*, Submitted.

Conference papers

1. Karim, H., Sheikh, M. N., and Hadi, M. N. S. (2014). "Confinement of circular concrete columns: A review." *Proc. of 1st Int. Engineering Conference (IEC2014) on developments in civil and computer engineering applications*, Ishik University, Erbil, Iraq, 28-36.

2. Karim, H., Noel-Gough, B., Sheikh, M. N., and Hadi, M. N. S. (2015). “Strength and ductility behavior of circular concrete columns reinforced with GFRP bars and helices.” *Proc. of 12th International Symposium on Fiber Reinforced Polymers for Reinforced Concrete Structures (FRPRCS-12) & 5th Asia-Pacific Conference on Fiber Reinforced Polymers in Structures (APFIS-2015)*, Nanjing, China.

ABSTRACT

Glass Fibre Reinforced Polymer (GFRP) bar has emerged as a preferable alternative to steel bar in Reinforced Concrete (RC) members in harsh, corrosive, and coastal environments. This is particularly because steel bars may corrode in such environments and may cause damage and deterioration of RC members. FRP bars are noncorrosive and possess high tensile strength to weight ratio. In spite of their high tensile strength, FRP bars are not recommended to reinforce concrete columns because of their low compressive strength and low modulus of elasticity in comparison to the steel bars. The behaviour of FRP bar reinforced concrete (FRP-RC) columns under axial compression and particularly under eccentric axial loads was not addressed adequately in the previous studies. Moreover, the effects of FRP wrapping on the behaviour of FRP-RC columns was not investigated in the previous studies.

This study aims to investigate experimentally and analytically the behaviour and performance of GFRP bar reinforced concrete (GFRP-RC) circular columns under different loading conditions. A total of 18 circular concrete specimens with 205 mm in diameter and 800 mm in height were cast and tested. The influences of reinforcing materials (steel and GFRP bars), helix pitches (30 mm and 60 mm), loading conditions (concentric, 25 mm eccentric, 50 mm eccentric and flexural loadings) and wrapping with CFRP sheets were investigated. In addition to the experimental works, analytical studies were conducted for the axial load-bending moment interactions of

FRP-RC columns. The developed analytical model well predicted the axial load-axial deformation and moment-curvature behaviours of FRP-RC columns with reasonable agreements to the experimental results.

The experimental and analytical results showed that GFRP bars can be used as longitudinal reinforcements to improve the performance of RC specimens in terms of axial load carrying capacity and bending moment. Also, the GFRP helices considerably confined the concrete core to sustain loads. In addition, well confined GFRP-RC columns can obtain two peak loads where the first peak load represents the capacity of unconfined cross-section and the second peak load represents the capacity of confined concrete core of the column.

TABLE OF CONTENTS

LIST OF FIGURES

LIST OF TABLES

ABBREVIATIONS

A_c = area of concrete in the compression side

A_{core} = area of concrete core with diameter d_c

A_{cver} = area of concrete cover

A_f = area of FRP reinforcement

A_g = gross area of concrete cross-section diameter h

b = width of concrete cross-section

b_f = width of flange

b_w = width of web

c = depth of neutral axis

c_s = depth of neutral axis at serviceability state

c_u = depth of neutral axis at ultimate state

CF = curvature factor

d = distance between FRP bars to the extreme fibre in compression side

d' = distance between FRP bars in compression to the extreme fibre in compression side

d_c = diameter of confined concrete enclosed by the centreline of the helices

DF = deformability factor

E_1 = modulus of elasticity of the first ascending part of stress-strain relationship of confined concrete

E_2 = modulus of elasticity of the second ascending part of stress-strain relationship of confined concrete

E_c = modulus of elasticity of unconfined concrete

E_f = modulus of elasticity of FRP bars

f_c = compressive concrete stress at any point

f_c' = cylinder concrete compressive strength at 28 days

f_{cc}' = confined concrete strength

f_{co}' = unconfined concrete strength which is equal to $0.85f_c'$

F_c = compression force in concrete

F_{cs} = compressive force in concrete at serviceability state

F_{cu} = compressive force in concrete at ultimate state

f_f = tensile or compressive strength in FRP bars

f_{fu} = ultimate tensile or compressive strength in FRP bars

F_f = tensile or compressive force in FRP bars

F_{fs} = tensile or compressive force in FRP bars at serviceability state

F_{fu} = tensile or compressive force in FRP bars at ultimate state

h = total depth of concrete cross-section

k_s = curvature at serviceability state

k_u = curvature at ultimate state

L = length of the specimens

MF = moment factor

M_s = bending moment at serviceability state

M_u = bending moment at ultimate state

n = numbers of FRP layers in the concrete cross-section

P = axial load on FRP-RC columns

$\bar{y}_s$ = distance of concrete compression force to the extreme fibre in the

compression side at serviceability state

$\bar{y}_u$ = distance of concrete compression force to the extreme fibre in the compression side at ultimate state

α_1 = ratio of concrete compressive strength in the members to f_c'

β_1 = ratio of depth of equivalent rectangular stress-block to c

ε_c = compressive concrete strain at any point

ε_{co} = unconfined concrete compressive strain corresponding to f_{co}'

ε_{cc} = confined concrete compressive strain corresponding to f_{cc}'

ε_{cs} = unconfined concrete compressive strain at serviceability state

ε_{cu} = unconfined concrete compressive strain at ultimate state

ε_f = tensile or compressive strain in FRP bars

ε_{fs} = tensile strain in FRP bars at serviceability state

ε_{fu} = tensile strain in FRP bars at ultimate state

γ = ratio of distance between FRP bars in tension side to FRP bars in compression side to h

λ_b = ratio of area of FRP bars in each layer to area of FRP bars in first layer

λ_c = ratio of area of FRP bars in each layer to total area of FRP bars

ρ_f = FRP reinforcement ratio

$\rho_{f\ min}$ = minimum FRP reinforcement ratio

$\rho_{f\ T\ \&\ L}$ = minimum FRP reinforcement ratio for T and L cross-section

ω = density of concrete

1 INTRODUCTION

1.1 Preamble

Fibre reinforced polymer (FRP) composite materials in the constructing of new structures and retrofitting of the existing structures is a novel invention that can replace the conventional steel bars and plates because FRP materials can eliminate the corrosion problem. Corrosion is a considerable issue in the humid, aggressive, and coastal areas that causes large maintenance cost and sometimes the structure loses its performance[1]. In general, FRP composite is produced in Glass (G), Carbon (C) and Aramid (A) fibre, while the glass fibre is most familiar to produce FRP bars because glass fibre is cheaper than carbon fibre and its characteristics is better than aramid fibre. However, the mechanical properties of GFRP bars are different than steel bars because GFRP bars have higher tensile strength to weight ratio and their modulus of elasticity is about a quarter of the steel bars. The behaviour of GFRP bars under compression is complex because some different parameters such as debonding or buckling of the fibres can play roles. Therefore, to figure out the behaviour and the effect of GFRP bars on the Reinforced Concrete (RC) columns and the lack of experimental studies in this field, 18 circular concrete columns were cast and reinforced with conventional steel and GFRP bars and helices. Four of the specimens were confined externally with CFRP sheets. The specimens were tested under concentric, eccentric and flexural loading in this study.

1.2 Overview

Concrete columns have traditionally been reinforced with steel bars because of the compatible properties of concrete and steel reinforcement. Normally, steel bars are protected from corrosion by the alkalinity of the concrete. However, concrete columns in marine structures and coastal areas are exposed to harsh and aggressive environments such as combination of moisture and temperature where chloride ingress or concrete carbonation can occur. The ingress of chloride or concrete carbonation may degrade the alkalinity of the concrete and cause corrosion of steel bars. The detrimental impact of corrosion is the formation of hydrated ferrous oxide around the surface of the steel bars and consequent volume expansion, which produces considerable internal stresses in the concrete. This stress leads to cracking of concrete and cover spalling, which causes the concrete structure to become unserviceable and eventually unsafe[2]. In addition, the cost of repair and rehabilitation of deteriorated structures may be significant[3]. For instance, in the United States, the annual repair and replacement cost for bridge substructures (bridge piers and columns) is two billion dollars and for marine piling is one billion dollars[3]. Although different methods such as the use of galvanised or stainless steel bars, epoxy coating and cathodic protection have been used to protect reinforcement from corrosion[4-7]. None of the methods, however, have eliminated the corrosion problem of steel reinforcement. Also, epoxy coating of steel bars may cause the loss of bond between concrete and the steel bars[8, 9].

FRP bars consisting of glass, carbon or aramid fibres encased in a matrix of epoxy, polyester or phenolic thermosetting resins were developed as economical substitute of conventional steel bars. Also, FRP materials possess high tensile strength to weight ratio and are nonmagnetic, noncorrosive and nonconductive. Fibre reinforced composite materials have been used for many decades in the aerospace, automotive and recreational products industries, while they have been used in construction fields over the last two decades. Fibre reinforced polymer (also known as fibre reinforced plastic or advanced composite material) is advantageous to use in new buildings and bridges and to upgrade or retrofit existing structures[10].

Application of FRP bars for reinforcing flexural concrete elements such as beams and slabs can be denoted as an incipient use of FRP bars to reinforce concrete members. Extensive research was conducted in the 1990s on the behaviour of concrete beams and slabs reinforced with various types of FRP bars[11, 12] and the research is still underway. Moreover, some standards from different countries such as United State[13], Japan[14] and Canada[15] were introduced to design of concrete members reinforced with FRP bars. However, none of the standards have recommended or proposed a design guideline for concrete columns that are reinforced with FRP bars due to the intricate behaviour of FRP bars under compression loading. This is because FRP bars are anisotropic materials and different parameters such as micro-buckling of the fibres or debonding of the fibres with the resin matrix play role in the failure of FRP bars under compression. Also, the lack of experimental studies in this field would be another substantial point that makes it impossible to scheme design guidelines for reinforcing concrete columns with FRP bars.

The traditional design philosophy should be changed for concrete members reinforced with FRP bars because FRP bars have different mechanical properties than steel reinforcing bars[13, 16]. For instance, the stress-strain behaviour of FRP bars does not have yield point; it is linear elastic until failure. In addition, FRP bars are anisotropic materials and characterised by high tensile strength only in the direction of the fibres. Consequently, it is thought that the failure mode of flexural concrete members reinforced with FRP bars should be changed to crushing of concrete in the compression zone rather than the failure of FRP bars in the tension zone. This is because tensile rupture of FRP bars happens suddenly and is more catastrophic and large crack-widths and deflection can be observed. However, in the crushing of concrete, the RC member undergoes in a large deformation and then followed by rupture of the FRP bars[17]. Therefore, in the design of concrete members with FRP bars these points should be considered. Accordingly, a direct substitution area of FRP bars for steel bars in reinforced concrete is not an appropriate option. This is because the mechanical properties of FRP bars vary from one product to another and are affected by the fibre volume fractions. Moreover, the resin matrix that is used to hold the fibres together and changing the diameter of the FRP bars makes it difficult to provide universal mechanical property values. Predominately, the serviceability limit state controls the flexural design of concrete members with FRP bars because the modulus of elasticity of FRP bars is about a quarter of the corresponding steel bars[2].

FRP sheets were developed for retrofitting existing concrete bridges and building structures to strengthen against static and quasi-static loads due to the increase of dead or live loads, or against increasing dynamic loads such as seismic loads or blast response in concrete members. FRP sheets have been used for flexural strengthening of concrete beams and slabs, shear strengthening of concrete beams, and axial strengthening and ductility enhancement of concrete columns. The retrofitting technique by using FRP sheets started approximately in the late 1980s in Europe and in Japan. Since then, research and applications on this technique have been initiated in the United States and Canada. Studies about flexural strengthening by FRP sheets initially started and was soon followed by research on confining of concrete columns known as FRP wrapping[10].

FRP wrapping techniques gained widespread use for strengthening RC bridges and structures because conventional techniques may be problematic. It can be noticed in one of the most popular techniques (which is externally bonded steel plate) it faces some issues such as deterioration of the bond between steel plates and concrete surfaces due to the corrosion of steel, difficulty in the adjusting of the steel plates at the construction site because of their heavy weight, need for scaffolding, and limited length of steel plates that can be delivered[18]. Providing proper FRP confinement promotes the ductility and rotation capacity of concrete columns in plastic hinge regions and prevents debonding in the lap splices of internal reinforcement. Also, FRP confinement may be advantageous in seismic and nonseismic zones where serviceability of explosive attacks is required or the axial load capacity of a concrete column must be increased due to increasing of vertical loads[19].

Based on the aforementioned discussion, this study aims to investigate experimentally and analytically the behaviour and performance of circular concrete columns reinforced with GFRP bars longitudinally and GFRP helices transversally. A total of 18 circular concrete specimens with 205 mm in diameter and 800 mm in height are cast and tested. The influences of reinforcing materials (steel and GFRP bars), helix pitches (30 mm and 60 mm), loading conditions (concentric, 25 mm eccentric, 50 mm eccentric and flexural loadings) and wrapping with CFRP sheets are investigated. In addition to the experimental works, analytical studies are conducted for the axial load-bending moment interactions of FRP-RC columns. The developed analytical model can predict the axial load-axial deformation and moment-curvature behaviours of FRP-RC.

1.3 Objectives

The main purpose of this study can be briefly outlined in the following points:

- Perceiving the behaviour of circular concrete columns that are reinforced with GFRP bars and different pitch of GFRP helices in the longitudinal and transversal directions, respectively.
- Demonstrating the effects of different monotonic loading conditions such as concentric, eccentric, and flexural on the GFRP reinforced circular concrete columns.
- Four column specimens are externally wrapped with CFRP sheets to investigate the effect of CFRP confinement on the circular columns containing GFRP bars and helices.

1.4 Outline of the content

This study consists of nine chapters. The background, significance and objective of this study were presented above (Chapter 1). In Chapter 2, the composition and the mechanical behaviour of concrete and FRP bars are explained based on the previous studies. A number of the available stress-strain models are also reported for concrete under uniaxial compression. The effect of unbraced length to diameter ratio on the compressive strength of GFRP bars is also demonstrated.

Chapter 3 is dedicated to review the behaviour of concrete members reinforced with FRP bars based on the available literature. The effect of longitudinal and transverse FRP bars on strength, ductility and failure modes of FRP-RC columns are discussed. The strength, failure modes, deflection, crack-width and deformability of FRP-RC flexural members are also explained.

In Chapter 4, a brief history of confined concrete under compressive load is illustrated. The effect of volumetric ratio and strength of confining reinforcement, presence of longitudinal reinforcement and strength of confined concrete are discussed on the efficiency of internal confinement by steel helices and hoops. Also, a number of the available stress-strain models proposed in the literature for confined concrete by steel bars or FRP jackets are reviewed.

Chapter 5 consists of an extensive study to limit the minimum and maximum FRP reinforcement ratio for FRP-RC flexural members. The minimum FRP reinforcement ratio is limited to prevent the brittle tensile rupture of FRP bars or to control the

crack-width in the tension region. Also, the maximum FRP reinforcement ratio is limited to ensure a considerable deformation before complete failure of FRP-RC members.

In Chapter 6, an experimental work is presented about 18 circular concrete columns. The preliminary tests for the materials used in casting of the specimens are conducted. Also, the preparing, instrumentation, casting and testing of the specimens are reported.

Chapter 7 is dedicated for analytical modelling of the FRP-RC columns. The behaviours such as peak axial load-bending moment diagrams, axial load-axial deformation and moment curvature for the FRP-RC columns are investigated.

In Chapter 8, the analytical models presented in Chapter 7 are verified with experimental results presented in Chapter 6. Also, parametric studies are conducted to investigate the effect of longitudinal and transverse reinforcement ratio and slenderness ratio on the peak axial load-bending moment diagrams.

In Chapter 9, summary and concluding remarks gained from experimental and analytical studies and recommendations for further research studies are expressed.

2 MATERIAL PROPERTIES

2.1 Introduction

Steel reinforcing bars have been used for a very long time for reinforcing concrete members because concrete cannot resist tensile loads. Therefore, using steel bars in those parts of concrete members that face tensile stress make concrete members a desirable choice in building structures. However, sometimes steel reinforced members may be constructed in coastal areas or harsh and aggressive environments that deteriorate the steel reinforcing bars. So, in these cases steel bars would not be a reasonable choice because of high maintenance cost or sometimes failure of the structures. Hence, using fibre reinforced polymer (FRP) as noncorrosive reinforcing bars with concrete members in these cases can give concrete members more durability and lower maintenance cost. Also, FRP bars have some other advantages such as low weight, high tensile strength and no conductivity which makes FRP bars acceptable in areas that require these properties. This chapter gives a brief introduction to the mechanical and stress-strain behaviour of concrete as well as composition and the mechanical properties of FRP bars that are relevant to the reinforcing of concrete members.

2.2 Concrete

Concrete is a composite anisotropic material. In general, concrete is composed of fine and coarse aggregate (sand and gravel) that chemically bounded together by hydrated Portland cement[20]. Concrete is essentially used to carry compressive loads. The compressive stress-strain relationship of concrete depends on many interrelated

variables including water-cement ratio, rate of loading and aggregate properties[21]. Therefore, many studies have been conducted to predict the stress-strain behaviour of concrete empirically. The proposed equations for the stress-strain behaviour of concrete can be divided into two main groups. In the first group, a single equation was used to model the whole stress-strain behaviour of concrete. In the second group, two equations were used for the ascending and the descending parts of the concrete stress-strain behaviour. Table 2.1 reports some of the equations that proposed by different authors.

Unconfined concrete strain (ε_{co}) corresponding to the peak stress of concrete (f'_{co}) is a function of f'_{co}. Different equations have been introduced based on experimental studies and Table 2.2 shows a number of the proposed equations to estimate ε_{co}.

Table 2.1. Proposed equations to estimate ε_{co}

Popovics[22]	$\varepsilon_{co} = 0.00073\ {f'_{co}}^{0.25}$
Ford et al.Ford et al.[23]	$\varepsilon_{co} = 2\ f'_{co}/E_1$
Carreira and Chu[24]	$\varepsilon_{co} = (0.071\ f'_{co} + 16.8)\ \text{x}\ 10^{-4}$
Hsu and Hsu[25]	$\varepsilon_{co} = (0.129\ f'_{co} + 21.14)\ \text{x}\ 10^{-4}$
Almusallam and Alsayed[21]	$\varepsilon_{co} = (0.398\ f'_{co} + 18.174)\ \text{x}\ 10^{-4}$
Wee et al. [26]	$\varepsilon_{co} = 0.00078\ {f'_{co}}^{0.25}$
Légeron[27]	$\varepsilon_{co} = 0.0005\ {f'_{co}}^{0.4}$
Yang et al.[28]	$\varepsilon_{co} = 0.0016\ \exp(240\ f'_{co}/E_1)$

Table 2.2. Stress-strain models for unconfined concrete

Popovics[22] Carreira and Chu[24]	$f_c = \frac{f'_{co}\,\beta\,(\varepsilon_c/\varepsilon_{co})}{\beta - 1 + (\varepsilon_c/\varepsilon_{co})^{\beta}}\;;\;\beta = \frac{E_1}{E_1 - f'_{co}/\varepsilon_{co}}\;;\;E_1 = 0.043\,\omega^{1.5}\sqrt{f'_{co}}$
Wang et al.[29]	$f_c = \frac{A(\varepsilon_c/\varepsilon_{co}) + B(\varepsilon_c/\varepsilon_{co})^2}{1 + C(\varepsilon_c/\varepsilon_{co}) + D(\varepsilon_c/\varepsilon_{co})^2}\,f'_{co}$ For $\varepsilon_c \le \varepsilon_{co}$: $A = 1.300501\,, B = -0.835818\,, C = -0.699498\,, D = 0.164182$ For $\varepsilon_c > \varepsilon_{co}$: $A = 0.349777\,, B = -0.104963\,, C = -1.650222\,, D = 0.895036$
Ford et al.[23]	$f_c = f'_{co}\left[2\left(\frac{\varepsilon_c}{\varepsilon_{co}}\right) - \left(\frac{\varepsilon_c}{\varepsilon_{co}}\right)^2\right]$ For $\varepsilon_c \le \varepsilon_{co}$ and $f_c = f'_{co}[1 - 20(\varepsilon_c - \varepsilon_{co})]$ For $\varepsilon_{co} < \varepsilon_c \le \varepsilon_{cu}$
Hsu and Hsu[25]	$f_c = \frac{f'_{co}\,k\,\beta\,(\varepsilon_c/\varepsilon_{co})}{k\beta - 1 + (\varepsilon_c/\varepsilon_{co})^{k\beta}}$ For $\varepsilon_c \le \varepsilon_{cd}$ and $f_c = 0.3f'_{co}\exp\left[-0.8\left(\frac{\varepsilon_c}{\varepsilon_{co}} - \frac{\varepsilon_{cd}}{\varepsilon_{co}}\right)^{0.5}\right]$ For $\varepsilon_{cd} < \varepsilon_c \le \varepsilon_{cu}$ $\beta = \frac{E_1}{E_1 - f'_{co}/\varepsilon_{co}}\;;\;E_1 = 124.31f'_{co} + 22653\;;\;\varepsilon_{cd} =$ strain at $0.3f'_{co}$ in the descending part ; For $\varepsilon_c \le \varepsilon_{co}$: $k = 1$ For $\varepsilon_c > \varepsilon_{co}$: $k = 1$ If $f'_{co} < 62$ MPa, $k = 2$ If $62 \le f'_{co} < 76$ MPa, $k = 3$ If $76 \le f'_{co} < 90$ MPa, $k = 5$ If $f'_{co} \ge 90$ MPa

Table 2.1. (Continued)

Almusallam and Alsayed[21]	$f_c = \frac{(E_1 - E_2)\varepsilon_c}{(1 + [(E_1 - E_2)\varepsilon_c / f_o]^n)^{1/n}} + E_2\varepsilon_c \; ; \; n = \frac{-\ln 2}{\ln[f_1/f_o - E_1/(E_1 - E_2)]}$ $f_1 = f'_{co}\left[2\left(\frac{\varepsilon_1}{\varepsilon_{co}}\right) - \left(\frac{\varepsilon_1}{\varepsilon_{co}}\right)^2\right] \; ; \; \varepsilon_1 = \frac{f_o}{E_1 - E_2} \; ; \; f_o = 5.6 + 1.02f'_{co} - E_2\varepsilon_o \; ; \; E_1 = 3320\sqrt{f'_{co}} + 6900$ $E_2 = 5470 - 375f'_{co}$ For $f'_{co} \leq 55$ MPa and $E_2 = 16398.23 - 676.82f'_{co}$ For $f'_{co} > 55$ MPa
Wee et al.[26]	$f_c = \frac{f'_{co}\, k_1\, \beta\, (\varepsilon_c/\varepsilon_{co})}{k_1\beta - 1 + (\varepsilon_c/\varepsilon_{co})^{k_2\beta}} \; ; \; \beta = \frac{E_1}{E_1 - f'_{co}/\varepsilon_{co}} \; ; \; E_1 = 10200\, {f'_{co}}^{1/3}$ $k_1 = k_2 = 1$ For $\varepsilon_c \leq \varepsilon_{co}$; $k_1 = \left(\frac{50}{f'_c}\right)^3 \leq 1$ and $k_2 = \left(\frac{50}{f'_c}\right)^{1.3} \leq 1$ For $\varepsilon_c > \varepsilon_{co}$
Tasnimi[30]	$f_c = \left[(2\beta - 3)\left(\frac{\varepsilon_c}{\varepsilon_{co}}\right)^4 + (4 - 3\beta)\left(\frac{\varepsilon_c}{\varepsilon_{co}}\right)^3 + \beta\left(\frac{\varepsilon_c}{\varepsilon_{co}}\right)\right] f'_{co} \; ; \; \beta = \frac{E_1\varepsilon_{co}}{f'_{co}} \; ; \; E_1 = 2250 \ln\left(\frac{{f'_{co}}^{2.8}}{\omega^{0.2}}\right) + 50f'_{co}$
Yang et al.[28]	$f_c = \frac{f'_{co}(\beta + 1)(\varepsilon_c/\varepsilon_{co})}{\beta + (\varepsilon_c/\varepsilon_{co})^{\beta+1}} \; ; \; E_1 = 8470\, {f'_{co}}^{1/3}\, (\omega/2300)^{1.17}$ $\beta = 0.2\exp\left[0.73\left(\frac{f'_{co}}{10}\right)^{0.67}\left(\frac{2300}{\omega}\right)^{1.17}\right]$ For $\varepsilon_c \leq \varepsilon_{co}$ and $\beta = 0.41\exp\left[0.77\left(\frac{f'_{co}}{10}\right)^{0.67}\left(\frac{2300}{\omega}\right)^{1.17}\right]$ For $\varepsilon_c > \varepsilon_{co}$

where f'_{co}, E_1 and E_2 are in MPa and ω is in kg/m^3.

One of the most applicable equations that has been used in many studies is the equation that was proposed in Popovics[22]. This equation is simplified in Wight and MacGregor[20] for the design purpose within the range of normal strength concrete as bellow,

$$f_c = \frac{2\,(\varepsilon_c/\varepsilon_{co})}{1+(\varepsilon_c/\varepsilon_{co})^2}\ \text{x}\ 0.9\,f_c' \tag{2.1}$$

$$\varepsilon_{co} = 1.71\,\frac{f_c'}{E_1} \tag{2.2}$$

where, ε_c is the axial concrete strain at any concrete stress f_c, f_c' is the cylinder compressive strength at age 28-days, ε_{co} is the unconfined concrete strain corresponding to $0.9\,f_c'$ and E_1 is the elastic modulus of the concrete. The reduced strength $(0.9\,f_c')$ accounts for the differences between cylinder strength and member strength.

2.3 GFRP bars

Glass fibre reinforced polymer (GFRP) bars are composed of continuous strand mat (also called continuous strand filament mat) and a resin matrix. The filaments have a high tensile strength and modulus of elasticity and they are responsible for the high carrying loads and strength of FRP bars. The matrix works as a bonding material to hold the fibres together to prevent shear between the fibres and protect the fibres from degradation and give them required shape, dimension and stability[31].

There are four main types of glass fibres. The most commercially used one is E-glass (electrical) fibre because it has good tensile strength, electrical resistance, acid resistance and low cost. If higher strength, stiffness and ultimate tensile strength were required, S-glass fibre would be better, but it is more expensive and susceptible to degradation in alkaline environment than E-glass. Also, C-glass (chemical) fibre is used in acidic environments because of its chemical stability. The alkali-resistant (AR) glass fibres are used to minimize weight and strength loss in alkaline environment[31]. The properties of different types of glass fibres are shown in Table 2.3.

Table 2.3. Typical physical and mechanical property of commercial glass fibres[31]

Parameters	E-glass	S-glass	C-glass	AR-glass
Tensile strength (GPa)	3.45	4.3	3.03	2.5
Tensile modulus (GPa)	72.4	86.9	69	70
Ultimate strain (%)	4.8	5.0	4.8	3.6
Poisson's ratio	0.2	0.22	-	-
Density (g/cm^3)	2.54	2.49	2.49	2.78
Diameter (μm)	10	10	4.5	-

There are different types of resin matrices that are used in producing GFRP bars. Thermoset polyester is one of them, which consists of an unsaturated ester polymer dissolved in a crosslinking monomer such as styrene. Depending on the mix of ingredients, the properties of polyesters can vary widely. The main advantages of polyesters are low viscosity, fast curing time, dimensional stability, excellent

chemical resistance, and moderate cost. The disadvantage of polyesters is their high volumetric shrinkage during processing. The cost of polyesters is about half of that of epoxy, however their properties are not much better in comparison to the properties of epoxy[31]. The physical and mechanical properties of polyester resin are shown in Table 2.4.

Epoxy resins have high strength and creep resistance, strong adhesion to fibres, chemical and solvent resistance, good electrical properties, high glass transition temperature, and low shrinkage and volatile emission during curing. Epoxy resins can be used in all FRP manufacturing processes[31]. The physical and mechanical properties of epoxy resin are shown in Table 2.4.

Vinyl ester resins are produced by the reaction of a monofunctional unsaturated acid, such as methacrylic or acrylic acid, and an epoxy resin. Vinyl ester resins are better than polyesters in terms of chemical resistance, high temperature resistance and vinyl esters have better resilience than polyesters. Also, they are easier to handle during processing than either polyester or epoxy resins. They also have excellent wet-out and high interfacial strength. They are suitable for the manufacture of FRPs due to their low viscosity and short curing time, but they have a high volumetric shrinkage in comparison to epoxies during curing and they are more expensive than polyester resins[31]. The physical and mechanical properties of vinyl ester resin are shown in Table 2.4.

Table 2.4. Typical physical and mechanical properties of commercial matrix materials[31]

Parameters	Polyester	Epoxy	Vinyl ester
Tensile strength (MPa)	20 – 100	55 – 130	70 – 80
Tensile modulus (GPa)	2.1 – 4.1	2.5 – 4.1	3.0 – 3.5
Ultimate strain (%)	1 – 6	1 – 9	3.5 – 5.5
Poisson's ratio	–	0.2 – 0.33	–
Density (gm/cm^3)	1.0 – 1.45	1.1 – 1.3	1.1 – 1.3
Cure shrinkage (%)	5 – 12	1 – 5	5.4 – 10.3

GFRP bars are composed of a type of glass fibre that binds together with a type of resin material. They are manufactured by pultrusion process, as shown in Figure 2.1. This process consists of pulling resin impregnated reinforcing fibres through a heated curing die[18]. This process helps to make high-fibre content products, 60% to 80% by volume, with a homogeneous distribution of fibres in the cross-section of the rebar.

The surface deformation can be obtained by wrapping an additional resin-impregnated strand around the bar prior to entering or after coming out of the heated die to enhance the mechanical bond to concrete. Some types of bars have a layer of sand coating to improve mechanical bonding to concrete[31].

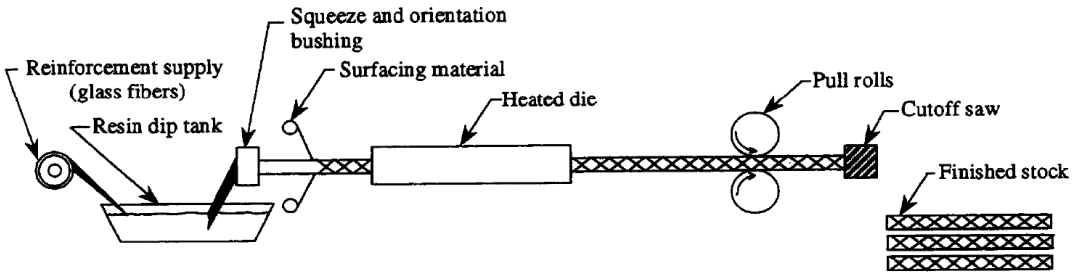

Figure 2.1. Pultrusion process of GFRP bars[31]

2.3.1 Mechanical properties of GFRP bars

The mechanical properties of GFRP bars vary significantly from one product to another. Also, factors such as volume and type of fibre and resin, fibre orientation, quality control during the manufacturing process, all play a major role in the mechanical properties of the GFRP bars[31]. According to the previous studies, it can be observed that the short and long term behaviours of GFRP bars subjected to high stress level (80% of the ultimate tensile strength), aggressive environment and the presence of fibre cracking does not affect considerably the mechanical properties of the GFRP bars[32].

2.3.1.1 Tensile behaviour

Generally, FRP bars are made from an anisotropic material and they are stronger than steel bars in the longitudinal direction. The tensile behaviour of FRP bars is a linear elastic stress-strain relationship until failure, and they do not have plastic behaviour before rupture. Tensile properties of some different types of FRP bars are compared with steel bars in Table 2.5. In Figure 2.2, it can be seen that the GFRP

stress-strain curve is linear and elastic until failure and its failure is brittle, unlike steel, with no ductile plateau present.

Table 2.5. Tensile properties of different types reinforcing bars[13]

Parameters	Steel	GFRP	CFRP	AFRP
Nominal yield stress (MPa)	276–517	N/A	N/A	N/A
Tensile strength (MPa)	483–690	483–1600	600–3690	1720–2540
Elastic modulus (GPa)	200	35–51	120–580	41–125
Yield Strain (%)	0.14–0.25	NA	NA	NA
Rupture strain (%)	6.0–12.0	1.2–3.1	0.5–1.7	1.9–4.4

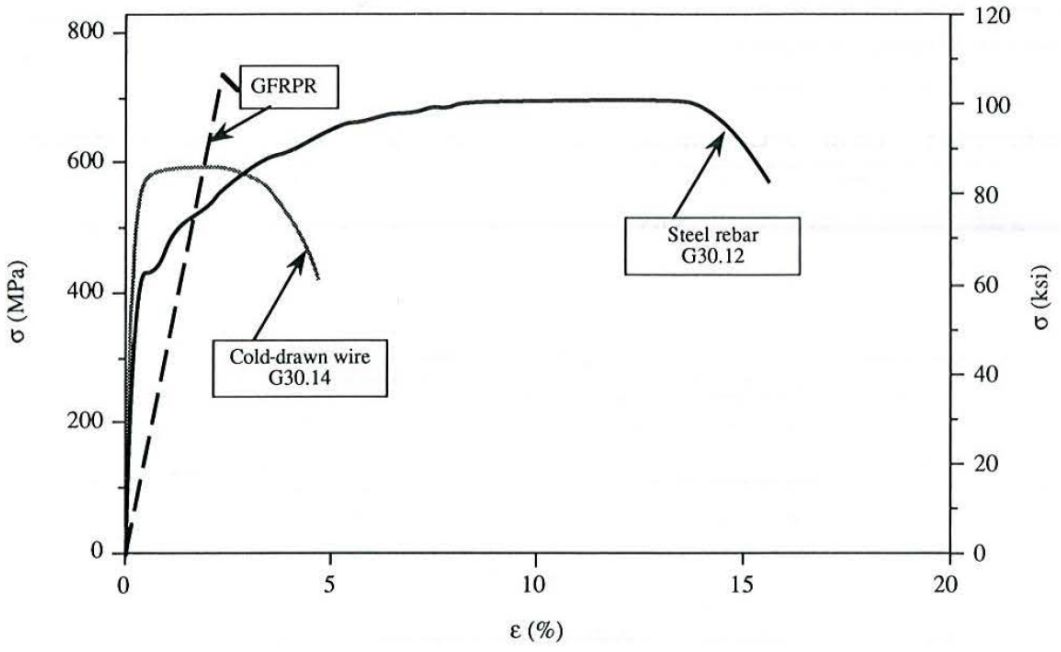

Figure 2.2. Tensile stress-strain relations of GFRP, steel and cold-draw wire[33]

There are several factors that affect the tensile strength of GFRP bars. The fibres in FRP bars are the main load carrying component, so the ratio of fibre to the overall volume of the FRP bars (fibre-volume fraction) significantly affects the tensile behaviour of FRP bars. Also, the rate of curing, the manufacturing process, and the manufacturing quality control also affect the mechanical characteristics of the bars[34]. In addition, the tensile strength of FRP bars is affected by the bar's diameter. It is reported that the tensile strength decreases with increasing bar diameter due to shear lag effect. The fibres located near the surface of the bars are subjected to a higher stress than the fibres located near the centre of the bars, so this variation in the distribution of the stress results in the reduction of strength and efficiency in larger diameter bars[31, 35].

Chaallal and Benmokrane[33] studied different diameters of GFRP bars and they reported that the tensile strength varied between 674 to 719 MPa with an average of 689 MPa, which is greater than the yield tensile strength of reinforcing steel bars (f_y = 500 MPa). However, the average strain obtained at failure was 1.8%, which is lower than that of steel bars (15% – 18%).

Kocaoz et al.[35] investigated four types of GFRP bars which were similar in diameter (12.7 mm), constituent material, shape and fibre-volume fraction, but they were only different in coating type. They observed that all specimens failed suddenly and the failures started with splitting and ended with rupture of the bars, while the numbers and sizes of pieces were different depending on the type of the coating. They also

reported that coating may have an effect on the tensile strength of the GFRP bars and a coating using filler could slightly increase the tensile strength.

The tensile modulus of elasticity is not significantly affected by the change in the diameter of the FRP bars, but rather by the level of fibre contained. The modulus of elasticity and Poisson's ratio of GFRP bars have been studied by Chaallal and Benmokrane[33] and they were equal to 42 GPa and 0.28, respectively. The modulus of elasticity of GFRP bars is lower than the steel bars, but it is an advantage for prestressing application because it results in a reduction of prestress loss due to shrinkage and creep of concrete. Also, Kocaoz et al.[35] determined the modulus of elasticity of GFRP bars with 55% fibre-volume fraction of E-glass ranging from 40 to 47 GPa.

Carvelli et al.[36] investigated the effect of speed testing on the tensile strength of GFRP bars. They performed a test on 16 mm diameter sand coated GFRP bars. The speed was 2 kN/s for the first specimen, 5 kN/s for the second and 8 kN/s for the third, but no difference was observed in the test results.

2.3.1.2 Compressive behaviour

The compressive strength of GFRP bars is normally lower than its tensile strength; about 40% to 60% of its tensile strength. Higher compressive strength is expected for bars with higher tensile strength and it also depends on the type of fibre, the fibre-volume fraction, and the type of resin[31, 34]. The compressive behaviour of FRP bars is

a linear elastic stress-strain relationship until failure and they do not have plastic behaviour before failure, similar to its tensile behaviour.

Chaallal and Benmokrane[33] carried out compression tests on three different GFRP bar diameters (15.9, 19.1 and 25.4 mm) and the slenderness ratio was 11 for all specimens. The results are presented in Table 2.6. The typical stress-strain curve is shown in Figure 2.3 and the transverse versus longitudinal strain curve is shown in Figure 2.4. The results showed that the average ultimate GFRP compressive strength was 532 MPa, which was smaller than the ultimate tensile strength (690 MPa). The ultimate compressive strain was 1.25%, which was also smaller than that in tension.

Table 2.6. Compression characteristics of the GFRP bars[33]

Diameter (mm)	Compressive strength (MPa)	Strain at rupture (%)	Modulus of Elasticity (GPa)	Poisson's ratio
15.9	492	1.2	43	0.31
19.1	575	1.3	46	0.31
25.4	527	-	41	0.3
Average	532	1.25	43	0.31

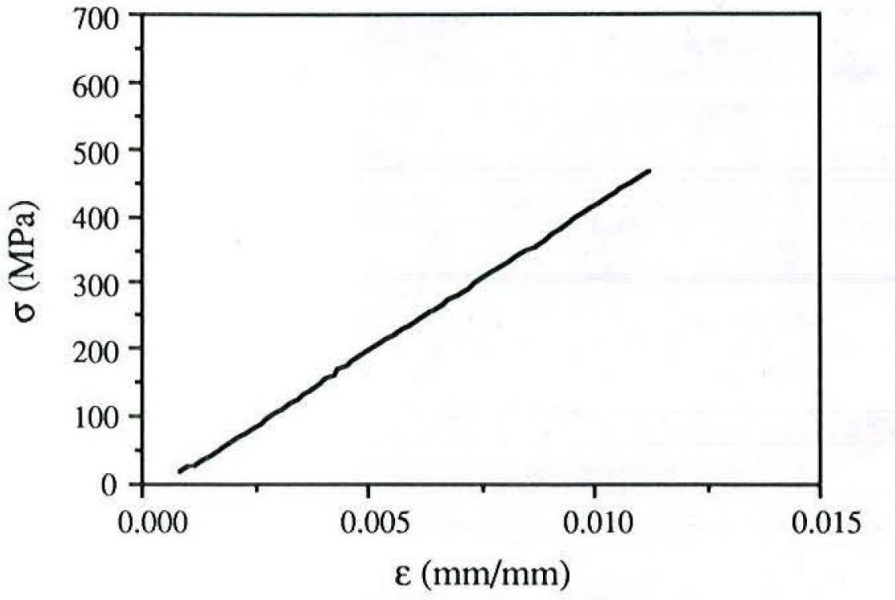

Figure 2.3. Typical GFRP stress strain curve in compression[33]

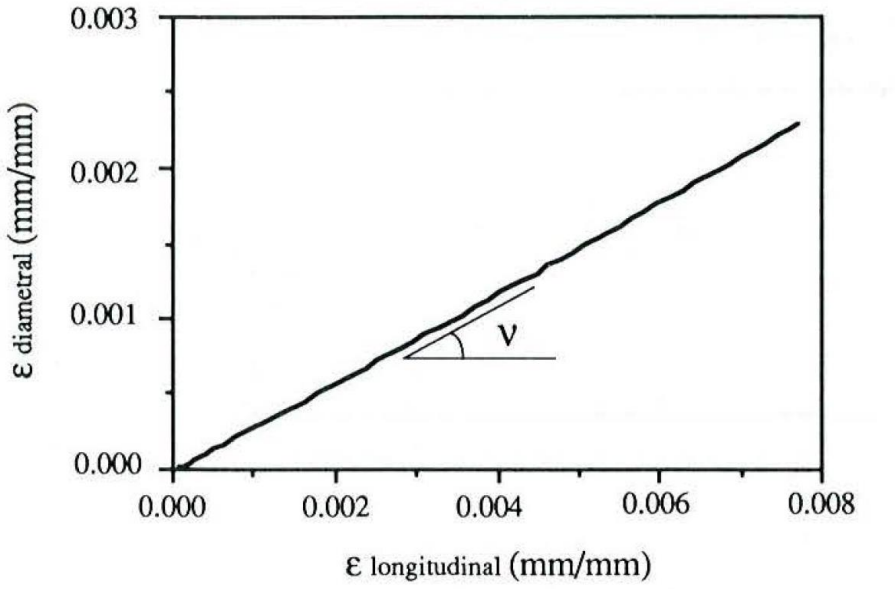

Figure 2.4. Typical diametric versus longitudinal strain curve in compression[33]

The failure mode for GFRP bars under longitudinal compression can include transverse tensile failure, fibre microbuckling, or shear failure[34]. The effect of the unbraced length to the diameter ratio of GFRP bars in compression was studied by

Deitz et al.[37]. They investigated GFRP bars with 15 mm in diameter, 610 MPa in ultimate tensile strength and 40 GPa in modulus of elasticity. The main parameter was the length of the GFRP bars which varied between 50 mm to 380 mm. They categorized the failure of GFRP bars into three different categories as shown in Figure 2.5, depending on the unbraced length of the specimens. The first failure mode was crushing of the specimens, and can be known as micromechanical failure as the glass fibres separated from the resin matrix and buckled individually. This mode of failure happened in the shorter specimens or in the specimens with unbraced length from 50 mm to 110 mm and the compressive strength remained constant as in Equation 2.1[37].

$$f_{fu,c} = 325\ MPa \quad for: 0\ mm \leq L_u \leq 110\ mm \tag{2.3}$$

The second failure mode was a combination of the crushing and buckling mode. In some cases, the GFRP specimens buckled first, and with continuity of loading followed with crushing failure. This mode of failure happened in the specimens with unbraced lengths from 110 mm to 210 mm and the compressive strength of the specimens decreased linearly with the increase of unbraced length as shown in Figure 2.5[37]. Therefore, the ultimate compressive strength could be expressed as:

$$\begin{aligned} f_{fu,c} &= 325 - 0.5(L_u - 100) \ \text{MPa} \\ for: 110\ mm &< L_u < 210\ mm \end{aligned} \tag{2.4}$$

The third failure mode was the buckling of the entire unbraced length of the GFRP specimens. This mode of failure happened in the specimens with unbraced length from 210 mm to 380 mm[37] and the ultimate compressive strength can be estimated as:

$$f_{fu,c} = \frac{\pi^2 E_{f,c}}{\left(\frac{k L_u}{r}\right)} \text{ MPa} \quad \text{for : } 210\,mm \leq L_u \tag{2.5}$$

where $f_{fu,c}$ = ultimate compressive stress; L_u = unbraced length; $E_{f,c}$ = compressive modulus of elasticity; k = effective length factor for buckling; and r = radius of gyration of the GFRP bar.

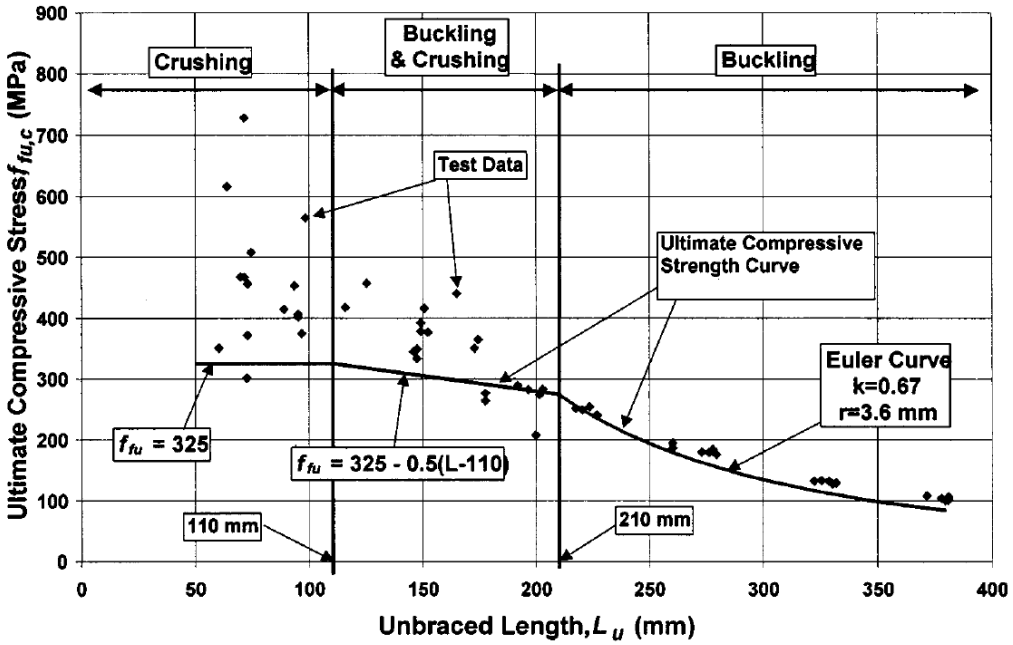

Figure 2.5. Proposed ultimate strength curve for 15 mm GFRP bars in compression[37]

Also, Kobayashi and Fujisaki[38] investigated carbon, glass and aramid FRP bars under compression. They reported that the compressive capacity of carbon, glass and aramid FRP bars was approximately 30-50%, 30-40% and 10% of their tensile capacity, respectively.

The compressive modulus of GFRP bars is slightly smaller than its tensile modulus of elasticity. The test results of specimens with 55 to 60% E-glass fibre-volume fraction indicated the compressive modulus of elasticity to be around 35 to 48 MPa, which is approximately equal to 80% of its tensile modulus of elasticity[34]. However, the test results of Chaallal and Benmokrane[33] showed that the compressive modulus of elasticity and Poisson's ratio (43 GPa and 0.31, respectively) were somehow greater than corresponding values in tension (42 GPa and 0.28, respectively).

Deitz et al.[37] also tested three different unbraced length (80, 200 and 300 mm) GFRP bars under compression to determine the modulus of elasticity. They reported that the compressive modulus of elasticity was approximately equal to the tensile modulus of elasticity (42.5 GPa). The slightly lower values of modulus of elasticity in compression could be referring to the premature failure in the test resulting from end brooming and internal fibre microbuckling under compressive loading.

2.4 Summary

This chapter focused on the stress strain behaviour of concrete and the composition and mechanical properties of FRP bars. It clarified what the ingredients of the FRP bars were, and the production process. Also, the mechanical properties such as tensile strength, compressive strength, and modulus of elasticity of FRP bars were discussed.

The following chapter explains the behaviour of concrete columns and beams as concrete structural elements that are reinforced internally with FRP bars longitudinally and transversally. The behaviour and contribution of FRP bars in carrying load and confining of concrete core are studied. Also, the failure mode of FRP concrete columns is explained and compared with the steel reinforced concrete columns.

3 CONCRETE MEMBERS REINFORCED WITH FRP BARS

3.1 Introduction

A review of the use of FRP bars in reinforcing of concrete members is presented in this chapter. The influence of longitudinal and transverse FRP reinforcement is addressed on the behaviour, performance and failure modes of concrete columns based on the previous studies. Also, the effects of the FRP bars on the load carrying capacity, deflection, crack, and deformability on the RC flexural members is reviewed in this chapter.

3.2 Overview of FRP use in structure

Polymers and polymer composites have been used since World War II in the manufacturing of Radomes to house electronic radar equipment. Because of the ease of use and flexibility to make complex shapes and moulding, they became attractive to designers and they were available in the form of translucent sheets in the 1950s, while they were very expensive[2]. The use of FRP composites in civil infrastructures has been in use for 50 years in the construction of new or retrofitting of the existing structures[10]. The FRP composite bars as prestressed or non-prestressed internal reinforcement for concrete developed since the 1960s in the United States and the 1970s in Europe and Japan, whereas in the 1980s, the use of FRP composites progressed in the way of research, demonstration and commercialization[18].

In the United States, GFRP bars were initially developed by Marshall-Vega Inc., as GFRP bars were a suitable alternative to steel in the reinforcing of polymer concrete

due to the incompatibility of thermal expansion between polymer concrete and steel bars[13]. In addition, in the early 1980s, the American Society of Civil Engineers (ASCE) published some papers on the use of FRP profile sections in structures. It can be seen from the historical review about the FRP composites that more attention is paid to the application of FRP composites from the 1990s and the codes to design with FRP materials have been established in Japan, Canada, United States and Europe. Moreover, in 1997, the ASCE published the *Journal of Composites for Construction* which today is the main international archive for reporting on research and development in the field of FRP composites. Also, the International Institute for FRP in Construction (IIFC) was established in Hong Kong in 2003. Nowadays, there are a lot of research studies and structural engineering projects that use FRP materials for building new and retrofitting existing structures.

3.3 Concrete columns reinforced with FRP bars

In general, a concrete column that is reinforced with steel bars obtains some different behavioural limits such as capacity, curvature and deformability that make it different than plain concrete columns. Also, the behaviour and effects of steel reinforcement have been addressed thoroughly in the literature. Whereas, the appearance of using FRP bars for reinforcing concrete columns made the researchers be concerned about the effect of FRP bars in concrete columns because of their intricate behaviour like having higher tensile strength than compressive strength. In addition, because of the lack of studies and not having a global standard for testing FRP bars under compression, ACI 440.1R-06[39] does not recommend the use of FRP bars in compression members and CAN/CSA S806-12[15] recommend to ignore the

contribution of FRP in the capacity of concrete columns. Therefore, some authors have investigated the impact of replacing longitudinal and transversal steel reinforcement with FRP reinforcement on the behaviour and failure mode of concrete columns.

3.3.1 FRP-RC columns under concentric load

3.3.1.1 Longitudinal reinforcement

Longitudinal or main reinforcement in concrete columns, as it is clear from its name, is responsible for the upstanding of the concrete columns. Even in situations that longitudinal reinforcement is not required for carrying load, it should be provided at least 1% of the concrete cross section area[40] (for steel reinforcement) because of the effect of sustainable loads and creep. Because FRP bars have different mechanical behaviour in comparison with conventional steel reinforcement, it is necessary to precisely address the behaviour and contribution of FRP bars in concrete columns.

Castro et al.[41] investigated eight square concrete columns (100 mm × 100 mm × 1600 mm) under concentric compressive loading. The columns were cast with two different concrete strengths (20 and 40 MPa) and half of them were reinforced with four 6.35 mm GFRP bars and the rest were plain concrete. They noticed that GFRP bars could increase the load carrying capacity of the concrete columns in comparison with plain concrete and GFRP bars were more effective in columns with lower concrete strength and greater column's length because of the effect of buckling.

Alsayed et al.[42] tested 15 rectangular concrete columns (450 mm × 250 mm × 1200 mm) under concentric axial loading. The concrete columns were cast with 38.6 MPa concrete and they were reinforced longitudinally with steel (six bars of 16 mm) or GFRP bars (six bars of 15.7 mm) and three of them were plain concrete as control specimens. The GFRP-RC columns gained 13% lower load carrying capacity than the steel counterpart. Also, they suggested a 60% reduction in the ultimate tensile strength of the GFRP bars in computing the compressive load carrying capacity of the GFRP-RC columns as:

$$P_o = 0.85\, f_c' \left(A_g - A_f\right) + 0.6\, f_{fu}\, A_f \tag{3.1}$$

where f_c' and f_{fu} are the compressive strength of the concrete and the ultimate tensile strength of the GFRP bars, respectively, and A_g and A_f are the gross area of the concrete and the area of GFRP bars, respectively.

Lotfy[43] carried out tests on eight square concrete columns (250 mm × 250 mm × 1250 mm) under concentric axial compressive loading. The concrete columns had three different compressive strengths (25, 30 and 35 MPa) and were reinforced longitudinally with steel and three different GFRP reinforcement ratios (0.72, 1.08 and 1.45%). He found that the capacity of GFRP-RC columns was 16% lower than the steel counterpart. Also, increasing the longitudinal GFRP reinforcement ratio led to an increase in the ductility and had a significant effect on the initial cracking load, ultimate strain and ultimate loads.

De Luca et al.[44] studied five full-scale square concrete columns (610 mm × 610 mm × 3050 mm) under monotonic axial loading with 34.5 MPa concrete compressive strength. The columns were reinforced longitudinally with steel and two different GFRP bars. The longitudinal reinforcement ratio of the columns was 1%. They reported that the contribution of the GFRP bars was about 2.9 and 4.5% of the total peak load, while the contribution of the steel bars was approximately 11.6% of the total peak load. The lower contribution of the GFRP bars was due to lower modulus of elasticity of the GFRP bars than that of the steel bars. Hence, De Luca et al.[44] suggested to ignore the contribution of GFRP bars in the load carrying capacity of the concrete columns. In addition, the axial strain of GFRP bars was greater than the steel bars. It means that the steel bars failed by buckling rather than crushing. Also, in the case of large tie spacing the failure is controlled by bar buckling because of light lateral confinement.

Tobbi et al.[45] investigated eight full-scale square concrete columns (350 mm × 350 mm × 1400 mm) under monotonic axial loading. The columns were cast with 32.6 MPa concrete and reinforced horizontally with 1.9% steel or GFRP bars. They found that the contribution of the GFRP bars was about 10% of the peak load which was very close to the contribution of steel bars (12% of the peak load). The failure of GFRP longitudinal bars in the large lateral spacing is caused by buckling, while in the smaller pitch spacing the bars ruptured. Also, they suggested using 0.35 reduction factor of the ultimate tensile strength of the GFRP bars in calculating the capacity of the concrete columns that are reinforced with GFRP bars as in Equation 3.2 instead

of ignoring it because this causes an underestimate of the capacity of the concrete columns.

$$P_o = 0.85\, f_c' \left(A_g - A_f\right) + 0.35\, f_{fu}\, A_f \tag{3.2}$$

Pantelides et al.[46] investigated 10 circular concrete columns, 254 and 711 mm in diameter and height, respectively, under concentric axial loading. The columns were cast with 36 MPa concrete and reinforced longitudinally with steel or GFRP bars with 1.0 or 1.7% reinforcement ratio, respectively. They found that the GFRP-RC columns gained 16% lower strength capacity compared to the steel-RC columns counterpart. Therefore, concrete columns that are reinforced with GFRP bars needs larger reinforcement ratios of longitudinal and transverse reinforcements to achieve a comparable performance to the steel-RC columns.

Afifi et al.[47] conducted an experimental study on 12 circular concrete columns with 300 mm in diameter and 1500 mm in height that were reinforced with steel and GFRP bars under compressive axial loading. The columns were cast with 42.6 MPa concrete having three different GFRP reinforcement ratios (1.1%, 2.2% and 3.2%). The contribution of the GFRP bars in the load carrying capacity of the concrete columns was about 5% to 10% of the peak load, whereas the contribution of the steel bars was approximately 16%. The GFRP-RC columns behaved in a more ductile manner than the steel counterpart. As such, the ductility index for the GFRP concrete columns was 2.0 in comparison with 1.9 for steel-RC columns. In addition, the effect of increasing the GFRP longitudinal reinforcement ratios were more considerable on the ductility and confinement efficiency than the axial strength of the concrete

columns because it could be observed that by increasing the longitudinal GFRP reinforcement ratio from 1.1% to 3.2%, the vertical strain in the concrete columns and the GFRP bars reduced by 20% and 25%, respectively, and the strain in the helix reduced by 86%, while the gain in strength was only 6%. Depending on the Tobbi et al.[45] study and their results, Afifi et al.[47] suggested to use 0.35 as a reduction factor for the ultimate tensile strength of the GFRP bars in computing the axial capacity of the GFRP concrete columns as in Equation 3.2.

Afifi et al.[48] investigated 11 full-scale circular concrete columns with 300 mm in diameter and 1500 mm height under concentric axial loading. The columns were cast with 42.9 MPa concrete and reinforced with steel and three different CFRP reinforcement ratios (1.0%, 1.7% and 2.4%). They explained that the contribution of the CFRP bars in the peak load carrying capacity was around 11 to 15% in comparison with 16% of the steel bars. At the peak axial load level, the average axial strain in the CFRP and steel bars in the concrete columns was 0.0021 which equals approximately to 15% of the ultimate tensile strain and yield strain of the CFRP and steel bars, respectively. In addition, by increasing the longitudinal CFRP reinforcement ratio from 1% to 2.4%, the contribution of the CFRP bars in the peak axial load was also increased from 11% to 19% and it led to an increase in the concrete column capacities by 12%. Moreover, this increase in the reinforcement ratio reduced the strain in the transverse CFRP helix by 66% at the peak load. The failure of the vertical CFRP bars was in the form of breaking into small pieces rather than buckling of the bars because CFRP bars do not have high bending capacity.

Also, they suggested 0.25 as a reduction factor for the ultimate tensile strength of the CFRP bars in the calculation of the CFRP-RC column capacities as:

$$P_o = 0.85\, f_c' \left(A_g - A_f\right) + 0.25\, f_{fu}\, A_f \tag{3.3}$$

Mohamed et al.[49] carried out an experimental study on 14 circular concrete columns (300 mm in diameter and 1500 mm in height) under axial compression load. The columns were cast with normal-strength concrete with cylinder compressive strength of 42.9 MPa. The columns were reinforced longitudinally with steel, GFRP, or CFRP bars. They reported that reinforcing the columns with GFRP, CFRP, and steel bars increased the peak loads to 1.2, 1.24, and 1.27 times that of the plain concrete, respectively. At the peak load, the average axial strain in the GFRP and CFRP bars were about 15% of their ultimate tensile strain, while the steel bars yielded. Also, the contribution of the steel bars in the peak load carrying capacity of the columns was about 15%, whereas the contribution of the GFRP and CFRP bars in the peak loads were about 5 to 10% and 6 to 19%, respectively. The CFRP longitudinal bars failed before buckling because CFRP bars do not have high bending capacity. Mohamed et al.[49] introduced Equation 3.4 to estimate the peak load of FRP-RC columns under axial compression load.

$$P_o = 0.85\, f_c' \left(A_g - A_f\right) + \varepsilon_p\, E_f\, A_f \tag{3.4}$$

where ε_p is the strain limit to be considered in the FRP strength contribution at the initiation of microcracks in the concrete's plastic stage and E_f is the elastic modulus of the FRP bars.

Tobbi et al.[50] conducted an experimental investigation on 20 concrete columns measuring 350 mm × 350 mm × 1400 mm under concentric compression load. The columns were reinforced longitudinally with steel, GFRP, or CFRP bars and cast with three different concrete strengths (27 MPa, 33 MPa, and 35 MPa). They reported that the effect of the longitudinal bars was more pronounced at the pre-peak phase before activation of the confinement effects. Increasing the longitudinal reinforcement ratio increased the load at peak before activation of confinement. The peak load of steel-RC columns was greater than the FRP-RC columns with the same longitudinal reinforcement ratio. After peak load, the GFRP-RC columns showed stabilization of the load carrying capacity and it was nearly horizontal plateau until failure, while the load carrying capacity of the steel-RC columns decreased after the peak loads. These differences in the post-peak behaviour of the RC columns were because of the longitudinal reinforcing materials. As, the stress-strain behaviour of the steel bars were elastic perfectly plastic and the FRP bars were linearly elastic until failure. Tobbi et al.[50] proposed Equation 3.5 to estimate the peak load of the FRP-RC columns under axial loads.

$$P_o = 0.85\, f_c' \left(A_g - A_f\right) + \varepsilon_{co}\, E_f\, A_f \tag{3.5}$$

where ε_{co} is the unconfined concrete strain corresponding to f_c'.

3.3.1.2 Transverse reinforcement

Transverse or lateral reinforcement laterally generates pressure on the concrete columns against lateral expansion due to Poisson's effect. Transverse reinforcement

passively confines columns because it is not active until the concrete columns are pressured and laterally expanded which is when the lateral reinforcement becomes active and makes the failure of concrete columns more ductile rather than brittle or sudden failure. Because of the different mechanical behaviour of FRP bars, this becomes more concerning and has been studied by some researchers.

Alsayed et al.[42] studied 15 rectangular concrete columns that were reinforced transversally with the same amount of steel or GFRP ties. They reported that at low level of loading or up to about 80% of the peak load the GFRP ties had little or no contribution in the confining of the concrete columns and the columns behaved as the plain concrete specimens because of low modulus of elasticity of the GFRP ties. Whereas, the increasing of applied load, the contribution of the GFRP ties in confining the concrete columns became more effective and reduced the lateral expansion and increased the ultimate capacity of the concrete columns. In contrast, the contribution of steel ties started at the beginning of loading and increased with the increasing of loading, so the concrete columns with steel ties exhibited higher resistance to axial shortening. They concluded that replacing only the steel ties by the same amount of the GFRP ties caused reduction by 10% of the axial capacity of the concrete columns.

De Luca et al.[44] investigated five square concrete columns with two different spacing of GFRP transverse reinforcement (305 mm and 76 mm). They revealed that the Poisson's ratio for the specimens with large GFRP lateral reinforcement remained constant between 0.15 and 0.2 up to an axial strain of about 0.002, whereas for the

steel lateral reinforcement is 0.25 through axial strain about 0.0028 and after that it rapidly increased. Moreover, for the specimens with small lateral GFRP reinforcement, the Poisson's ratio started at a value of 0.2 and increased linearly up to an axial strain of about 0.0028. Beyond the peak load, Poisson's ratio increased more rapidly and reached approximately 0.9 at failure. In addition, using smaller tie spacing did not increase the peak capacity of the concrete columns but it changed the failure mode and increased the ductility of the concrete columns.

Tobbi et al.[45] studied eight square concrete columns that were reinforced laterally with four different GFRP reinforcement configurations with two different spacing (120 and 80 mm) as shown in Figure 3.1. They observed that during the ascending part lateral reinforcement had low or no effect and in the first peak load its strain was around 0.001 which is lower than 10% of its ultimate tensile strain. After spalling of the concrete cover, the strain in ties increased considerably and the well confined specimens could reach second peak load. At this stress level the strain in transverse reinforcement for lightly confined specimens reached about 0.01 which is 70% of its ultimate tensile strain and the strain in transverse reinforcement for well confined specimens reached about 0.008 which is 55% of its ultimate tensile strain. Reducing tie spacing from 120 mm to 80 mm could increase the concrete columns strength by more than 20%. Also, lateral confinement led to improve the ductility of concrete columns as their ductility was four to eight times greater than the unconfined specimens.

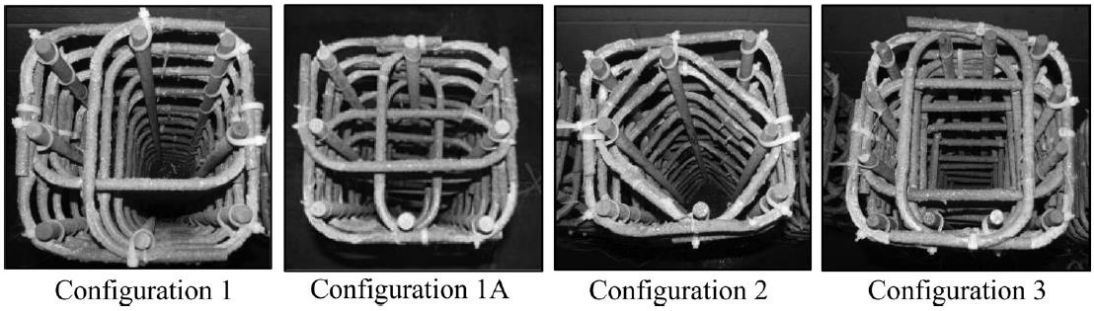

Figure 3.1. GFRP reinforcement configurations[45]

Afifi et al.[47] carried out tests on 12 circular concrete columns that were transversally reinforced with five different volumetric ratios and spacing of GFRP helices as shown in Figure 3.2. They observed that the transverse reinforcement at the peak load was not active and its strain was about 0.000305 which is less than 2.0% of its ultimate tensile strain. However, with the progressing of axial stress and reaching the concrete columns ultimate stress, the strain in the GFRP helix continuously increased and reached around 80% of its ultimate tensile strain. Increasing the volumetric ratios or reducing the spacing of the GFRP helix positively affected the behaviour of the concrete columns. For example, by increasing the volumetric ratio of GFRP helices from 1% to 3%, 6% in axial strength, 208% in the ductility, 29% of bar-strength contribution and 34% in the confinement efficiency was obtained. Moreover, the well-confined specimens (40 mm spacing) could reach a second peak load and their post-peak behaviour until failure was more stable and ductile. Within the same amount of volumetric ratio of GFRP helix, using smaller bar diameters with smaller spacing was more effective than larger bar diameters with larger spacing in improving ductility. Moreover, using 6.4 mm GFRP helix with 35 mm instead of 12.7 mm with 145 mm spacing could increase 140% in the ductility, 35% in the

strength of the concrete core and 3% in the maximum axial load of the concrete columns.

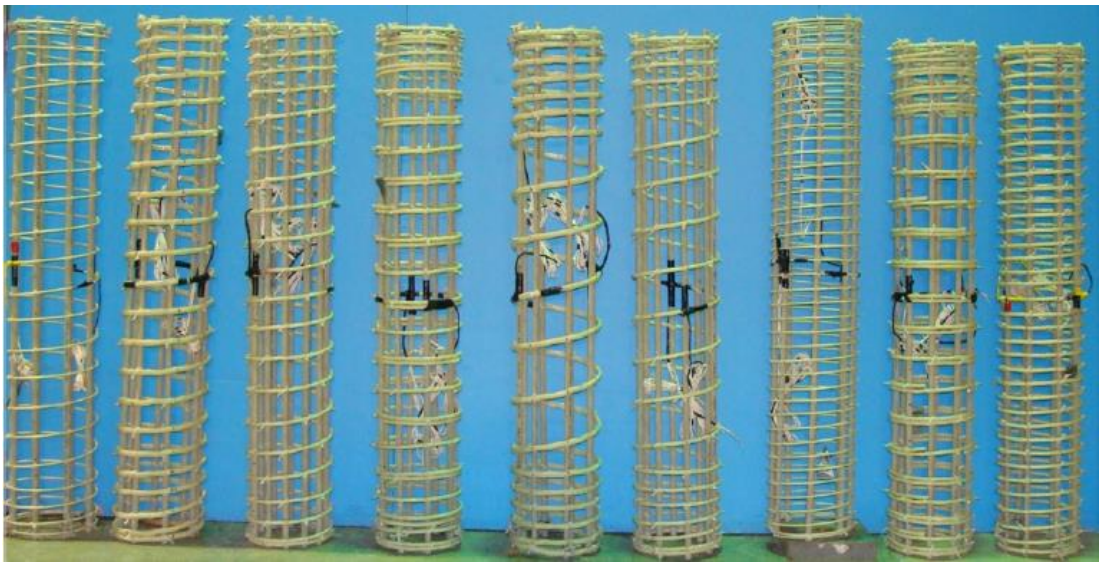

Figure 3.2. GFRP assembled cages[47]

Afifi et al.[48] investigated 11 full-scale circular concrete columns that were reinforced with five different volumetric ratios and spacing of CFRP helices as shown in Figure 3.3. They reported that at the peak load, the average strain in the CFRP and steel helices were about 0.0002 and 0.000282, respectively, which is less than 2.0 and 15% of the ultimate tensile strain of CFRP and yield tensile strain of steel bars, respectively. The ductility index for the CFRP columns was about 96% of the steel RC columns. Furthermore, by increasing volumetric ratio of CFRP helix from 1% to 3%, an increase of 3% in the axial strength, 57% in the ductility, 37% in the longitudinal CFRP bars contribution and 21% in the confinement efficiency was gained. Therefore, increasing CFRP helix reinforcement has more effect on confinement efficiency and ductility rather than on axial strength capacity. Within a constant volumetric ratio of CFRP helix reinforcement, using smaller diameter bars

with closer spacing was much more effective in improving the behaviour of specimens. As such, an increase of 25% in ductility, 16% in strength of the concrete core and 7% in maximum load carrying capacity were seen when using 6.35 mm helix with 35 mm spacing instead of using 12.7 mm helix with 145 mm spacing.

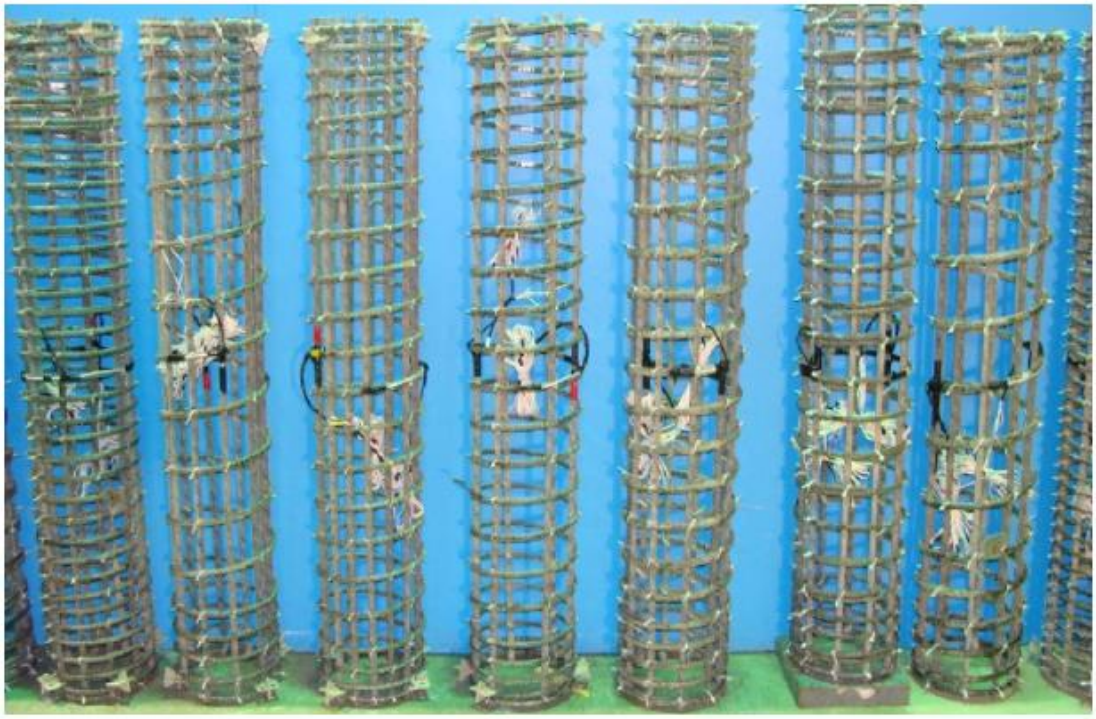

Figure 3.3. CFRP assembled cages[48]

Mohamed et al.[49] tested circular concrete columns under concentric loads that were reinforced longitudinally and transversally with GFRP and CFRP bars. The transverse reinforcement consisted of three different volumetric ratios (0.7%, 1.5%, or 2.7%) of hoops or helices as shown in Figure 3.4. They reported that columns with GFRP and CFRP helices obtained 1.3% and 2.2% higher strength, respectively, compared with the columns confined with GFRP and CFRP hoops. Also, the RC columns with CFRP helices and hoops achieved 3.4% and 2.16%, respectively,

greater peak loads than the counterpart RC-columns with GFRP helices and hoops. At the peak load level, the hoop strain at the CFRP and GFRP helices were about 2% of their ultimate tensile strain. The GFRP-RC columns showed more ductile behaviour compared with the counterpart steel-RC columns, as the ductility indexes were 2.0 and 1.9 for the GFRP- and steel-RC columns, respectively. However, the CFRP-RC columns exhibited little ductile behaviour compared with the counterpart GFRP-RC columns, as the ductility indexes were 2.0 and 1.82 for the GFPR- and steel-RC columns, respectively. The test results indicated that the CFRP and GFRP helices performed better than counterpart columns with CFRP and GFRP hoops in the ways of ductility and strength enhancement ratio. This is because of the fact that greater concrete core was confined by the helices and the confined pressures were almost uniform than that of the hoops. Finally, it was concluded that the GFRP (helices and hoops) were more effective in improving the ductility and confined concrete strength than the CFRP (helices and hoops) because the CFRP helices and hoops did not have high bending and shear capacity.

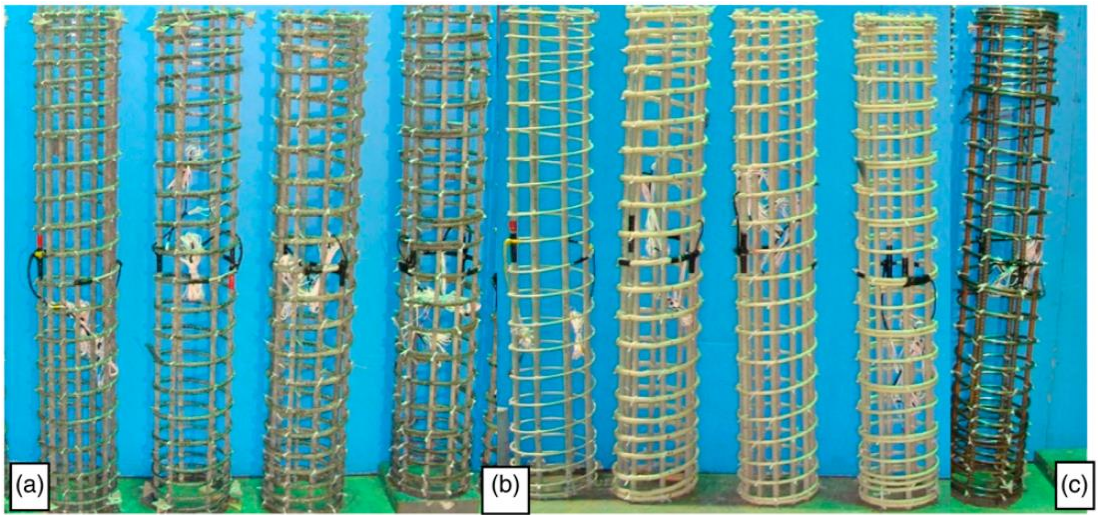

Figure 3.4. Assembled cages: (a) CFRP; (b) GFRP; and (c) Steel[49]

Tobbi et al.[50] investigated the effects of FRP reinforcement on square concrete columns under concentric axial loads. The parameters that considered in this study were transverse reinforcement materials (CFRP and GFRP), shape of transverse reinforcement (C-shaped parts assembly or closed ties as shown in Figure 3.5), transverse reinforcement ratios and configurations (Figure 3.6). They reported that closed transverse reinforcement performed better in confining concrete core than C-shaped transverse reinforcement. This is because of the material continuity that eliminates slippage, increasing the lateral confinement pressure rather than confinement degradation. A higher confined concrete strength and peak stress could be achieved with Configuration 3 rather than Configuration 1. The test results indicated that with CFRP ties a higher confined concrete strength could be obtained that the counterpart GFRP ties. This is because the CFRP ties were stiffer and tended to open less than the GFRP ties. Finally, they concluded that the configuration and spacing of the transverse reinforcement were more important parameters than modulus of elasticity. In a given transverse reinforcing material and volumetric ratio, Configuration 3 performed better than Configuration 1 in terms of ultimate strain.

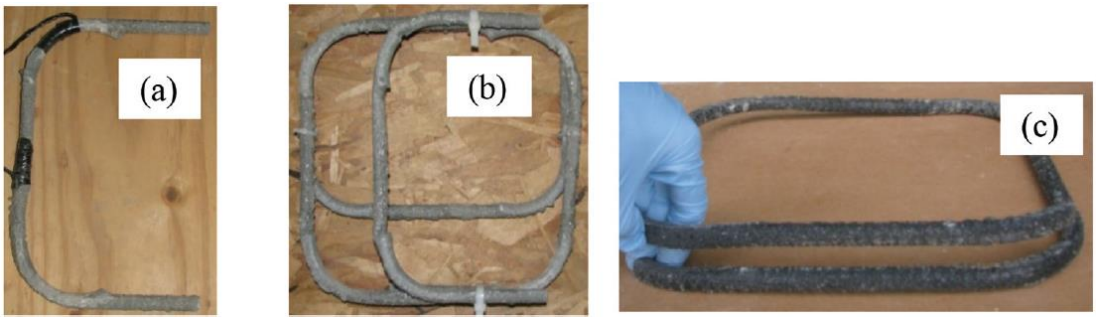

Figure 3.5. (a) and (b) C-shaped; and (c) closed transverse reinforcement[50]

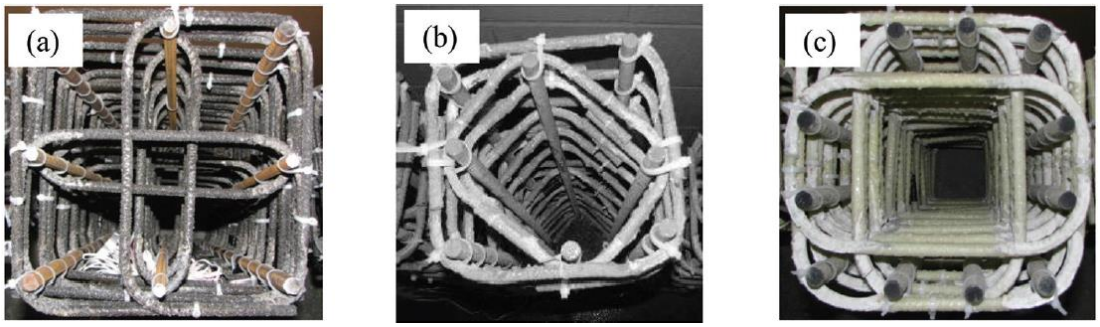

Figure 3.6. Transverse reinforcement: (a) Configuration 1; (b) Configuration 2; and (c) Configuration 3[50]

3.3.1.3 Failure modes

Because studies on FRP bars and their modes of failure started with using FRP bars in reinforcing flexural members, the failure mode of concrete columns could be somehow predicted with having differences between columns and flexural members. In flexural members a great amount of FRP bars should be provided in order to gain a compression failure mode, which is the most ductile failure mode in FRP concrete columns. Also, for crack width and deflection control, a great amount of FRP bars is provided in the tension zone. Thus, the compression zone receive a large compressive force and compression failure of FRP bars would happen because of its small compressive strength[38]. However, FRP concrete columns have differences with flexural members because different loading modes and reinforcement bars are distributed almost symmetrically around the perimeter of the column cross sections. For this purpose, some studies have been undertaken to understand the failure mode of FRP concrete columns under concentric and eccentric compressive load.

Kawaguchi[51] stated that crushing of concrete in the compression region controlled the failure of the GFRP concrete columns under eccentric loading and no rupture happened in the GFRP bars. In addition, the ultimate strain in the compression zone was recorded between 0.004 and 0.005. Also, Amer et al.[52] studied eight square (152 mm × 152 mm × 2438 mm) slender concrete columns under four different eccentric loading (28, 64, 127, and 305 mm). The columns were cast with 32.11 and 41.37 MPa concrete and the columns were reinforced with four 7.5 mm diameter longitudinal CFRP bars and 9.53 mm steel ties with 152 mm spacing. They reported that the failure of the CFRP concrete columns was due to concrete crushing in the compression zone and the cracks were symmetrically distributed. The CFRP concrete columns followed the conventional steel reinforced column pattern in the way of curvature and deflection of the CFRP bars.

Alsayed et al.[42] showed that failure of the GFRP concrete columns was caused by crushing of the concrete and breaking of the bars at the mid-height of the columns, while the failure of steel reinforced specimens resulted from buckling of the longitudinal bars at the mid-height of the columns.

Kobayashi and Fujisaki[38] classified the failure modes of FRP-RC columns into three types which were tension failure of FRP longitudinal bars, compression failure of concrete in the compressive region and compression failure of FRP bars in the compressive region. In monotonic loading, compression failure of FRP bars does not seriously reduce the capacity of the columns because the modulus of elasticity of FRP bars is close to the concrete. However, compression failure of FRP bars should

be considered in cyclic loading because the FRP bars cannot carry tensile load after its compression failure. More attention should be paid for concrete columns reinforced with aramid fibre reinforced polymer (AFRP) bars because it has low compression strain and easily fails under compression loading. In contrast, concrete columns that are reinforced with glass or carbon FRP bars do not face compressive bar failure because the ultimate compressive strain of the concrete at failure is between 0.3% and 0.5%, therefore the concrete fails under compression before the bars.

Choo et al.[53] clarified that FRP concrete columns in some cases are susceptible to tension failure. This failure happens when the outermost concrete fibres reach its ultimate compressive strain ($\varepsilon_c = \varepsilon_{cu} = 0.003$) and at that moment the outermost FRP bars reach their ultimate tensile strength ($\varepsilon_f = \varepsilon_{fut}$). This failure is more common in concrete columns that have low FRP reinforcement ratio.

De Luca et al.[44] reported that the GFRP-RC columns behaved almost like the steel-RC columns. The failure started with vertical cracks and then the vertical bars started deflecting, followed by splitting of the concrete cover and then the concrete core started crushing and finally the longitudinal bars buckled. The stiffness of the GFRP-RC columns started decreasing as they reached about 60% of their peak load, while the steel-RC columns about 80% of their peak load. In addition, all specimens obtained about 85.9 to 93.2% of the average concrete strength in their peak loads with axial strain approximately between 0.0022 and 0.0027. The failure of the specimens with large tie spacing (305 mm) was sudden and had explosive noises.

Also, their failure after peak load was brittle and their strength instantly dropped without cracking or early warning until the final crushing. However, the specimens with smaller tie spacing (76 mm) were more ductile by increasing their axial deformation and delaying of the concrete core crushing and their strength beyond the peak load decreased more steadily.

Tobbi et al.[45] stated that the concrete columns during the ascending part until the first peak were visually free of cracks. After peak load they lost 10 to 15% of their maximum axial stress value due to the sudden spalling of the concrete cover and then they failed either by crushing of the concrete core or the GFRP bars buckled or fractured (Figure 3.7) depending on the spacing of the lateral reinforcement. Eventually, an inclined shear sliding surface divided the concrete core into two parts and it caused a considerable drop in the axial strength of the concrete columns. Conversely, the concrete columns with smaller tie spacing (80 mm) could gain second peak load which was greater than the first peak load, while with the larger tie spacing (120 mm) the second peak was not observable.

Pantelides et al.[46] reported that the failure mode of steel-RC column was buckling of the longitudinal bars, while the failure mode of GFRP-RC columns was buckling and crushing of the longitudinal bars and tensile rupture of GFRP helix.

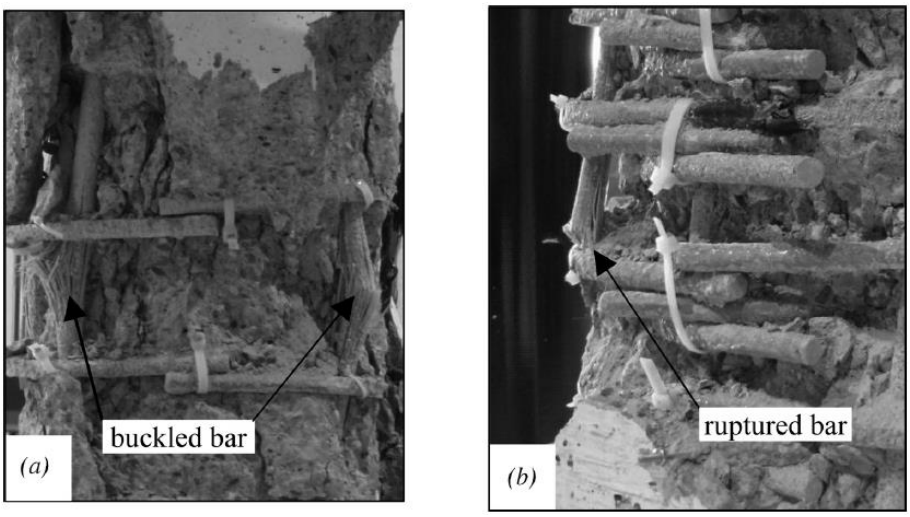

Figure 3.7. GFRP bars failure modes[45]

Afifi et al.[47] stated that the ascending part of the stress-strain curve of the GFRP and steel reinforced concrete columns were almost similar and linear up to the peak or starting of concrete cover spalling. During the ascending part, the cover was visually free of cracks and the cracks appeared at about 85% to 95% of the peak load and then widened up to the peak load. After that, the cover suddenly separated as large pieces of concrete and the columns lost 10% to 15% of their maximum capacities, while the average axial strain was recorded ranging between 0.0026 to 0.004. Furthermore, the failure of the concrete columns with larger helix spacing (145 and 120 mm) was caused by buckling of the bars, whereas the columns with closer helix spacing (80 and 40 mm) after reaching the second peak, they failed by concrete core crushing and helix rupture as shown in Figure 3.8. After crushing of the concrete core, a single inclined shear sliding surface occurred (Figure 3.8) and the columns lost their axial capacity rapidly.

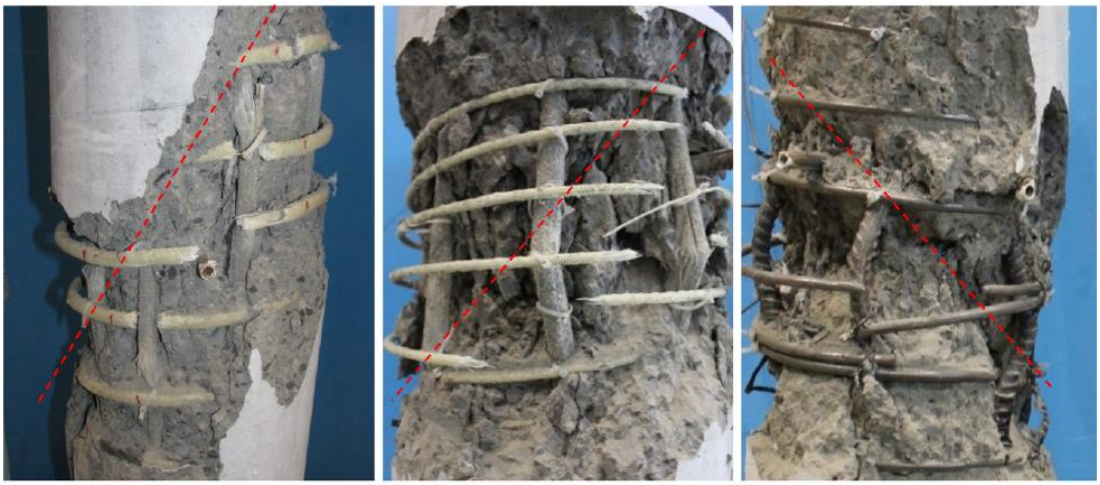

Figure 3.8. Failure of the RC columns: (a) rupture of GFRP helix; (b) buckling and rupture of longitudinal GFRP bars; and (c) buckling of longitudinal steel bars and rupture of helices[47]

Afifi et al.[48] demonstrated that the ascending branch of the stress-strain relationship of the CFRP-RC columns were nearly linear and similar to the steel-RC counterpart up to the peak load and beginning of the cover spalling. At the beginning, the concrete cover was visually free of cracks and then vertical hairline cracks started to appear near 85% to 95% of their peak load. With the progression of loading, the vertical cracks gradually increased and widened up to the peak point. Then, the initial spalling started on one side due to imperfections in the concentric loading and it soon spread to the other sides and suddenly the concrete cover started spalling as large pieces of concrete, so the columns lost about 15% to 20% of their maximum capacities. At peak load level, the axial strain was between 0.0026 to 0.0036. The failure of the specimens with large spacing helix (120 and 145 mm) or with small volumetric ratio (0.7%) was controlled by a shear diagonal plane (Figure 3.9).

However, the failure of the specimens with closer spacing (40 and 80 mm) was controlled by crushing of the concrete core and rupture of the helix (Figure 3.9).

Figure 3.9. Failure of the columns: (a) plain concrete; (b) rupture of CFRP helices; (c) inclined plane failure and rupture of longitudinal CFRP bars; and (d) buckling of longitudinal steel bars and rupture of helices[48]

Mohamed et al.[49] categorised the failure modes of 14 RC columns on two modes. The steel- and GFRP-RC columns failed in a ductile manner with the gradual spalling of the concrete cover, followed by buckling of the longitudinal bars and then rupture of the helices or hoops (Figure 3.10). The CFRP columns failed in a rather sudden and brittle manner, closely similar to the failure of the plain specimen (Figure 3.10). The failure of the GFRP-RC columns with a small volumetric ratio of transverse reinforcement (0.75%) was controlled by buckling of the longitudinal bars. However, the failures of the GFRP-RC columns with moderate and high volumetric ratios of lateral reinforcement (1.5% and 2.7%) were attributed to the crushing of the concrete core and rupture of the helices. Finally, it was concluded

that the failure of the CFRP resulted from the formation of a single inclined failure plane due to shear sliding of the top and bottom parts of the column. However, the GFRP helices and hoops were ruptured due to the confinement action.

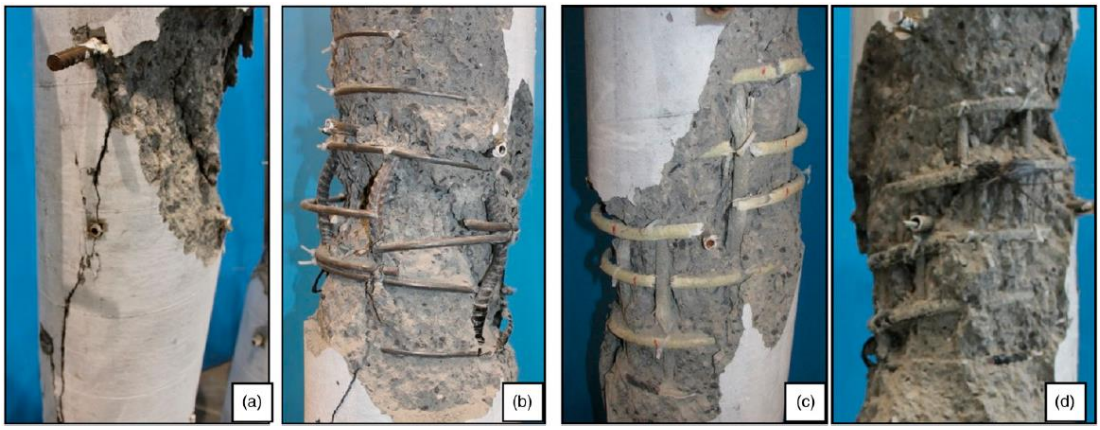

Figure 3.10. Failure of the columns: (a) plain concrete; (b) buckling and rupture of the steel bars and helices; (c) buckling and rupture of the GFRP bars and helices (d) crushing and rupture of the CFRP bars and helices[49]

Tobbi et al.[50] stated that the failure modes were governed by the shape, configuration, diameter of the transverse reinforcement, and longitudinal bars material. The failure of FRP-RC columns followed this progression: (1) crushing or buckling of the longitudinal bars; and (2) rupture of the transverse reinforcement, as shown in Figure 3.11. In general, the FRP-RC columns with C-shaped transverse reinforcements experienced brittle failure because slipping of the outer C-shaped ties at the slice location occurred due to dilation of the concrete core. However, the FRP-RC columns with closed transverse reinforcement failed progressively due to successive crushing of the longitudinal bars before crushing of the concrete core.

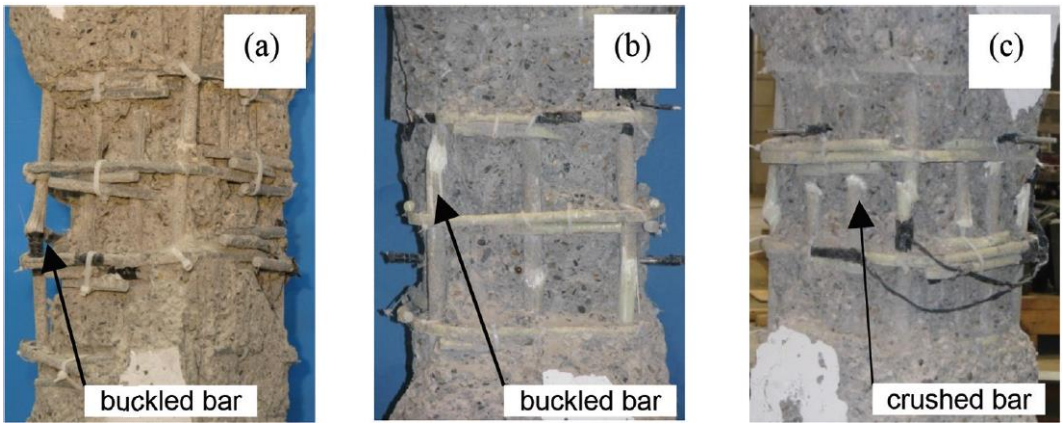

Figure 3.11. Failure of FRP-RC columns[50]

3.3.2 FRP-RC columns under eccentric load

Kawaguchi[51] studied twelve rectangular concrete columns (150 x 200 mm) under eccentric (200 mm) compressive loading. The columns were cast with 39.2 MPa concrete with four 12 mm sand coated aramid bars. They reported that depending on their material properties and reinforcement ratio, the balance AFRP reinforcement was 0.2% and with reducing this ratio the failure of the columns would be caused by rupture of the AFRP bars.

Mirmiran[54] and Mirmiran et al.[55] clarified that concrete columns with FRP bars are more susceptible to length effect than their steel counterpart because of the lower stiffness of FRP bars. Also, they suggested reducing slenderness limits by 5% for AFRP, 15% for CFRP and 22% for GFRP bars, if the minimum reinforcement is held at 1%.

Choo et al.[53] concluded that FRP-RC column cross section interaction strength diagrams do not have balance points (Figure 3.12) because the stress-strain response of FRP bars which are linear elastic until failure. They also observed that reducing FRP reinforcement ratio results in a great tensile strain in the tension side of the FRP-RC cross-sections with increasing load-eccentricity, particularly in the flexural loading condition. Insufficient FRP reinforcement ratio sometimes leads to a brittle tensile failure of the FRP bars before the interaction strength diagrams reach to the pure bending condition as shown in Figure 3.12. Choo et al.[56] proposed a set of equations to limit the minimum ρ_f for rectangular cross-section columns to prevent brittle tensile failure of FRP bars in the tension side under pure bending loads.

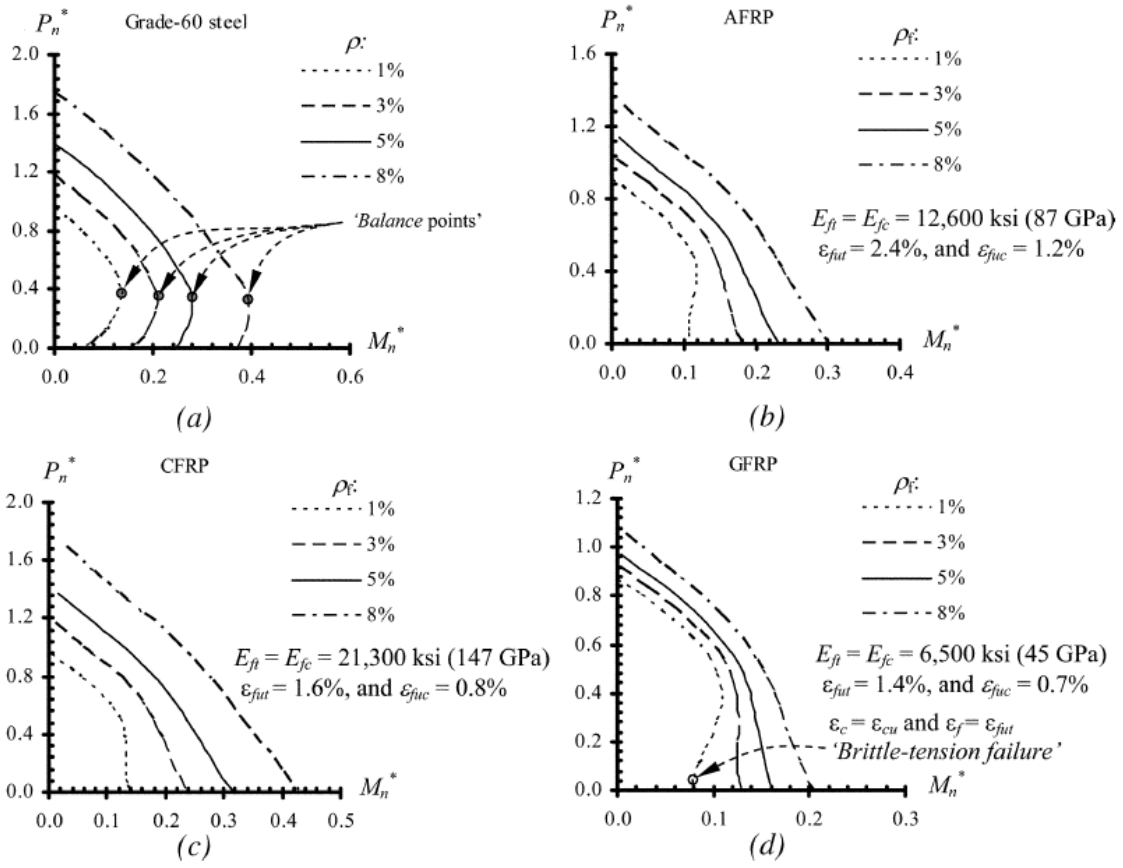

Figure 3.12. Normalized axial load-moment interaction diagrams for steel, AFRP, CFRP, and GFRP-RC column cross-sections for different reinforcement ratios[53]

3.4 Concrete flexural members reinforced with FRP bars

Fibre reinforced polymer bars have different properties and behaviours than steel bars that make FRP bars different to steel reinforcing bars. For instance, FRP bars have higher tensile strength than the corresponding steel bars, while their higher strength cannot be exploited because the modulus of elasticity of FRP bars is smaller than the steel bars. Therefore, for controlling the crack width in tension regions and serviceability requirement, it is compulsory to reduce the serviceability strength of FRP bars. Moreover, the crack width and spacing are affected by the bond between the FRP bars and the surrounding concrete which is also a function of the surface texture and the Poisson's ratio of FRP bars (which are different with steel bars). Despite the differences between the FRP and steel bars, the same analytical moment-curvature relationship for steel reinforced section can be used for FRP reinforced section under the following assumptions: (1) Perfect bond between concrete and reinforcement; (2) plane sections remain plane under loading; and (3) simplification of the stress-strain relationship for the constituent materials[11]. For understanding the practical behaviour of concrete flexural members reinforced with FRP bars, researchers have been experimentally studying the different aspects of the FRP reinforced concrete beams with different type of FRP bars, reinforcement ratios and concrete strength.

3.4.1 Load carrying capacities and failure modes

Failure of FRP reinforced concrete beams in flexure can be caused by rupture of FRP bars in the tension zone when the reinforcement ratio is smaller than the balance

ratio, which is called under reinforcement, or by crushing the concrete in the compression zone when the reinforcement ratio is greater than the balance ratio which is also called over reinforcement. For each case, the ultimate flexural strength can be calculated by using the same equations when the reinforcement is steel or FRP bars[57]. This phenomenon has been addressed by the different authors by studying and testing concrete beams reinforced with different types of FRP bars and different reinforcement ratios and different concrete strengths.

Benmokrane et al.[12] investigated eight concrete beams under monotonic four-point loading. The cross-section dimensions of the beams were 200 mm in width and 300 and 550 mm in height and the clear span was 3000 mm. The specimens were reinforced with the same amount of GFRP or steel bars in tension and steel bars in compression. They observed that the maximum experimental moment was similar for GFRP and steel reinforced beams for 300 mm height, while it was approximately 8% greater in GFRP-RC beams than steel-RC beams for 550 mm height. Also, the specimens failed either in tension for under reinforced beams or in compression (concrete crushing) for over reinforced beams, as they had been designed.

Masmoudi et al.[58] studied ten concrete beams under cyclic four-point loading with 200 mm × 300 mm × 3300 mm in width, height and length, respectively. The specimens were reinforced with either GFRP or steel bars and had different reinforcement ratios according to their predicted failure modes which were balance, tension and compression failure. The compressive strength of the concrete was varied between 45 MPa to 52 MPa. They noticed that with the increasing of the

reinforcement ratio, the ultimate moment capacity also increased. However, this increase in the GFRP reinforcement ratio was limited by the concrete compressive failure strain. The failure of over reinforced specimens consisted of two stages. The first stage was the crushing of the concrete which was followed instantly by the decrease and then the increase of the moment resistance strength. The second stage was the initiation of failure of the GFRP bars. In addition, it was observed that, if the reinforcement was more than one level, a partial failure can occur. When a partial failure happens, the specimens can regain the elastic deflection component with a large deformation.

The effect of CFRP reinforcement ratio on the flexural behaviour of the concrete beams has been studied by El-Salakawy et al.[59]. They constructed 14 full-scale concrete beams with 200 mm × 300 mm × 3300 mm in width, depth and length, respectively. The specimens were cast with 39.3 to 44.8 MPa concrete and tested under four-point loading and were reinforced with different reinforcement ratios of CFRP bars or steel bars. They concluded that increasing the reinforcement ratio by 50% to 100% led to increase the load carrying capacity of the beams by 4% to 11%. Also, the failure of the specimens was caused by concrete crushing, as they were designed with an over reinforcement ratio, except the specimen that was reinforced with a 1.2 balanced reinforcement ratio. For this beam a simultaneous failure by concrete crushing and CFRP rupture occurred.

Kassem et al.[60] conducted a test on 24 concrete beams to investigate the flexural behaviour under four-point loading. The beams were 200 mm × 300 mm × 3300 mm

in width, depth and length, respectively and they were cast with 40 MPa concrete. The beams were reinforced with carbon, glass and aramid FRP bars which had different surface textures and different reinforcement ratios. They noticed that the failures of specimens were controlled by the concrete compressive strength, while the increase of reinforcement ratio did not significantly increase the flexural capacities. The flexural capacity increased by 4% and 16% as a result of increasing the reinforcement ratio by 50% and 100%, respectively.

The effect of concrete strength and FRP reinforcement ratio on the flexural capacity of concrete beams were studied by Kalpana and Subramanian[61]. They conducted an experimental investigation on nine concrete beams with 200 mm × 250 mm × 1800 mm in width, depth and length, respectively and reinforced with GFRP bars under four-point monotonic loading. The specimens were reinforced with three different reinforcement ratios and they were cast with three different concrete strengths (20, 40 and 60 MPa). They observed that increasing the reinforcement ratio by 0.52%, it resulted in increases of 13% and 17% of the ultimate load capacity in the normal and high strength concrete specimens, respectively. Also, increasing the reinforcement ratio by 1.3% resulted in a better increase of 28% and 36% in the ultimate load carrying capacity for the normal- and high-strength concrete, respectively. However, a comparable improvement in the ultimate load carrying capacity of the specimens cast with moderate concrete strength could not be observed due to change in the reinforcement ratio.

In a study by El-Nemr et al.[62] about the impact of the concrete strength and FRP reinforcement ratio on the flexural behaviour of concrete beams, they revealed that for normal strength concrete beams, increasing reinforcement ratio from 0.36 to 1.47% increased the load carrying capacity of the specimens by 143% and increasing the reinforcement ratio from 0.55 to 1.78% increased the load carrying capacity by 224%. In addition, for high strength concrete beams, increasing the reinforcement ratio from 0.36 to 1.47% increased the load carrying capacity of the specimens by 28% and increasing the reinforcement ratio from 0.55 to 1.78% increased the ultimate capacity by 116%. These results were deduced through testing 14 concrete beams which were 200 mm × 400 mm × 4250 mm in width, depth and length, respectively under four-point monotonic loading. The specimens were reinforced with different type and ratio of GFRP bars and they were cast with 30 and 65 MPa concrete strength.

3.4.2 Deflection

Initially, the RC-members are uncracked and have high stiffness, with the increasing of the applied moment, cracking occurs at mid-span and when the applied moment exceeds the cracking moment, the stiffness of the beams reduces. The reduction of stiffness is greater in GFRP-RC members than steel-RC members and the cracks in GFRP-RC members are wider and their spacing is narrower than steel-RC members[63]. Therefore, the maximum deflection of GFRP-RC members at service load is three to four times greater than the maximum deflection of steel-RC members because of the differences in the modulus of elasticity and other physical and

mechanical properties such as bond behaviour and Poisson's coefficient of the GFRP bars with steel bars[12, 58].

Thériault and Benmokrane[64] carried out an experimental study on 12 concrete beams reinforced with GFRP bars under four-point cyclic loading. The specimen dimensions were 130 mm × 180 mm × 1800 mm in width, height and length, respectively. The beams were cast with three different concrete strengths and two different reinforcement ratios which were greater than the balanced reinforcement ratio. They concluded that the increase in concrete strength could not considerably increase the stiffness of the specimens, while increasing the reinforcement ratio resulted in greater stiffness than the smaller reinforcement ratio. In addition, by increasing the reinforcement ratios by 50% and 100%, the measured deflection was reduced by about 31% and 43%, respectively[59].

The deflection of concrete beams reinforced with GFRP bars versus steel bars that had the same flexural strength, has been studied by Alsayed[65] through testing of 12 concrete beams under four-point monotonic loading. The specimens had the same width (200 mm) with three different heights (210, 250 and 260 mm) and 2700 mm in length. The midspan deflection of the steel reinforced specimens corresponding to the ultimate load was 20 mm, while it was 39 mm for the GFRP-RC beams. Hence, replacing steel bars with GFRP bars without changing the cross-section dimensions resulted in doubling the deflection corresponding to the ultimate load.

Toutanji and Saafi[66] studied the flexural behaviour of concrete beams reinforced with GFRP bars under four-point monotonic loading by testing six concrete beams of 180 mm × 300 mm × 3000 mm in width, depth and length, respectively. The beams were designed with balanced and over reinforced ratios with 35 MPa concrete. They reported that the moment-deflection relationship of the specimens was linear until cracking and almost linear in post-cracking with reduction in stiffness until failure. This behaviour caused by the linear characteristics of the GFRP bars and a perfect bond between the concrete and the GFRP bars. However, the moment-deflection for CFRP-RC beams was bilinear for the first part up to the cracking moment represented by the behaviour of the uncracked cross-section beams. However, the second part represented the cracked cross-section beams with reduced second moment of area[59].

The effect of FRP reinforcement ratios has been investigated in Kassem et al.[60] by constructing 24 concrete beams that were reinforced with carbon, glass and aramid FRP bars with different surface textures and reinforcement ratios. They reported that at service load levels (corresponding to 30% of the nominal moment capacity) the measured deflection was 16% and 36% lower for the beams reinforced with CFRP sand-coated bars and 25% and 36% lower for the beams reinforced with CFRP ribbed bars due to the 50% and 100% increase of reinforcement ratio, respectively. Also, the deflection reduction was 27% for the beams reinforced with GFRP sand-coated bars and 20% for the beams reinforced with GFRP ribbed bars as a result of the 33% increase of reinforcement ratio. In addition, the deflection reduction of 15%

was achieved for the beams reinforced with AFRP bars because of increasing the reinforcement ratio by 33%.

3.4.3 Crack distribution and width

The flexural crack characteristics are influenced by the FRP reinforcement ratio and the concrete strength. With increases in the reinforcement ratio or concrete strength the width and spacing of the cracks decrease, while the number of cracks increases[60, 62]. The cracks of the FRP reinforced concrete beams in the flexural span are generally vertical and perpendicular to the direction of maximum principal stress that results by pure bending moment. The cracks outside the pure bending region start as flexural cracking, whereas when the loading is increased, shear stresses become important and cause inclined cracks[58]. According to the results that were obtained in Benmokrane et al.[12] and Masmoudi et al.[58] the formation of cracks was sudden and started when the applied moment approached the cracking moment. Then, the cracks became closer towards the load points on the compression face of the beams. The average crack spacing at low loading level (25% of nominal bending moment) in GFRP-RC beams was similar to the corresponding steel-RC beams. However, at moderate and high loading levels, it was approximately 65% that of steel-RC beams. When the load level reached around 67% of the nominal moment, the formation of new cracks stopped and only widening of the existing cracks could be observed[60].

The average crack spacing in GFRP-RC beams was approximately 109 and 97 mm at moderate and high loading level, respectively[12]. The effect of the reinforcement ratio and concrete strength on the crack spacing were negligible and the crack spacing

slightly decreased with increasing the load due to the formation of new cracks and the average crack spacing was about 139, 104 and 99 mm at low, moderate and high loading, respectively, according to the study by Masmoudi et al.[58]. Also, the crack spacing was about 120, 88 and 80 mm at low, moderate and high loading, respectively, according to the study by Thériault and Benmokrane[64]. The crack width of GFRP-RC beams was about three to five times that of steel-RC beams[58].

The width of cracks increases with increasing the concrete strength because higher stress is needed in the crack initiations which lead to a sudden high crack formation. However, increasing the reinforcement ratios cause a smaller crack width as higher reinforcement ratio can resist higher stresses and tempering the crack initiation[64, 66]. Also, the reduction of the maximum crack width by 36% to 39% and 55% to 56% has been reported by El-Salakawy et al.[59] due to increasing the reinforcement ratio by 50% and 100%, respectively. Moreover, the effect of different types of FRP and reinforcement ratios on crack width were studied in Kassem et al.[60]. They reported that at service load levels, the crack width was 54% and 64% smaller due to increasing the reinforcement ratio by 50% and 100%, respectively, for the beams reinforced with CFRP bars. Also, the crack width was 32% smaller because of increasing the reinforcement ratio by 33% for the beams reinforced with GFRP bars. For the beams reinforced with AFRP bars, the reduction in crack width was 22% as a result of increasing 33% of reinforcement ratio.

3.4.4 Ductility and deformability

Ductility of reinforced concrete beams is the capacity of energy absorption through plastic deformation which is measured in conventional steel-RC beams by the ratio of deflection or curvature or rotation value at ultimate to yield. However, this interpretation is unavailable for FRP-RC beams because in the stress-strain relationship of FRP bars there is no yield point as it is linear until failure. The deformability factor (or J-factor) that has been introduced in Jaejer et al.[67] can be used to evaluate the deformability of concrete beams which are reinforced with FRP or steel bars. This factor is the ratio of product of moment and curvature at ultimate to the corresponding values of moment and curvature when the concrete compressive strain is equal to 0.001 as defined in Equation 3.6. The concrete compressive strain of 0.001 is chosen to demonstrate the linear stress-strain behaviour in concrete above the neutral axis during the post cracking stage to make comparisons with the ductility of steel-RC beams.

$$\begin{matrix} deformability \\ factor\ (J) \end{matrix} = \begin{matrix} moment \\ factor \end{matrix} x \begin{matrix} curvature \\ factor \end{matrix} \tag{3.6}$$

$$\begin{matrix} moment \\ factor \end{matrix} = \frac{Moment\ at\ ultimate}{Moment\ at\ \varepsilon_c = 0.001} \tag{3.7}$$

$$\begin{matrix} curvature \\ factor \end{matrix} = \frac{curvature\ at\ ultimate}{curvature\ at\ \varepsilon_c = 0.001} \tag{3.8}$$

In conventional steel-RC beams, flexural failure of a concrete beam is accompanied by a large deformation which is significant when the failure is due to yielding of the steel reinforcement in the tension region (under reinforced section). However, deformability reduces when the failure is due to crushing of the concrete in the tension region. Therefore, the design codes have generally recommended to design the flexural members as under reinforced or the reinforcement ratio should be smaller than the balanced reinforcement ratio. However, for FRP reinforced cross-sections under flexure load, it is recommended that the reinforcement ratio should be greater than the balanced reinforcement ratio to ensure that failure would be caused by crushing of concrete without rupture of the FRP bars.

Providing greater reinforcement ratios than the balanced reinforcement ratio sometimes is not applicable, especially in T-sections with wide flanges because the reinforcement area becomes very large and cannot be practically placed in the web of the sections. Therefore, it is better to consider the deformability factor rather than the balanced reinforcement ratio. Also, it has been experienced that both rectangular and T-section can have an acceptable value of deformability factor which is 4 for rectangular sections and 6 for T-sections[57].

Figure 3.13 has been prepared with the allowable value of strain in service in the GFRP bars equal to 2000 x 10^{-6} mm/mm. It can be observed that the deformability factor has almost constant and high value when the reinforcement ratio is much smaller than the balanced reinforcement ratio. Also, the deformability factor

decreases with the increase in reinforcement ratio and the decrease of concrete strength[57].

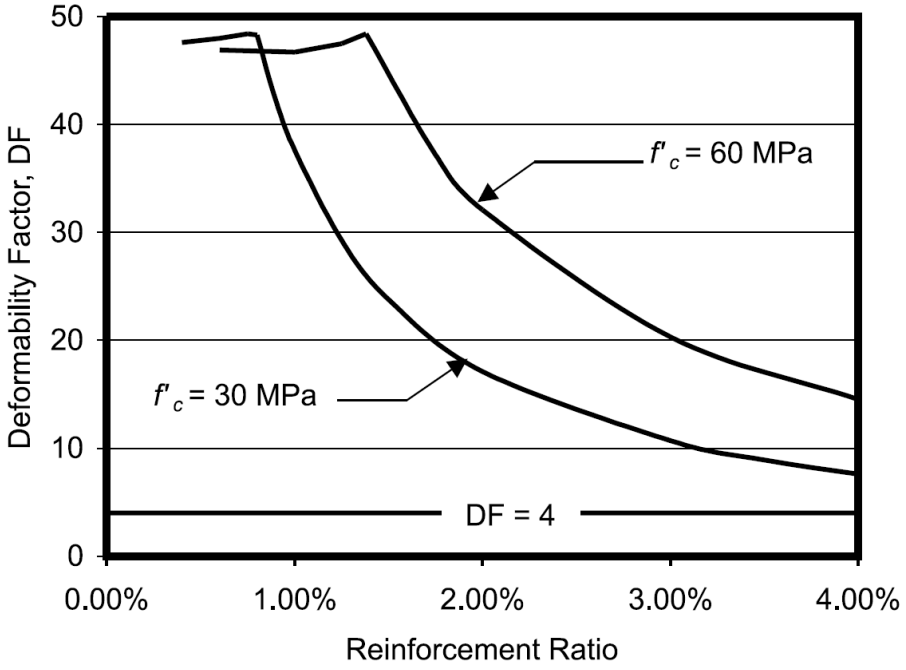

Figure 3.13 Deformability factor for GFRP reinforced section[57]

A detail study on the deformability factor of FRP-RC flexural members can be found in Chapter 5 of this study.

3.5 Summary

Despite the lower compressive strength and modulus of elasticity of FRP bars with respect to the steel bars, they can be used in reinforcing concrete columns, especially carbon and glass FRP bars. In order to have a comparable behaviour of FRP concrete columns to steel one, it should be reinforced with larger longitudinal and transversal

reinforcement ratios. However, the behaviour of circular concrete columns reinforced with GFRP bars and helices under eccentric loading has not been addressed. Therefore, studies about FRP reinforced circular concrete columns under different eccentric loading must be conducted to understand the behaviour of longitudinal and transversal reinforcement and their failure mode.

The next chapter explains the confinement of circular concrete columns. This confinement might be provided internally as steel or FRP helix or hoops, or externally by FRP sheet wrapping.

4 CONFINEMENT OF CONCRETE COLUMNS

4.1 Introduction

The main philosophy behind the confining of concrete columns is to prevent lateral expansion under the effect of Poisson's ratio. This technique can enhance the column's performance such as capacity and deformability because of the stress compatibility. However, the effect of confinement is more pronounced in improving the ductility and after peak stress deformability rather than load carrying capacity. Traditionally, the confinement is provided by using steel helices, hoops or ties which is named internal confinement. In addition, during the last century some different techniques such as steel plate or FRP wrapping had been introduced which is called external confinement. Therefore, this chapter focuses on the internal confinement with steel helices and hoops and external confinement with FRP sheets.

4.2 Internal confinement

Transverse reinforcement in concrete columns has two main duties which are holding the longitudinal reinforcement and confining the concrete columns against lateral expansion. Circular columns are generally confined by helices or hoops which confine an area (A_{core}) that is smaller than the gross concrete area (A_g) by providing concrete cover to protect the reinforcement from external environments and corrosion. Also, the confined concrete section has a diameter (d_c) which is equal to the centreline of the confining reinforcement and is smaller than the diameter of the column (h) as shown in Figure 4.1. The lateral expansion of the concrete column

triggers a tensile force in the transverse reinforcement that also makes a lateral pressure (f_l) on the concrete column.

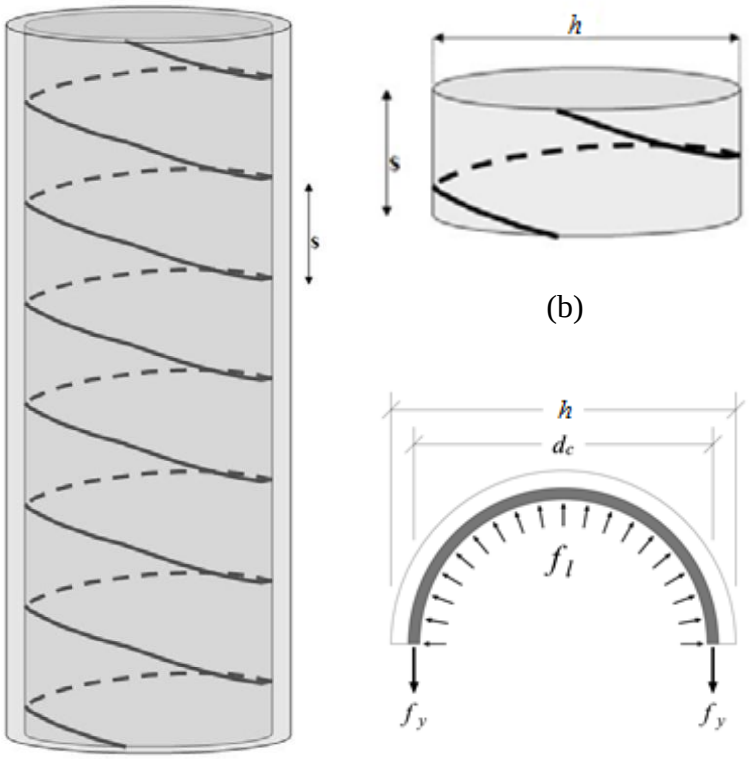

(a) (b) (c)

Figure 4.1 (a) Confinement of concrete core by steel helix; (b) An isolated part of pitch height; (c) Stresses action on half-loop

The f_l can be calculated by equilibrium of forces in Figure 4.1(c).

$$f_l \, d_c \, s = 2 \, A_s \, f_y \tag{4.1}$$

$$f_l = \frac{2 \, A_s \, f_y}{d_c \, s} \tag{4.2}$$

where s is the pitch or centre-to-centre spacing between two hoops, A_s is the area of the confining reinforcement and f_y is the yield tensile strength of the confining reinforcement. The volumetric ratio of transverse reinforcement (ρ_{st}) for an isolated pitch as shown in Figure 4.1 can be calculated (Equation 4.3) by dividing the volume of one cycle of helix or one hoop by the volume of confined concrete with diameter d_c and height s.

$$\rho_{st} = \frac{4\,A_s}{d_c\,s} \tag{4.3}$$

Therefore, from Equations 4.2 and 4.3 the lateral pressure (f_l) can be expressed only by ρ_{st} and f_y as in Equation 4.4.

$$f_l = \frac{1}{2}\,\rho_{st}\,f_y \tag{4.4}$$

Some different parameters such as volumetric ratio and spacing of lateral reinforcement, concrete strength of confined concrete and longitudinal reinforcement have different effects on the behaviour, capacity and deformability of the confined concrete as has been addressed in the following points depending on the previous literature.

4.2.1 Volumetric ratio of confinement steel

Generally, increasing lateral reinforcement ratio of a specific grade of steel increases the peak stress (f'_{cc}), the strain at peak stress (ε_{cc}), the fracture strain (ε_{cu}) and

ductility, and decreases the slope of the stress-strain relationship after peak stress[68]. Providing only 0.6% lateral confinement ratio could increase the strength and ductility of concrete columns[69] which is found by dividing the axial strain at the first helix rupture, or when the stress drops to 85% of the peak stress, by axial strain corresponding to the peak confined stress on the initial tangent to the stress-strain relationship, in comparison to the unconfined columns[70]. Also, it is reported that a circular concrete column with 2% lateral confinement ratio could gain 0.06 axial strain in the first hoop fracture, while the core concrete still sustained a stress in excess $0.85\ f_c'$ [69].

Sheikh and Toklucu[71] investigated 27 circular concrete columns with three different diameters which were confined with steel helices and hoops. They concluded that the effect of increasing the volumetric ratio of lateral confinement steel on ductility was much greater than on strength and that in some cases doubling the confinement ratio did not affect the strength by much. Also, they found that the optimum values of s/d_c (the ratio of helices spacing to confined concrete diameter) and ρ_{st} (volumetric ratio of lateral confinement) were about 0.24 and 1.2%, respectively. In addition, it is observed through testing 12 concrete columns with volumetric confinement ratio from 0.58% to 3.18% that concrete columns with higher confinement ratio could achieve a second peak stress which was greater than the spalling stress (first peak stress), while the specimens with lower confinement ratio could gain only a first peak stress[72]. However, when the volumetric ratio of lateral confinement in the concrete columns was reduced to 1%, the high-strength concrete columns behaved similar to unconfined concrete columns[73].

4.2.2 Strength of confinement steel

A concrete section that is confined with high-strength steel is possible to reduce its ductility due to premature fracture of the transverse steel and loss of effective confinement[69]. Zahn[74] tested six circular concrete columns reinforced with steel helices, and they revealed that the volumetric ratio of high-strength steel can be reduced without a reduction in the compressive strength of confined concrete columns, and the ductility of the confined columns will not reduce considerably. However, Razvi and Saatcioglu[75] revealed that high-strength steel was effective in confinement of the concrete core and the specimens confined with high-strength steel behaved in a ductile manner and sustained 1.2% of axial strain with little strength decay until the first hoop fracture depending on testing of 20 circular concrete columns that were confined with three different steel grades (400, 660 and 1000 MPa). Therefore, they concluded that the volumetric ratio of confinement could be decreased with increasing the yield strength of steel without adversely affecting the deformability of the confined concrete columns.

4.2.3 Spacing of lateral reinforcement

For a given volumetric ratio of confinement, it is better to use smaller diameter reinforcement with smaller spacing rather than greater diameter reinforcement with greater spacing[47, 48]. However, Mander et al.[69] revealed that increasing the lateral spacing from 36 mm to 93 mm did not significantly influence the peak stress and ultimate strain.

Sheikh and Toklucu[71] reported that the reduction in helix spacing resulted in an improvement in confinement and higher concrete stress after an initial drop due to cover spalling. They also recommended determining the helix spacing based on s/d_c ratio for confinement instead of an absolute limit and s/d_b (the ratio of helix spacing to the bar diameter) for buckling of the longitudinal bars.

Pessiki and Pieroni[70] observed that decreasing the size and pitch of the helix reinforcement within a constant volumetric ratio of confinement resulted in a decrease of the ductility of the concrete columns because of the differences in the strain capacity on different sizes of the helix reinforcement that had been used. Also, close spacing of the helices leads to forming a mesh of reinforcement with longitudinal reinforcement and produces a natural plane of separation between the concrete cover and the core which makes cover spalling due to instability rather than crushing[75].

Bing et al.[73] tested 40 circular and square concrete columns with 20 to 70 mm in the lateral reinforcement spacing. They observed that increasing the hoop spacing detrimentally affected the behaviour of confined concrete columns and each of ductility, strength enhancement and longitudinal strain at the first hoop fracture were decreased. Therefore, they recommended that the maximum pitch should not be greater than $5d_b$ to achieve satisfactory behaviour.

4.2.4 Longitudinal reinforcement

The presence of longitudinal reinforcement could improve the confinement mechanism, strength and ductility of the concrete columns[75]. Pessiki and Pieroni[70] investigated eight circular concrete columns that were reinforced longitudinally with 1.65% (8 No. 8) and 4.2% (16 No. 9) steel reinforcement ratios and transversally with steel helices. They figured out that the concrete columns with 8 No. 8 longitudinal bars displayed more ductility than those with 16 No. 9 longitudinal bars. This may be because the longitudinal bars set a greater stress on the helices reinforcement, as the helix reinforcement fractured directly over the longitudinal bars in the tested specimens. However, the specimens with 16 No. 9 longitudinal bars could attain higher peak stresses than those with 8 No. 8 longitudinal bars.

Bing et al.[73] reported that the longitudinal reinforcement cannot affect the behaviour of confined concrete columns as increasing of the volumetric ratio or decreasing of the spacing of transverse reinforcement can do. However, the distribution of longitudinal reinforcement for a given amount of reinforcement is important for confinement effectiveness. Also, they suggested to provide at least eight longitudinal bars to be distributed along the perimeter of the concrete columns.

4.2.5 Concrete strength

It is clear that normal-strength plain concrete is more ductile than high-strength plain concrete, therefore it is reasonable that more confinement is needed for high-strength concrete to obtain a comparable deformability with normal strength concrete[68].

Pessiki and Pieroni[70] studied eight circular concrete columns that were reinforced transversally with steel helices and cast with low, medium and high strength concrete which were 37.9, 51.9 and 84.7 MPa, respectively. They pointed out that the higher strength concrete columns experienced lesser ductility than the lower strength concrete columns. Therefore, they suggested the minimum helix reinforcement that is limited by ACI 318-89[76] should be increased for high-strength concrete to gain the same ductility as low strength-concrete. They also observed that the confined concrete columns with low concrete strength (37.9 MPa) failed by helix fracture, while the medium (51.9 MPa) and high-strength (84.7 MPa) concrete strength specimens failed by the formation of an inclined failure plane developed in the columns.

Razvi and Saatcioglu[75] investigated 20 circular concrete columns with three different concrete strengths (60, 92 and 124 MPa) and the specimens were confined with steel helices. They reported that development of vertical surface cracks in the concrete cover was affected by concrete strength. In 124 MPa concrete, cracks appeared in 0.15% to 0.30% of axial strain, in 92 MPa concrete, they appeared in 0.17% to 0.25% of axial strain and in 60 MPa concrete, they appeared in 0.20% to 0.41% of axial strain. In addition, they concluded that the strength enhancement ratio (f'_{cc}/f'_{co}) for 60 MPa concrete was greater than for 92 and 124 MPa concrete. Also, Bing et al.[73] tested 40 circular and square concrete columns with four different concrete strengths from 35.2 to 82.5 MPa. They indicated that the lateral confinement was less effective with higher concrete strength because the lateral dilation of high-strength concrete is smaller than normal-strength concrete. Also, with the same volumetric

confinement ratio (2.86%), the strength enhancement ratio was about 2.04, 1.57 and 1.28 for low, medium and high concrete strength, respectively.

4.3 Stress-strain relationship for internally confined circular concrete columns

From the reviewing of the literature it was shown that internal confinement can positively change the behaviour of the concrete columns. This means the capacity and stress-strain relationship of confined concrete is different than unconfined concrete. The confined concrete has higher capacity and is more ductile, or undergoes a larger deformation until failure. Therefore, for modelling the stress-strain relationship and computing the strength and strain enhancement of confined concrete, different authors have investigated confined concrete with different parameters and they have introduced models to propose the stress-strain curve of confined concrete. Some models have been presented in this part for circular-cross section concrete columns that are laterally confined with steel helices or hoops.

The model of Richart et al.[77] was the first attempt to define the effect of lateral confinement on the compressive strength of confined concrete members. They introduced Equation 4.5 to estimate the confined compressive strength of concrete columns.

$$f'_{cc} = f'_{co} + k_1 f_l \tag{4.5}$$

The value of k_1 was found from experimental results of testing a series of concrete cylinders, 250 mm in diameter and 1000 mm in height, and it came out to be 4.1.

The confined strain (ε_{cc}) corresponding to the confined maximum strength (f_{cc}) is obtained by Equation 4.6.

$$\varepsilon_{cc} = \left[1 + k_2 \left(\frac{f_l}{f'_{co}}\right)\right] \varepsilon_{co} \tag{4.6}$$

$$k_2 = 5\, k_1 \tag{4.7}$$

where ε_{co} is the strain corresponding to f_{co} and k_2 is the strain coefficient of the effective lateral confinement pressure.

Ahmad and Shah[78] developed a model for confinement based on testing eight series of normal and light weight concrete cylinders (75 x 300 mm and 75 x 150 mm) without longitudinal reinforcement and cover with different pitch and yield strength of the helices. They suggested the ultimate confined strength and corresponding strain as in Equations 4.8 and 4.9.

$$f'_{cc} = f'_{co} + k_1\, f'_l \tag{4.8}$$

$$\varepsilon_{cc} = \varepsilon_{co} + k_2\, f'_l \tag{4.9}$$

$$f'_l = k_e\, f_l \tag{4.10}$$

$$k_e = 1 - \sqrt{\frac{s}{1.25\, d_c}} \tag{4.11}$$

$$k_1 = \frac{6.6}{\sqrt{f_{co}}} (f_l')^{0.04} \quad (4.12)$$

$$k_2 = \frac{0.047}{(f_{co})^{1.2}} (f_l')^{0.19} \quad (4.13)$$

They adapted a model by Sargin et al.[79]; counting on the octahedral failure theory, the three stress invariants and the experimental results:

$$Y = \frac{AX + (B-1)X^2}{1 + (A-2)X + BX^2} \quad (4.14)$$

$$Y = \frac{f_{co}}{f_{cc}} \quad (4.15)$$

$$X = \frac{\varepsilon_{co}}{\varepsilon_{cc}} \quad (4.16)$$

$$A = \frac{E_c}{E_{sec}} \quad (4.17)$$

where *B* is a parameter that governs the descending branch. They also observed that when spacing of the helices was greater than 1.25 times the diameter of confined concrete (d_c), the effect of confinement was negligible.

Martinez et al.[80] deduced a model for confinement by studying 78 normal and light weight concrete columns without longitudinal reinforcement and cover. The columns were different in dimensions, 100 x 200 mm, 100 x 400 mm and 125 x 600 mm in

diameter and height, respectively. They used different concrete strength and tensile yield strength of the steel helices to construct the specimens.

Martinez et al.[80] concluded Equation 4.18 to find the strength of confined normal weight concrete.

$$f'_{cc} = f'_{co} + 4\, k_e\, f_l \tag{4.18}$$

$$k_e = 1 - \frac{s}{d_c} \tag{4.19}$$

They concluded that the modulus of elasticity of helically confined and unconfined concrete columns are almost equal.

Fafitis and Shah[81] proposed that maximum capacity could be achieved when the concrete cover starts spalling. Their experimental program consisted of four concrete columns that were cast with different concrete strength and equal longitudinal reinforcement. They also had different lateral reinforcement ratios. The authors proposed two equations for the ascending and descending parts of the stress-stain curve as Equations 4.20 and 4.21, respectively.

$$f_c = f'_{cc}\left[1 - \left(1 - \frac{\varepsilon_c}{\varepsilon_{cc}}\right)^A\right] \qquad 0 \le \varepsilon_c \le \varepsilon_{cc} \tag{4.20}$$

$$f_c = f'_{cc}\, exp[-k(\varepsilon_c - \varepsilon_{cc})^{1.15}] \qquad \varepsilon_{cc} \le \varepsilon_c \tag{4.21}$$

$$A = \frac{E_c\, \varepsilon_{cc}}{f'_{cc}} \tag{4.22}$$

$$k = 0.17\, f'_{cc}\, exp(-0.01\, f_l) \tag{4.23}$$

Also, they found f'_{cc} and ε_{cc} by Equations 4.24 and 4.25, respectively.

$$f'_{cc} = f'_{co} + \left(1.15 + \frac{3048}{f_{co}}\right) f_l \tag{4.24}$$

$$\varepsilon_{cc} = 1.027\, x\, 10^{-7}\, f'_{co} + 0.0296\, \frac{f_l}{f'_{co}} + 0.00195 \tag{4.25}$$

Mander et al.[82] developed a new confinement model (Figure 4.2) based on an equation suggested by Popovics[22] as in Equation 4.26.

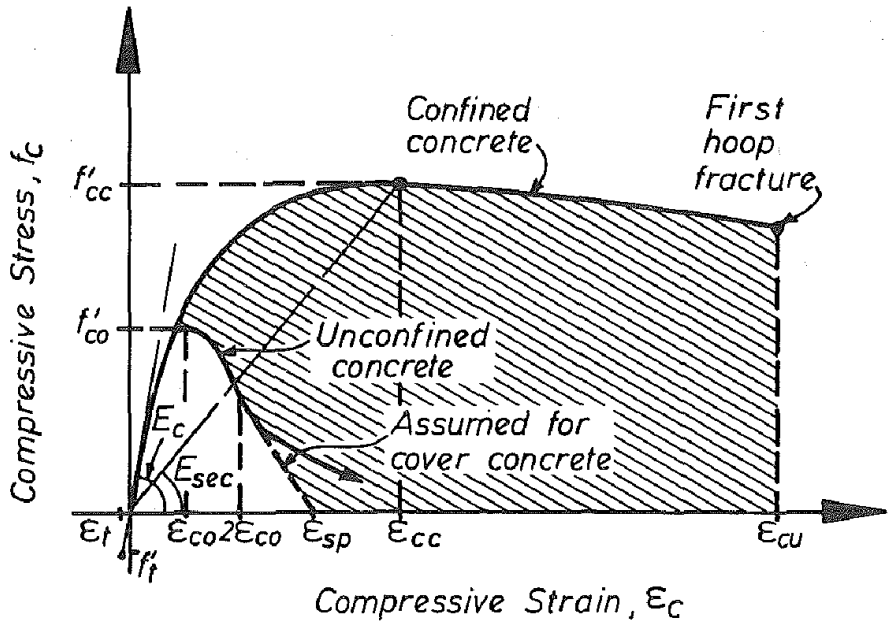

Figure 4.2 Stress-strain model proposed for confined and unconfined concrete by Mander et al.[82]

$$f_c = \frac{f'_{cc}\, x\, r}{r - 1 + x^r} \tag{4.26}$$

$$x = \frac{\varepsilon_c}{\varepsilon_{cc}} \tag{4.27}$$

$$r = \frac{E_c}{E_c - E_{sec}} \tag{4.28}$$

Also, the f'_{cc} and ε_{cc} could be expressed as Equations 4.29 and 4.30, respectively.

$$f'_{cc} = f'_{co}\left(-1.254 + 2.254\sqrt{1 + \frac{7.94\, f'_l}{f'_{co}}} - 2\,\frac{f'_l}{f'_{co}}\right) \tag{4.29}$$

$$\varepsilon_{cc} = \varepsilon_{co}\left[1 + 5\left(\frac{f'_{cc}}{f'_{co}} - 1\right)\right] \tag{4.30}$$

$$f'_l = k_e\, f_l \tag{4.31}$$

where for circular cross-section with helices or hoops lateral reinforcement the k_e can be found by Equations 4.32 or 4.33, respectively.

$$k_e = \frac{1 - \frac{s'}{2\, d_c}}{1 - \rho_{cc}} \tag{4.32}$$

$$k_e = \frac{\left(1 - \frac{s'}{2\, d_c}\right)^2}{1 - \rho_{cc}} \tag{4.33}$$

The model that has been introduced by Saatcioglu and Razvi[83] for confinement (Figure 4.3) adopted a variable ratio for the effect of lateral pressure on the capacity

of the confined concrete. The value of (k_1) in Equation 4.34 has an inverse relation with the lateral pressure (Equation 4.35) based on the experimental data of Richart et al.[77].

$$f'_{cc} = f'_{co} + k_1 f_l \tag{4.34}$$

$$k_1 = 6.7\,(f_l)^{-0.17} \tag{4.35}$$

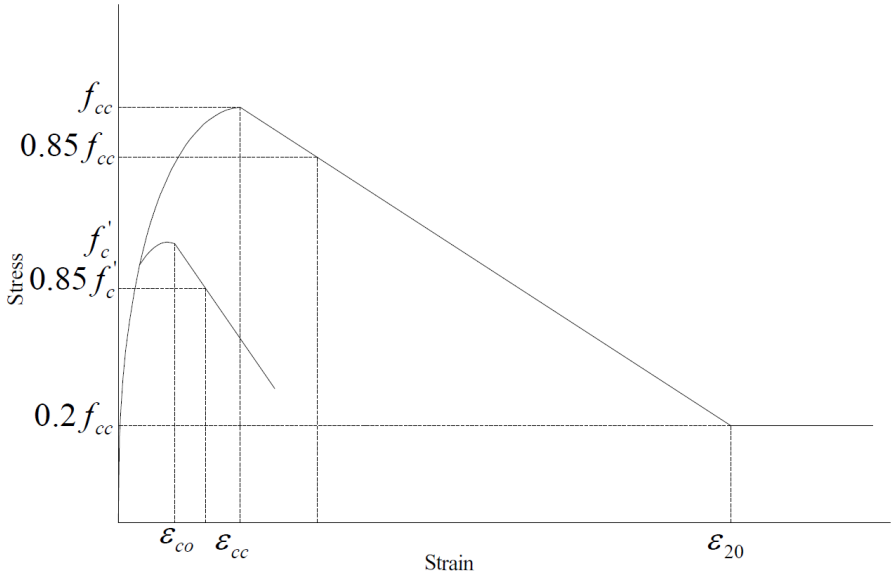

Figure 4.3 Proposed stress-strain relationship by Saatcioglu and Razvi[83]

Also, they expressed the stress-strain relationship as in Equation 4.36.

$$f_c = f'_{cc}\left[2\left(\frac{\varepsilon_c}{\varepsilon_{cc}}\right) - \left(\frac{\varepsilon_c}{\varepsilon_{cc}}\right)^2\right]^{1/(1+2\,K)} \tag{4.36}$$

$$\varepsilon_{cc} = \varepsilon_{co}\,(1 + 5\,K) \tag{4.37}$$

$$K = \frac{k_1 f_l}{f'_{co}} \tag{4.38}$$

El-dash and Ahmad[84] concluded that the diameter and yield strength of the helix reinforcement, the volumetric ratio of confining reinforcement, the dimension of the columns and the pitch of the helices manipulate the stress-strain relationship of confined concrete. Through using the model that had been introduced by Sargin et al.[79], they proposed a model for the stress-strain relationship of confined normal and high strength concrete. Also, they deduced a new equation to find the peak strength of confined concrete.

$$Y = \frac{AX + (B-1)X^2}{1 + (A-2)X + BX^2} \tag{4.39}$$

$$Y = \frac{f_c}{f'_{cc}} \tag{4.40}$$

$$X = \frac{\varepsilon_c}{\varepsilon_{cc}} \tag{4.41}$$

$$f'_{cc} = f'_{co} + k_1 f'_l \tag{4.42}$$

$$\varepsilon_{cc} = \varepsilon_{co} + k_2 \frac{f'_l}{f'_{co}} \tag{4.43}$$

$$f'_l = k_e f_l \tag{4.44}$$

$$k_e = 1 - \sqrt{\frac{s}{1.25\, d_c}} \tag{4.45}$$

Also, The values of *A*, *B*, k_1 and k_2 are defined by the following equations:

$$A = \frac{E_c}{E_{sec}} \tag{4.46}$$

$$B = \frac{16.5}{\sqrt{f_c'}} \left(\frac{f_l'}{s/d_b} \right)^{0.33} \quad (4.46)$$

$$k_1 = 5.1 \left(\frac{f_{co}}{f_y} \right)^{0.5} \left(\frac{d_b}{\rho_{st}} \right)^{0.25} \quad (4.47)$$

$$k_2 = \frac{66}{\left(s/d_b \right) (f_{co})^{1.7}} \quad (4.48)$$

Assa et al.[85] studied the confinement effect on 24 concrete cylinders (145 x 300 mm) under monotonic axial load. The cylinders were cast with different concrete strength from 20 to 90 MPa and reinforced transversally with helix or hoop steel reinforcement without cover. Based on their experimental results, they suggested Equation 4.49 to predict the ultimate confined concrete strength.

$$f_{cc}' = f_{co}' + 3.36\, f_l \quad (4.49)$$

$$\varepsilon_{cc} = \varepsilon_{co} \left(1 + 21.5 \frac{f_l}{f_{co}'} \right) \quad (4.50)$$

$$\varepsilon_{80} = \varepsilon_{co} \left(2.74 + 32.84 \frac{f_l}{f_{co}'} \right) \quad (4.51)$$

$$\varepsilon_l = 0.0021 + 0.016 \frac{f_l}{f_{co}} \quad (4.52)$$

They also proposed stress-strain relationship by Equation 4,53.

$$Y = \frac{AX + (B-1)X^2}{1 + (A-2)X + BX^2} \quad (4.53)$$

$$Y = \frac{f_c}{f'_{cc}} \tag{4.54}$$

$$X = \frac{\varepsilon_c}{\varepsilon_{cc}} \tag{4.55}$$

$$A = \frac{E_c}{E_{sec}} \tag{4.56}$$

$$B = \frac{\left(\frac{\varepsilon_{80}}{\varepsilon_{cc}}\right)^2 - (0.2\,A + 1.6)\,\frac{\varepsilon_{80}}{\varepsilon_{cc}} + 0.8}{0.2\,\left(\frac{\varepsilon_{80}}{\varepsilon_{cc}}\right)^2} \tag{4.57}$$

Recently, Karim et al.[86] proposed two equations to compute the ultimate confined concrete strength and strain based on reviewing about 150 experimental data.

$$f'_{cc} = k_c\, f'_{co} \tag{4.58}$$

$$\varepsilon_{cc} = {k_c}^2\, \varepsilon_{co} \tag{4.59}$$

$$k_c = \frac{f'_{co} + 5\, f_l}{f'_{co} + 0.5\, f_l} \tag{4.60}$$

Karim et al.[86] also proposed minimum lateral reinforcement ratio (Equation 4.61) to have the load carrying capacity of the confined concrete core comparable to the load carrying capacity to the gross concrete cross-section (concrete core and cover)

$$\rho_{st} = 3.4\left(\frac{A_g - A_{core}}{10\,A_{core} - A_g}\right)\left(\frac{f'_c}{f_y}\right) \tag{4.61}$$

4.4 External confinement by FRP

External confinement of concrete columns consists of confining the external circumference of the columns by a material that can resist tensile strength such as steel plates or FRP sheets. The confinement can be provided as strips or whole wrapping of the columns. For passive confinement by FRP, the confinement is produced as a result of lateral expansion of the concrete columns under compression loading that generate tension stresses in the hoop direction of the FRP. This tension stress becomes a lateral pressure (f_l) that is proportional to the axial pressure on the concrete columns until the failure of the column and ruptures of the FRP and makes the confined columns stronger and more ductile.

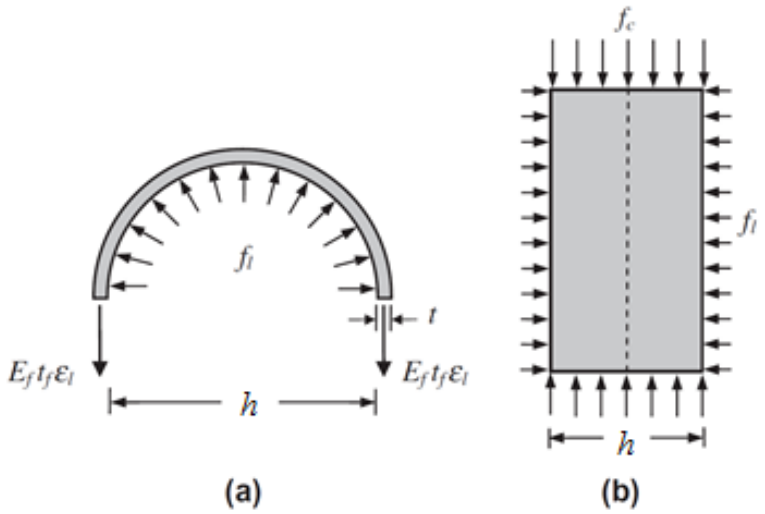

Figure 4.4. Confining action of FRP on concrete core: (a) FRP; (b) concrete core[87]

In the FRP confined circular cross-sections, the lateral FRP confining pressure is assumed to be uniformly distributed around the circumference of the concrete cross-section as shown in Figure 4.4. The ultimate lateral confining pressure (f_l) that is

produced by an FRP shell on the concrete can be determined theoretically based on the deformation compatibility between the confining FRP shell and the concrete surface from Equation 4.59. Also, it can be observed from the previous studies that the ultimate tensile strain that has been achieved for the FRP shell at the time of FRP hoop rupture $(\varepsilon_{h,rup})$ is lower than the ultimate tensile strain (ε_f) of the FRP sheet that is measured from coupon test[88-92]. To estimate the actual relationship between the hoop rupture strain and the ultimate tensile strain, Pessiki et al.[88] introduced the strain reduction factor (k_ε) to account for the premature failure of the FRP confining system as in Equation 4.60. Therefore, the actual confining pressure $(f_{l,a})$ defined in Lam and Teng[89] can be displayed as Equation 4.61.

$$f_l = \frac{2\, E_f\, t_f\, \varepsilon_f}{D} \tag{4.59}$$

$$\varepsilon_{h,rup} = k_\varepsilon\, \varepsilon_f \tag{4.60}$$

$$f_{l,a} = \frac{2\, E_f\, t_f\, \varepsilon_{h,rup}}{D} \tag{4.61}$$

The FRP strain reduction factor (k_ε) has been studied experimentally by many authors. Based on the experimental studies, Lam and Teng[89] computed an average value of 0.586 for k_ε and Carey and Harries[93] counted average value of 0.58, 0.57 and 0.61 for small, medium and large scale circular concrete columns, respectively. Also, the value of 0.55 for k_ε has been suggested in ACI 440.2R-08[94], depending on the previous studies. In addition, Ozbakkaloglu et al.[92] based on a database of over 250 data sets determined an average value of 0.685 for the FRP strain reduction

factor (k_ε). However, it can be seen from the databases by Lim and Ozbakkaloglu[95] and Ozbakkaloglu and Lim[87] that the value of (k_ε) varies with changing the compressive strength of the confined concrete (f'_c) and the elastic modulus of confining FRP materials (E_f) rather than having a constant value. The recorded hoop rupture strain $(\varepsilon_{h,rup})$ from the previous experimental studies has been reduced with increasing each of concrete strength and modulus of elasticity of the FRP materials. Therefore, Ozbakkaloglu and Lim[87] introduced Equation 4.62 to reasonably predict the value of the FRP strain reduction factor.

$$k_\varepsilon = 0.9 - 2.3\, f'_{co}\, x\, 10^{-3} - 0.75\, E_f\, x\, 10^{-6} \tag{4.62}$$

Where f'_{co} and E_f are in MPa

Different types of FRP confining materials such as CFRP and GFRP have different impacts on confined concrete columns. In general, the previous studies[96-103] show that for a given lateral confining pressure to unconfined concrete compressive strength $(f_{l,a}/f_{co})$, the enhancement of confined compressive strength to unconfined compressive strength (f'_{cc}/f'_{co}) is not considerably affected, while the ultimate compressive strain of confined concrete (ε_{cu}) is much more sensitive to the properties of confining FRP materials. The value of ultimate confined compressive strain (ε_{cu}) increases with the increase of the ultimate tensile strain of FRP confining materials.

4.5 Stress- strain relationship for externally FRP confined circular concrete columns

Providing external FRP confinement for concrete columns changes the stress-strain relationship of the confined concrete in comparison with unconfined concrete as well as its ultimate compressive strength and strain. In general, it can be represented in a bilinear stress-strain curve[104] where the first ascending part represents the unconfined concrete behaviour and the second ascending part represents the activation and behaviours of FRP passive confinement. This bilinear curve has a transition point that is named the first peak $(f'_{c1}, \varepsilon_{co})$ which is equal to or somehow greater than the compressive strength of unconfined concrete $(f'_{co}, \varepsilon_{co})$ and a final point $(f'_{cc}, \varepsilon_{cu})$ at the ultimate condition, as shown in Figure 4.5.

The typical bilinear stress-strain relationship of FRP confined concrete has been modelled by many authors with different types of curves. Karbhari and Gao[96] and Xiao and Wu[104] used two straight lines to represent the relationship as shown in Figure 4.5(a). This model is simple and cannot represent the actual stress-strain relationship of FRP confined concrete. Figure 4.5(b) shows another type of proposed models for FRP confined concrete behaviour by different authors[105, 106] that used the Hognestad[107] parabola to model the first ascending part of the relationship and for the second part a straight line was used to connect the first peak point to the ultimate point $(f'_{cc}, \varepsilon_{cu})$ in the stress-strain curve.

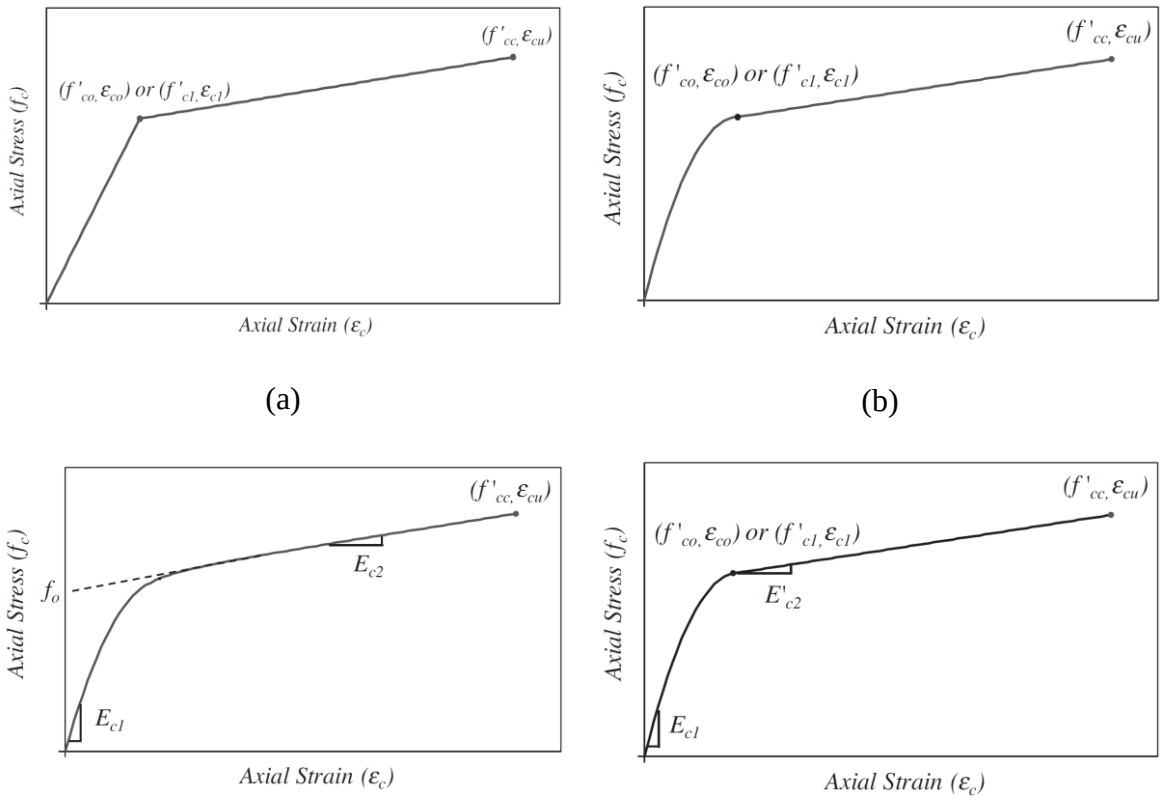

Figure 4.5. Different shapes of proposed stress-strain relationship for FRP confined concrete columns[92]

Another type of model used by different authors[89, 108-110] is based on the four parameter curve by Richard and Abbott[111]. The first part of the bilinear stress-strain curve is named the elastic portion of the first ascending branch (E_1), and the post peak second branch (E_2) follows, as shown in Figure 4.5(c). This model is represented by a single equation where a curve-shape parameter (n) controls the transition from the first portion to the second portion. Also, the modulus of elasticity of concrete $\left(E_c = 4730\sqrt{f_c'}\right)$ given by ACI 318-14[40], has been used by most of the proposed models to determine the slope of the first ascending part (E_1). Figure 4.5(d)

shows another type of proposed model for FRP confined concrete which is based on the modified model of Sargin et al.[79] by Toutanji[112]. In this model, the first part which has a slope of (E_1) is connected with the second part which has a slope of (E_2) at the first peak point (f_c', ε_{c1}) to the ultimate point $(f_{cc}', \varepsilon_{cu})$ by a straight line in the stress-strain relationship. Table 4.1 reports some of the proposed stress-strain models for the confined concrete by FRP.

The most familiar stress-strain models that have been used for confined concrete in literature are Samaan et al.[108] and Lam and Teng[89]. In the Samaan et al.[108] model, the whole stress-strain curve are represented by one equation as:

$$f_c = \frac{(E_{c1} - E_{c2})\varepsilon_c}{\left[1 + \left(\frac{E_{c1} - E_{c2}}{f_o}\varepsilon_c\right)^n\right]^{1/n}} + E_{c2}\,\varepsilon_c \tag{4.62}$$

$$E_2 = \frac{f_{cc}' - f_o}{\varepsilon_{cc}} \tag{4.63}$$

$$f_o = 0.872\,f_c' + 0.371\,f_l + 6.258 \tag{4.64}$$

$$n = 1 + \frac{1}{E_{c1}/E_{c2} - 1} \tag{4.65}$$

where f_o is the intercept of the second ascending part with the stress axis.

In Lam and Teng[89] model, the first portion is represented by a parabolic curve which connects smoothly to the linear second portion.

$$f_c = E_{c1}\,\varepsilon_c - \frac{(E_{c1} - E_{c2})^2}{4\,f_{co}'}\varepsilon_c{}^2 \quad \text{for} \quad \varepsilon_c < \varepsilon_t \tag{4.66}$$

$$f_c = f_{co}' + E_{c2}\,\varepsilon_c \quad \text{for} \quad \varepsilon_t \le \varepsilon_c \le \varepsilon_{cc} \tag{4.67}$$

$$\varepsilon_t = \frac{2\,f_{co}'}{E_{c1} - E_{c2}} \tag{4.68}$$

$$E_{c2} = \frac{f'_{cc} - f'_{co}}{\varepsilon_{cc}} \tag{4.69}$$

Many authors proposed equations for the ultimate confined axial strength (f'_{cc}) and corresponding axial strain (ε_{cc}) for concrete confined by FRP. Table 4.1 reports a number of empirical equations for f'_{cc} and ε_{cc} that have been proposed based on experimental results. It can be noticed that there is a linear relationship between the confined concrete strength and the lateral pressure (f_l) in almost all of the proposed equations in Table 4.1.

Table 4.1. Proposed equation to estimated ultimate confined concrete strength and corresponding strain

Authors	Strength	Strain
Samaan et al.[108]	$f'_{cc} = f'_{co} + 6\, f_l^{0.7}$	$\varepsilon_{cc} = \frac{f'_{cc} - f_o}{E_{c2}}$
Saafi et al.[113]	$f'_{cc} = f'_{co} + k_1\, f_l$ $k_1 = 2.2\left(\frac{f_l}{f'_{co}}\right)^{-0.16}$	$\frac{\varepsilon_{cc}}{\varepsilon_{co}} = 1 + k_2\left(\frac{f'_{cc}}{f'_{co}} - 1\right)$ $k_2 = 573\varepsilon_{lu} + 2.6$
Spoelstra and Monti[114]	$f'_{cc} = f'_{co}\left(0.2 + 3\sqrt{f_l}\right)$	$\frac{\varepsilon_{cc}}{\varepsilon_{co}} = 2 + 1.25E_c\varepsilon_{lu}\sqrt{f_l}$
Toutanji[112]	$f'_{cc} = f'_{co} + k_1\, f_l$ $k_1 = 3.5\left(\frac{f_l}{f'_{co}}\right)^{-0.15}$	$\frac{\varepsilon_{cc}}{\varepsilon_{co}} = 1 + k_2\left(\frac{f'_{cc}}{f'_{co}} - 1\right)$ $k_2 = 310.57\varepsilon_{lu} + 1.9$
Thériault and Neale[115]	$f'_{cc} = f'_{co} + 2\, f_l$	NA

Table 4.1. (Continued)

Lin and Chen[97]	$f'_{cc} = f'_{co} + 2\,f_l$	NA
Lam and Teng[116]	$f'_{cc} = f'_{co} + 2\,f_l$	NA
Shehata et al.[117]	$f'_{cc} = f'_{co} + 2\,f_l$	$\frac{\varepsilon_{cc}}{\varepsilon_{co}} = 1 + 632\left(\frac{f_l}{f'_{co}}\frac{f'_{cc}}{E_f}\right)^{0.5}$
Lam and Teng[89]	$f'_{cc} = f'_{co} + 3.3\,f_l$	$\frac{\varepsilon_{cc}}{\varepsilon_{co}} = 1.75 + 12\left(\frac{f_l}{f'_{co}}\right)\left(\frac{\varepsilon_{h,rup}}{\varepsilon_{co}}\right)^{0.45}$
Saiidi et al.[118]	$f'_{cc} = f'_{co} + 6.2\,f_l^{0.7}$	$\varepsilon_{cc} = \frac{\varepsilon_{h,rup}}{0.1 - 0.25\ln\left(\frac{f_l}{f'_{co}}\right)}$
Matthys et al.[119]	$\frac{f'_{cc}}{f'_{co}} = 1 + 3.5\left(\frac{f_l}{f'_{co}}\right)^{0.85}$	$\frac{\varepsilon_{cc}}{\varepsilon_{co}} = 1 + k_2\left(\frac{f'_{cc}}{f'_{co}} - 1\right)$ $k_2 = 310.57\varepsilon_{lu} + 1.9$
Wu and Wang[120]	$\frac{f'_{cc}}{f'_{co}} = 1 + 2.23\left(\frac{f_l}{f'_{co}}\right)^{0.96}$	NA
Wu et al.[121]	$f'_{cc} = f'_{co} + 3.2\,f_l$	$\frac{\varepsilon_{cc}}{\varepsilon_{co}} = 1 + 9.5\left(\frac{f_l}{f'_{co}}\right)$
Benzaid et al.[122]	$f'_{cc} = f'_{co} + 2.2\,f_l$	$\frac{\varepsilon_{cc}}{\varepsilon_{co}} = 2 + 7.6\left(\frac{f_l}{f'_{co}}\right)$

4.6 Summary

It is shown that confinement can improve the behaviour of concrete columns in the way of obtaining higher capacity and deformability before failure. However, the internally confined concrete columns by steel helices have lower improvements in comparison with externally confined concrete columns by FRP wrapping. This is

because internal confinement only has a considerable impact on the ductility, while in external confinement; the second peak load is greater than the first peak load. Despite having a limited study about FRP confinement helices for concrete columns, its effectiveness and compatibility have not been studied. Also, it is expected that the existing models cannot accurately predict the stress-strain relationship of concrete columns confined with FRP helices because FRP bars have higher tensile strength with smaller modulus of elasticity and FRP bars do not have yielding point like steel bars. In addition, the impact of external FRP confinement could not be known because there is no study about such area. Therefore, it is needed to introduce a model that can predict the stress-strain relationship and peak capacity for concrete columns confined with FRP helices.

The following chapter is a detailed study on the FRP reinforcement limitation for FRP-RC flexural members. The minimum FRP reinforcement ratio can be selected either to prevent rupture of FRP bars or to control the crack width. The limiting maximum reinforcement ratio takes into account the deformability of the FRP-RC members.

5 REINFORCEMENT LIMITATION FOR FRP-RC MEMBERS

5.1 Introduction

This chapter consists of an extensive study to limit the minimum and maximum FRP reinforcement ratio for FRP-RC flexural members. The minimum FRP reinforcement ratio is limited to prevent the brittle tensile rupture of FRP bars or to control the crack-width in the tension region. Also, the maximum FRP reinforcement ratio is limited to ensure a considerable deformation before complete failure of FRP-RC members.

5.2 Overview

Fibre Reinforced Polymer (FRP) is a composite material which has been used for many decades in the aerospace, automotive and recreational product industries, while they have been used in the construction industries only over the last two to three decades. FRP is advantageous for the construction of new structures and upgrading or retrofitting existing structures[10]. Extensive research was conducted in the 1990s on the behaviour of concrete beams and slabs reinforced with various types of FRP bars[11, 12, 58] and further research is still ongoing. Also, few experimental studies were conducted on the behaviour of concrete columns reinforced with FRP bars under concentric loads[44, 45, 47]. Recently, Sonobe et al.[14], CAN/CSA S806-12[15] and ACI 440.1R-15[13] introduced design guidelines for concrete members reinforced with FRP bars.

The traditional design philosophy for steel-RC members should be changed for concrete members reinforced with FRP bars because FRP bars have different mechanical properties than steel reinforcing bars[13, 16]. For instance, the stress-strain behaviour of FRP bars does not have a yield point and is linearly elastic until failure[53]. In addition, FRP bars consist of anisotropic materials and characterised by high tensile strength only in the direction of the fibres[31, 33]. Consequently, the failure mode of flexural concrete members reinforced with FRP bars should be changed to crushing of concrete in the compression side rather than failure of FRP bars in the tension side. This is particularly because tensile rupture of FRP bars is sudden and catastrophic. Also, large crack-widths and deflection cannot be observed. However, for failure in the crushing of concrete, FRP-RC members undergo larger deformation followed by rupture of the FRP bars[17].

In general, three types of failure modes were indicated in the literature for FRP-RC members: (i) brittle tension failure of FRP bars in the tension side; (ii) compression failure of concrete in the compression side; and (iii) premature compression failure of FRP bars in the compression side[53]. A set of equations were recommended in Choo et al.[56] to calculate minimum FRP reinforcement ratio for rectangular columns under pure bending to prevent the tensile failure of FRP bars in the tension side. However, RC columns are usually subjected to the combination of axial load and bending moment. Also, the axial load influences considerably in the reduction of the amount of FRP reinforcement to prevent tension failure. In addition, ACI 440.1R-15[13] proposed an equation to calculate the balanced FRP reinforcement ratio (when extreme concrete fibre in the compression side and FRP bars in the tension side reach

the ultimate strain simultaneously) for FRP-RC beams. The proposed equation in ACI 440.1R-15[13] can be used to limit the minimum FRP reinforcement ratio to prevent rupture of FRP bars in the tension side. However, this equation is only applicable for a single layer of FRP reinforcement. The increase in the number of layers of the FRP bars in the tension side should increase the limit of the minimum FRP reinforcement. As the stress-strain behaviour of FRP bars is linearly elastic until failure, the strain in the first layer of FRP bars in the tension side should be considered in the design calculation. Also, the maximum tensile strain is attained first in the first layer of the FRP bars in the tension side.

One of the common and preferable failure modes of FRP-RC members is the compression failure of concrete in the compression side. Previous studies reported that compression failure of concrete in the compression side was accompanied by a large deformation before complete failure of the FRP-RC members[17]. Jaejer et al.[67] introduced the Deformability Factor (DF) to measure the deformability of FRP-RC flexural members failed due to crushing of concrete in the compression side. The DF is a ratio of the product of moment and curvature at ultimate to the product of moment and curvature at serviceability limit state. Jaejer et al.[67] recommended that FRP-RC members should have a DF not less than 6. However, the CAN/CSA S6-06[123] limited the DF for FRP-RC members to a minimum of 4 and 6 for rectangular and T cross-section, respectively. Newhook et al.[57] evaluated the DF of rectangular and T cross-section flexural members reinforced with different types of FRP bars (glass, carbon and aramid fibre) through a parametric study. They reported that the DF did not increase considerably for a T cross-section when the depth of the neutral

axis was equal to or less than the depth of the flange. Also, they concluded that an increase in the FRP reinforcement ratio led to a reduction in the DF .

The objective of this study is to determine the limit of minimum FRP reinforcement ratio to prevent the brittle tensile rupture of longitudinal FRP bars in the tension side and to determine the limit of maximum longitudinal FRP reinforcement ratio to ensure failure in a ductile manner for FRP-RC members. In this study, different cross-sectional geometries (rectangular, circular, T and L cross-sections) as well as different FRP reinforcement arrangements were considered in proposing minimum and maximum longitudinal FRP reinforcement ratios for FRP-RC members.

5.3 Basic assumptions

In order to analyse the FRP-RC members, the following assumptions are considered,

- Plane sections remain plane after deformation.
- Perfect bond exists between the FRP reinforcing bars and the surrounding concrete.
- Tensile strength of concrete in the tension side can be neglected.
- The moduli of elasticity of FRP bars are equal in tension and compression.
- The area of the concrete displaced by the FRP bars in the compression side is negligible.
- The serviceability and ultimate limit state concrete compressive strain are 0.001 and 0.003, respectively.

- The compressive strain, stress and force are positive and the tensile strain, stress and force are negative.

5.4 Flexural behaviour

FRP-RC members under flexural loads can be analysed based on the stress-strain behaviour of the concrete and the FRP bars. The stress-strain behaviour of FRP bars is linearly elastic until failure[31, 34] as shown in Figure 5.1. The compressive strength of the FRP bars is relatively lower than the tensile strength, while the tensile and compressive moduli of elasticity are almost equal[33, 37].

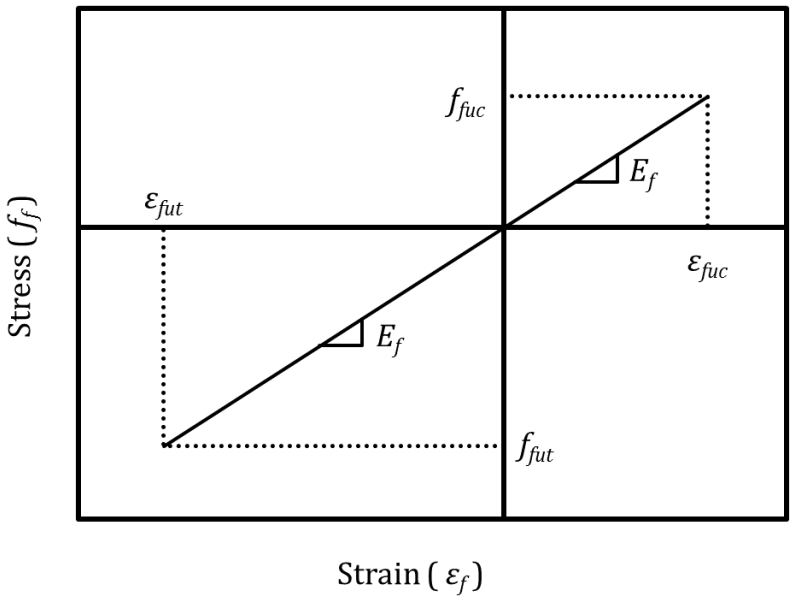

Figure 5.1. Stress-strain behaviour of FRP bars in compression and tension

The stress–strain relationship adopted for concrete in compression is shown in Figure 5.2. The adopted model consists of a single curve proposed by Popovics[22] and simplified in Wight and MacGregor[20] for normal-strength concrete.

$$f_c = \frac{2(\varepsilon_c/\varepsilon_{co})}{1+(\varepsilon_c/\varepsilon_{co})^2} \times 0.9 f_c' \tag{5.1}$$

$$\varepsilon_{co} = 1.71 \frac{f_c'}{E_c} \tag{5.2}$$

$$E_c = 4730\sqrt{f_c'} \quad \text{(MPa)} \tag{5.3}$$

where f_c is the axial concrete stress at any concrete strain (ε_c), f_c' is the cylinder compressive strength at 28-days, ε_{co} is the unconfined concrete strain corresponding to $0.9 f_c'$ and E_c is the elastic modulus of the concrete. The reduced concrete strength $(0.9 f_c')$ accounts for the differences between cylinder strength and member strength.

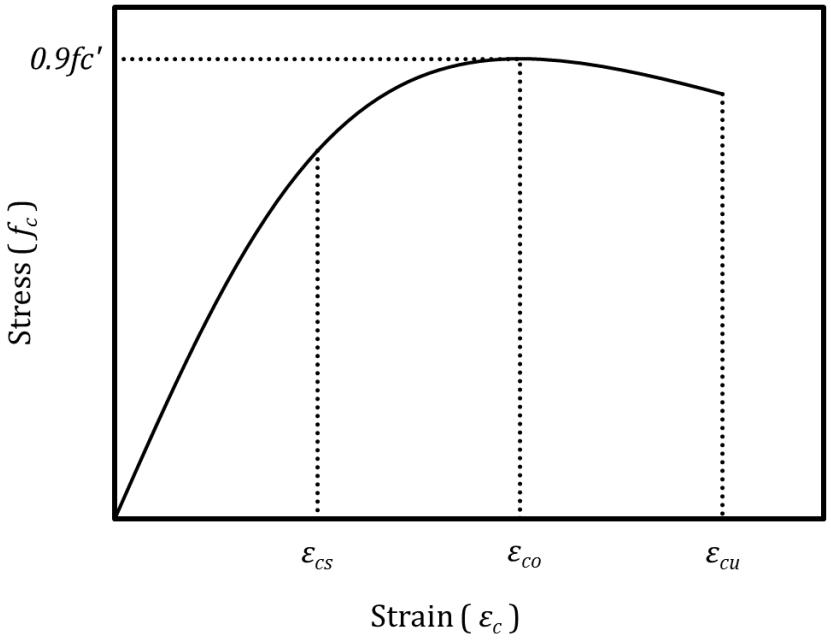

Figure 5.2. Stress-strain behaviour of concrete in compression

The stress of concrete in the compression side can be simplified to an equivalent rectangle, if the strain in the extreme fibre in the compression side reaches the ultimate limit state which is equal to 0.003 as in ACI 318-14[40]. Figure 5.3 shows the equivalent rectangular stress-block which has a width of $\alpha_1 f_c'$ and a depth of $\beta_1 c$. The α_1 is the ratio of concrete compressive strength in the members to the concrete cylinder compressive strength at 28-days which is equal to 0.85 for normal-strength concrete. The β_1 is the ratio of depth of equivalent rectangular stress-block to depth of neutral axis which varies from 0.65 to 0.85 as:

$$\text{For } f_c' \leq 28 \text{ MPa}, \ \beta_1 = 0.85 \tag{5.4}$$

$$\text{For } 28 \text{ MPa} < f_c' \leq 55 \text{ MPa}, \ \beta_1 = 0.85 - 0.05(f_c' - 28 \text{ MPa})/7 \text{ MPa} \tag{5.5}$$

$$\text{For } f_c' > 55 \text{ MPa}, \ \beta_1 = 0.65 \tag{5.6}$$

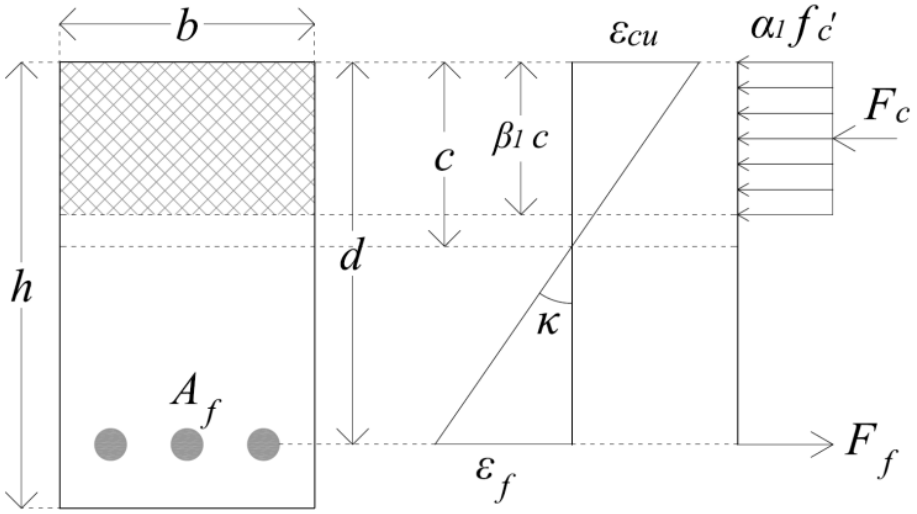

Figure 5.3. Equivalent rectangular stress-block for concrete in compression

5.5 Minimum FRP reinforcement for FRP-RC beams

The main concept of providing a minimum FRP reinforcement ratio is to prevent the brittle tensile failure of FRP bars in the tension side before concrete reaches the ultimate compressive strain in the compression side. However, the modulus of elasticity of the FRP bars is small. Hence, in some cases the minimum FRP reinforcement ratio should be limited to control the crack width in the tension side. This requirement is because the crack opening might be very large at the ultimate tensile strain of the FRP bars. In this study the minimum FRP reinforcement ratio is expressed as a function of the tensile strain of FRP bars in the tension side.

5.5.1 Rectangular cross-section

5.5.1.1 Single layer FRP reinforcement

The beams are reinforced with only one layer of FRP reinforcement in the tension side. The depth of the neutral axis (c) can be determined as a function of the ultimate strain in the extreme compression concrete fibre (ε_{cu}) and the maximum tensile strain in the FRP reinforcement (ε_f) (Figure 5.3).

$$c = \frac{d\varepsilon_{cu}}{\varepsilon_{cu} - \varepsilon_f} \tag{5.7}$$

where d is the distance between the centre of the FRP reinforcement to the extreme compression fibre. The compression force in the concrete (F_c) can be determined using the equivalent rectangular stress-block parameters. Also, the tensile force in the FRP bars (F_f) can be calculated as:

$$F_c = \alpha_1 \beta_1 f_c' bd \frac{\varepsilon_{cu}}{\varepsilon_{cu} - \varepsilon_f} \tag{5.8}$$

$$F_f = E_f \varepsilon_f A_f \tag{5.9}$$

where b is the width of the beam cross-section, E_f is the elastic modulus of the FRP bars and A_f is the area of the FRP bars. Based on the equilibrium of the forces in the cross-section, the F_c and the F_f should be equal. Hence, the minimum FRP reinforcement ratio $(\rho_{f\min})$ can be estimated as:

$$\rho_{f\min} = \alpha_1 \beta_1 \frac{f_c'}{E_f} \frac{\varepsilon_{cu}}{\varepsilon_f} \frac{1}{\varepsilon_{cu} - \varepsilon_f} \tag{5.10}$$

where $\rho_{f\min} = A_f / bd$.

5.5.1.2 Multiple layers of FRP reinforcement

A beam cross-section reinforced with $n+1$ layers of FRP bars is shown in Figure 5.4. Because the stress-strain behaviour of FRP bars is linearly elastic until failure, the strain of the first layer of FRP bars in the tension side should be considered, as explained above. It is assumed that the ratio of the area of FRP bars in each layer to the first layer is $A_{fi} = \lambda_{bi} A_f$, and the distance from the centre of each layer of FRP bars to the extreme compression fibre is d_i. Hence, the strain (ε_{fi}) and force (F_{fi}) in each layer of the FRP bars can be calculated as:

$$\varepsilon_{fi} = \varepsilon_{cu} - (\varepsilon_{cu} - \varepsilon_f)\frac{d_i}{d} \tag{5.11}$$

$$F_{fi} = E_f \varepsilon_{fi} A_{fi} \tag{5.12}$$

The $\rho_{f\min}$ can be estimated based on the equilibrium of the forces in the cross-section as:

$$\rho_{f\min} = -\alpha_1\beta_1 \frac{f_c'}{E_f} \frac{\varepsilon_{cu}}{\varepsilon_{cu} - \varepsilon_f} \frac{1+\sum_{i=1}^{n}\lambda_{bi}}{\varepsilon_f + \sum_{i=1}^{n}\lambda_{bi}\varepsilon_{fi}} \tag{5.13}$$

where $\rho_{f\min} = A_{ftotal}/bd$ and $A_{ftotal} = \left(1+\sum_{i=1}^{n}\lambda_{bi}\right)A_f$. For the doubly reinforced FRP-RC beam (one layer of tension reinforcement and one layer of compression reinforcement), Equation 5.13 can be simplified as:

$$\rho_{f\min} = \alpha_1\beta_1 \frac{f_c'}{E_f} \frac{\varepsilon_{cu}}{\varepsilon_{cu} - \varepsilon_f} \frac{1+\lambda_b}{\left(1-\frac{d'}{d}\right)\lambda_b\varepsilon_{cu} - \left(1+\frac{d'}{d}\lambda_b\right)\varepsilon_f} \tag{5.14}$$

where λ_b is the ratio of the area of FRP bars in the compression side to the area of FRP bars in the tension side and d' is the distance from the centre of FRP bars in the compression side to the extreme compression fibre.

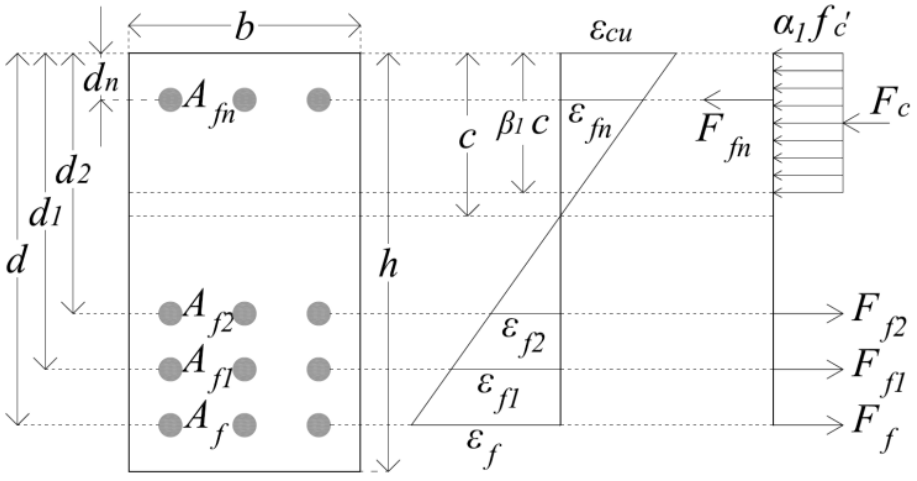

Figure 5.4. Concrete beam cross-section reinforced with $n+1$ layers of FRP bars

5.5.2 T and L cross-section

FRP-RC beams with T and L cross-section (Fig. 5.5) normally need more FRP reinforcement to attain the ultimate strain in concrete in the compression side due to increased amount of concrete in the compression side. The depth of the neutral axis in the T and L cross-section is either smaller or greater than the depth of the flange. In this study, however, it is considered that the depth of the neutral axis is equal to or smaller than the flange depth. By considering the same calculation principles for the rectangular cross-section, the minimum FRP reinforcement ratio $(\rho_{T\&L})$ can be estimated for the T and L cross-sections.

$$\rho_{T\&L} = \rho_{f\min}\left(\frac{b_f}{b_w}\right) \tag{5.15}$$

where $\rho_{T\&L} = A_{ftotal}/b_w d$, $\rho_{f\min}$ is the minimum FRP reinforcement ratio for rectangular cross-section (Equation 5.13), b_w is the width of the web and b_f is the width of the flange.

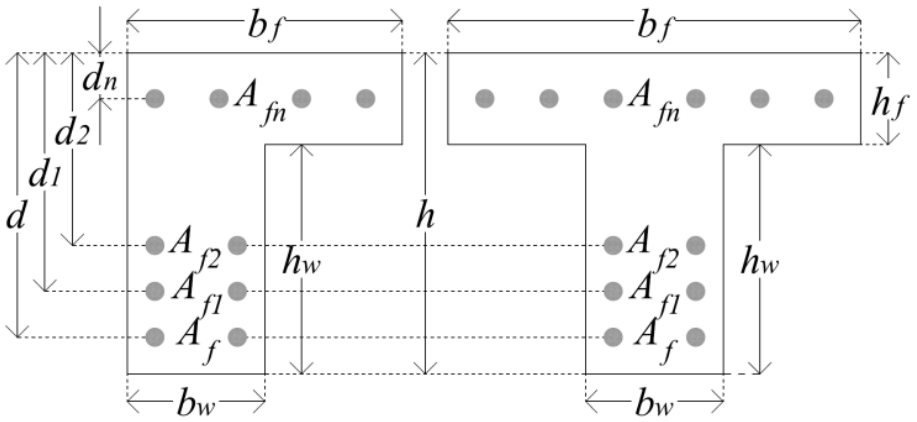

Figure 5.5. T and L beam cross-sections reinforced with $n + 1$ layers of FRP bars

5.6 Minimum FRP reinforcement for FRP-RC columns

5.6.1 Rectangular cross-section

A concrete column cross-section reinforced with n layer of FRP bars along the h direction is shown in Figure 5.6. The depth of the neutral axis (c) and the strain in each layer of the FRP bars (ε_{fi}) can be expressed as:

$$c = \frac{1}{2} h \varepsilon_{cu} \frac{1+\gamma}{\varepsilon_{cu} - \varepsilon_f} \tag{5.16}$$

$$\varepsilon_{fi} = \varepsilon_{cu} - \left[1 + \left(2\frac{n-i}{n-1} - 1\right)\gamma\right] \frac{\varepsilon_{cu} - \varepsilon_f}{1+\gamma} \tag{5.17}$$

where γ is the ratio of the distance between the centre of the first layer of FRP bars in the tension side to the last layer of the FRP bars in the compression side to h (Figure 5.6). The compression force of concrete (F_c) and the forces in each layer of the FRP bars (F_{fi}) can be expressed as:

$$F_c = \frac{1}{2} \alpha_1 \beta_1 f_c' b h \varepsilon_{cu} \frac{1+\gamma}{\varepsilon_{cu} - \varepsilon_f} \tag{5.18}$$

$$F_{fi} = E_f \varepsilon_{fi} A_{fi} \tag{5.19}$$

As a result of the summation of the forces in the FRP-RC cross-section,

$$F_c + \sum_{i=1}^{n} F_{fi} = P \tag{5.20}$$

The minimum FRP reinforcement $(\rho_{f\min} = A_{ftotal}/bh)$ can be determined by substituting Equations 5.18 and 5.19 in Equation 5.20.

$$\rho_{f\min} = \left(-\frac{1}{2}\alpha_1 \beta_1 \varepsilon_{cu} \frac{f_c'}{E_f} \frac{1+\gamma}{\varepsilon_{cu} - \varepsilon_f} + \frac{P}{E_f A_g}\right) \frac{1}{\sum_{i=1}^{n} \lambda_{ci} \varepsilon_{fi}} \tag{5.21}$$

where A_g is the gross area of the concrete cross-section and λ_{ci} is the ratio of the area of FRP bars in each layer to the total area of the FRP bars $\left(A_{fi} = \lambda_{ci} A_{ftotal}\right.$ and $\left. A_{ftotal} = \sum_{i=1}^{n} A_{fi}\right)$.

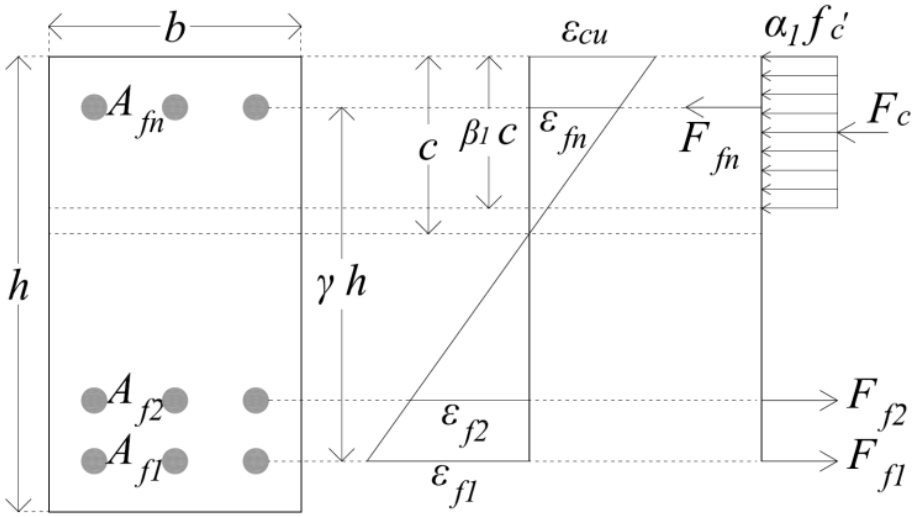

Figure 5.6. Concrete column cross-section reinforced with n layers of FRP bars

5.6.2 Circular cross-section

For the circular columns, c, ε_{fi} and F_{fi} are the same as the rectangular columns in the section above. However, F_c is different as shown in Figure 5.7.

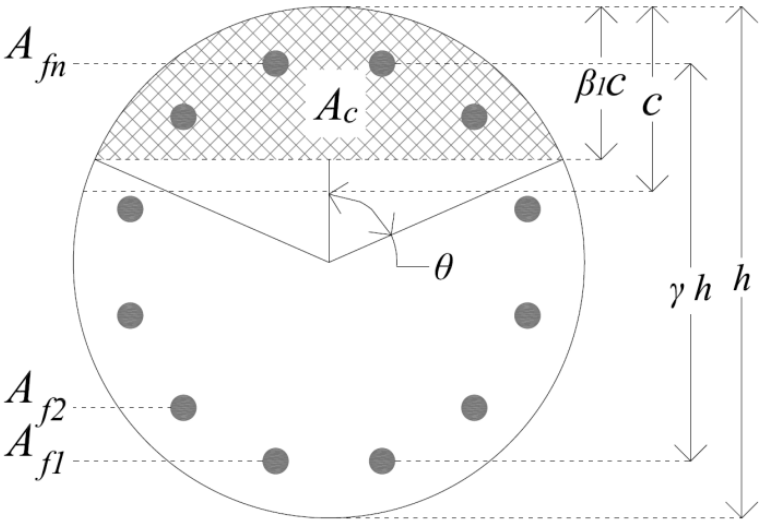

Figure 5.7. Circular concrete column reinforced with n layers of FRP bars

The F_c can be calculated as:

$$F_c = \alpha_1 f_c' A_c \tag{5.22}$$

$$A_c = \left(\frac{\theta - \sin\theta\cos\theta}{\pi} \right) A_g \tag{5.23}$$

$$\theta = \cos^{-1}\left(1 - \beta_1 \varepsilon_{cu} \frac{1+\gamma}{\varepsilon_{cu} - \varepsilon_f} \right) \tag{5.24}$$

where A_c is the area of concrete in the compression side and θ is explained in Fig. 5.7. Within the allowable range of β_1, γ, ε_{cu} and ε_f, the A_c can be simplified as Equation 5.25, if $\beta_1 \varepsilon_{cu} (1+\gamma) / (\varepsilon_{cu} - \varepsilon_f) \le 1.0$, which is commonly achieved (Figure 5.8).

$$A_c \approx \frac{1}{2} \left(\beta_1 \varepsilon_{cu} \frac{1+\gamma}{\varepsilon_{cu} - \varepsilon_f} \right)^{1.4} A_g \tag{5.25}$$

The $\rho_{f\,\min}$ can be determined based on the equilibrium of forces in the cross-section as:

$$\rho_{f\min} = \left[-\frac{1}{2}\alpha_1 \frac{f_c'}{E_f}\left(\beta_1 \varepsilon_{cu} \frac{1+\gamma}{\varepsilon_{cu} - \varepsilon_f} \right)^{1.4} + \frac{P}{E_f A_g} \right] \frac{1}{\sum_{i=1}^{n} \lambda_{ci} \varepsilon_{fi}} \tag{5.26}$$

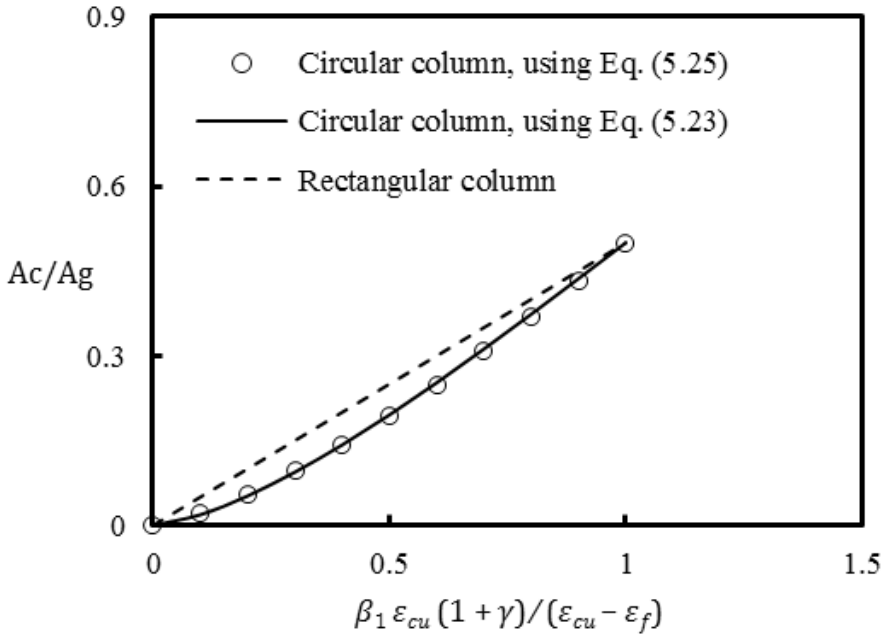

Figure 5.8. Differences in the area of concrete in compression side for rectangular and circular cross-section

5.6.3 General equation for minimum reinforcement ratio for FRP-RC columns

In the sections above, Equations 5.21 and 5.26 were derived to limit the $\rho_{f\min}$ for FRP-RC columns with rectangular and circular cross-sections. It can be observed that the $\rho_{f\min}$ for the circular cross-section is slightly smaller than the rectangular cross-section with the same material properties and maximum allowable tensile strain in FRP bars in the tension side. This is because the term $\beta_1 \varepsilon_{cu}(1+\gamma)/(\varepsilon_{cu} - \varepsilon_f)$

is generally smaller than 1. Hence, Equation 5.21 for the $\rho_{f\min}$ for rectangular columns can be generalized for circular columns.

In order to simplify Equation 5.21, parametric studies were conducted for different arrangements of the FRP reinforcement in FRP-RC columns. In general, the arrangements can be divided onto four different categories as shown in Figure 5.9. For the equal and symmetric arrangements (Figure 5.9 a, b) which are the usual arrangements for reinforcing the concrete columns:

$$\sum_{i=1}^{n} \lambda_{ci} \varepsilon_{fi} = \frac{\gamma \varepsilon_{cu} + \varepsilon_f}{1+\gamma} \tag{5.27}$$

For the descending arrangement (Figure 5.9 c) the area of the FRP bars in the tension side is greater than the compression side, the result of the term $\sum_{i=1}^{n} \lambda_{ci} \varepsilon_{fi}$ is greater than the result obtained from Equation 5.27. Hence, the limit of the $\rho_{f\min}$ is reduced. In the ascending arrangement (Figure 5.9 d), the area of the FRP bars in the tension side is smaller than the compression side. Also, the result of the term $\sum_{i=1}^{n} \lambda_{ci} \varepsilon_{fi}$ is smaller than the result obtained from Equation 5.27. Hence, the limit of the $\rho_{f\min}$ is increased. However, the ascending arrangement is rarely used and is not realistic. Therefore, Equation 5.21 can be generalized for rectangular and circular columns reinforced with equal, symmetric and descending arrangements of FRP bars as:

$$\rho_{f\min} = \left(-\frac{1}{2} \alpha_1 \beta_1 \varepsilon_{cu} \frac{f'_c}{E_f} \frac{1+\gamma}{\varepsilon_{cu} - \varepsilon_f} + \frac{P}{E_f A_g} \right) \frac{1+\gamma}{\gamma \varepsilon_{cu} + \varepsilon_f} \tag{5.28}$$

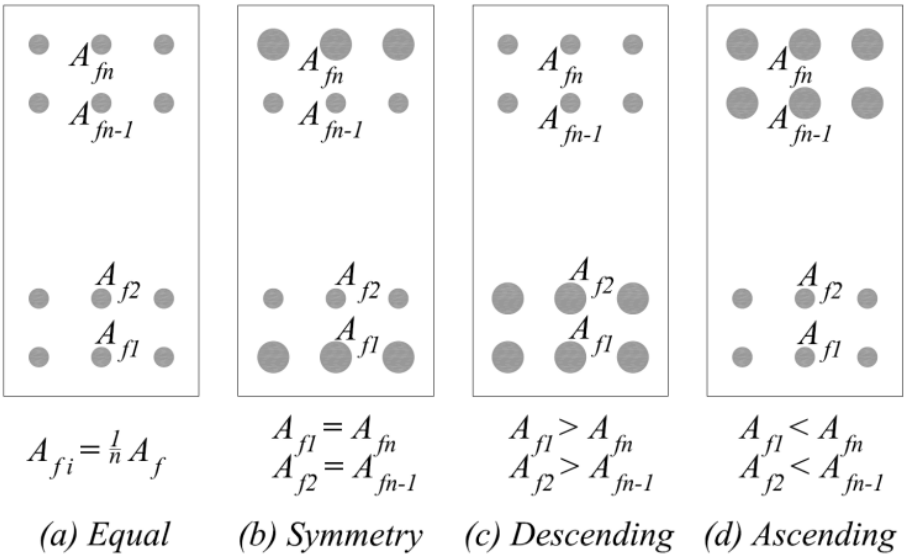

Figure 5.9. Different arrangements of FRP bars in RC columns

The derived equation for calculating the $\rho_{f\min}$ in the FRP-RC columns considerably decreases with the increase in the applied axial load (i.e. reducing eccentricity). If the condition in Equation 5.29 is satisfied,

$$P \geq \frac{1}{2}\alpha_1\beta_1\varepsilon_{cu} f_c' A_g \frac{1+\gamma}{\varepsilon_{cu} - \varepsilon_f} \tag{5.29}$$

The $\rho_{f\min}$ does not need to be checked. However, minimum FRP reinforcement ratio should be provided for shrinkage and creep of concrete due to sustained load.

Example No. 1 in Choo et al.[56] is solved in the Appendix A using Equation 5.28 to determine $\rho_{f\min}$ for a rectangular FRP-RC column. A small difference can be observed between the two results. This is particularly because Choo et al.[56] used a simplified procedure to calculate $\rho_{f\min}$. However, $\rho_{f\min}$ has been calculated accurately using Equation 5.28. In addition, at least three equations are needed to be

solved for the calculation of $\rho_{f\min}$ for FRP-RC rectangular columns using the procedure proposed in Choo et al.[56], whereas Equation 5.28 alone can calculate $\rho_{f\min}$ for different cross-section FRP-RC columns.

5.7 Maximum FRP reinforcement

Ductility of reinforced concrete members is the capacity of energy absorption through plastic deformation. The ductility in conventional steel-RC flexural members is measured by the ratio of deflection or curvature at ultimate to that at yield. However, this interpretation is not appropriate to FRP-RC members because there is no evident yield point in the stress-strain relationship of FRP bars, as the stress-strain behaviour is linearly elastic up to failure. The DF introduced by Jaejer et al.[67] can be used to evaluate the deformability of concrete members which are reinforced with FRP bars. DF is the product of Moment Factor (MF) to Curvature Factor (CF) as:

$$DF = MF \times CF \tag{5.30}$$

$$MF = M_u / M_s \tag{5.31}$$

$$CF = \kappa_u / \kappa_s \tag{5.32}$$

where M_u and κ_u are the moment and curvature, respectively, at the ultimate concrete strain which is equal to 0.003 as defined in ACI 318-14[40]. The M_s and κ_s are the moment and curvature, respectively, at serviceability limit state of the concrete strain which is equal to 0.001 as recommended in Jaejer et al.[67].

In conventional steel-RC members, flexural failure of a concrete member is accompanied by a large deformation which is reasonably observable when the failure mode is by yielding of the steel reinforcement in the tension side (under reinforced section). However, the *DF* reduces when the failure mode is changed to the crushing of the concrete in the compression side. Therefore, the design codes recommended to design the flexural members as under-reinforced cross-section (reinforcement ratio should be smaller than the balanced reinforcement ratio). However, for FRP-RC cross-sections under flexure, it is recommended that reinforcement ratio should be greater than the balanced reinforcement ratio to ensure that failure would be caused by crushing of concrete without rupture of the FRP bars[13].

5.8 Calculation of deformability factor

According to the definition of Jaejer et al.[67] for the *DF* of FRP-RC members, the bending moment and curvature of the members should be calculated for serviceability and ultimate limit states. However, the moment and curvature cannot simply be determined for serviceability limit state. This is because the stress-block parameters for the concrete in the compression side are not applicable, as the strain in the extreme compression fibre does not reach ultimate concrete strain. Therefore, instead of the stress-block parameters, the stress of concrete in the compression side was computed using integration technique. The stress-strain models presented above are used for the concrete in the compression side.

5.8.1 Serviceability limit state

The stress distribution along a RC cross-section in the serviceability limit state is shown in Figure 5.10(a). The compressive stress of concrete in the compression side can be expressed as:

$$f_c = \frac{1.8 \times \left(\frac{\varepsilon_{cs}}{\varepsilon_{co}} \frac{y}{c_s} \right)}{1 + \left(\frac{\varepsilon_{cs}}{\varepsilon_{co}} \frac{y}{c_s} \right)^2} f_c' \tag{5.33}$$

where ε_{cs} is the compressive concrete strain at the serviceability limit state which is taken as 0.001, y is the direction along the depth of the cross-section and c_s is the depth of the neutral axis for serviceability limit state. The compression force of concrete in the compression side (F_{cs}) can be determined according to Equation 5.34:

$$F_{cs} = \int_0^{c_s} f_c b dy \tag{5.34}$$

where b is the width of the cross-section. By solving Equation 5.34, the F_{cs} can be written as:

$$F_{cs} = 0.9 f_c' b c_s \frac{\varepsilon_{co}}{\varepsilon_{cs}} \ln \left[1 + \left(\frac{\varepsilon_{cs}}{\varepsilon_{co}} \right)^2 \right] \tag{5.35}$$

The centroid $(\bar{y}_s)$ of the area under the curve of f_c can be calculated by taking moment about the neutral axis and is equal to:

$$\bar{y}_s = (1 - n_s) c_s \tag{5.36}$$

where

$$n_s = 2\frac{\varepsilon_{co}}{\varepsilon_{cs}}\frac{\frac{\varepsilon_{cs}}{\varepsilon_{co}} - \tan^{-1}\frac{\varepsilon_{cs}}{\varepsilon_{co}}}{\ln\left[1+\left(\frac{\varepsilon_{cs}}{\varepsilon_{co}}\right)^2\right]} \tag{5.37}$$

The tension force in the FRP bars (F_{fs}) in the tension side can be calculated in terms of the maximum tensile strain (ε_{fs}) in the FRP bars for the serviceability limit state as:

$$F_{fs} = \varepsilon_{fs} E_f \rho_f bd \tag{5.38}$$

where ρ_f is the FRP reinforcement ratio. Based on the equilibrium of forces,

$$F_{cs} + F_{fs} = 0 \tag{5.39}$$

Also, based on the strain distribution in the concrete cross-section, the c_s can be written as:

$$c_s = \frac{d\varepsilon_{cs}}{\varepsilon_{cs} - \varepsilon_{fs}} \tag{5.40}$$

By substituting Equations 5.35, 5.38 and 5.40 in Equation 5.39, the ε_{fs} can be written as:

$$\varepsilon_{fs} = \frac{1}{2}\left(\varepsilon_{cs} - \sqrt{\varepsilon_{cs}^2 + 3.6\frac{a_s f_c'}{\rho_f E_f}\varepsilon_{cs}}\right) \tag{5.41}$$

where

$$a_s = \frac{\varepsilon_{co}}{\varepsilon_{cs}}\ln\left[1+\left(\frac{\varepsilon_{cs}}{\varepsilon_{co}}\right)^2\right] \tag{5.42}$$

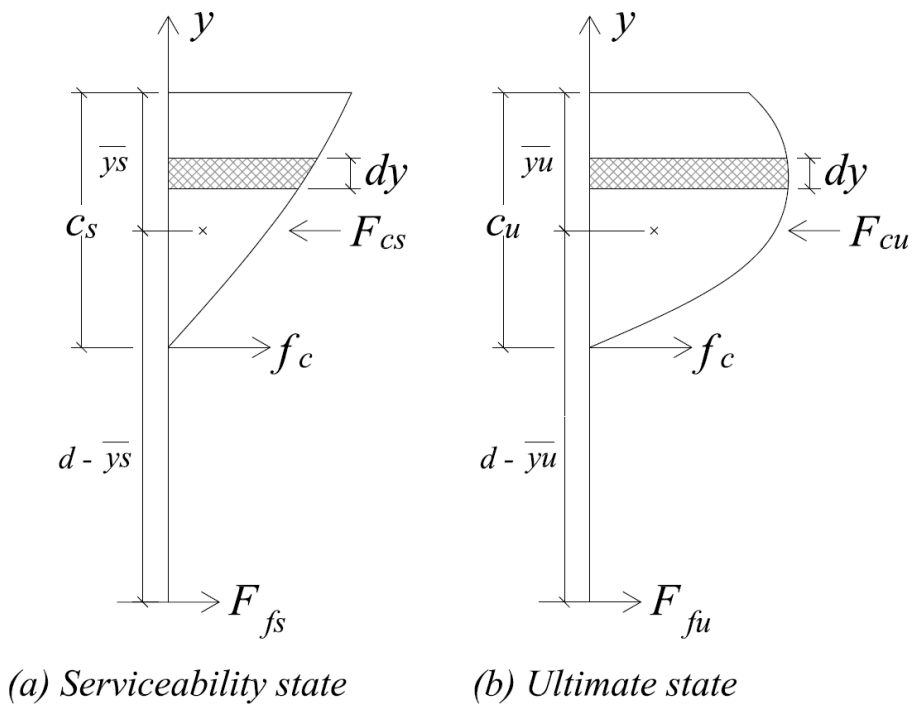

Figure 5.10. Distribution of stress and force in the RC member cross-section: (a) serviceability state; and (b) ultimate state

5.8.2 Ultimate limit state

The stress distribution along the RC cross-section in the ultimate limit state is shown in Figure 5.10(b). The compressive stress of concrete in the compression side can be expressed as:

$$f_c = \frac{1.8 \times \left(\frac{\varepsilon_{cu}}{\varepsilon_{co}} \frac{y}{c_u} \right)}{1 + \left(\frac{\varepsilon_{cu}}{\varepsilon_{co}} \frac{y}{c_s} \right)^2} f_c' \tag{5.43}$$

where ε_{cu} is the maximum concrete strain at the ultimate limit state which is taken as 0.003 and c_u is the depth of the neutral axis for ultimate limit state. The compression

force of concrete in the compression side (F_{cu}) can be calculated by the same principle as applied for the serviceability limit state.

$$F_{cu} = 0.9 f_c' b c_u \frac{\varepsilon_{co}}{\varepsilon_{cu}} \ln\left[1+\left(\frac{\varepsilon_{cu}}{\varepsilon_{co}}\right)^2\right] \tag{5.44}$$

The centroid of the area $(\bar{y}_u)$ under the curve of f_c can be determined by taking moment about the neutral axis and is equal to:

$$\bar{y}_u = (1-n_u)c_u \tag{5.45}$$

where

$$n_u = 2\frac{\varepsilon_{co}}{\varepsilon_{cu}} \frac{\frac{\varepsilon_{cu}}{\varepsilon_{co}} - \tan^{-1}\frac{\varepsilon_{cu}}{\varepsilon_{co}}}{\ln\left[1+\left(\frac{\varepsilon_{cu}}{\varepsilon_{co}}\right)^2\right]} \tag{5.46}$$

The tension force in the FRP bars (F_{fu}) in the tension side can be found in terms of the maximum tensile strain (ε_{fu}) in the FRP bars for the ultimate limit state as:

$$F_{fu} = \varepsilon_{fu} E_f \rho_f b d \tag{5.47}$$

Based on the equilibrium of forces in the concrete cross-section,

$$F_{cu} + F_{fu} = 0 \tag{5.48}$$

Also, based on the strain distribution in the concrete cross-section, the c_u can be written as:

$$c_u = \frac{d\varepsilon_{cu}}{\varepsilon_{cu} - \varepsilon_{fu}} \tag{5.49}$$

By substituting Equations 5.44, 5.47 and 5.49 in Equation 5.48, the ε_{fu} can be expressed as:

$$\varepsilon_{fu} = \frac{1}{2}\left(\varepsilon_{cu} - \sqrt{\varepsilon_{cu}^2 + 3.6\frac{a_u f_c'}{\rho_f E_f}\varepsilon_{cu}} \right) \tag{5.50}$$

where

$$a_u = \frac{\varepsilon_{co}}{\varepsilon_{cs}} \ln\left[1 + \left(\frac{\varepsilon_{cu}}{\varepsilon_{co}} \right)^2 \right] \tag{5.51}$$

5.8.3 Deformability factor

The DF is a product of the MF and CF as defined earlier. The CF can be calculated as:

$$CF = \frac{\kappa_u}{\kappa_s} = \frac{\varepsilon_{cu}/c_u}{\varepsilon_{cs}/c_s} \tag{5.52}$$

By substituting Equations 5.40 and 5.49 in Equation 5.52, the CF can be written as:

$$CF = \frac{\varepsilon_{cu} - \varepsilon_{fu}}{\varepsilon_{cs} - \varepsilon_{fs}} \tag{5.53}$$

Also, the MF can be calculated as:

$$MF = \frac{M_u}{M_s} = \frac{F_{fu}(d - \bar{y}_u)}{F_{fs}(d - \bar{y}_s)} \tag{5.54}$$

By substituting Equations 5.36, 5.38, 5.45 and 5.47 in Equation 5.54, the MF can be written as:

$$MF = \frac{\varepsilon_{fu}}{\varepsilon_{fs}} \times \frac{d - (1 - n_u)c_u}{d - (1 - n_s)c_s} \tag{5.55}$$

Eventually, the MF can be calculated by substituting Equations 5.40 and 5.49 in Equation 5.55 as:

$$MF = \frac{\varepsilon_{fu}}{\varepsilon_{fs}} \times \frac{n_u \varepsilon_{cu} - \varepsilon_{fu}}{n_s \varepsilon_{cs} - \varepsilon_{fs}} \times \frac{\varepsilon_{cu} - \varepsilon_{fu}}{\varepsilon_{cs} - \varepsilon_{fs}} \tag{5.56}$$

Finally, the DF can be determined from Equations 5.53 and 5.56 as:

$$DF = \frac{\varepsilon_{fu}}{\varepsilon_{fs}} \times \frac{n_u \varepsilon_{cu} - \varepsilon_{fu}}{n_s \varepsilon_{cs} - \varepsilon_{fs}} \tag{5.57}$$

For the FRP-RC members with T or L cross-section, the DF can be calculated same as the rectangular cross-section. However, the ε_{fs} and ε_{fu} can be determined as:

$$\varepsilon_{fs} = \frac{1}{2}\left(\varepsilon_{cs} - \sqrt{\varepsilon_{cs}^2 + 3.6 \frac{b_f}{b_w} \frac{a_s f_c'}{\rho_f E_f} \varepsilon_{cs}} \right) \tag{5.58}$$

$$\varepsilon_{fu} = \frac{1}{2}\left(\varepsilon_{cu} - \sqrt{\varepsilon_{cu}^2 + 3.6 \frac{b_f}{b_w} \frac{a_u f_c'}{\rho_f E_f} \varepsilon_{cu}} \right) \tag{5.59}$$

5.8.4 Simplified equation for deformability factor

It can be observed that Equation 5.57 for calculating DF is complicated for the design purpose as seven equations (Equations 5.37, 5.41, 5.42, 5.46, 5.50, 5.51 and 5.57) need to be solved. Therefore, the parameters that control the DF were taken in the allowable range to simplify Equation 5.57. The DF is dependent on two terms which are f_c' and $b_w \rho_f E_f / b_f$. Therefore, the DF can be expressed as:

$$DF = k \times f(f_c') \times g\left(\frac{b_w}{b_f} \rho_f E_f \right) \tag{5.60}$$

where k is a constant, f is a function of f_c' and g is a function of $b_w \rho_f E_f / b_f$. An MS-EXCEL spread-sheet was prepared to calculate the DF using Equation 5.57

with different values of the dependant terms $\left(f_c'\right.$ and $\left.b_w\rho_f E_f/b_f\right)$. Figure 5.11 shows the relationship between the DF and $\sqrt[4]{f_c'}$. The $f\left(f_c'\right)$ can be expressed as:

$$f\left(f_c'\right)=\sqrt[4]{f_c'}-3/5 \tag{5.61}$$

where f_c' is in MPa.

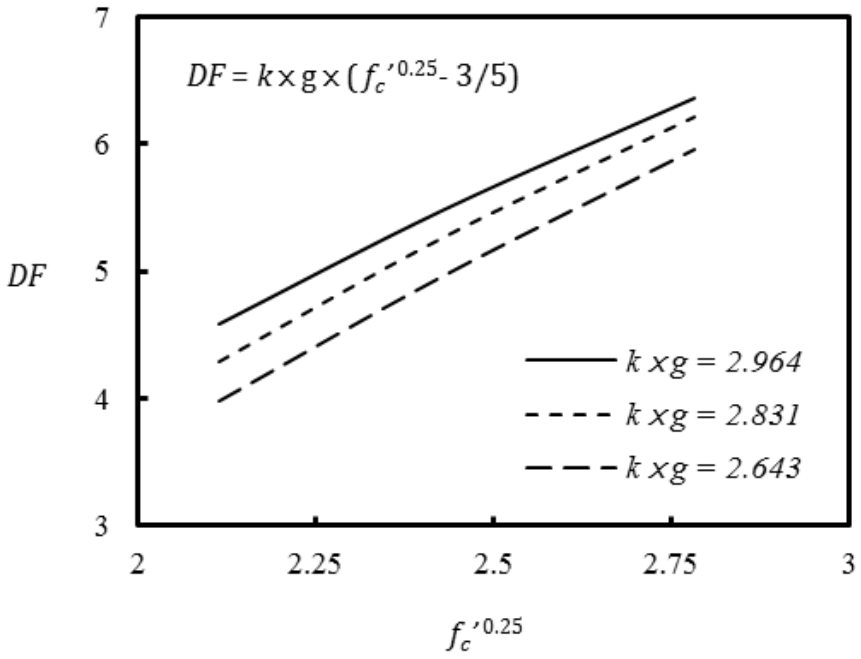

Figure 5.11. Relationship between f_c' and DF

Figure 5.12 shows the relationship between the DF and $\sqrt[4]{b_w\rho_f E_f/b_f}$. The function of $g\left(b_w\rho_f E_f/b_f\right)$ was determined by the best fit line using regression analysis technique.

$$g\left(\frac{b_w}{b_f}\rho_f E_f\right)=1-0.01\times\sqrt[4]{\frac{b_w}{b_f}\rho_f E_f} \tag{5.62}$$

where E_f is in MPa.

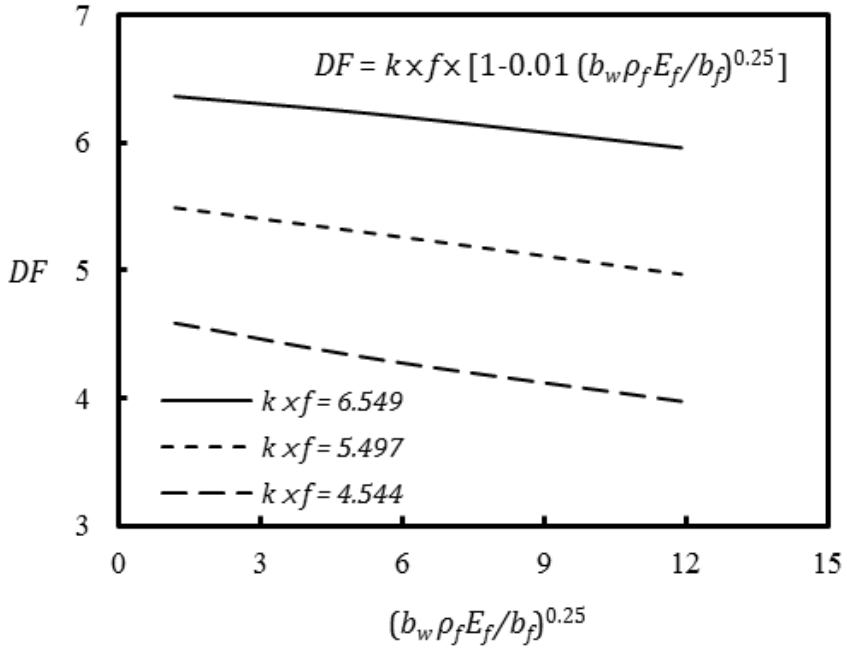

Figure 5.12. Relationship between $b_w \rho_f E_f / b_f$ and DF

Figure 5.13 shows the relationship between the DF using Equation 5.57 and the product of f and g functions using Equations 5.61 and 5.62, respectively, to find the value of k. Eventually, the simplified equation of the DF can be written as:

$$DF = 3 \times \left(\sqrt[4]{f_c'} - \frac{3}{5} \right) \times \left(1 - 0.01 \times \sqrt[4]{\frac{b_w}{b_f} \rho_f E_f} \right) \quad \text{(MPa)} \tag{5.63}$$

According to CAN/CSA S6-06[123] the value of DF should not be less than 4 for FRP-RC rectangular members to undergo an observable deformation before failure. However, the value of ε_{cu} significantly influences the value of DF. Equation 5.63 is proposed based on $\varepsilon_{cu} = 0.003$ as recommended in ACI 318-14[40]. If $\varepsilon_{cu} = 0.0035$ is used in Equation 5.57 instead of 0.003, Equation 5.63 increases approximately as a ratio of 15%. Hence, the minimum value of the DF can be reduced from 4 to 3.5 when $\varepsilon_{cu} = 0.003$. For a given FRP reinforcement ratio in the FRP-RC members,

DF slightly increases with increasing the number of layers of the FRP bars. This is because the FRP reinforcement ratio decreases in the first layer of the tension side. Therefore, the proposed equation for the DF with one layer of FRP bars can be used for any arrangement of FRP bars. By changing the cross-section of the concrete members from rectangular to T or L cross-section, the increase in the DF is very small for any ratio of b_w/b_f . Hence, the minimum DF limit for T and L cross-section can be reduced to the minimum DF limit of rectangular cross-section.

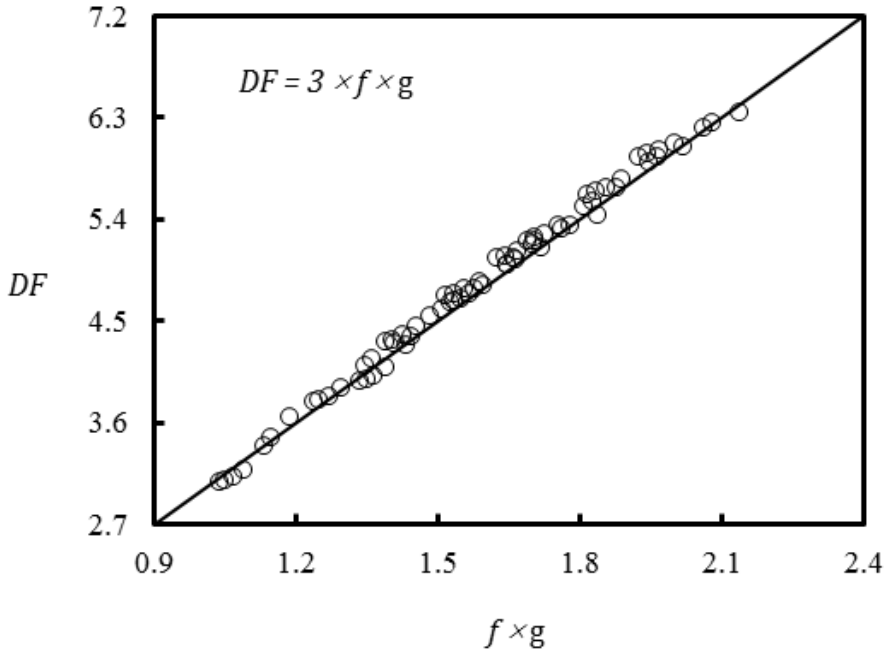

Figure 5.13. Relationship between $f(f_c')\times g(b_w\rho_f E_f/b_f)$ and DF

Example 9.2 in ISIS 2007[16] is solved in the Appendix A using Equations 5.57 and 5.63 to determine DF for a FRP-RC slab. It can be observed that Equation 5.57 can accurately calculate the DF. Also, the developed simplified equation (Equation 5.63) can calculate the DF reasonably accurately. In addition, the calculation

procedure of DF in ISIS 2007[16] is long, whereas only one equation (Equation 5.63) is needed in this study to calculate DF for different cross-section FRP-RC members.

5.9 Summary

Failure of FRP-RC flexural members can be due to the rupture of FRP bars in the tension side or due to the crushing of concrete in the compression side. Meanwhile, the preferable failure mode for FRP-RC flexural members is crushing of concrete in the compression side. In order to prevent rupture of FRP bars in the tension side and attain ultimate compressive strain in concrete in the compression side, analytical calculations were carried out for limiting minimum FRP reinforcement ratio. Different concrete cross-sectional geometries and FRP reinforcement arrangements were investigated. The analytical results showed that circular cross-sections need slightly lower minimum FRP reinforcement ratio than rectangular cross-sections. The minimum RFP reinforcement ratio should be increased by the ratio of b_f / b_w for concrete members with T and L cross-sections. Using more than one layer of FRP reinforcement in the tension side leads to increasing the minimum requirement of FRP reinforcement ratio to prevent rupture of the first layer of FRP bars. This increase in the minimum reinforcement ratio is because with increasing the reinforcement layers, the area of the first layer reduces with respect to the total reinforcement area. Hence, more reinforcement ratio is needed to achieve the required tensile strain in the first layer of the FRP bars.

Increasing FRP reinforcement ratio leads to the reduction in the DF of FRP-RC members because of the reduction in the curvature, as the depth of neutral axis increases with increasing of FRP reinforcement ratio. As a result, the FRP-RC members that fail by crushing of concrete become brittle and considerable deformations will not be observed before failure. An equation is proposed for calculating the DF using integration of the concrete stress in the compression side instead of using equivalent rectangular stress-block. This is because rectangular stress-block parameters cannot be applied for serviceability limit state as the strain in concrete in the compression side does not reach ultimate concrete compressive strain. Also, the DF equation was simplified in the range of normal-strength concrete in order to propose a simplified equation for the design purpose. It was also concluded that the minimum limit of the DF can be reduced to 3.5 if the ultimate strain of concrete in the compression side is considered as 0.003. Also, it is recommended that the minimum DF limit for T and L cross-section should be reduced to the minimum DF limit of rectangular cross-section.

This study did not consider the shrinkage and creep of concrete under sustained load in calculating minimum and maximum longitudinal reinforcement ratio for FRP-RC members. More studies are, therefore, needed to include the shrinkage and creep effects. Such studies are considered beyond the scope of this study. Finally, based on the developed equations in this study, the minimum FRP reinforcement ratio for FRP-RC members can be selected either to prevent rupture of FRP bars or to control crack width. Also, the maximum FRP reinforcement ratio can be selected for the design deformability of the FRP-RC members.

6 EXPERIMENTAL STUDY

6.1 Introduction

In order to a better understand and figure out the behaviour of GFRP-RC columns, it is necessary to design and conduct an experimental program in a laboratory. For this objective an experimental work is presented in this chapter to evaluate the behaviour of concrete columns that were reinforced longitudinally with GFRP bars and different volumetric ratios of GFRP helices. The GFRP-RC specimens were cast with or without external CFRP wrapping. The GFRP-RC specimens were tested under monotonic loading with 0, 25 and 50 mm eccentricity and four-point loading. Also, GFRP bars were tested with different unbraced length to diameter ratio to investigate the behaviour of GFRP bars under monotonic compression loading. The experimental program was carried out at the laboratories of the School of Civil, Mining and Environmental Engineering at the University of Wollongong, Australia. Finally, the experimental results were reported and discussed in detail.

6.2 Experimental design

In this study, 18 small scale circular concrete specimens were cast and tested under different loading conditions. Nine specimens were tested as columns and three specimens were tested as beams. All specimens were 205 mm in diameter and 800 mm in height or length (height to diameter (l/h) ratio is equal to 4). The dimensions were chosen to be suitable for the condition and capacity of the available testing equipment in the laboratory. It is noted that vertical support with l/h ratio of greater

than or equal to 2.5 is considered as a column in CAN/CSA S6-06[123] and AS 3600-2009[124]. The slenderness ratio of the specimens was about 16, which is within the limit of a short concrete column. In addition, the height of the columns was enough to have a sufficient development length for the longitudinal bars according to ACI 318-14[40]. The size effect of the RC columns on strength and ductility can be reasonably neglected for a short RC specimen[125-128].

The dimensions and reinforcement scheme and configuration of the tested specimens are presented in Figure 6.1. The specimens were divided into five groups. Specimens of the first group (GI) (reference specimens) were reinforced longitudinally with six N12 (nominal diameter=12 mm) steel bars (longitudinal reinforcement ratio=2.06%) and transversally with R10 (nominal diameter=10 mm) steel helices with a pitch of 60 mm (transversal reinforcement ratio=3.27%). Specimens of the second group (GII) were reinforced longitudinally with six #4 (nominal diameter=12.7 mm) GFRP bars (longitudinal reinforcement ratio=2.3%) and transversally with #3 (nominal diameter=9.5 mm) GFRP helices with a pitch of 60 mm (transversal reinforcement ratio=2.97%). Specimens of the third group (GIII) were reinforced longitudinally with six #4 GFRP bars and transversally with #3 GFRP helices with a pitch of 30 mm (transversal reinforcement ratio=5.94%). Specimens of the forth group (GIV) were reinforced longitudinally with six #4 GFRP bars transversally with #3 GFRP helices with a pitch of 30 mm and also confined externally with two layers of CFRP sheets with a total thickness of 0.9 mm. Specimens of the fifth group (GV) were only reinforced transversally with #3 GFRP helices with a pitch of 60 mm or 30 mm. The

reinforcements (longitudinal and transversal) of the reference group were provided to satisfy the requirements of ACI 318-14[40].

Table 6.1 provides reinforcement details of the specimens. Groups GI to GIV consist of three columns and one beam. One column was tested concentrically, one was tested under 25 mm eccentric load, the one was tested under 50 mm eccentric load. The beam was tested under four-point loading. Group GV consists of two columns which were tested under concentric load. The specimens are identified by the longitudinal reinforcement material and its number, the transversal reinforcement material and its spacing, and the applied loading condition. For example, Specimen G6-G60-E25 is reinforced longitudinally with six GFRP bars and transversally with a pitch of 60 mm of GFRP helix and tested under 25 mm eccentric load. Specimen 00-G30-C is reinforced only transversally with a pitch of 30 mm of GFRP helix and tested under concentric load. The letter "C" at the beginning of the specimens in the fourth group (GIV) name indicates that the specimens were confined externally with CFRP sheets.

6.3 Materials

The materials used in this study are concrete, longitudinal and helical steel reinforcement, longitudinal and helical GFRP and unidirectional CFRP sheets.

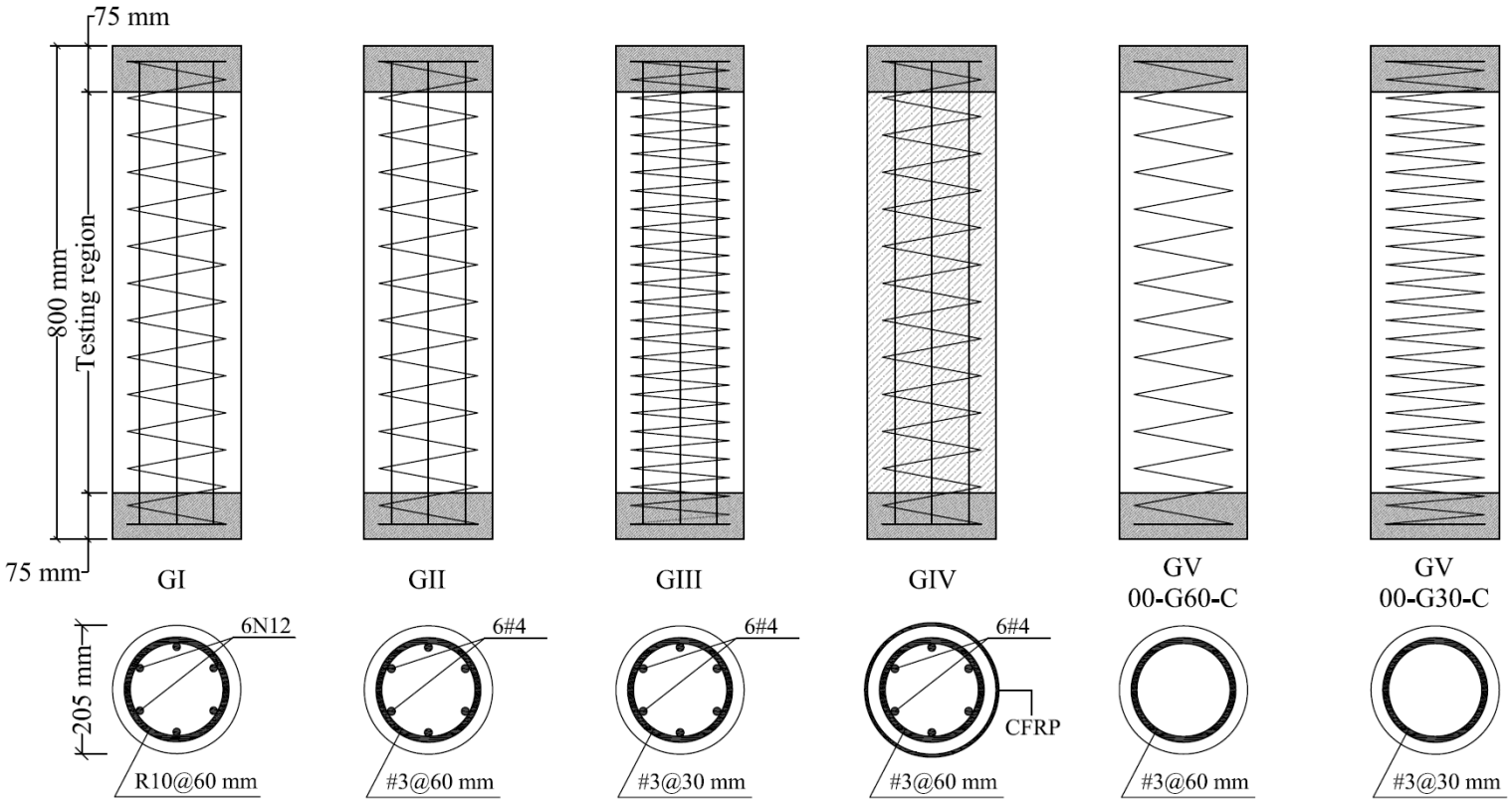

Figure 6.1. Reinforcement details and dimension of the specimens

Table 6.1. Experimental matrix

Group	Specimen Labels	Longitudinal Reinforcement				Transverse Reinforcement				CFRP External Confinement (ply numbers)	Loading Modes
		Material	Number of Bars	Diameter of Bars [a] (mm)	ρ_s% [b]	Material	Diameter of Bars [a] (mm)	Pitch (mm)	ρ_{st}% [b]		
GI	S6-S60-C	Steel	6	12	2.16	Steel	10	60	3.27	-	Concentric
	S6-S60-E25	Steel	6	12	2.16	Steel	10	60	3.27	-	e = 25 mm
	S6-S60-E50	Steel	6	12	2.16	Steel	10	60	3.27	-	e = 50 mm
	S6-S60-F	Steel	6	12	2.16	Steel	10	60	3.27	-	Flexural
GII	G6-G60-C	GFRP	6	12.7	2.42	GFRP	9.525	60	2.96	-	Concentric
	G6-G60-E25	GFRP	6	12.7	2.42	GFRP	9.525	60	2.96	-	e = 25 mm
	G6-G60-E50	GFRP	6	12.7	2.42	GFRP	9.525	60	2.96	-	e = 50 mm
	G6-G60-F	GFRP	6	12.7	2.42	GFRP	9.525	60	2.96	-	Flexural

Table 6.1. (Continued)

GIII	G6-G30-C	GFRP	6	12.7	2.42	GFRP	9.525	30	5.92	-	Concentric
	G6-G30-E25	GFRP	6	12.7	2.42	GFRP	9.525	30	5.92	-	e = 25 mm
	G6-G30-E50	GFRP	6	12.7	2.42	GFRP	9.525	30	5.92	-	e = 50 mm
	G6-G30-F	GFRP	6	12.7	2.42	GFRP	9.525	30	5.92	-	Flexural
GIV	CG6-G60-C	GFRP	6	12.7	2.42	GFRP	9.525	60	2.96	2	Concentric
	CG6-G60-E25	GFRP	6	12.7	2.42	GFRP	9.525	60	2.96	2	e = 25 mm
	CG6-G60-E50	GFRP	6	12.7	2.42	GFRP	9.525	60	2.96	2	e = 50 mm
	CG6-G60-F	GFRP	6	12.7	2.42	GFRP	9.525	60	2.96	2	Flexural
GV	00-G60-C	-	-	-	-	GFRP	9.525	60	2.96	-	Concentric
	00-G30-C	-	-	-	-	GFRP	9.525	30	5.92	-	Concentric

[a] Standard diameters

[b] Calculated based on standard areas of the bars

6.3.1 Concrete

Ready-mix normal-strength concrete was used to cast the specimens. The design compressive strength of the concrete was 32 MPa. The maximum size of the coarse aggregate for the concrete was 10 mm. Three concrete cylinders (100 mm x 200 mm) were cast according to AS[129] for 28 day to determine the compressive strength with the same concrete batch that was used for casting the specimens. After 24 hours, the concrete cylinders were taken out of the moulds and immersed into water to cure until the day of testing. Both ends of the concrete cylinders were capped with high-strength plaster in order to distribute the load uniformly. The result of the tested cylinder at 28-days is reported in Table 6.2 and the average compressive strength was 37 MPa.

Table 6.2. 28 day concrete compressive strength result

Specimen No.	Diameter (mm)	Load (kN)	Compressive strength (MPa)	Average compressive strength (MPa)
1	101.7	316	38.9	37
2	99.6	294	37.7	
3	101.6	279	34.4	

6.3.2 Steel bars

Two different diameters of steel bars were used to reinforce the reference specimens. Deformed N12 steel bars with nominal diameter of 12 mm and nominal tensile strength of 500 MPa were used for longitudinal reinforcement. Also, Plane R10 with nominal diameter of 10 mm and nominal tensile strength of 250 MPa were used for transverse reinforcement. The mechanical properties of the steel bars were determined according to AS[130] by testing three specimens of each diameter with a total length of 500 mm including 340 mm clear testing length and 80 mm gripping length at both ends as shown in Figure 6.2. The stress-strain behaviour of the tested steel bars is shown in Figure 6.3. The yield tensile strength and corresponding strain and elastic modulus of the R10 steel bar were 400 MPa, 0.0021 mm/mm and 190 GPa, respectively. Also, the yield tensile strength and corresponding strain and elastic modulus of the N12 steel bar were 600 MPa, 0.003 mm/mm and 200 GPa, respectively.

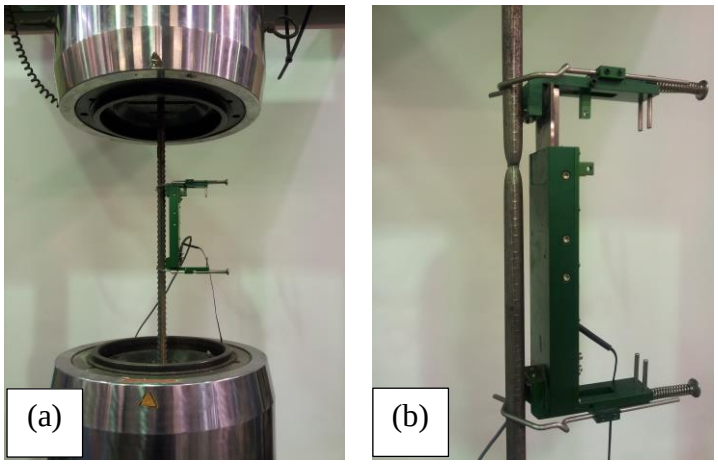

Figure 6.2. Tensile test of the steel bars: (a) test set up; and (b) failure of the tested specimen

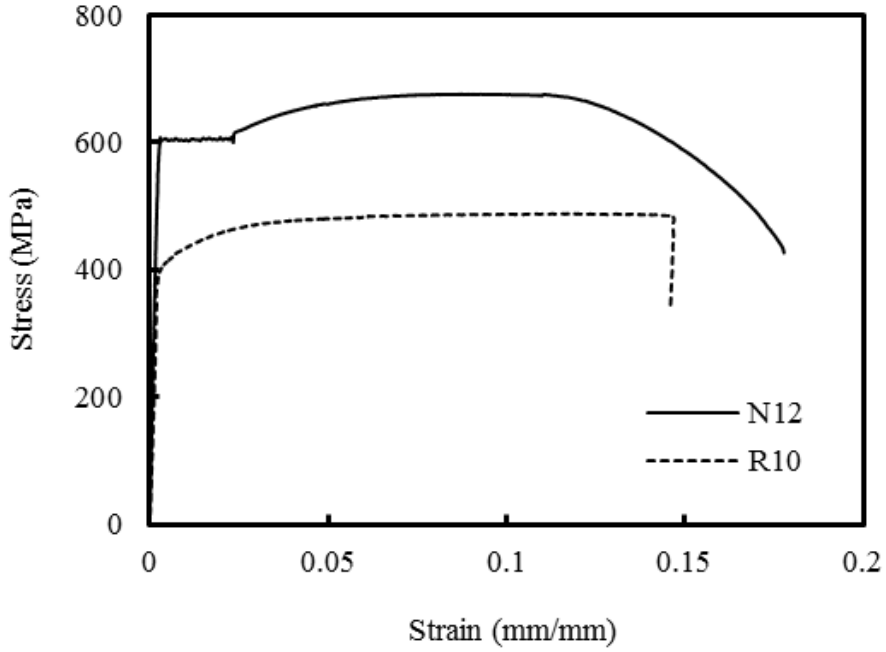

Figure 6.3. Stress-strain behaviour of steel bars

6.3.3 GFRP bars

Sand coated #4 GFRP bars were used for longitudinal reinforcement and sand coated #3 GFRP helices were used for transverse reinforcement. The GFRP bars and helices used in this study had a sand-coated surface to enhance the bond strength between the bars and the surrounding concrete. The GFRP bars and helices were provided by V-Rod Australia[131]. Cross-sectional areas of the #3 and #4 GFRP bars were determined by immersion test according to ISO 10406-1:2015[132]. Five pieces of GFRP bars of 100 mm long for each diameter bars were used to calculate representative cross-sectional dimensions. The average areas of the GFRP bars from the immersion test were 95 and 168 mm^2 for #3 and #4 bars, respectively. Also, five

pieces from the same GFRP bar for each of the two diameter bars with a test length (L) of 40 times the diameter of the bars plus the required gripping length at both ends as shown in Figure 6.4 were tested to determine the mechanical properties of the GFRP bars as recommended in ASTM D7205/D7205M−11[133]. The ultimate tensile strength and elastic modulus of the GFRP bars were determined using the standard areas of the GFRP bars because the sand coat only increases the bond between the bars and surrounding concrete. Figure 6.5 shows the stress-strain behaviour of the tested GFRP bars. The average ultimate tensile strength and corresponding strain and elastic modulus of #3 GFRP bars were 1700 MPa, 0.0224 mm/mm and 76 GPa, respectively. Also, the average ultimate tensile strength and corresponding strain and elastic modulus of #4 GFRP bars were 1600 MPa, 0.0242 mm/mm and 66 GPa, respectively.

6.3.4 CFRP sheets

In this study, CFRP sheets were used to fully wrap the specimens in Group CG6-G60 and the both ends of the other column specimens in the hoop direction. The CFRP sheet was 75 mm wide with a unidirectional fibre density of 340 g/m^2 and thickness of 0.45 mm. The mechanical properties of the CFRP sheets were found by coupon test as recommended in ASTM D7565/D7565M-10[134]. Five samples of two layers of CFRP sheets with 25 mm width and 250 mm length as shown in Figure 6.6 were tested. The average maximum tensile load and the corresponding strain were 1125 N/mm and 0.0147 mm/mm, respectively. Also, the tensile modulus of elasticity was 85 GPa. Figure 6.7 shows the stress-strain behaviour of the tested CFRP sheets.

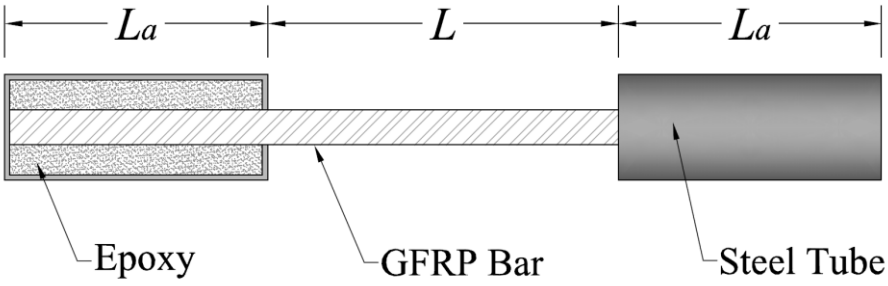

(a)

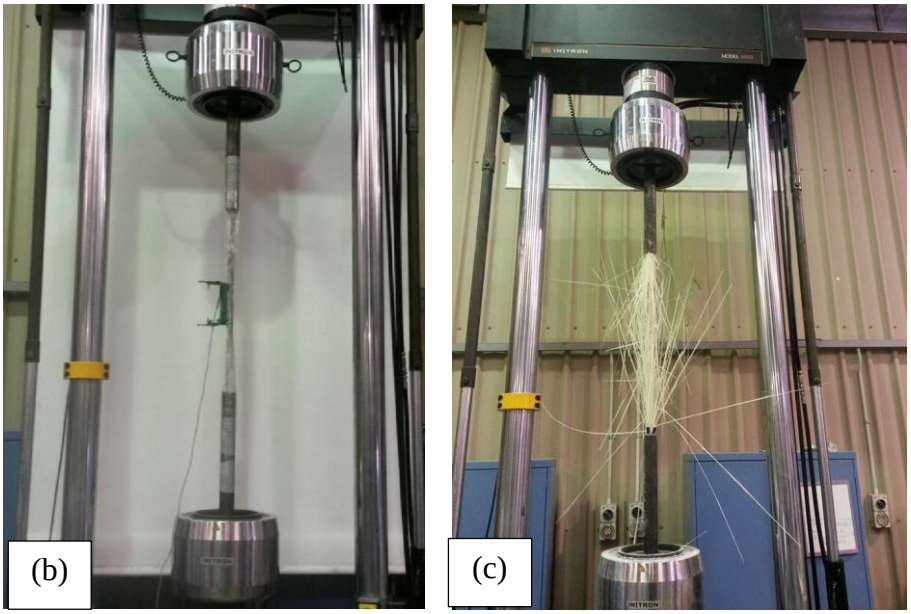

Figure 6.4. Tensile test of the GFRP bars: (a) dimensions for GFRP bars test; (b) test set up; and (c) failure of the tested specimen

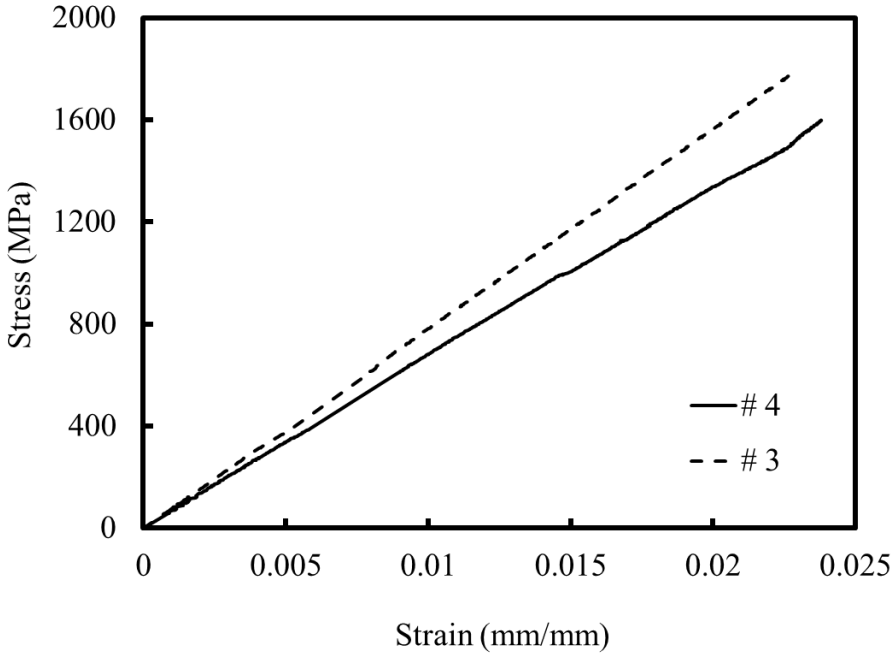

Figure 6.5. Stress-strain behaviour of GFRP bars

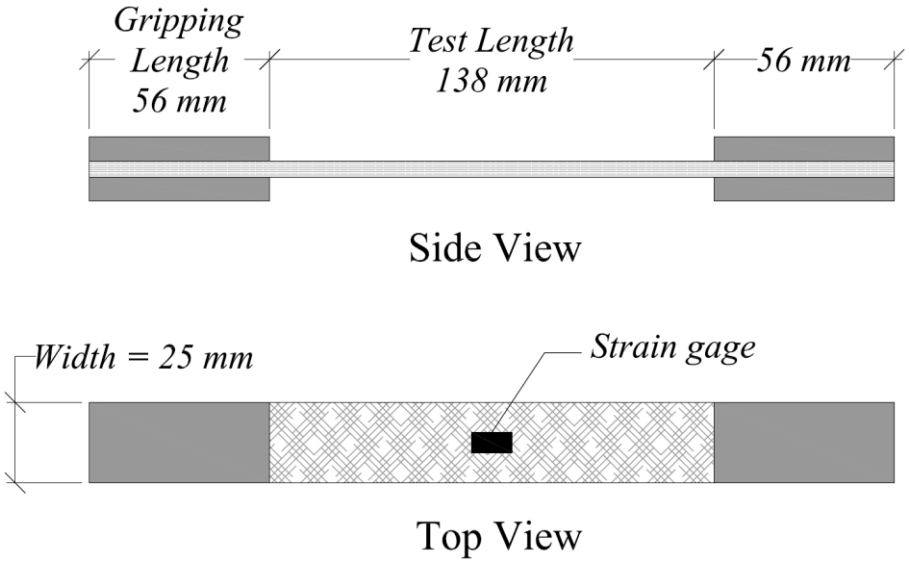

Figure 6.6. Coupon test dimensions for CFRP sheets

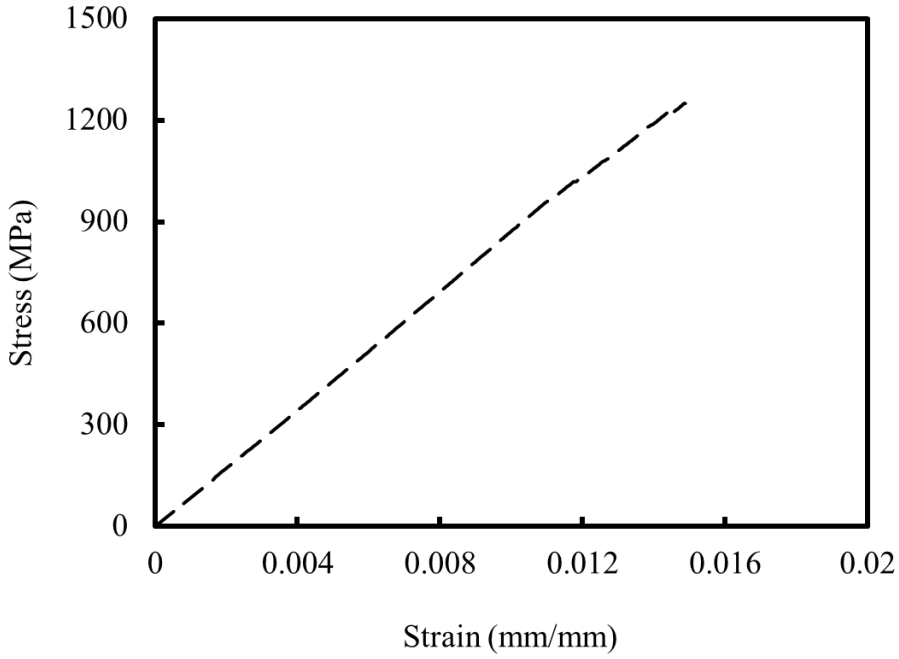

Figure 6.7. Stress-strain behaviour of CFRP sheets

6.4 Fabrication and testing of the specimens

6.4.1 Specimen fabrication

The formwork used for casting the concrete specimens was PVC pipe with internal diameter of 205 mm and 800 mm in length. Before pouring of the concrete the formworks were vertically fixed and tied by using plywood and timber in order to prevent movement during the pouring and vibrating of the concrete mix as shown in Figure 6.8. The longitudinal steel and GFRP reinforcement were prepared and cut to 760 mm length in order to have 20 mm clear cover at the top and bottom of the reinforcement cage. The transverse steel helix was prepared by forming a coil with 170 mm outer diameter and 60 mm pitch. The GFRP helices were manufactured in a

coil shape with 170 mm outer diameter by the manufacturer V-Rod Australia[131]. The clear covers to the face of the helices were 17.5 mm for all the specimens. The steel and GFRP reinforcement cages assembled for the specimens are shown in Figure 6.9. Concrete was placed into the formwork in three stages. In every stage concrete was vibrated using an electric vibrator to compact and to remove any air bubbles. The specimens were cured by covering them with wet hessian and plastic sheets to maintain the moisture conditions. The curing process lasted 28 days before testing the specimens.

Figure 6.8. PVC formworks

G6-G60 G6-G30 S6-S60 00-G60 00-G30

Figure 6.9. Reinforcement cages

6.4.2 CFRP wrapping of the specimens

The specimens in Group GIV were fully wrapped with two layers of CFRP sheets. The top and bottom parts of the unconfined column specimens were also wrapped by CFRP sheets to prevent the premature cracking of concrete during axial compression tests. The CFRP confinement was made by wrapping two layers of CFRP sheets in the hoop direction by a wet lay-up process. The bonding agent is a mixture of epoxy resin and hardener with a ratio of 5:1. Firstly, epoxy resin was spread onto the surface of the specimens and the first layer of CFRP is attached. After forming each layer, the specimens were left to develop enough bond strength with the CFRP layer for a couple of hours and the next layer was applied with a 100 mm overlap to maintain sufficient bonding strength. Also, the epoxy mixture was applied to the

surface of the last layer of CFRP in order to harden the CFRP and ensure perfect bonding.

6.4.3 Instrumentation

The specimens were instrumented internally and externally to capture the axial and lateral deformations of the specimens and the axial and hoop strain in the reinforcement as shown in Figure 6.10. For concentric loading, the axial deformation of the columns was recorded by two Linear Variable Differential Transducers (LVDT) attached vertically to the loading plate at two opposite corners. Also, before casting the concrete, two electrical strain gauges were attached at the mid-height in the two opposite longitudinal bars (one in the compression side and the other in the tension side) in order to capture the axial strain at these bars. In addition, two electrical strain gauges were attached at mid-height in the two opposite sides of the helical reinforcement to measure the strain in the hoop direction. For the specimens with CFRP sheets, two electrical strain gauges were also attached at the mid-height in the two opposite sides of the CFRP wrap to measure the strain in the hoop direction. In addition, a lazer triangulation was used for the columns under eccentric loads to record the lateral deformation at the mid-height of the columns. For the flexural loading, the lazer triangulation was fixed vertically at the bottom of the beams to record the mid-span deflection.

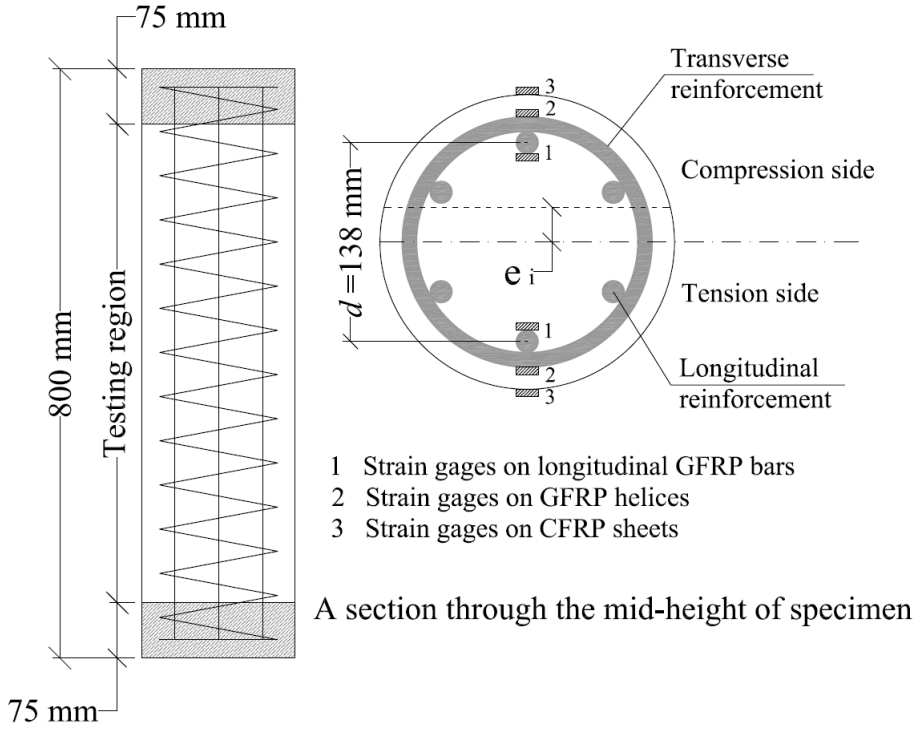

Figure 6.10. Strain gauges location

6.4.4 Testing Procedure

The Denison 5000 kN compression testing machine was used to test the specimens. The top and bottom of the specimens were wrapped by a single layer of CFRP sheet to prevent the premature failure of the concrete during axial compression tests. The width of the CFRP sheet was 75 mm. Also, both ends of the specimens were capped with high-strength plaster in order to distribute the load uniformly. The eccentric loading system consisted of two steel loading heads with two steel plates on top and bottom of the columns with an overhang edge (or loading knives) as shown in Figure 6.11(a). Also, the flexural loading system consisted of two rigs at top and bottom of the beams. The span of the beam specimens was 700 mm and spacing between the loads was 233.3 mm, as shown in Figure 6.11(b).

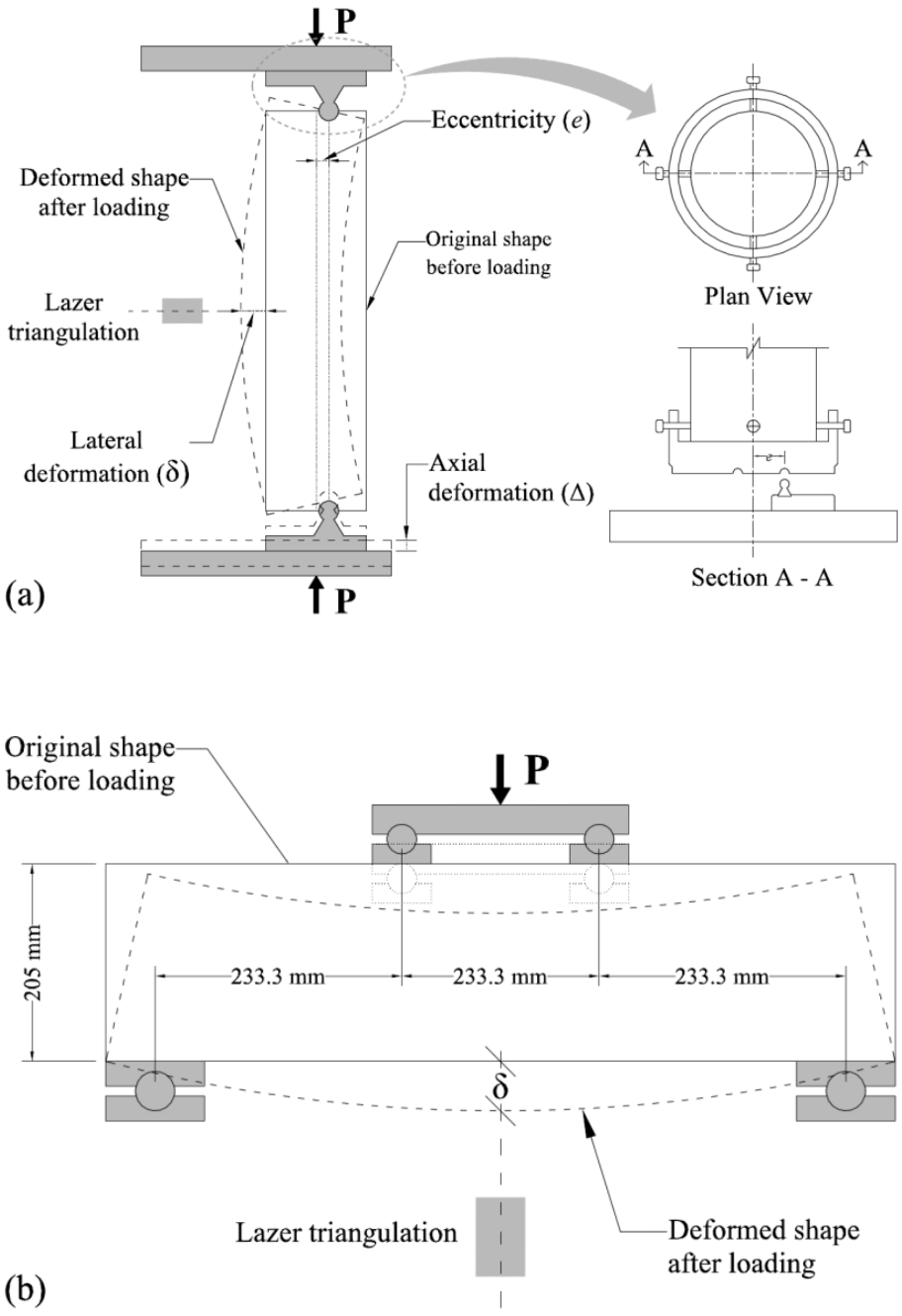

Figure 6.11. Testing of specimens: (a) columns under eccentric load; and (b) beams under flexural load

The test stared with a force-controlled pre-loading the specimens at a rate of 2 kN/s to about 10% of the yield loads of the specimens and then unloading the specimens to 20 kN. Afterwards, the test resumed with displacement control loading (0.005 mm/s) until the resistance of the specimens dropped to 30% of the yield load or until the axial displacement reached 40 mm. The applied axial load and displacement of the tested specimens were recorded through the internal load cell of the Denison testing machine. Also, the experimental test results were recorded through the LVDTs, lazer triangulation, the strain gauges, and a sensor located on the bottom of the testing machine to capture the applied axial load and displacement of the specimens. The LVDTs, strain gauges, the lazer triangulation and the sensor were connected to a data-logger to record the readings at every 2 seconds. Typical test set ups for a column and a beam specimens are shown in Figure 6.12.

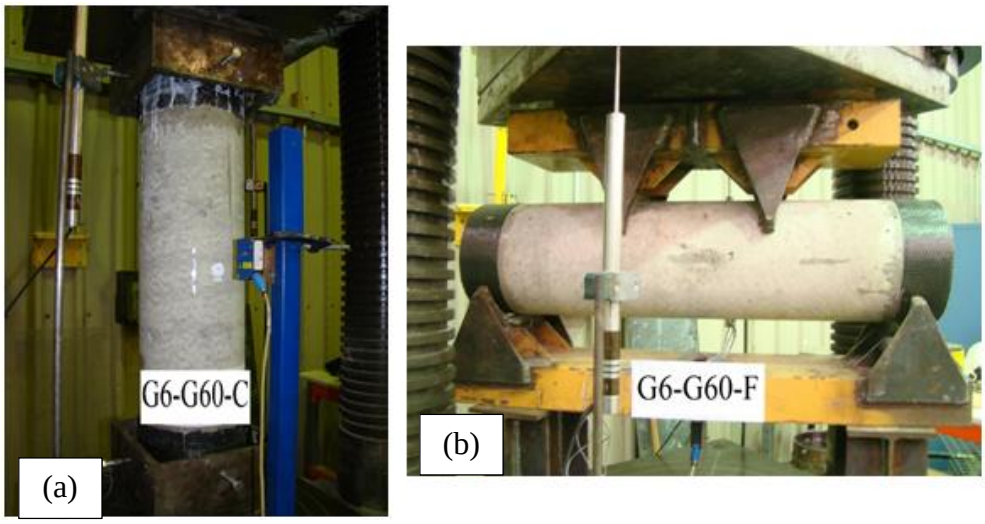

Figure 6.12. Typical testing set up of the tested specimens: (a) Column specimen; and (b) Beam specimen

6.5 Experimental results

6.5.1 Failure modes

All the specimens were tested to failure. The failure modes depended on the reinforcement materials and the loading conditions. For the specimens under concentric loads, the vertical hairline cracks appeared at around 90% of the first peak loads. With the progression of the applied axial loads, the cracks propagated and caused cover spalling in the specimens without CFRP sheet. Afterwards, the cracks were initiated in the concrete core, which led to dilate the concrete core and produce stresses in the confining material (helices and sheets). The produced stresses in the confining materials held the concrete core and provided enough stiffness to carry sustained loads without failure. The failure of the reference specimen (S6-S60-C) under concentric loading was caused by buckling of the longitudinal bars followed by crushing of the concrete core. However, the failure of the GFRP-RC specimens under concentric loads was due to the rupture of the GFRP helices and CFRP sheets followed by buckling and fracturing of the longitudinal bars and crushing of the concrete core. The failure mode of the tested specimens under concentric loads is shown in Figure 6.13.

S6-S60-C

G6-G60-C

G6-G30-C

00-G60-C

00-G30-C

CG6-G60-C

Figure 6.13. Failure mode of tested specimen under concentric loads

The specimens under eccentric loads failed due to crushing of the concrete in the compression side. The horizontal hairline cracks of the unwrapped column specimens appeared at about 85% of the first peak load in the compression side. The cracks led to spalling of the concrete cover after first peak load and reduction of the load carrying capacity of the column specimens. With progression of the applied load, the strain in the GFRP helices increased due to dilation of the concrete core in the compression region. Therefore, the specimens carried more load and the second ascending part was observed for most of the specimens. However, because cover

spalling did not happen in the CFRP wrapped specimens, the load did not reduce and continuously increased until failure of the specimens. The confined specimens with CFRP sheets failed by rupture of the CFRP sheets in the compression side. The spacing of the horizontal cracks in the tension side depended on the reinforcing materials and the pitch of the helices. The spacing of the cracks in the steel-RC specimens was about 60 mm, which was approximately 6.3% smaller than the crack spacing of the corresponding GFRP-RC specimens. The spacing of the cracks in the specimens with 30 mm pitch of GFRP helix (about 54 mm) were about 15.6% smaller than the specimens with 60 mm pitch of GFRP helix (about 64 mm). The failure modes of the tested specimens under eccentric loads are shown in Figure 6.14.

The failure of the beam specimens (S6-S60-F and G6-G30-F) was also caused by concrete crushing in the compression region. The failure of Specimen G6-G30-F was marked as a brittle failure because of the behaviour of GFRP bars which is linear elastic until failure. However, Specimen G6-G60-F failed in shear after reaching the yield load because the provided lateral reinforcement was not enough to carry the shear force until the ultimate flexural load carrying capacity. Also, the shear span of the tested beam specimens was less than twice of the effective depth of the cross-section. Beam Specimen CG6-G60-F failed by concrete crushing at the supports. The failure modes of the tested specimens under flexural loads are shown in Figure 6.15.

S6-S60-E25 G6-G60-E25 G6-G30-E25 CG6-G60-E25

S6-S60-E50 G6-G60-E50 G6-G30-E50 CG6-G60-E50

Figure 6.14. Failure mode of tested specimen under eccentric loads

S6-S60-F G6-G60-F G6-G30-F CG6-G60-F

Figure 6.15. Failure mode of tested specimen under flexural loads

6.5.2 Behaviour of column specimens

In general, the axial load and deformation (axial or lateral) behaviour of the column specimens can be divided into three phases. The first phase is the ascending part of the load-deformation curve. The second phase is a sharp descend of the axial load within a small amount of axial and lateral deformation which is caused by the spalling of concrete cover. The third phase is a descending or an ascending axial load of the column specimens with increasing axial and lateral deformation until failure of the column specimens. There were also two main points which were the first and the second peak load in the load-deformation curve of the GFRP-RC specimens. The first peak load in the load-deformation curve shows the maximum axial load carried by the reinforced gross concrete cross-section (concrete core and cover). At this point, the concrete covers may have been cracked and cover spalling started afterwards. The second peak load expresses the maximum axial load carried by the confined concrete core (without concrete cover). In some cases, the second peak load was greater than the first peak load depending on the confinement conditions. However, the steel-RC specimens only experienced the first peak load because the longitudinal steel bars reached the yield strain and the steel helices reached about 50% of yield strain at the first peak load. The CFRP confined specimens, however, only achieved the second peak load because concrete cover spalling did not take place. Also, the transition between the first and the second ascending parts of the load-deformation curve was a continuous smooth curve.

The ductility based on energy absorption of the column specimens after the first peak load (P_1) was used in this study. The ductility $(I_5 \text{ and } I_{10})$ defined in Foster and

Attard[135] was computed based on area under the axial load-axial deformation curves. I_5 is the area of ADE (Figure 6.16) divided by the area ABC, where C corresponds to Point Δ_{75} and E corresponds to Point $3\Delta_{75}$. Also, I_{10} is the area of AFG divided by the area of ABC, where G corresponds to Point $5.5\Delta_{75}$. Point Δ_{75} is the deformation corresponding to the intersection point of an extension line through the origin and 0.75 times of the first peak axial load and a horizontal line from the first peak axial load, as shown in Figure 6.16.

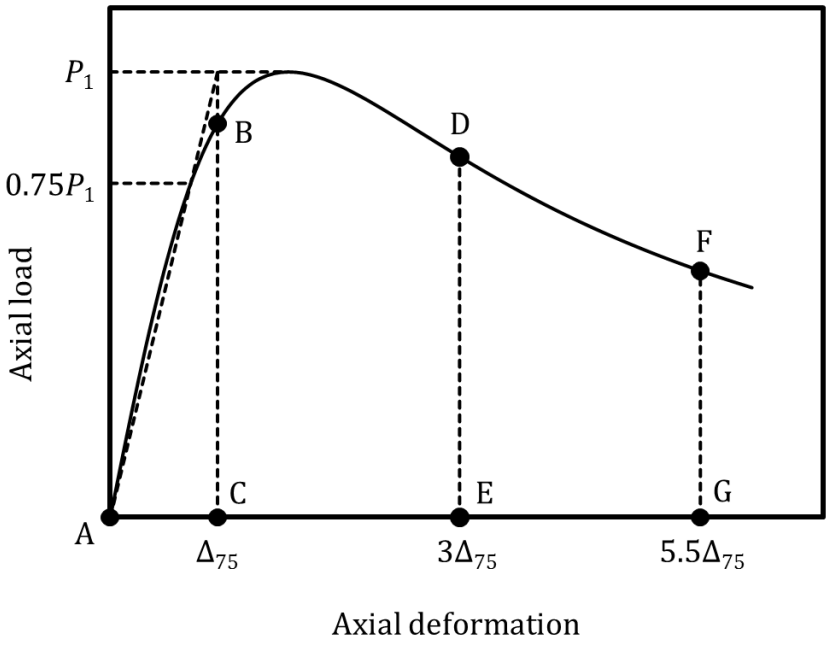

Figure 6.16. Ductility measurement for the column specimens

6.5.2.1 Column specimens under concentric load

Figure 6.17 shows the axial load-axial deformation behaviour for the tested column specimens under concentric loads. It can be seen that the ascending part of the load-

deformation curve of the column specimens followed the same pattern until first peak load and was dominated mainly by the concrete strength. It can be noticed that the ascending part of Specimen 00-G60-C is slightly smaller than the other specimens, although the difference is not significant. This slight difference may be because concrete is a composite and non-homogeneous material that different factors such as placing, compacting and curing may affect the strength and properties of concrete[136].

Specimen G6-G60-C obtained about 20% lower first peak load than the first peak load of the reference specimen (S6-S60-C) because of the lower modulus of elasticity of the GFRP bars. However, the ductility of the GFRP-RC specimen (G6-G60-C) was slightly greater than the reference specimen (S6-S60-C). This is because the axial and hoop strain of the GFRP bars and helices at first peak load were less than 20% and 5%, respectively, of their ultimate strain. Whereas, the steel bars reached the yield strain and the steel helices reached about 50% of the yield strain at first peak load. Therefore, it is expected that the GFRP-RC columns will carry more loads and deformations after the first peak load. Hence, most of the GFRP-RC column specimens achieved greater second peak load than the first peak load. Also, it can be observed that the contribution of the longitudinal steel bars in the first peak load of the columns was about 26.6%. The contribution of the steel bars was about two times greater than the contribution of the longitudinal GFRP bars (about 13.4%).

Reducing the spacing of the GFRP helices from 60 to 30 mm led to increase in the first peak load and ductility by about 7% and 29%, respectively. It can also be

observed that increasing the lateral GFRP reinforcement could improve the ductility more than the first peak load. This is because the GFRP helices were not completely activated before the cover spalling. The strains in the GFRP helices were smaller than 5% of the ultimate tensile strain. In contrast, after cover spalling and dilation of the concrete core, the GFRP helices were activated and resulted in improving the second peak load and ductility of the GFRP-RC column specimens.

In general, the specimens with longitudinal GFRP bars performed better in comparison with the corresponding specimens without longitudinal bars in terms of load carrying capacity and ductility. The specimens with longitudinal GFRP bars achieved about 13% and 52% greater first and second peak loads, respectively, than the corresponding specimens without longitudinal bars. Also, the contribution of the longitudinal GFRP bars in the first and the second peak load of the GFRP-RC column specimens was about 13.4 and 23%, respectively. The longitudinal GFRP bars considerably improved the ductility of the specimens with 60 mm pitch of GFRP helix, which may be because the longitudinal GFRP bars reduced the unconfined concrete areas between the helices and caused the concrete core to undergo a large axial deformation. However, the influence of the longitudinal GFRP bars in the improvement of the ductility in the specimens with 30 mm pitch of GFRP helix was not very significant. This may be because the smaller pitch GFRP helix effectively confined the concrete core and the effect of longitudinal bars in confining the concrete core was not as significant. Confining the specimens with CFRP sheet led to the increase of the second peak loads by 115%. Also, the ductility of the

specimens improved considerably by reducing the pitch of GFRP helices and externally confining the specimens with CFRP sheets.

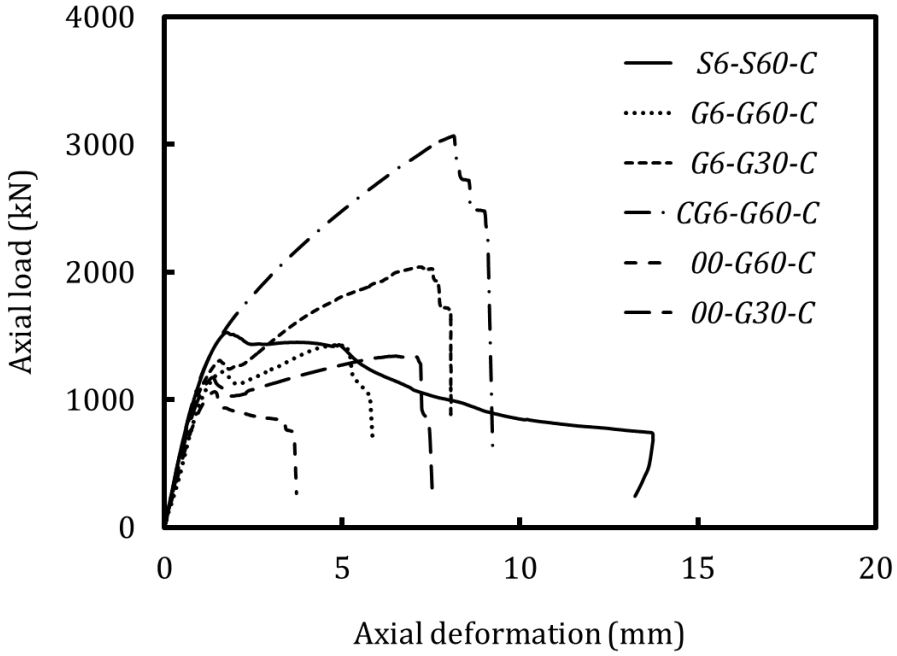

Figure 6.17. Axial load-axial deformation behaviour of column specimens tested under concentric loads

Table 6.3 reports the experimental results of tested column specimens under concentric load. The experimental results of unconfined concrete strength (f'_{co}) were calculated as:

$$f'_{co} = \frac{P_1 - P_{bar\,1}}{A_g - A_{bar}} \tag{6.1}$$

where P_1 and $P_{bar\,1}$ are the first peak load and the corresponding loads carried by the longitudinal bars, respectively, A_g is the gross cross-sectional areas of the specimens and A_{bar} is the total area of the longitudinal reinforcing bars. The results showed that the ratio of unconfined concrete strength to the cylinder compressive strength

(f'_{co}/f'_c) is on average greater than 0.85 which is defined in ACI 318-14[40]. However, the ratio of f'_{co}/f'_c was in the range of the recorded values between 0.81 to 0.97 in the previous studies[44, 137-139].

The experimental confined concrete strength (f'_{cc}) of the column specimens under concentric loads was calculated as:

$$f'_{cc} = \frac{P_2 - P_{bar\,2}}{A_{core} - A_{bar}} \tag{6.2}$$

where P_2 and $P_{bar\,2}$ are the second peak load and the corresponding loads carried by the longitudinal bars, respectively, and A_{core} is the area of confined concrete core with diameter d_c that is measured as the distance between the centreline of the GFRP helices. It can be observed that reducing the pitch of the GFRP helices from 60 to 30 mm improved the performance of the column specimens, as the second peak increased by about 43%. Also, CFRP wrapping of Specimen CG6-G60-C led to the increase in the second peak load by more than twice the corresponding specimen (G6-G60-C) without CFRP wrap. Reducing the GFRP pitch from 60 to 30 mm led to increasing the confined concrete strength by about 38%. Also, the CFRP wrap increased the confined concrete strength by about 36%. The ratio of hoop rupture strain to the ultimate tensile strain (k_ε) was about 0.333 and 0.75 for the GFRP helices and CFRP sheets, respectively. This difference is due to the fact that the concrete core in the case of the GFRP helices was not fully confined. Therefore, a lesser ratio of the GFRP ultimate strain was utilised by the dilation of the concrete core. In addition, the ultimate tensile strain of the GFRP helices was about two times of the CFRP sheet.

Table 6.3. Experimental results of column specimens tested under concentric loads

Specimen	First peak			Second peak			Ductility	
	Axial load (kN)	Bar load [a] (kN)	f'_{co} [b] (MPa)	Axial load (kN)	Bar load [a] (kN)	f'_{cc} [c] (MPa)	I_5	I_{10}
S6-S60-C	1528	407	34.0	-	-	-	4.8	8.7
G6-G60-C	1220	163	32.0	1425	307	57.4	5.0	9.0
G6-G30-C	1309	148	35.2	2041	494	79.4	5.1	11.6
CG6-G60-C	-	-	-	3068	593	76.8	-	-
00-G60-C	1063	0.0	32.2	945	0.0	46.7	4.4	5.1
00-G30-C	1170	0.0	35.4	1343	0.0	66.4	4.7	9.9

[a] Bar load = (Strain x Elastic modulus x Area) of bars

[b] Calculated using Equation 6.1

[c] Calculated using Equation 6.2

6.5.2.2 Column specimens under eccentric load

Table 6.4 reports the experimental results of tested column specimens under eccentric loads. Figure 6.18 shows the axial load versus the axial and lateral deformations behaviour of the tested column specimens under 25 mm eccentric loads. In general, the GFRP-RC columns under eccentric loads exhibited a slightly smaller stiffness in the ascending part of the load-deformation curves than the steel-RC column specimens because of the lower modulus of elasticity of the GFRP bars than the steel bars. Similar to the columns under concentric loads, the GFRP-RC column specimen gained lower first peak load by about 13% than the first peak load of the reference column specimen. Also, the ductility of Specimen G6-G60-E25 was slightly greater than the ductility of the reference specimen (S6-S60-E25). Increasing the amount of GFRP helices did not increase the first peak load of the column specimens because the smaller spacing of GFRP helix created a separation plane between the concrete cover shell and the concrete core which led to instability of the concrete shell and cover spalling at an early stage[68, 70]. However, the ductility and second peak load of the columns increased due to the reduction of the spacing of the GFRP helices from 60 mm to 30 mm. Also, wrapping the column specimens with CFRP sheets also increased the second peak load by 93% under 25 mm eccentric loads in comparison with the corresponding specimens without wrapping (G6-G60-E25).

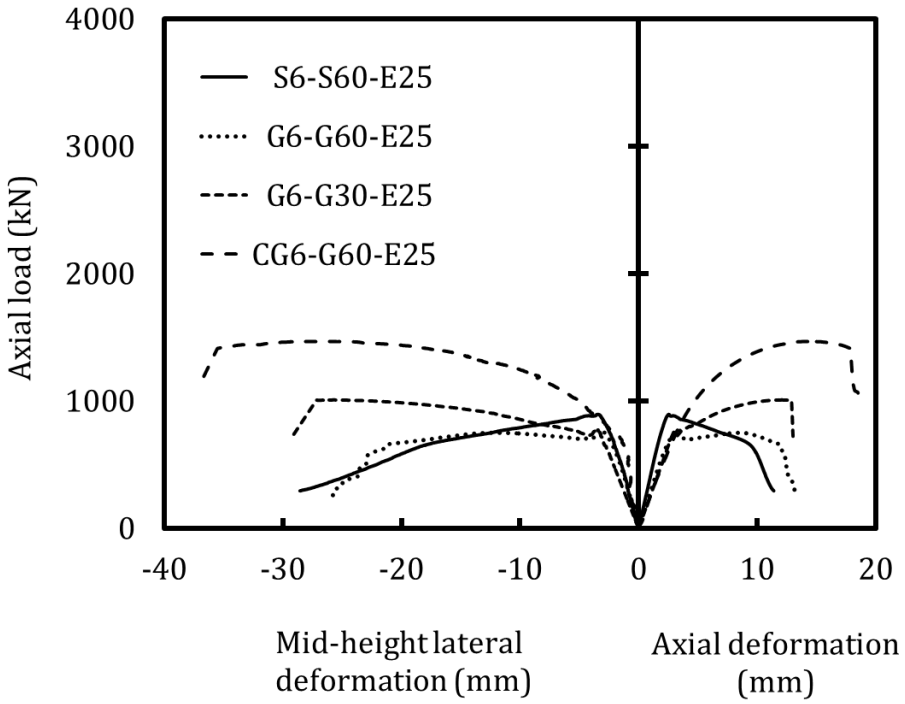

Figure 6.18. Axial load-deformation behaviour of column specimens tested under 25 mm eccentric loads

Figure 6.19 shows the axial load versus axial and lateral deformations behaviour of the tested column specimens under 50 mm eccentric loads. Specimen G6-G60-E50 achieved about 17% lower first peak load and slightly greater ductility compared to the first peak load and ductility of the reference specimen (S6-S60-E50). Similar to the specimens under 25 mm eccentric loads, the specimens with 60 mm pitch achieved about 3% greater first peak load than the first peak load of specimens with 30 mm pitch. However, the ductility (I_{10}) increased by about 57% as a result of the reduction of helices spacing from 60 mm to 30 mm. This is because the smaller spacing helix led to better confined concrete core and allowed the columns to sustain

more loads with increasing axial deformation. Confining the column specimens with CFRP sheets also increased the second peak load by 75% under 50 mm eccentric loads in comparison with the corresponding specimens without wrapping (G6-G60-E50).

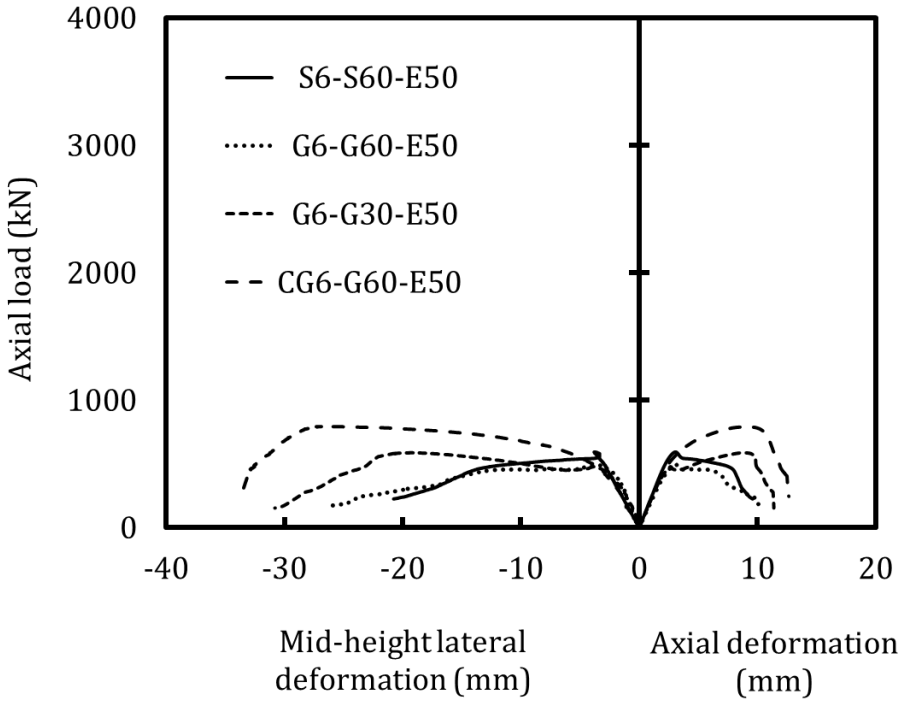

Figure 6.19. Axial load-deformation behaviour of column specimens tested under 50 mm eccentric loads

Table 6.4. Experimental results of column specimens tested under eccentric loads

Specimen	First peak			Second peak			Ductility	
	Axial load (kN)	Lateral deformation (mm)	Bending moment (kN.m)	Axial load (kN)	Lateral deformation (mm)	Bending moment (kN.m)	I_5	I_{10}
S6-S60-E25	895	2.4	24.5	-	-	-	4.7	8.1
G6-G60-E25	781	2.5	21.5	751	11	27	4.8	8.6
G6-G30-E25	767	2.8	21.3	1003	19	44.1	5.5	9.2
CG6-G60-E25	-	-	-	1450	21	66.7	-	-
S6-S60-E50	594	3.2	31.6	-	-	-	4.6	5.4
G6-G60-E50	494	3.4	26.4	459	15	29.8	4.7	5.8
G6-G30-E50	479	3.7	25.7	592	22	42.6	5.5	9.1
CG6-G60-E50	-	-	-	805	28	62.8	-	-

The effects of eccentricity on the behaviour of the column specimens have been shown in Figure 6.20. In general, increase in the eccentricity led to decrease the performance of the column specimens in terms of axial load carrying capacity and ductility. In general, the first peak load of the column specimens decreased by about 40 and 60% under the 25 and 50 mm eccentricity, respectively, compared to the column specimens under concentric load.

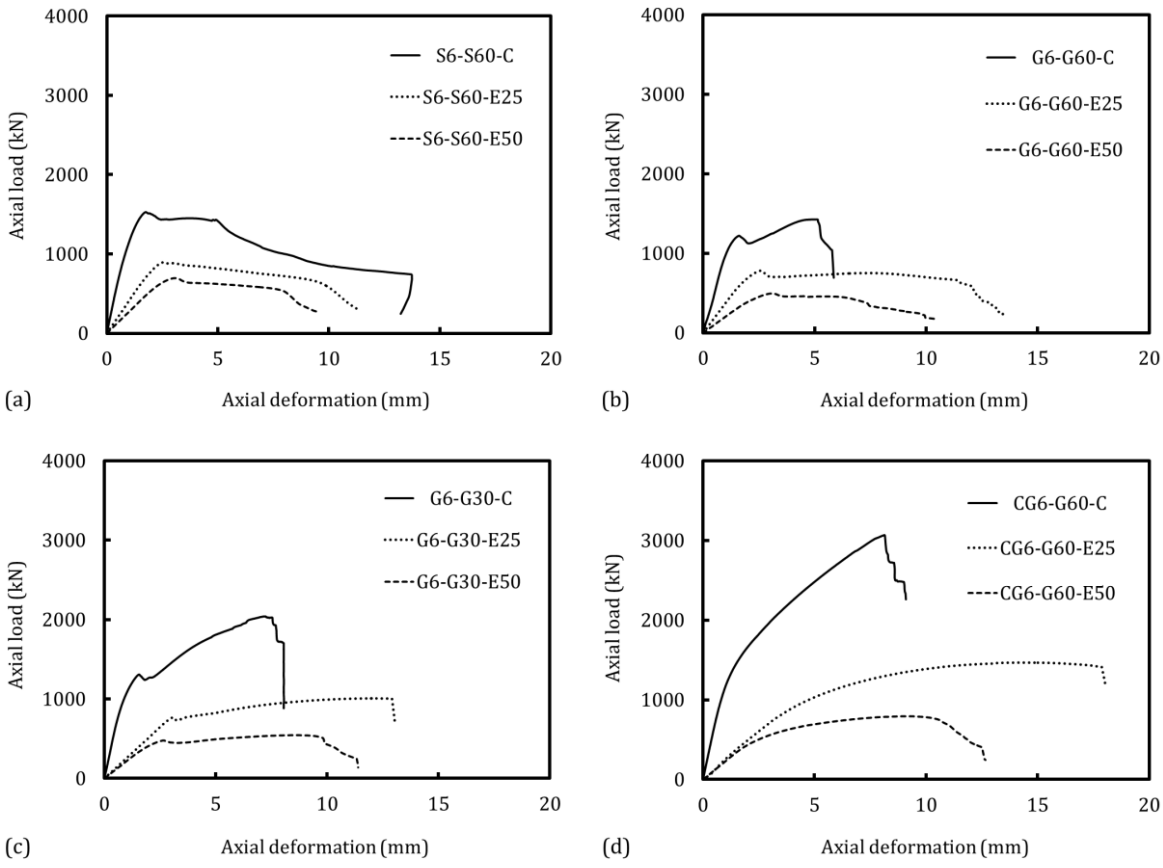

Figure 6.20. Axial load-axial deformation behaviour of column specimens tested under eccentric axial load: (a) S6-S60; (b) G6-G60; (c) G6-G30; and (d) CG6-G60

6.5.3 Behaviour of beam specimens

Figure 6.21 shows the load versus midspan deflection behaviour of the tested beam specimens under flexural loadings. It can be observed that the ascending part of the load-midspan deflection curve of the steel-RC beam has greater stiffness than the GFRP-RC beams because of the smaller modulus of elasticity of the GFRP bars. The load and midspan deflection curve of the steel-RC beam consisted of three parts which represent the yielding of the reinforcement in each layer. The first (Point A to B) and second (Point B to C) ascending parts of the load and midspan deflection curve represent the yielding of the first and the second layer of the steel reinforcement, respectively, followed by stabilizing the load-midspan deflection curve (Point C to D). With the progression of the applied load, the concrete in the compression zone reached its crushing strain and led to complete failure of the steel-RC beam specimen. However, the load-midspan deflection behaviour of the GFRP-RC beams consisted of only an ascending part and followed by a descending part because of the linear elastic stress-strain behaviour of GFRP bars.

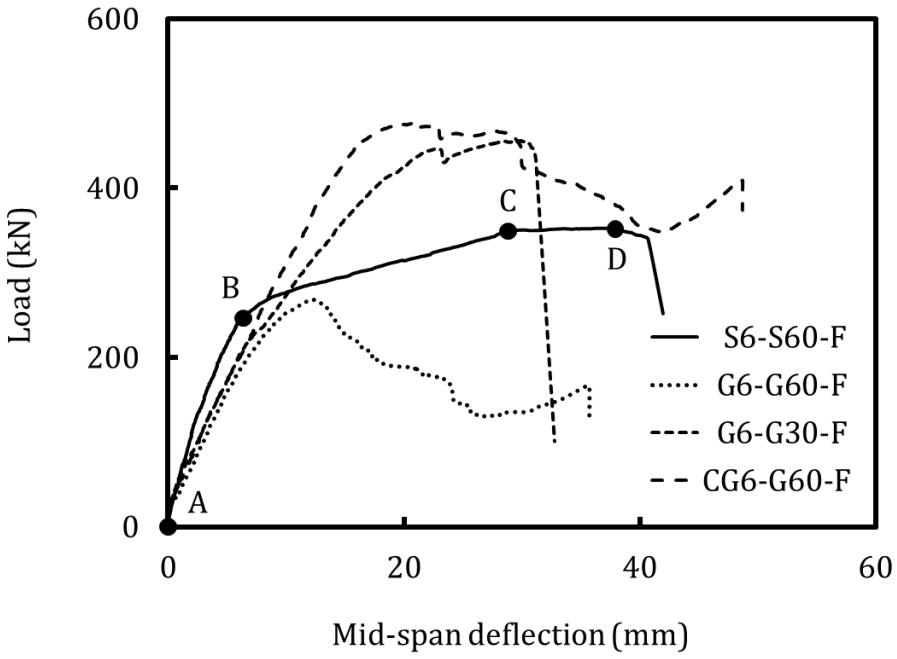

Figure 6.21. Axial load-deflection behaviour of beam specimens tested under flexural loads

Table 6.5 reports the experimental results of the tested beam specimens. Similar to the column specimens under eccentric loads, the beam specimens with 30 mm GFRP pitch obtained slightly lower first peak load than the beam specimen with 60 mm pitch because of early cover spalling. However, the smaller pitch of GFRP helix increased the second peak load of the specimens by about 69%. Wrapping the specimens with CFRP sheet also led to increasing the second peak load by about 78%. The descending part of the load-midspan deflection curve of Specimen G6-G60-F is less steep than Specimen G6-G30-F because Specimen G6-G60-F failed in shear.

Table 6.5. Experimental results of beam specimens tested under flexural loads

Specimen	First peak			Second Peak		
	Load (kN)	Midspan deflection (mm)	Bending moment (kN.m)	Load (kN)	Midspan deflection (mm)	Bending moment (kN.m)
S6-S60-F	344	6.5	40.1	-	-	-
G6-G60-F	247	9.4	28.8	268	17.5	31.3
G6-G30-F	242	8.1	28.2	452	29.9	52.7
CG6-G60-F	-	-	-	478		55.8

6.5.4 Experimental peak axial load-bending moment diagrams

Based on the axial load-deformation behaviour of the GFRP-RC specimens, there were two main points which are the first and the second peak loads. The first peak load represents the maximum load carried by the gross concrete cross-section (concrete core and cover). At this point, concrete covers may have been cracked and cover spalling started afterwards. The second peak load represents the maximum load carried by the confined concrete core. However, the confined specimens with CFRP sheets only experienced second peak load because cover spalling did not happen. Therefore, two sets of the peak axial load-bending moment $(P-M)$ diagrams were drawn for the GFRP-RC specimen corresponding to the first and the second peak loads.

The experimental bending moments at the mid-height of the column specimens under eccentric loads were calculated as:

$$M_1 = P_1\ (e_i + \delta_1) \tag{6.3}$$

$$M_2 = P_2\ (e_i + \delta_2) \tag{6.4}$$

where M_1 and δ_1 are the bending moment and lateral deformation corresponding to the first peak load (P_1), respectively; M_2 and δ_2 are the bending moment and lateral deformation corresponding to the second peak load (P_2), respectively; and e_i is the applied initial eccentricity at the end of the column specimens (

Figure 6.11a). The experimental bending moments at midspan of the beam specimens were calculated as:

$$M_1 = \frac{1}{2} P_1\ a \tag{6.5}$$

$$M_2 = \frac{1}{2} P_2\ a \tag{6.6}$$

where a is the shear span length or the distance between the support and the closer loading point (a = 233.3 mm in this study,

Figure 6.11b). The experimental bending moment of the column and beam specimens are reported in Table 6.4 and Table 6.5, respectively.

Figure 6.22 shows the peak axial load-bending moment diagrams for the tested specimens in terms of the first peak loads. It can be seen that the conventional steel-RC specimens obtained greater load and moment capacity than the GFRP-RC

specimens because of greater modulus of elasticity of the steel reinforcement. Reduction in the spacing of the GFRP helices did not considerably change the peak axial load-bending moment diagram of the GFRP-RC specimens because the passive confinement due to the GFRP helices was not considerably activated in the first peak load.

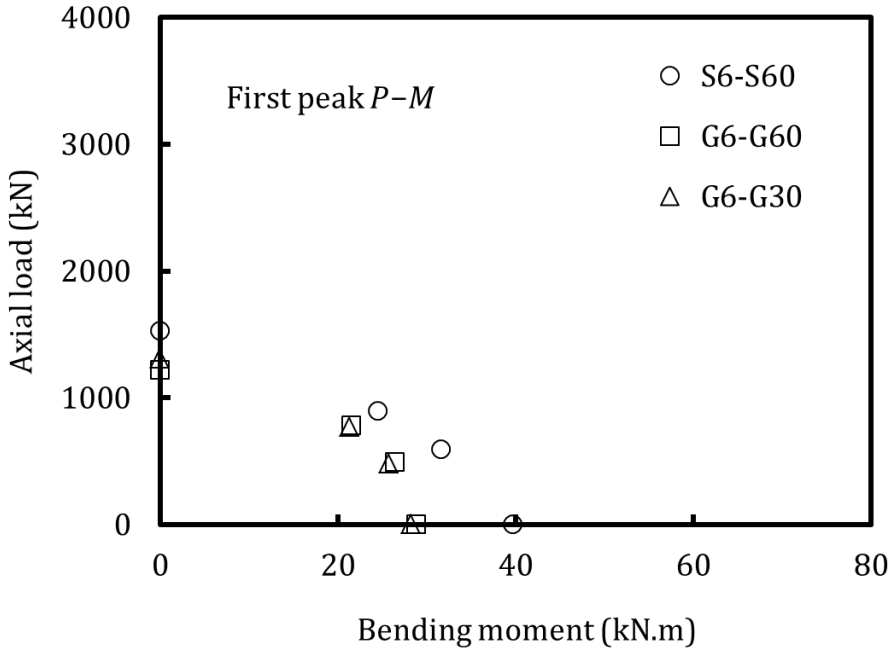

Figure 6.22. Experimental first peak $P - M$ diagram for the tested specimens

However, it is clear in Figure 6.23 that the GFRP bars and helices improved the peak axial load-bending moment diagram of the GFRP-RC specimens. This is because the modulus of elasticity of the GFRP bars is small, so larger deformation and lateral expansion are needed to achieve higher stress in the GFRP bars and helices. The efficiency of confining the specimens with the CFRP sheet on improving the strength capacity of the specimens increased with decreasing the eccentricity of the applied

axial load. This is because the area of confined concrete in the compression region increases with reducing the eccentricity.

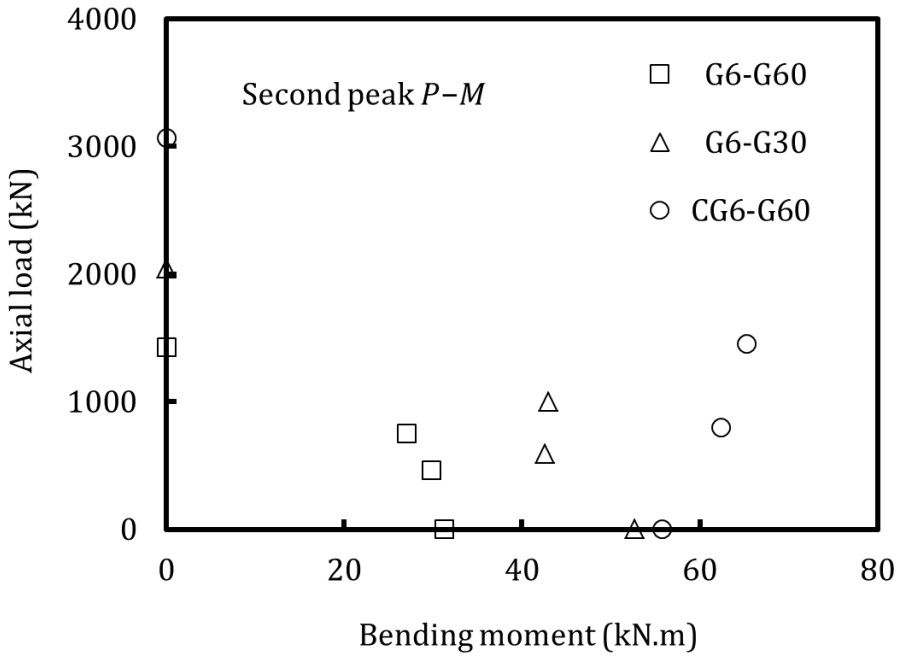

Figure 6.23. Experimental second peak $P - M$ diagram for the tested specimens

6.5.5 Experimental moment-curvature

The experimental bending moments (M) at mid-height of the tested column specimens under eccentric loads were calculated based on the applied axial load (P), the initial eccentricity (e_i) at the end of the column specimens and the mid-height lateral deformation (δ) as:

$$M = P\ (e_i + \delta) \tag{6.7}$$

The experimental curvatures (κ) corresponding to the bending moments were calculated based on the strain gauge readings at the longitudinal GFRP bars in the compression (ε_{fc}) and the tension side (ε_{ft}) and the distance between them (d) (Figure 6.10) as:

$$\kappa = \frac{\varepsilon_{fc} - \varepsilon_{ft}}{d} \tag{6.8}$$

where the compression strain, stress and force are considered as positive and the tension strain, stress and force are considered as negative, in this study.

Figure 6.24(a and b) shows the experimental moment-curvature $(M - \kappa)$ behaviour of the tested specimens under 25 and 50 mm eccentricity, respectively. It can be observed that reducing the pitch of the GFRP helices from 60 to 30 mm did not considerably change the bending moment of the specimens corresponding to the first peak load. This is because the passive confinement from the GFRP helices was not considerably activated at the first peak load. In addition, the ascending part of the $M - \kappa$ curve of the specimens with 30 mm pitch was slightly smaller than the 60 mm pitch GFRP helices before the first peak moment (before cover spalling). This may be because the smaller pitch of GFRP helix create a separation plane between the concrete cover shell and the concrete core which led to instability of the concrete cover shell and cover spalling at an early stage[68, 70]. The effect of the CFRP confinement can be observed clearly at the second ascending part of the $M - \kappa$ curve and improved the performance of the CFRP confined specimens in terms of the axial load carrying capacity and bending moment.

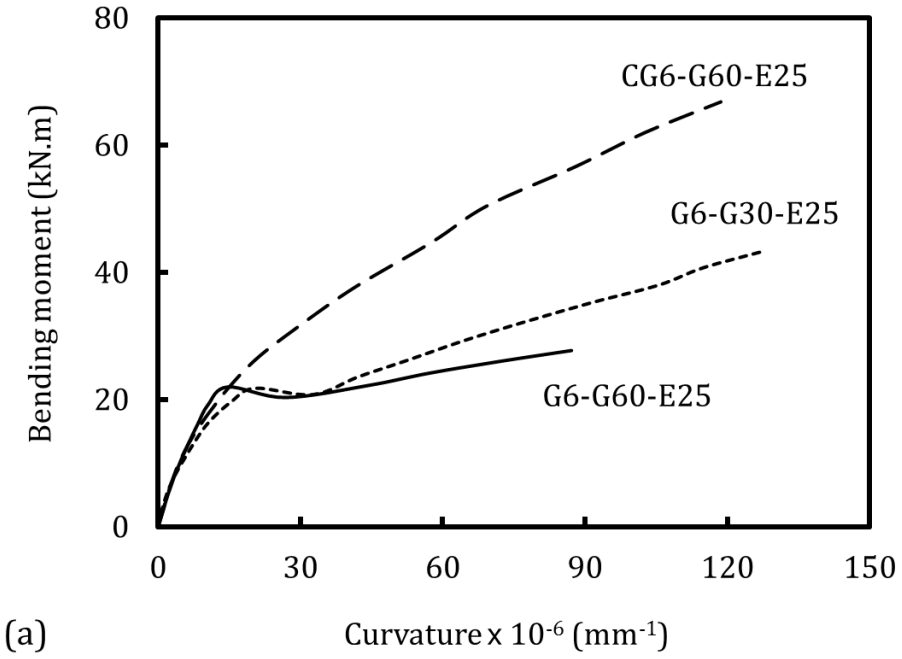

(a)

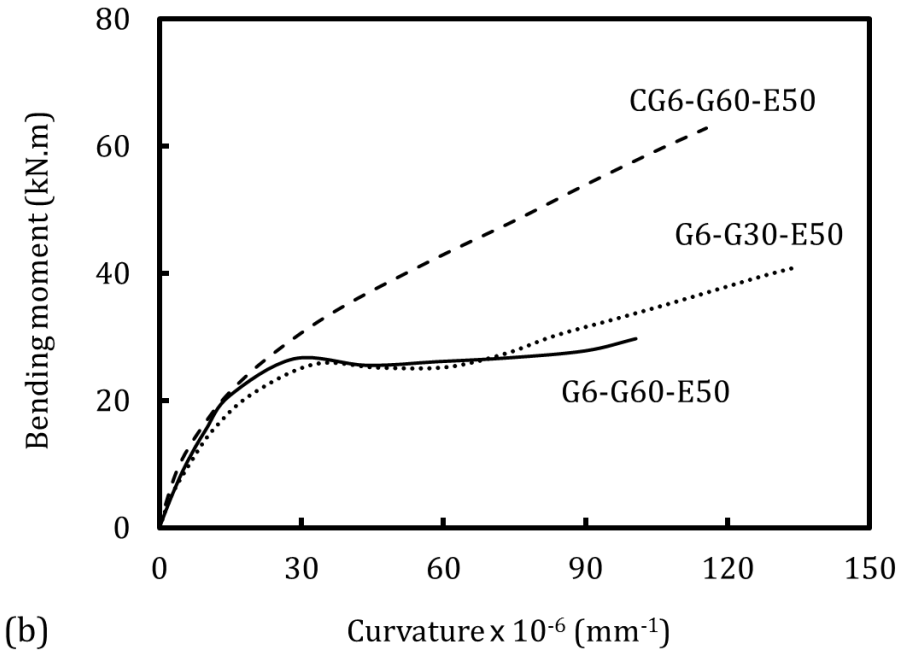

(b)

Figure 6.24. Experimental $M - \kappa$ behaviour of tested column specimens: (a) 25 mm eccentric load; and (b) 50 mm eccentric load

6.6 Summary

A detailed descriptions of preparing and testing 18 circular concrete specimens reinforced with steel, GFRP bars and GFRP helices are presented in this chapter. The specimens were divided into five groups based on reinforcing materials, spacing of the helices, external confinement with CFRP sheets and the longitudinal reinforcement ratio. The specimens of each group were tested under for different loading conditions. However, the specimens of the fifth group were only tested under concentric loads. Preliminary tests were conducted for the materials used in this study. Casting, instrumentation and testing procedures of the RC-specimens were also explained in detail. Afterward, the experimental results such as load carrying capacities, axial and lateral deformations, bending moments and ductility of the RC-specimens were presented. In addition, the axial load-bending moment diagrams and moment-curvature behaviour of the tested specimens were explained. It was observed that the strength capacity of the GFRP-RC specimens was smaller than the conventional steel-RC specimens. However, the ductility of the GFRP-RC specimens was slightly greater than the steel-RC specimens. Reduction in the spacing of the GFRP helices or confining the specimens with CFRP sheets improved the performance of the RC-specimens in terms of load carrying capacity, bending moments and ductility.

7 ANALYTICAL STUDY

7.1 Introduction

In this chapter, analytical calculation procedures were developed for different behaviour of the GFRP-RC specimens. In general, analytical modelling of the GFRP-RC specimens can be proposed by the behaviour of the components such as longitudinal GFRP bars, unconfined concrete cover and confined concrete core by the GFRP helices of CFRP sheets. Two analytical peak axial load-bending moment diagrams were drawn for the GFRP-RC specimens corresponding to the first and the second peak loads base on the experimental investigations. The peak axial load-bending moment diagrams were developed using two different techniques which are equivalent rectangular stress-block and numerical integration method to calculate the compression force of concrete in the compression region. In addition, the analytical axial load-axial deformation behaviour of the GFRP-RC specimens under concentric loads was demonstrated. Finally, the analytical moment-curvature behaviour of the GFRP-RC specimens under eccentric loads was explained in detail.

7.2 Section analysis

The cross-section of the specimens were analysed based on the assumptions that: (i) plane sections remain plane after deformation; (ii) perfect bond exits between the reinforcement and surrounding concrete; (iii) the tensile strength of concrete can be neglected[53]; and (iv) compressive strain, stress and force are considered as positive and tensile strain, stress and force are considered as negative. Similar assumptions are usually considered for analysing steel-RC cross-sections. The section analysis

herein is carried out considering the stress-strain behaviour of the RC cross-sectional components. The cross-section of the specimens can be divided into three components: concrete cover, concrete core and longitudinal GFRP bars. The stress-strain behaviour of concrete in the literature was based on concentric compression tests. It is usually assumed that the stress-strain behaviour of unconfined concrete under concentric load can be used for concrete in the compression region for columns under eccentric loads. However, the assumption is questionable for the stress-strain behaviour of confined concrete[140]. In contrast, Saadatmanesh et al.[141]; Yuan et al.[142]; and Jiang and Teng[143] reported that this assumption may be applicable for circular confined concrete cross-sections. Hence, the stress-strain behaviour of concrete under concentric load was used to model the stress-strain behaviour of concrete in the compression side under eccentric and flexural loads. A full composite action was also assumed between concrete core and cover.

7.2.1 Longitudinal GFRP bras

Based on the experimental studies on GFRP bars[31, 33], the stress-strain behaviour of the bars is linear elastic until failure. The compressive strength of the GFRP bars is relatively lower than the tensile strength. However, it can be assumed that tensile and compressive moduli of elasticity of GFRP bars are equal[33, 37] as shown in Figure 7.1. Therefore, the axial stress of the longitudinal GFRP bars at different points (f_f) can be represented by Equation 7.1. Also, it is assumed that the axial strain of the concrete and GFRP bars are equal at any point, considering the assumption that a perfect bonding exists between the GFRP bar and the surrounding concrete.

$$f_f = E_f\ \varepsilon_c \tag{7.1}$$

where and E_f is the modulus of elasticity of the GFRP bars and ε_c is the axial strain of the concrete.

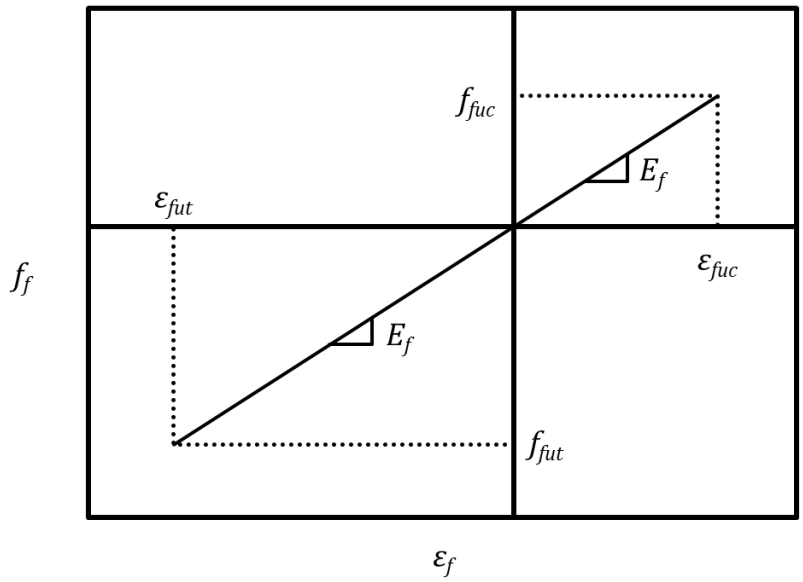

Figure 7.1. Stress-strain behaviour of GFRP bars in compression and tension

7.2.2 Unconfined concrete

The stress-strain behaviour of unconfined concrete proposed in Yang et al.[28] has been adopted in this study to model the behaviour of unconfined concrete cover for specimens without CFRP sheets.

$$f_c = \frac{(\beta + 1)(\varepsilon_c/\varepsilon_{co})}{\beta + (\varepsilon_c/\varepsilon_{co})^{\beta+1}}\ f'_{co} \tag{7.2}$$

$$\beta = 0.20\exp(0.73\xi) \quad \text{For} \quad \varepsilon_c \leq \varepsilon_{co} \tag{7.3}$$

$$\beta = 0.41\exp(0.77\xi) \quad \text{For} \quad \varepsilon_c > \varepsilon_{co} \tag{7.4}$$

$$\xi = (f_{co}/10)^{0.67}(2300/\omega_c)^{1.17} \tag{7.5}$$

$$\varepsilon_{co} = 0.0016\exp(240\ f_{co}/E_1) \tag{7.6}$$

$$E_1 = 8470(f'_{co})^{0.33}(\omega_c/2300)^{1.17} \tag{7.7}$$

where ε_c is the axial concrete strain at any concrete stress (f_c), f'_{co} is the unconfined concrete strength which is equal to 85% of cylinder compressive strength (f'_c) at age 28-days, ε_{co} is the unconfined concrete strain corresponding to f'_{co} (Figure 7.2), ω_c is the density of concrete which can be taken as 2300 kg/m^3 for normal-weight concrete and E_1 is the compressive modulus of elastic of concrete. Figure 7.2 shows the adopted stress-strain behaviour of unconfined concrete in compression used in this study.

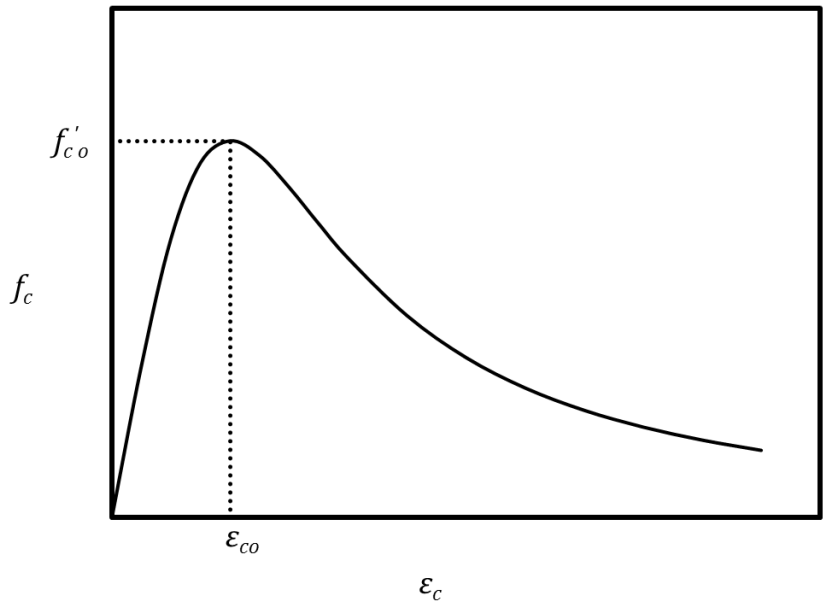

Figure 7.2. Stress-strain behaviour of unconfined concrete in compression

7.2.3 Confined concrete

The stress-strain relationship proposed in Samaan et al.[108] is adopted to model the stress-strain behaviour of the confined concrete core by the GFRP helices or the CFRP sheets in this study.

$$f_c = \frac{(E_1 - E_2)\,\varepsilon_c}{\left[1 + \left(\frac{E_1 - E_2}{f_o}\varepsilon_c\right)^n\right]^{1/n}} + E_2\,\varepsilon_c \quad \text{For} \quad \varepsilon_c \le \varepsilon_{cc} \tag{7.8}$$

$$f_c = 0 \quad \text{For} \quad \varepsilon_c > \varepsilon_{cc} \tag{7.9}$$

$$E_2 = \frac{f'_{cc} - f_o}{\varepsilon_{cc}} \tag{7.10}$$

$$n = 1 + \frac{1}{E_1/E_2 - 1} \tag{7.11}$$

where E_2 is the slope of the second ascending part of stress–strain curve of confined concrete, ε_{cc} is the compressive axial strain corresponding to the ultimate confined concrete strength (f'_{cc}), n is the curve-shape parameter and f_o is the intercept of the second ascending slope with the stress axis as shown in Figure 7.3. The $f_o = f'_{co}$ can be used for simplicity as proposed in Lam and Teng[89].

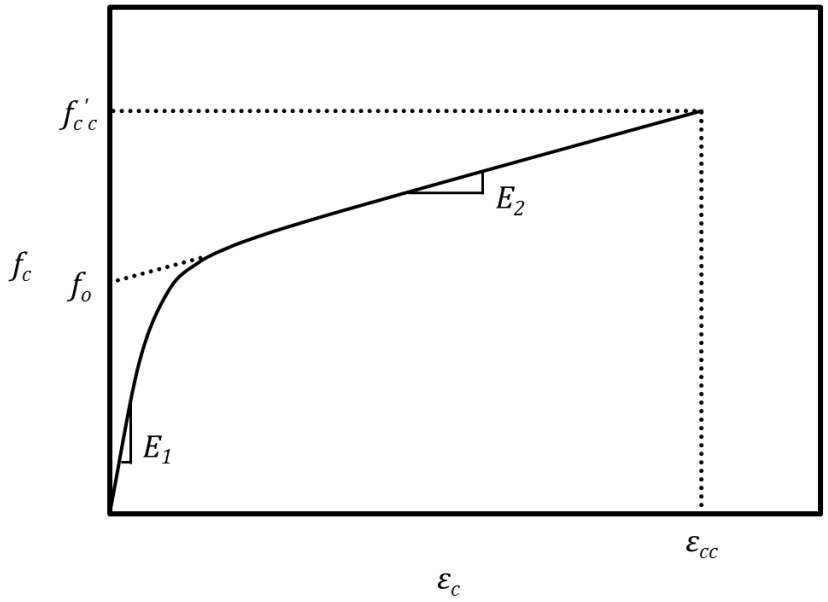

Figure 7.3. Stress-strain behaviour of confined concrete in compression

The f'_{cc} and ε_{cc} can be calculated using Equations 7.12 and 7.13 as proposed in Karim et al.[86].

$$f'_{cc} = k_c\, f'_{co} \tag{7.12}$$

$$\varepsilon_{cc} = {k_c}^2\, \varepsilon_{co} \tag{7.13}$$

$$k_c = \frac{f'_{co} + 5f_l}{f'_{co} + 0.5f_l} \tag{7.14}$$

where k_c is the confinement coefficient factor and f_l is the lateral pressure which can be calculated using Equations 7.15 and 7.16, for GFRP helices and CFRP sheets, respectively.

$$f_l = \frac{2\, A_h\, k_\varepsilon\, f_{fb}}{d_c\, s} \tag{7.15}$$

$$f_l = \frac{2\, t_f\, k_\varepsilon\, f_{fu}}{h} \tag{7.16}$$

where A_h is the area of the GFRP helices, k_ε is the ratio of the hoop rupture strain to the ultimate tensile strain of the confining materials, f_{fb} is the tensile strength of the bent GFRP bar or GFRP helix, d_c is the diameter of the confined concrete core enclosed by the centreline of the GFRP helices, s is the pitch of the GFRP helices, t_f is the total thickness of the CFRP sheet, f_{fu} is the ultimate tensile strength of the CFRP sheet and h is the diameter of the specimens. The value of k_ε is recommended as 0.55 for the CFRP sheet in ACI[94]. However, k_ε = 0.55 underestimates the actual value of the k_ε [144-146]. Therefore, the value of k_ε was found using Equation 7.17 as proposed in Ozbakkaloglu and Lim[87].

$$k_\varepsilon = 0.9 - 2.3\, f'_{co} \times 10^{-3} - 0.75\, E_f \times 10^{-6} \qquad (7.17)$$

where E_f is the tensile modulus of elasticity of the CFRP sheet. The value of k_ε for the GFRP helices has not been generalized due to insufficient experimental studies. Hence, the recorded strain value for the GFRP helices was used in this study. The hoop rupture strain of the GFRP helices was about 33.3% and 25% ($k_\varepsilon = 0.333$ and 0.25) of the ultimate tensile strain of the GFRP bars for the specimens with and without longitudinal GFRP bars, respectively, as reported in "Experimental study" chapter. The tensile strength of the bent GFRP bar or helix is lower than its ultimate tensile strength because GFRP bars are not isotropic. Hence, different directions of the applied load lead to reducing the ultimate tensile strength of the GFRP bars[147]. The tensile strength of the GFRP helices can be found using Equation 7.18, as recommended in ACI 440.1R-15[13].

$$f_{fb} = \left(0.05\frac{r_b}{d_b} + 0.3\right) f_{fu} \quad \leq f_{fu} \tag{7.18}$$

where r_b is the inner radius of the helices, d_b is the diameter of the helices bars and f_{fu} is the ultimate tensile strength of the GFRP bars. For the specimens reinforced with GFRP helices and confined with CFRP sheet, the concrete cover is confined by CFRP sheet and concrete core is confined by GFRP helices and CFRP sheet as shown in Figure 7.4. The confined concrete strength can be found using the following equation, as recommended in Lee et al.[148], Hu and Seracino[149], and Shirmohammadi et al.[150].

$$f'_{cc} = \frac{f'_{cc,cover}\, A_{cover} + f'_{cc,core}\, A_{core}}{A_g} \tag{7.19}$$

where $f'_{cc,cover}$ and $f'_{cc,core}$ are the confined concrete strength of the concrete cover and core, respectively, and A_{cover} and A_{core} are the areas of concrete cover and core, respectively, and A_g is the gross area of the concrete cross-section.

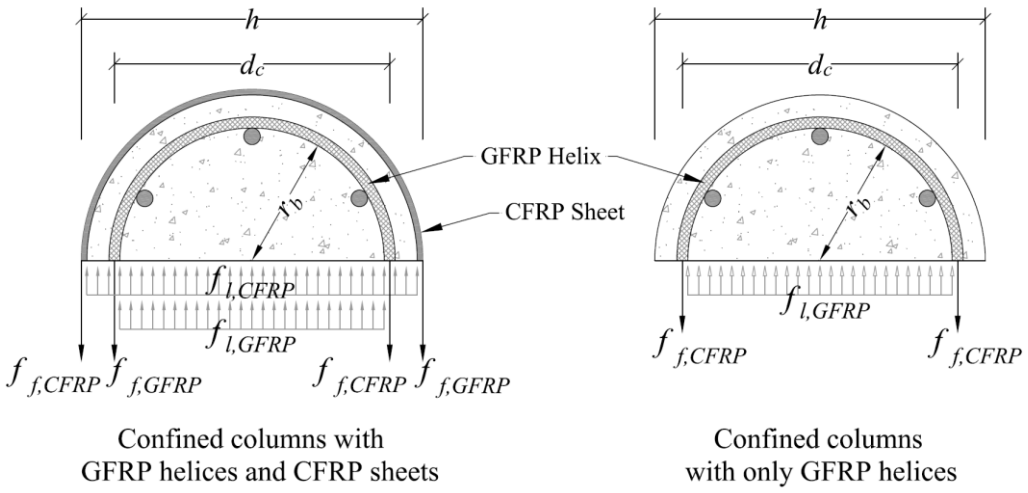

Figure 7.4. Confining mechanism for concrete confined by GFRP helices and CFRP sheet

7.2.4 Equivalent rectangular stress-block

The stress of concrete in the compression side can be simplified to an equivalent rectangle, if the strain in the extreme fibre in the compression side reaches the ultimate limit state which is equal to 0.003 as in ACI 318-14[40]. Figure 7.5 shows the equivalent rectangular stress-block which has a width of $\alpha_1 f_c'$ and a depth of $\beta_1 c$. The α_1 is the ratio of concrete compressive strength in the members to the concrete cylinder compressive strength at 28-days which is equal to 0.85 for normal-strength concrete. The β_1 is the ratio of depth of equivalent rectangular stress-block to depth of neutral axis which varies from 0.65 to 0.85 as:

$$\text{For} \quad f_c' \leq 28 \text{ MPa}, \quad \beta_1 = 0.85 \tag{7.20}$$

$$\text{For} \quad 28 \text{ MPa} < f_c' \leq 55 \text{ MPa}, \quad \beta_1 = 0.85 - 0.05(f_c' - 28 \text{ MPa})/7 \text{ MPa} \tag{7.21}$$

$$\text{For} \quad f_c' > 55 \text{ MPa}, \quad \beta_1 = 0.65 \tag{7.22}$$

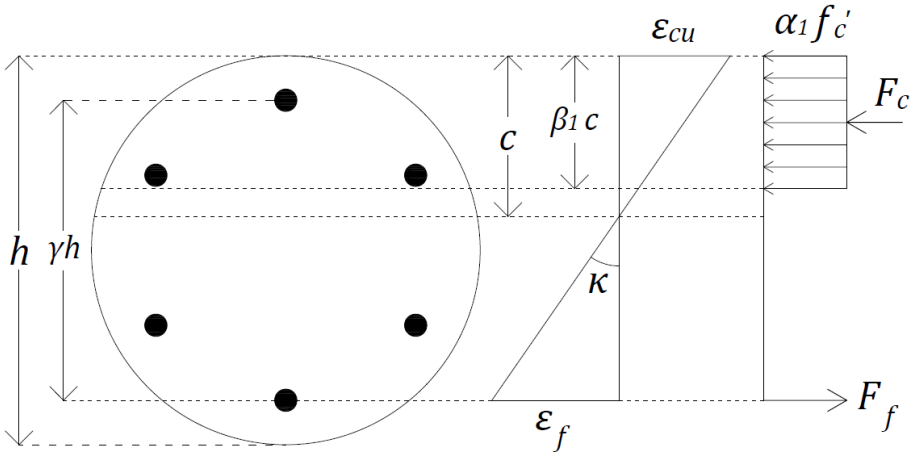

Figure 7.5. Equivalent rectangular stress block for concrete in compression

7.3 Curve-shape parameter

Figure 7.6 shows the stress-strain behaviour of unconfined and confined concrete drawn using Equation 7.2 and 7.8, respectively. It can be observed that the ascending part of the confined concrete is smaller than the unconfined concrete. It is evident that the differences are caused by inaccurate estimation of the curve-shape parameter (n) calculated using Equation 7.11.

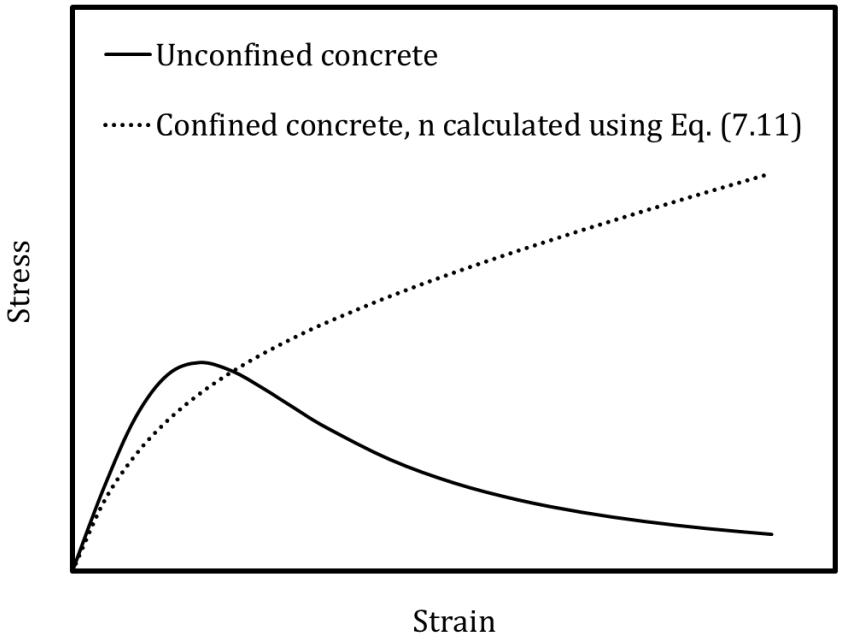

Figure 7.6. Stress-strain behaviour of unconfined and confined concrete

In general, increasing the value of n means the reduction of the radius of the transition curve that connects the first and the second ascending parts of the confined concrete stress-strain curve. In order to estimate a reasonable value of n, it was assumed that the first ascending part of the stress-strain curve of unconfined and confined concrete are equal within the elastic limit range of the concrete core. This assumption is reasonable as concrete core within the elastic axial strain is not cracked

and the lateral pressure is not considerably activated. The axial strain value at the end of the elastic limit state is assumed to be $0.5\varepsilon_{co}$ [67]. From this assumption, Equation 7.23 was proposed.

$$f_{c,unconf.} = f_{c,conf.} \quad \text{For} \quad \varepsilon_c \leq 0.5\varepsilon_{co} \tag{7.23}$$

where $f_{c,unconf.}$ and $f_{c,conf.}$ Are the unconfined and confined concrete stresses, respectively, corresponding to ε_c. By substituting Equation 7.8 in Equation 7.23 and considering $\varepsilon_c = 0.5\,\varepsilon_{co}$, the relationship between n and the other influencing parameters can be established in Equation 7.24.

$$\frac{E_1 - E_2}{2f'_{co,0.5}/\varepsilon_{co} - E_2} = \left[1 + \left(\frac{E_1 - E_2}{2f_o/\varepsilon_{co}}\right)^n\right]^{1/n} \tag{7.24}$$

where $f'_{co,0.5}$ is the unconfined concrete stress corresponding to $0.5\varepsilon_{co}$. The $f'_{co,0.5}$ and ε_{co} can be expressed as a function of E_1 using Equations 7.2, 7.6 and 7.7. Finally, the value of n is a function of E_1, E_2 and f_o. However, the relationship between n and the parameters that affect n is complex. Hence, a parametric study was conducted to estimate the relationship between E_1, E_2 and f_o with n. An algorithm was written in MATLAB[151] to numerically solve Equation 7.24 with the change of the parameters within reasonable range to obtain a representative value of n. The flow chart of the algorithm is shown in Figure 7.7 and the MATLAB code is written in Appendix B.

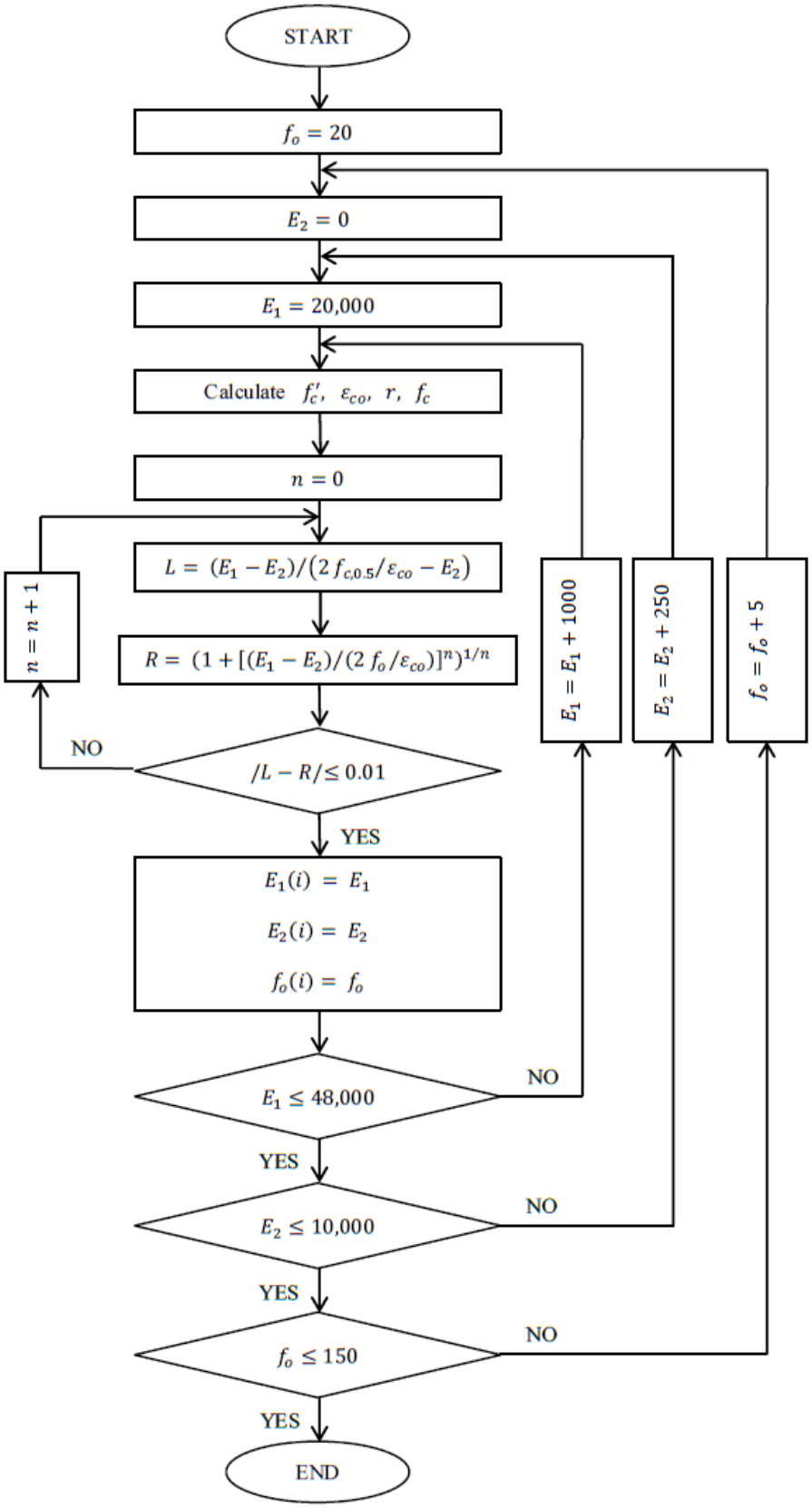

Figure 7.7. Stress-strain behaviour of unconfined and confined concrete

7.3.1 Influence of the concrete parameters on *n*

Figure 7.8 shows the effect of E_1 on n with fixed values of E_2 and f_o. In this study, the values of E_1 was considered to vary from 20,000 to 48,000 MPa which corresponds to f_c' between 20 to 100 MPa. Figure 7.9 shows the relationship between E_1 and n. It can be observed that the value of n increased with increasing of E_1 because increasing the value of E_1 leads to the reduction of the radius of the transition curve between the first and second ascending parts of the confined stress-strain curve.

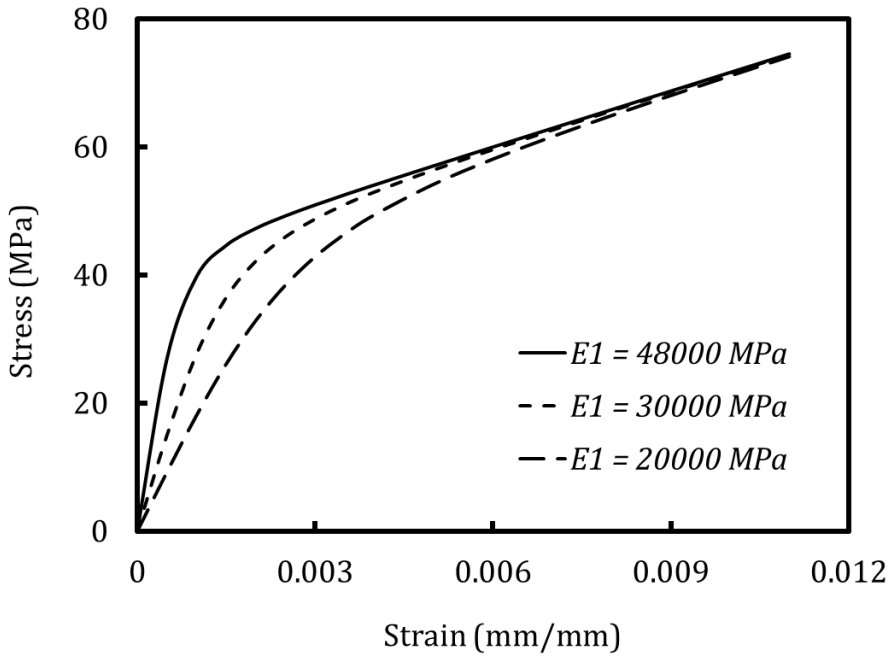

Figure 7.8. Influence of E_1 on stress-strain behaviour

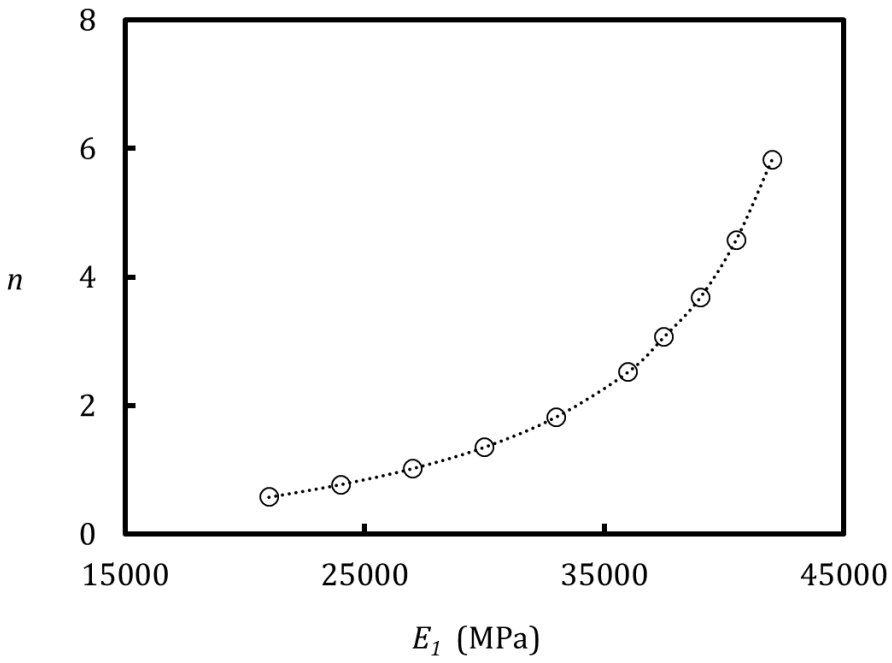

Figure 7.9. Influence of E_1 on n

Figure 7.10 shows the effect of changing E_2 on n with fixed values of E_1 and f_o. It is clear that the radius of the transition curve should be reduced with the increase in the value of E_2 in order to have the ascending part of the confined stress-strain curve the same as the ascending part of the unconfined concrete. To demonstrate the influence and relationship between E_2 and n, the values of E_2 were considered to vary from 0 to 10,000 MPa which are equivalent to the ratio of f'_{cc}/f'_{co} between 1 to more than 7. It can be observed that increasing the value of E_2 leads to the reduction of n as shown in Figure 7.11.

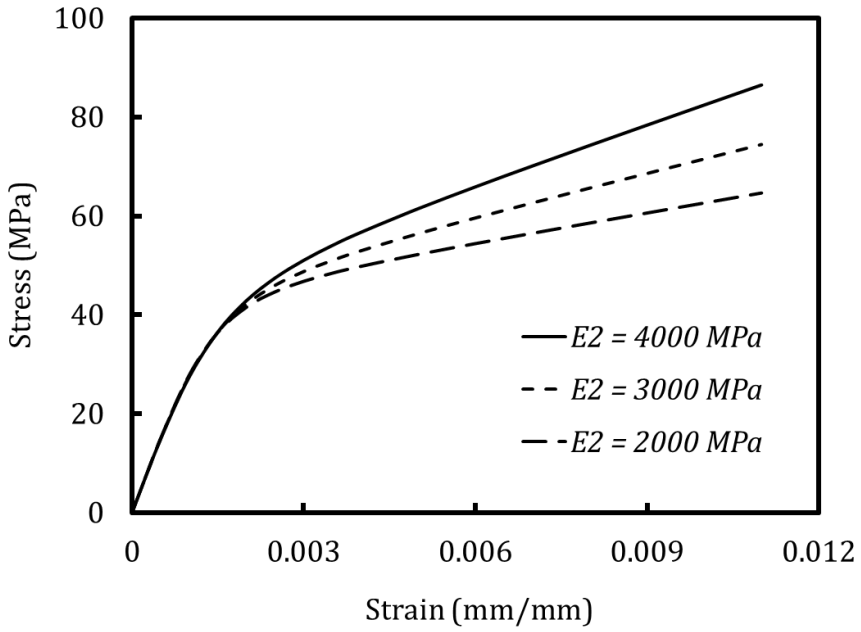

Figure 7.10. Influence of E_2 on stress-strain behaviour

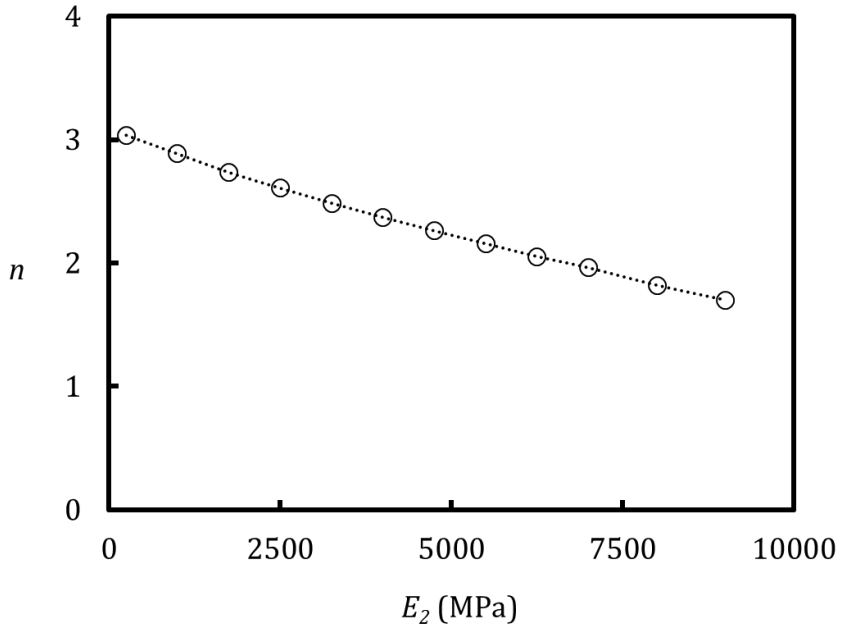

Figure 7.11. Influence of E_2 on n

Figure 7.12 shows the effects of changing f_o on the value of n with fixed values of E_1 and E_2. It is clear that reducing the value of f_o leads to the increase of the value of

n in order to have the ascending part of the confined stress-strain curve the same as the ascending part of the unconfined concrete. The values of f_o was varied between 20 to 150 MPa (Figure 7.13).

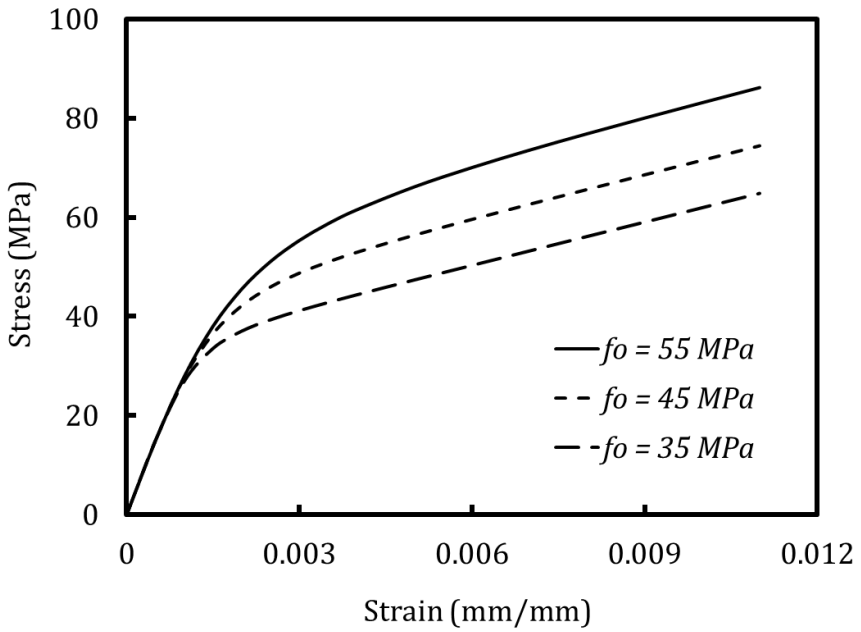

Figure 7.12. Influence of f_o on stress-strain behaviour

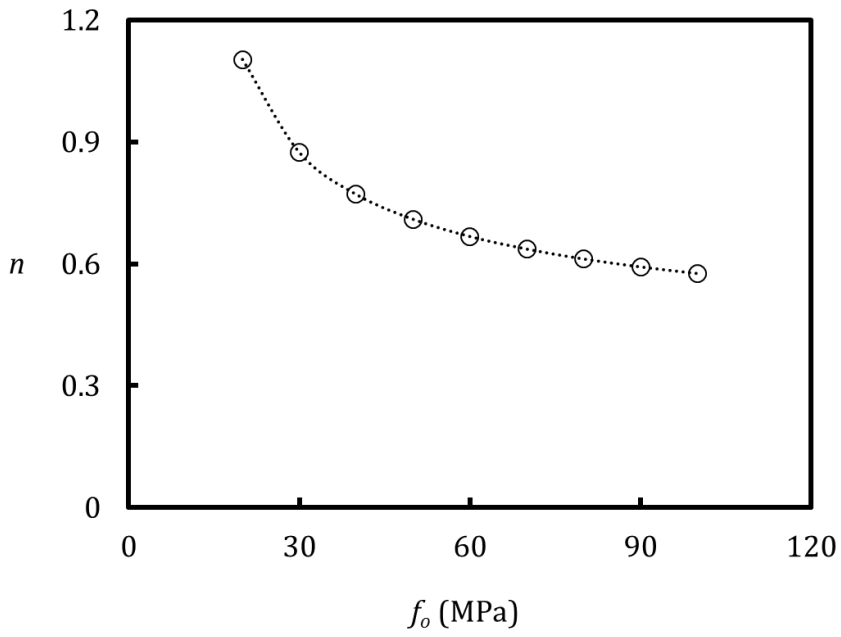

Figure 7.13. Influence of f_o on n

The relationship between the different parameters and the value of n are drawn in Figure 7.14, based on the parametric study discussed above. A regression analysis was performed to propose an equation to estimate the value of n. The proposed equation (Equation 7.25) can estimate the value of n in such a way that the ascending part of the confined concrete stress-strain curve within the elastic range is the same as the ascending part of unconfined concrete as shown in Figure 7.15.

$$n = 0.4\, e^{0.35x} \tag{7.25}$$

$$x = \frac{E_1 - E_2}{{f_o}^{0.45}} \times 10^{-3} \tag{7.26}$$

where the units of E_1, E_2 and f_o are in MPa.

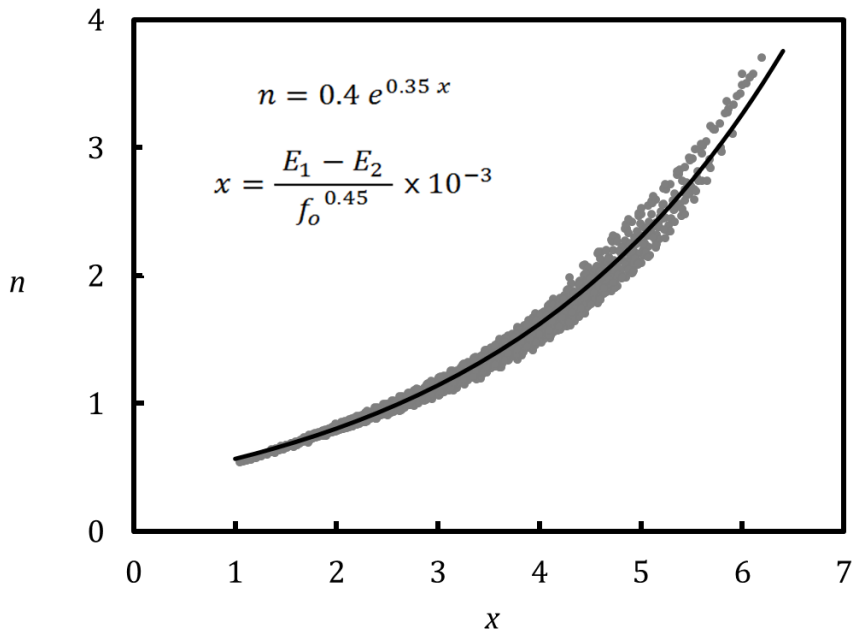

Figure 7.14. Relationship between E_1, E_2 and f_o with n

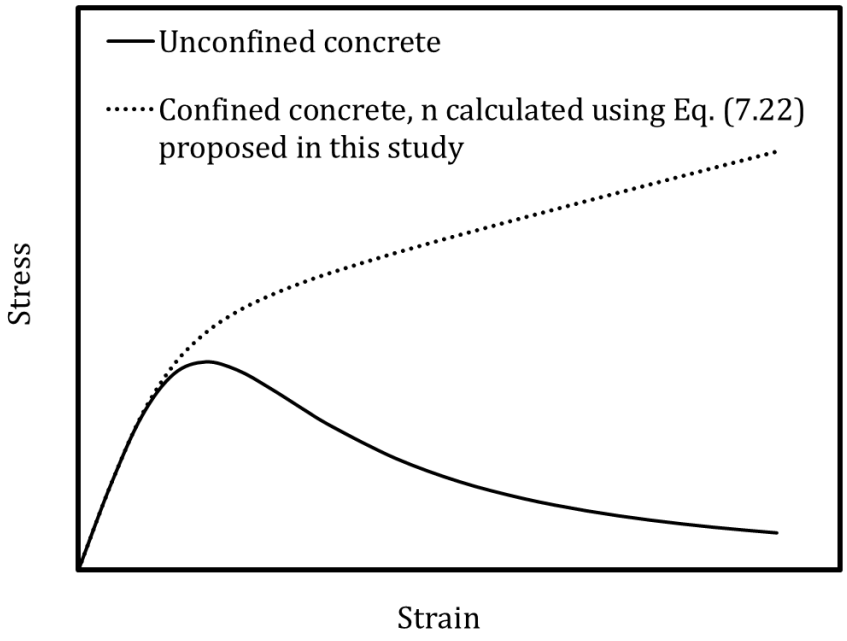

Figure 7.15. Stress-strain behaviour of unconfined and confined concrete with proposed value of n in this study

7.4 Peak axial load-bending moment diagram

Based on the experimental axial load-axial deformation behaviour of the tested specimens, two analytical peak axial load-bending moment $(P-M)$ diagrams were drawn for the GFRP-RC specimens. Figure 7.16 shows a typical axial load-axial deformation curve of a GFRP-RC specimen. The first peak $P-M$ diagram corresponds to the first peak load and the second peak $P-M$ diagram corresponds to the second peak load. The analytical peak axial load-bending moment diagrams were drawn based on five points (Points A to E) as demonstrated in Figure 7.17. These points (Points A to E) can demonstrate the entire peak $P-M$ diagrams for over-reinforced FRP-RC cross-sections reasonably accurately. It is noted that the

analytical peak $P-M$ diagrams presented herein did not consider the slenderness effect, as the specimens were considered short specimens.

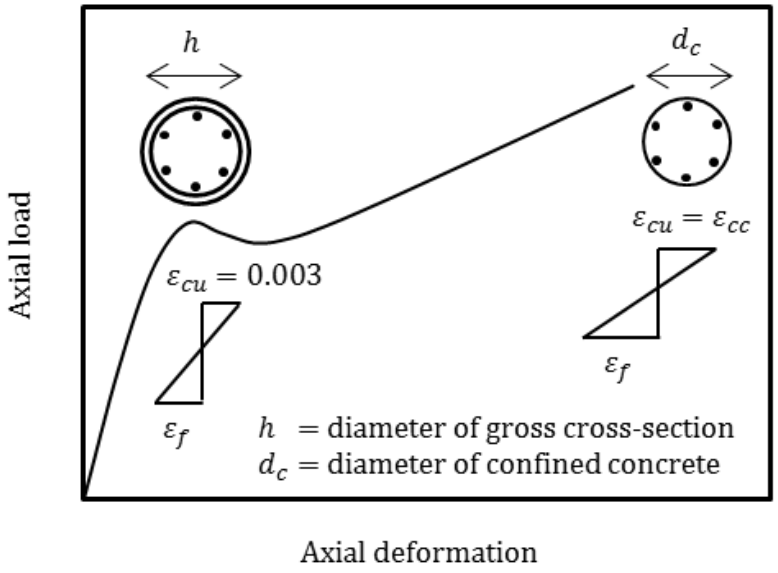

Figure 7.16. Typical axial load-axial deformation behaviour of GFRP-RC column specimens

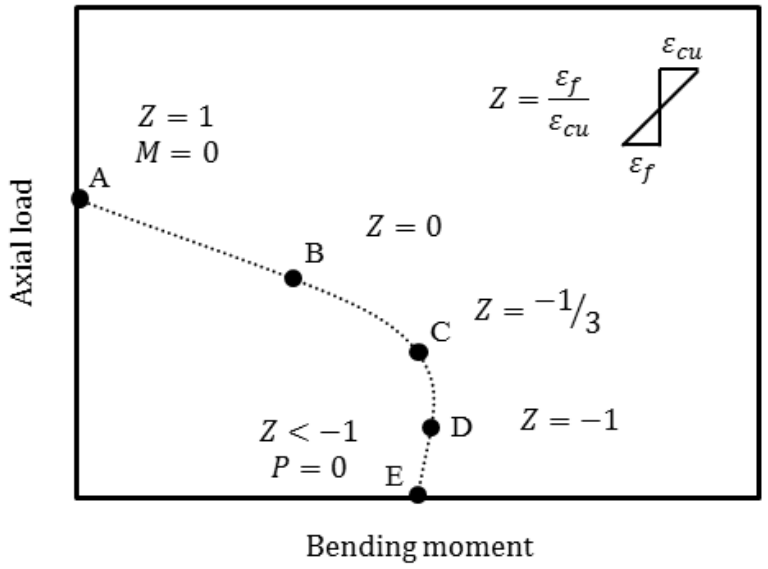

Figure 7.17. Drawing of analytical peak axial load-bending moment diagram

As explained above, the compressive stress of concrete in the compression region under flexural load can be represented either as stress-strain behaviour of concrete under axial concentric load or as equivalent rectangular stress-block. In this study, both of the methods were used to determine the compressive concrete stress in the compression region. A numerical integration method was also used to calculate the stress-strain curve of concrete.

7.4.1 Equivalent rectangular stress-block

The GFRP bars do not reach the ultimate compressive strain when the concrete reach the ultimate compressive strain. Also, the ultimate compressive strength of the GFRP bars is smaller than their ultimate tensile strength. Therefore, the nominal load carrying capacity of GFRP-RC columns under concentric loads (Point A in Figure 7.17) can be calculated based on the CSA S806-12[15], which ignores the contribution of the longitudinal GFRP bars.

$$P_{n1} = 0.85\, f_c'\, A_g \tag{7.27}$$

$$P_{n2} = 0.85\, f_{cc}'\, A_{core} \tag{7.28}$$

where P_{n1} and P_{n2} are the nominal load carrying capacity of the columns corresponding to the first and the second peak loads, respectively, A_g and A_{core} = the areas of gross concrete cross-section and confined concrete core, respectively, and f_c' and f_{cc}' = the unconfined concrete cylinder compressive strength at 28-days and the confined concrete core strength, respectively.

Also it is reasonable to assume that the strain in the GFRP bars is approximately equal to the concrete ultimate strain, which is equal to 0.003 for the first peak load as defined in ACI 318-14[40] and equal to ε_{cc} for the second peak load. As a result, the nominal load carrying capacity of the GFRP-RC columns under concentric loads can also be computed using Equations 7.29 and 7.30 for the first and the second peak loads, respectively. It can be assumed that the compressive and tensile moduli of elasticity of GFRP bars is approximately equal, based on the experimental studies of Chaallal and Benmokrane[33] and Deitz et al.[37].

$$P_{n1} = 0.85\, f_c' \left(A_g - A_f\right) + 0.003\, E_f\, A_f \tag{7.29}$$

$$P_{n2} = 0.85\, f_c' \left(A_c - A_f\right) + \varepsilon_{cc}\, E_f\, A_f \tag{7.30}$$

where A_f is the total area of the longitudinal GFRP bars and E_f is the modulus of elasticity of the longitudinal GFRP bars.

The analytical peak $P - M$ diagrams for the GFRP-RC specimens under eccentric and flexural loads (Points B to E) were calculated based on the principles of equilibrium and strain compatibility in the concrete cross-sections between GFRP bars and concrete. The equivalent rectangular stress-block as defined in ACI 318-14[40] and Mohamed and Masmoudi[152] were used to calculate the concrete stress in the compression region for the first and the second peak loads, respectively. A linear elastic stress-strain relationship was used for the GFRP bars in tension and compression. In order to investigate the effect and contribution of the GFRP bars in compression, two different calculation procedures were conducted for the GFRP-RC columns. In the first calculation procedure, the contribution of the GFRP bars in the

compression region was ignored and replaced with an equivalent area of concrete, as recommended in Zadeh and Nanni[153]. In the second calculation procedure, however, the contribution of the GFRP bars was considered.

In order to calculate the peak $P-M$ diagram in the Points B to E, arbitrarily values for Z were taken as shown in Figure 7.17, where Z is the ratio of maximum tensile strain of the GFRP bars in the tension side to the ultimate compressive strain in the extreme compression fibre in the compression side. In this study, compression strain, stress and force are considered as positive and tensile strain, stress and force are considered as negative. From Figure 7.18(a, b), by similar triangles, the depth of neutral axis (c) and strain in each of the GFRP bars (ε_{fi}) can be calculated as,

$$c = \frac{d_4}{1-Z} \tag{7.31}$$

$$\varepsilon_{fi} = \left(1 - \frac{d_i}{c}\right)\varepsilon_{cu} \tag{7.32}$$

where d_i is the distance between the centre of the i^{th} GFRP bar to the extreme compression fibre in the compression side, ε_{cu} is the ultimate concrete compressive strain which is equal to 0.003 in the first peak load and equal to ε_{cc} in the second peak load. Also, the forces in each of the GFRP bars (F_{fi}) and the compression force in concrete (F_c) in the compression side can be determined as:

$$F_{fi} = \varepsilon_{fi}\, E_f\, A_{fi} \tag{7.33}$$

$$F_c = \alpha_1\, f_{cu}\, A_c \tag{7.34}$$

$$A_c = (\theta - \sin\theta\cos\theta)\, {r_c}^2 \tag{7.35}$$

$$\theta = \cos^{-1}\left(1 - \frac{\beta_1 c}{r_c}\right) \tag{7.36}$$

where A_{fi} and A_c are the areas of the i^{th} GFRP bar and concrete in the compression side, respectively, f_{cu} is the maximum concrete compressive strength which is equal to f_c' in the first peak load and equal to f_{cc}' in the second peak load. Also, α_1 is the ratio of the member concrete compressive strength to the cylinder concrete compressive strength at age 28-days, β_1 is the ratio of height of the equivalent rectangular stress block to the depth of neutral axis as defined in ACI 318-14[40]. The r_c is the radius of the concrete cross-section which is equal to $h/2$ in the first peak load and equal to $d_c/2$ in the second peak load (Figure 7.16 and Figure 7.18). However, r_c is equal to $h/2$ for the externally confined specimens with CFRP sheets because cover did not spall off.

The nominal axial load (P_n) and bending moment (M_n) of the GFRP-RC specimens can be calculated by summation of the forces in the concrete cross-section and taking moment of the forces around the centroid of the concrete cross-section:

$$P_n = F_c + \sum_{i=1}^{m} F_{fi} \tag{7.37}$$

$$M_n = F_c\,\bar{y} + \sum_{i=1}^{m} F_{fi}(r_c - d_i) \tag{7.38}$$

$$\bar{y} = \frac{2\,r_c}{3}\left(\frac{\sin^3\theta}{\theta - \sin\theta\cos\theta}\right) \tag{7.39}$$

Where m is number of the longitudinal GFRP bars and $\bar{y} =$ the distance between the centroid of concrete in the compression side to the centroid of the concrete cross-section.

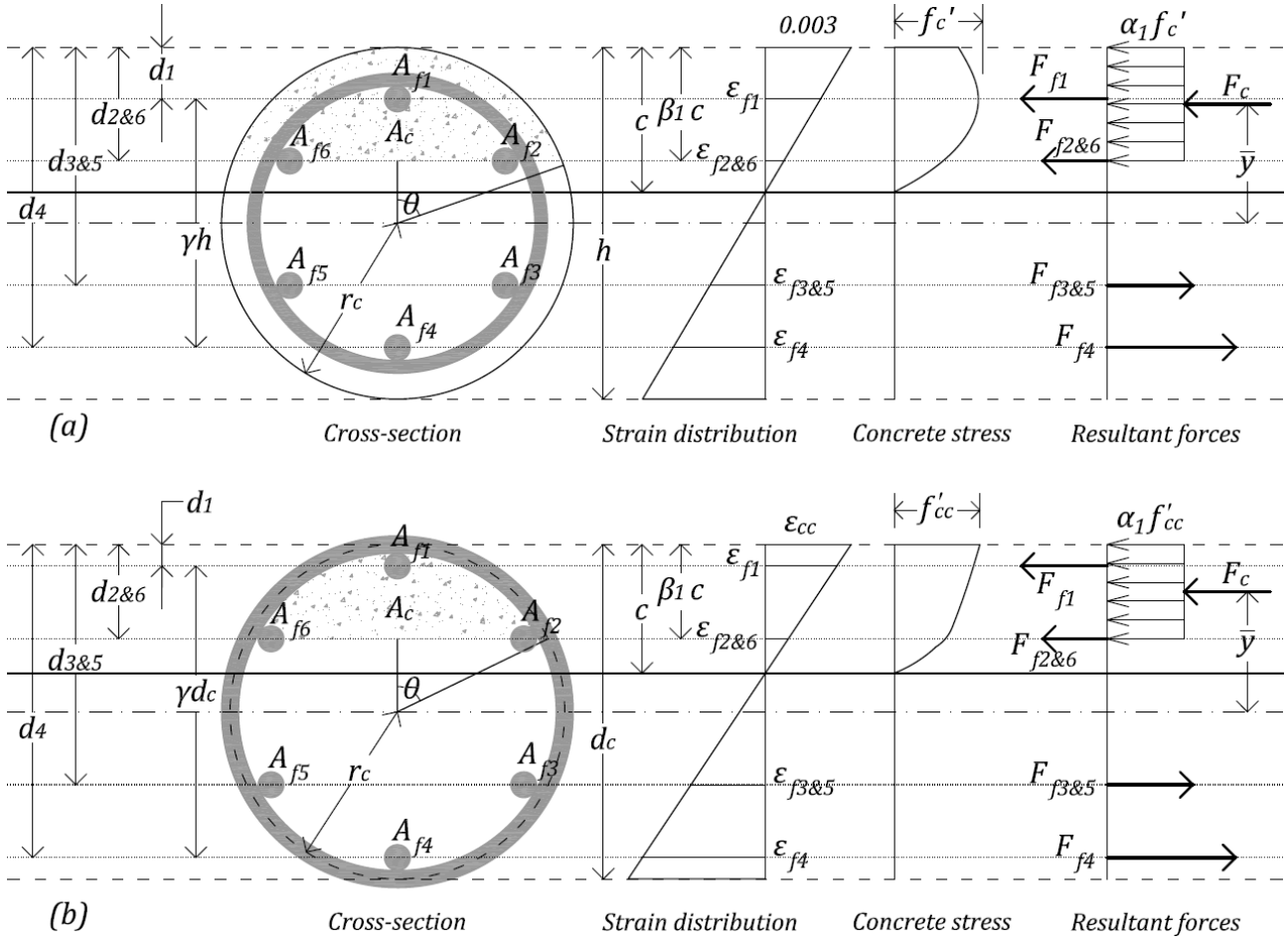

Figure 7.18. Stress and strain profile of GFRP-RC cross-section: (a) first peak load; and (b) second peak load

7.4.2 Numerical integration method

In order to calculate the axial loads and bending moments at Points A to E in Figure 7.17, arbitrarily values for Z were considered, where Z is the ratio of maximum tensile strain of the GFRP bars in the tension side to the ultimate compressive strain in the extreme compression fibre in the compression side. In this study, compression strain, stress and force are considered as positive and tensile strain, stress and force are considered as negative. From Figure 7.19(a, b), by similar triangles, the depth of neutral axis (c) and strain in each of the GFRP bars (ε_{fi}) can be calculated as:

$$c = \frac{d_4}{1 - Z} \tag{7.40}$$

$$\varepsilon_{fi} = \left(1 - \frac{d_i}{c}\right)\varepsilon_{cu} \tag{7.41}$$

where d_i is the distance between the centre of the i^{th} GFRP bar to the extreme compression fibre in the compression side as shown in Figure 7.20, ε_{cu} is the ultimate concrete compressive strain which is equal to 0.003 in the first peak load and equal to ε_{cc} in the second peak load. The d_i can be calculated using the following equation:

$$d_i = \left[1 - \gamma \cos\frac{2\pi}{m}(i - 1)\right] r_c \tag{7.42}$$

where γ is the distance between the GFRP bar in the tension side to the GFRP bar in the compression side to the diameter of the specimens, as shown in Figure 7.2, m is number of the longitudinal GFRP bars in the specimen's cross-section and r_c is the radius of the concrete cross-section which is equal to $h/2$ for the first peak load and equal to $d_c/2$ for the second peak load. For the specimens confined with CFRP sheets the value of r_c is equal to $h/2$ for the second peak load because concrete cover did not spall off. Also, the forces in each of the GFRP bars (F_{fi}) and the compression force (F_c) in concrete in the compression side can be determined as:

$$F_{fi} = E_f \, \varepsilon_{fi} \, A_{fi} \tag{7.43}$$

$$F_c = \int_0^c \int_{-x}^{x} f_c \, d_x \, d_y \tag{7.44}$$

where ε_{fi} and A_{fi} are the strain and the cross-sectional area of the i^{th} GFRP bar, respectively, f_c is the concrete stress which is considered as unconfined concrete stress (Equation 7.2) for the first peak load and considered as confined concrete stress (Equation 7.8) for the second peak load, and d_x and d_y are shown in Figure 7.19.

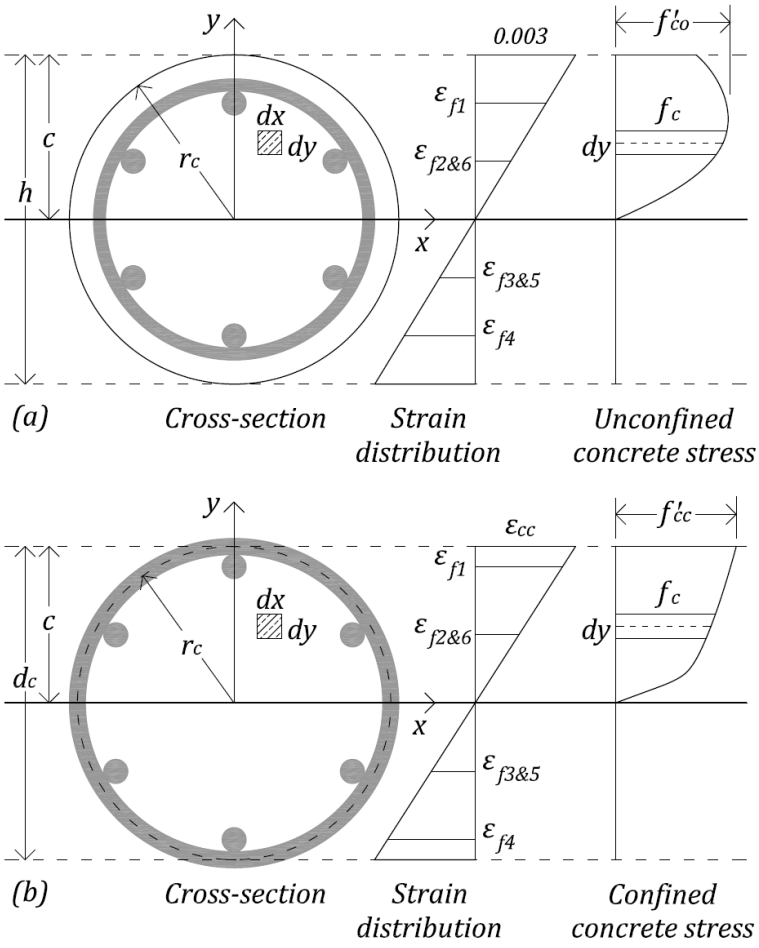

Figure 7.19. Stress-strain profile of GFRP-RC cross-section: (a) first peak load; and (b) second peak load

Small strip method was used to numerically solve Equation 7.44. This method has been widely used in analysing of RC cross-sections[154, 155]. The cross-section of the specimens was divided into N number of strips which are small enough to obtain accurate results as shown in Figure 7.20. The average width and strain of each concrete strip can be calculated as:

$$b_i = 2\sqrt{{r_c}^2 - \left[r_c - \left(i - \frac{1}{2}\right)t\right]^2} \tag{7.45}$$

$$\varepsilon_{ci} = \left[1 - \left(i - \frac{1}{2}\right)\frac{t}{c}\right]\varepsilon_{cu} \tag{7.46}$$

where b_i is the width of the i^{th} concrete strip, ε_{ci} is the strain of the i^{th} concrete strip, and t is the depth of the strips which is taken as 0.5 mm in this study. By substituting the values of ε_{ci} in Equations 7.2 and 7.8, the unconfined and confined concrete stress can be calculated in each concrete strip in the compression side. Eventually, the compression force of each concrete strip (F_{ci}) in the compression side can be determined as:

$$F_{ci} = f_{ci}\, b_i\, t \tag{7.47}$$

The nominal axial load (P_n) and the bending moment (M_n) of the GFRP-RC specimens can be calculated by summation of the forces in the concrete cross-section and taking moment of the forces around the centroid of the concrete cross-section:

$$P_n = \sum_{i=1}^{n} F_{ci} + \sum_{i=1}^{m} F_{fi} \tag{7.48}$$

$$M_n = \sum_{i=1}^{n} F_{ci}\left[r_c - \left(i - \frac{1}{2}\right)t\right] + \sum_{i=1}^{m} F_{fi}(r_c - d_i) \tag{7.49}$$

An MS-Excel spread-sheet was prepared to calculate the calculation procedures presented in this section.

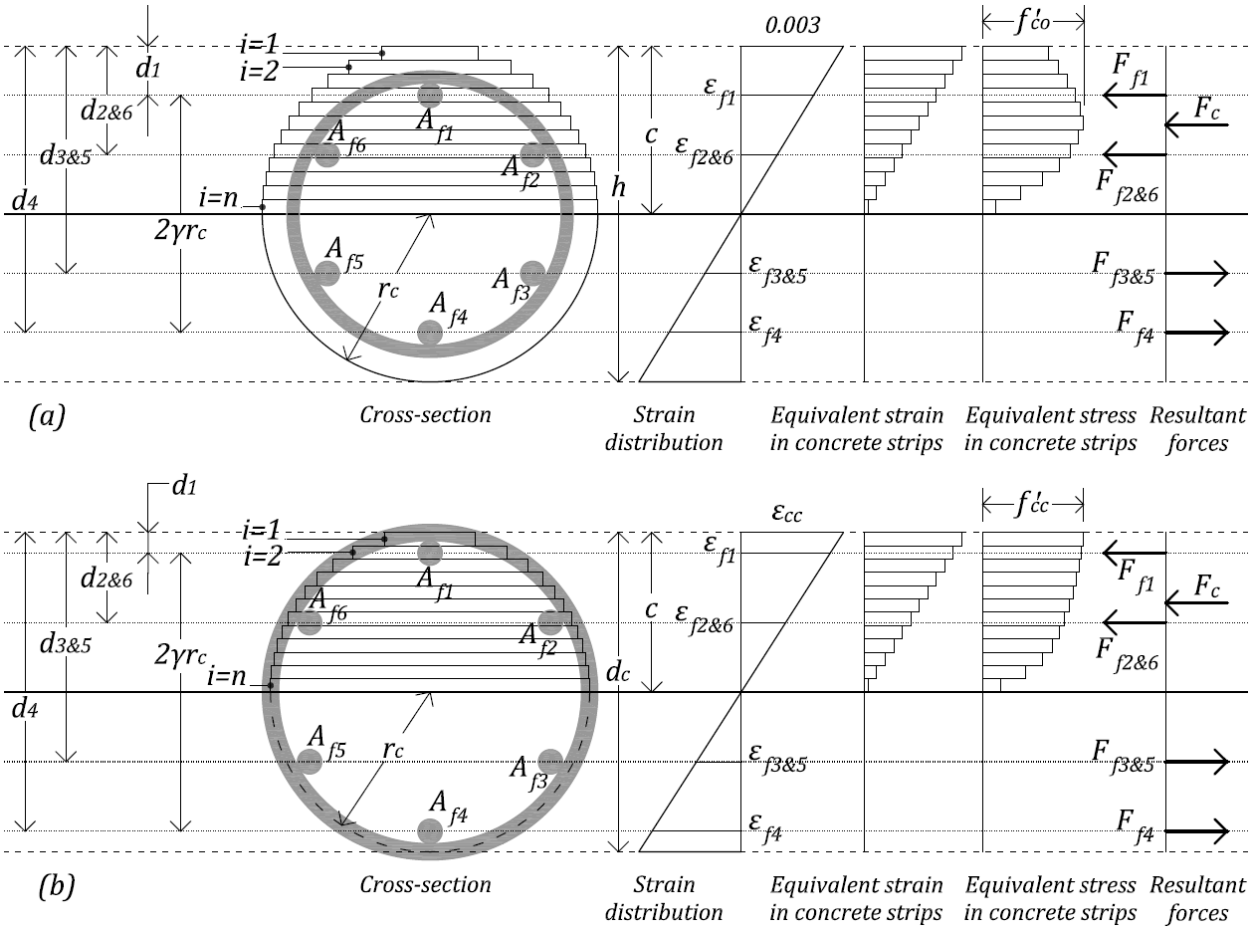

Figure 7.20. Section analysis of GFRP-RC cross-section: (a) first peak load; and (b) second peak load

7.5 Axial load-axial deformation behaviour

The analytical axial load-axial deformation curves of the GFRP-RC specimens were developed by the superposition of the axial load-axial deformation of the different components (longitudinal bars, confined concrete core and unconfined concrete cover) of the GFRP-RC specimens. The axial load-axial deformation behaviour of each component of the GFRP-RC specimens was drawn in Figure 7.21 based on the stress-strain behaviour and the assumptions presented in Section 7.2. In addition, a full composite action was considered between the concrete cover and the concrete core. An MS-Excel spread-sheet was used to perform the calculations and drawing of the axial load-axial deformation behaviour of the GFRP-RC specimens. The axial load of a specimen at any axial deformation can be calculated using the following equation.

$$P = f_f\, A_f + f_{c,core}\, A_{core} + f_{c,cover}\, A_{cover} \tag{7.50}$$

where P is the total load of the GFRP-RC specimens; f_f, $f_{c,core}$ and $f_{c,cover}$ are the axial stresses in the longitudinal GFRP bars, the concrete core and the concrete cover, respectively; and A_f, A_{core} and A_{cover} are the cross-sectional areas of the longitudinal GFRP bars, the concrete core and the concrete cover, respectively.

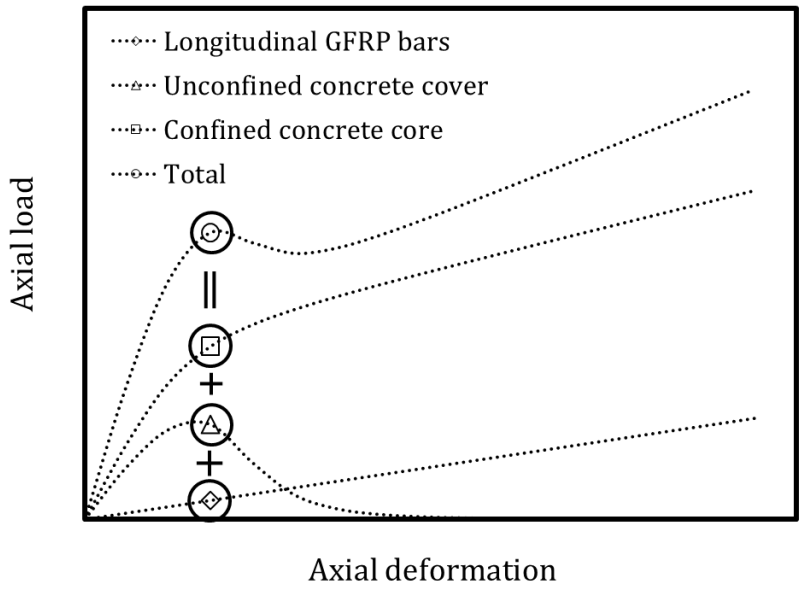

Figure 7.21. Analytical axial load-axial deformation behaviour of different components of the specimens

7.6 Moment-curvature behaviour

For a RC cross-section as shown in Figure 7.22, the distance from the centre of each GFRP bar to the extreme compression fibre can be calculated as:

$$d_i = \frac{1}{2}\left[1 - \gamma \cos\frac{2\pi}{m}(i-1)\right]h \tag{7.51}$$

where γ is the distance between the GFRP bar in the tension side to the GFRP bar in the compression side to the diameter of the specimens (h) as shown in Figure 7.22, m is the total number of the longitudinal GFRP bars in the cross-section. Also, strain distribution along the cross-section and each of the GFRP bars (ε_{fi}) can be calculated by similar triangles, if the strain in the extreme concrete compression fibre (ε_{cu}) and the depth of neutral axis (c) are known.

$$\varepsilon_{fi} = \left(1 - \frac{d_i}{c}\right)\varepsilon_{cu} \tag{7.52}$$

where $\varepsilon_{cu} = \varepsilon_{cc}/(1 - 0.5\,(h - d_c)/c)$ for specimens without CFRP wrapping and $\varepsilon_{cu} = \varepsilon_{cc}$ for specimens with CFRP wrapping. Also, the forces in each of the GFRP bars (F_{fi}) can be determined as:

$$F_{fi} = E_f\ \varepsilon_{fi}\ A_{fi} \tag{7.53}$$

where A_{fi} is the cross-sectional area of the i^{th} GFRP bar and E_f is the elastic modulus of the GFRP bars. The compression force of concrete was calculated by numerically integrating the stress-strain curve for unconfined (Equation 7.2) and confined (Equation 7.8) concrete in the compression side. Numerical integration method has been widely used in the analysis of RC specimens[53, 154, 155]. The cross-section of the specimens is divided into N number of horizontal small strips parallel to the neutral axis as shown in Figure 7.22. The average width and strain of each strip can be calculated as:

$$b_{core,i} = 0 \quad \text{For} \quad \frac{d_c}{2} \le \left|\frac{h}{2} - \left(i - \tfrac{1}{2}\right)t\right| \tag{7.54}$$

$$b_{core,i} = 2\sqrt{\left(\frac{d_c}{2}\right)^2 - \left(\frac{h}{2} - \left(i - \tfrac{1}{2}\right)t\right)^2} \quad \text{For} \quad \frac{d_c}{2} > \left|\frac{h}{2} - \left(i - \tfrac{1}{2}\right)t\right| \tag{7.55}$$

$$b_{cover,i} = 2\sqrt{\left(\frac{h}{2}\right)^2 - \left(\frac{h}{2} - \left(i - \tfrac{1}{2}\right)t\right)^2} - b_{core,i} \tag{7.56}$$

$$\varepsilon_{ci} = \left[1 - \left(i - \tfrac{1}{2}\right)\frac{t}{c}\right]\varepsilon_{cu} \tag{7.57}$$

where $b_{core,i}$ and $b_{cover,i}$ are the average width of the i^{th} strip of concrete core and cover, respectively, t is the depth of the strips which is taken as 0.5 mm in this study, and ε_{ci} is the strain for the i^{th} concrete strip. By substituting the value of ε_{ci} in Equations 7.2 and 7.8, the unconfined and the confined concrete stress can be calculated, respectively, in each concrete strip in the compression side. Eventually, the compression force of each concrete strip in the compression side can be determined as:

$$F_{core,i} = f_{ci}\, b_{core,i}\, t \tag{7.58}$$

$$F_{cover,i} = f_{ci}\, b_{cover,i}\, t \tag{7.59}$$

where $F_{core,i}$ and $F_{cover,i}$ are the compression force of the i^{th} strip of concrete core and cover, respectively, and f_{ci} is the stress in the i^{th} concrete strip calculated using Equations 7.2 and 7.8 for unconfined and confined concrete, respectively. The nominal axial load (P_n) and bending moment (M_n) of the GFRP-RC specimens can be calculated by summation of the forces in the concrete cross-section and taking moment of the forces around the centroid of the concrete cross-section:

$$P_n = \sum_{i=1}^{n} \left(F_{core,i} + F_{cover,i}\right) + \sum_{i=1}^{m} F_{fi} \tag{7.60}$$

$$M_n = \sum_{i=1}^{n} \left(F_{core,i} + F_{cover,i}\right) \left(\frac{h}{2} - \left(i - \tfrac{1}{2}\right) t\right) + \sum_{i=1}^{m} F_{fi} \left(\frac{h}{2} - d_i\right) \tag{7.61}$$

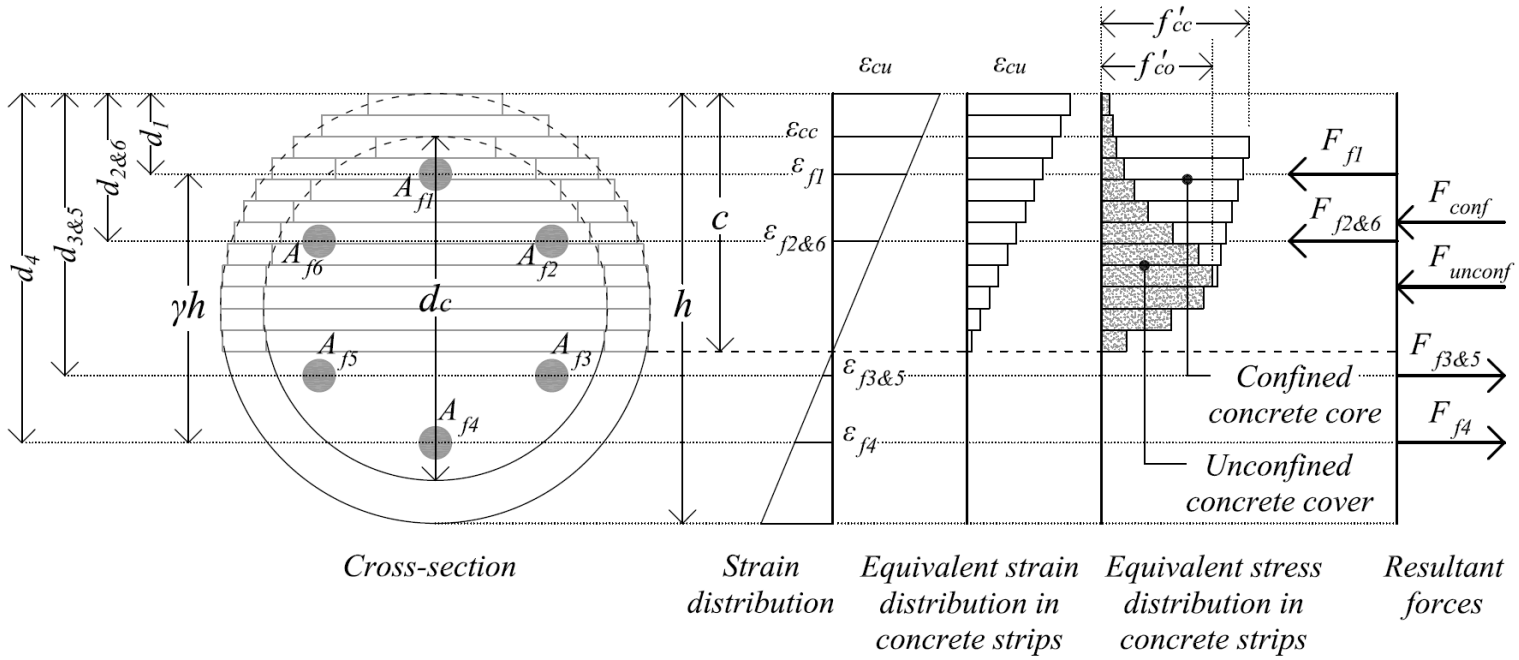

Figure 7.22. Stress-strain profile of GFRP-RC cross-section

When a column is loaded with an initial eccentricity (e_i), the cross-section is supposed to carry bending moments due to applied initial eccentricity at the ends of the column and the lateral deformation due to the curvature along the height of the column as shown in Figure 7.23. Hence, the bending moment at the mid-height of the columns (M_{mid}) can be calculated as:

$$M_{mid} = P\,(e_i + \delta_{mid}) \tag{7.62}$$

where P is the axial load and δ_{mid} is the lateral deformation at mid-height of the columns. For a pin ended column, the maximum deformation is at the mid-height of the column (Figure 7.23) and the deformed shape can be assumed to be a half-sine wave as explained in previous studies[143, 156]. Hence, the δ_{mid} can be calculated as:

$$\delta_{mid} = (L/\pi)^2\,\kappa_{mid} \tag{7.63}$$

$$\kappa_{mid} = \varepsilon_{cu}/c \tag{7.64}$$

where L is the height of the columns and κ_{mid} is the curvature at mid-height of the columns.

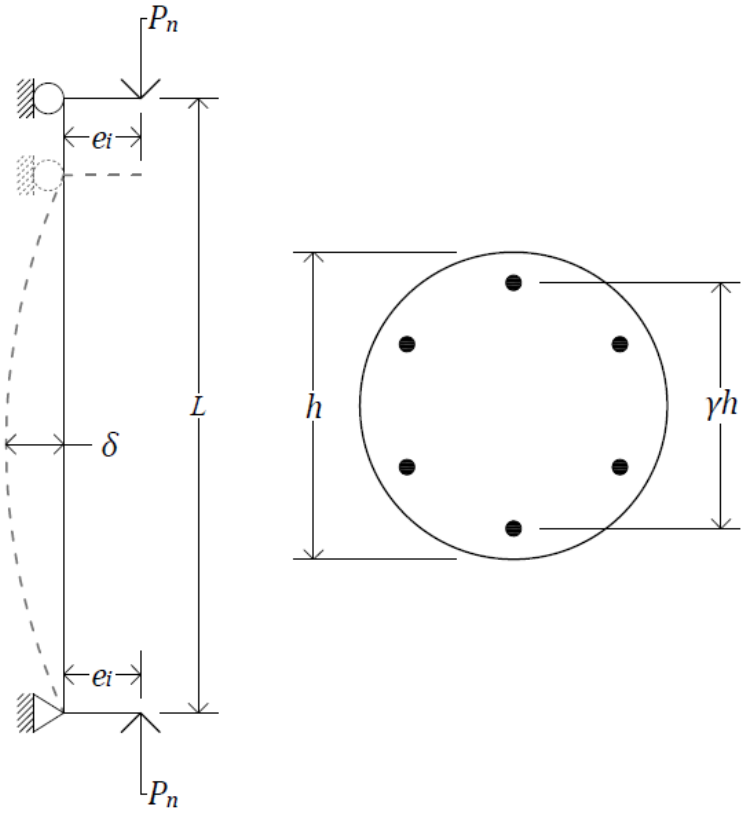

Figure 7.23. Typical deformation of pin-ended single curvature column

The flowchart of analytical development of the moment-curvature $(M-\kappa)$ diagram is shown if Figure 7.24 and is summarized in the following steps:

1. Select a small value for the depth of the concrete strips (t). The initial value of t is better to be not more than 1% of the h to achieve reasonably accurate results.
2. Select a small initial value for the concrete strain at the extreme concrete fibre in the compression side (ε_c). In this study, the initial value of ε_c was chosen to be 0.0002 mm/mm.
3. Select an initial value for the depth of the neutral axis (c). The initial value for c can be between 15 to 20% of the h.

4. Determine distance (d_i), strain (ε_{fi}) and force (F_{fi}) for each of the GFRP . Determine width $(b_{core,i}$ and $b_{cover,i})$, strain (ε_{ci}) and force (F_{ci}) for each of the concrete strips. Determine the axial load (P_n), bending moment (M_n), lateral deformation (δ_{mid}) and curvature (κ_{mid}) using the equations presented above.
5. Calculate error using the following equation:

$$error = \frac{|e_i + \delta_{mid} - M_n/P_n|}{e_i + \delta_{mid}} \text{ x } 100 \tag{7.65}$$

   If the calculated error is greater than 2%, repeat Steps 3 to 5 with an increment that is equal to the depth of concrete strips (t) for the value of c until the calculated error becomes smaller than 2%.
6. Repeat Steps 2 to 5 with increments for the value of ε_c until the value of ε_c becomes equal to ε_{cu}. In this study, each increment for the value of ε_c was chosen to be 0.0002 mm/mm.

A computer program was developed to implement the calculations and numerical procedures presented above using MATLAB[151] and the MATLAB code is written in Appendix B. The presented analytical procedures are also applicable for slender GFRP-RC columns with or without externally bonded FRP.

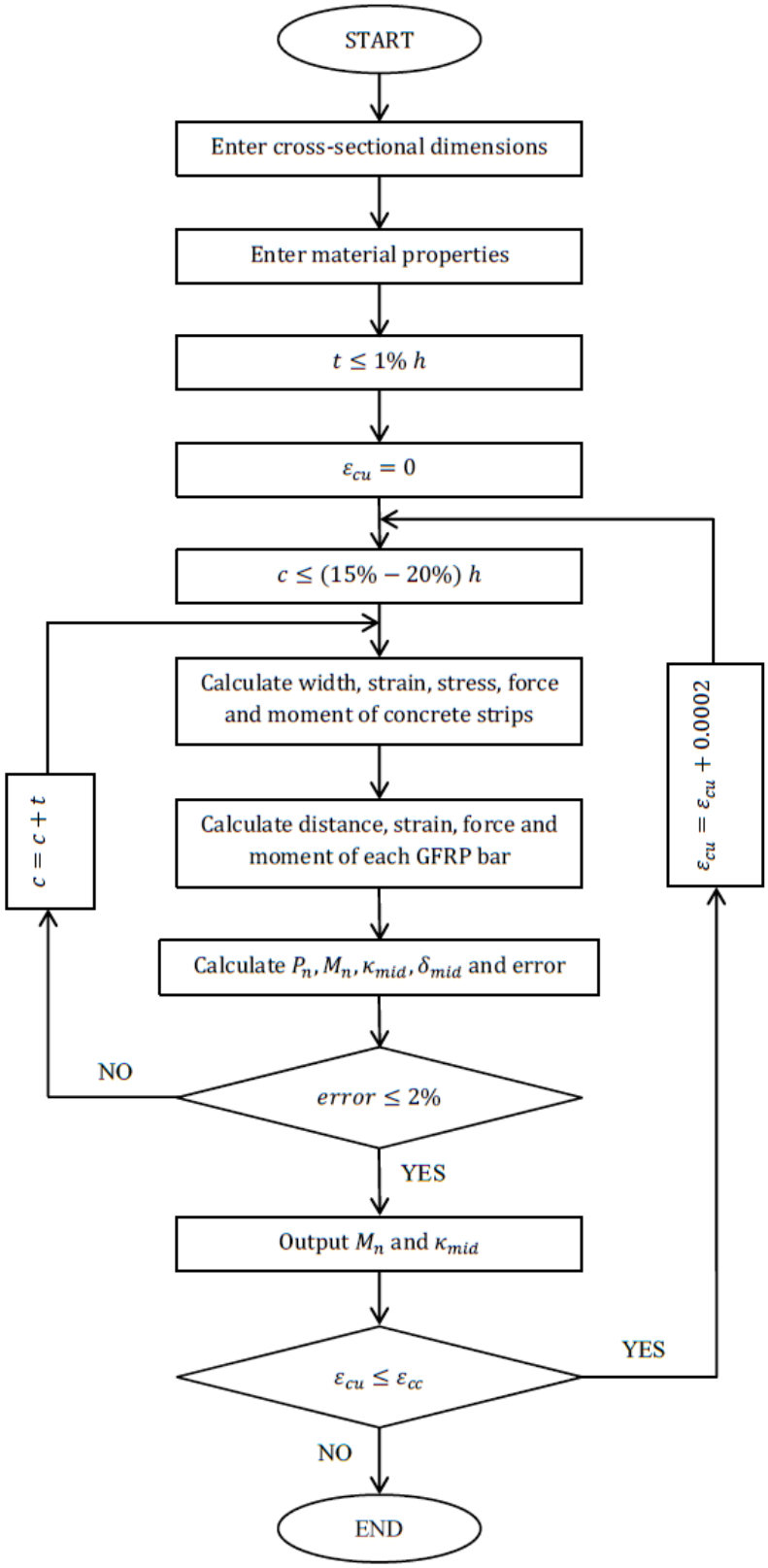

Figure 7.24. Flowchart of analytically development of $M - \kappa$ diagram

7.7 Summary

In this chapter, analytical studies were carried out to demonstrate the peak axial load-bending moment diagrams, axial load-axial deformation and moment-curvature behaviour of the GFRP-RC specimens. Five points were suggested to represent the entire peak axial load-bending moment diagram for over-reinforced FRP-RC cross-section. A new equation was also proposed to estimate a representative value of the curve-shape parameter for the stress-strain behaviour of confined concrete. In addition, a MATLAB[151] code was written to develop the moment-curvature behaviour of the GFRP-RC specimens with considering to the secondary bending moments due to the lateral deformation along the height of the specimens.

In the next chapter, comparisons are performed between experimental and analytical results to validate the presented analytical calculations presented in this chapter.

8 ANALYSIS OF RESULTS

8.1 Introduction

This chapter explains the comparisons between the experimental results in Chapter 6 (Experimental study) and analytical results in Chapter 7 (Analytical study). In addition, a parametric study was conducted to investigate the effects of different parameters such as longitudinal GFRP reinforcement ratio, transverse GFRP reinforcement ratio and slenderness effect on the behaviour of GFRP-RC specimens. The behaviours such as peak axial load-bending moment diagrams, axial load-axial deformation and moment-curvature of the GFRP-RC specimens are discussed in this chapter.

8.2 Analytical versus experimental results

8.2.1 Peak axial load-bending moment diagrams

8.2.1.1 Rectangular stress-block parameters

Figure 8.1 and Figure 8.2 show the peak axial load-bending moment $(P_n - M_n)$ diagrams of the experimental and analytical results corresponding to the first and the second peak loads, respectively, for the GFRP-RC specimens. Two analytical peak $P_n - M_n$ diagrams were drawn for the GFRP-RC specimens. In the first curve (Analytical 1), the contribution of the GFRP bars in compression was ignored. In the second curve (Analytical 2), the contributions of the GFRP bars in compression were taken into account. It can be seen that there is a large difference between the

experimental and calculated results when the effect of the GFRP bars was ignored in the compression region. However, the experimental results are in a better agreement with the analytical results when the effect of the GFRP bars in compression is taken into account. The experimental bending moments of the GFRP-RC beam specimens were greater than the calculated results. This may be because the shear span of the RC beam specimens was smaller than twice of the effect depth of the concrete cross-section. Eventually, it can be concluded that ignoring the contribution of GFRP bars in compression is not reasonable and very conservative.

8.2.1.2 Numerical integration method

Figure 8.3 and Figure 8.4 show the experimental and analytical peak $P_n - M_n$ diagrams corresponding to the first and the second peak loads, respectively, for the tested specimens. The calculated results show good agreements with the experimental results especially for the column specimens. However, the experimental bending moment of the GFRP-RC beam specimens was greater than the calculated results. This may be because the shear span of the beam specimens was smaller than two times of the effective depth of the concrete cross-section. It can be observed that all experimental results are greater than the analytical results. Except the beam specimens, the differences between the experimental and analytical results were about 10%.

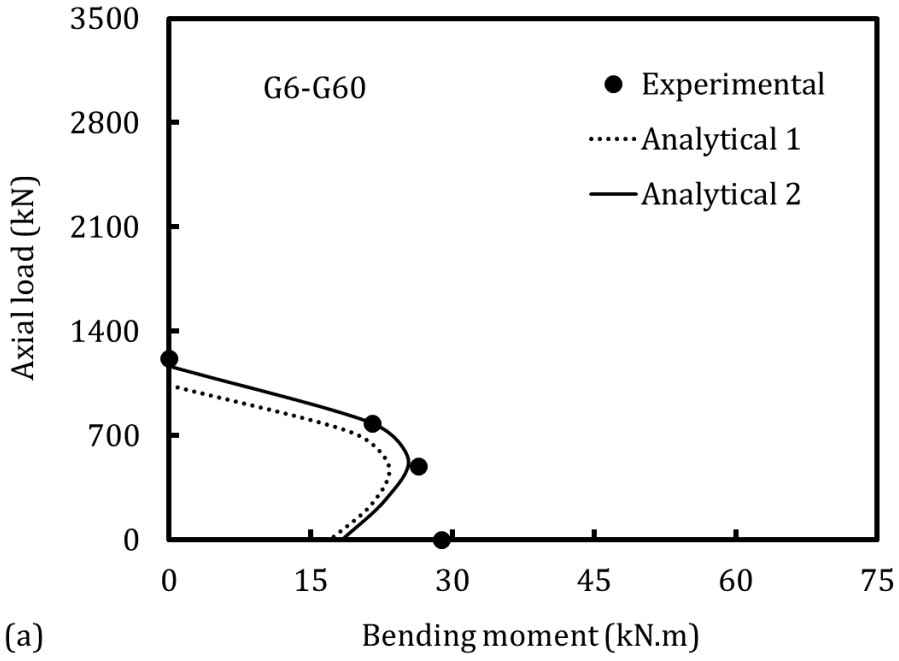

(a)

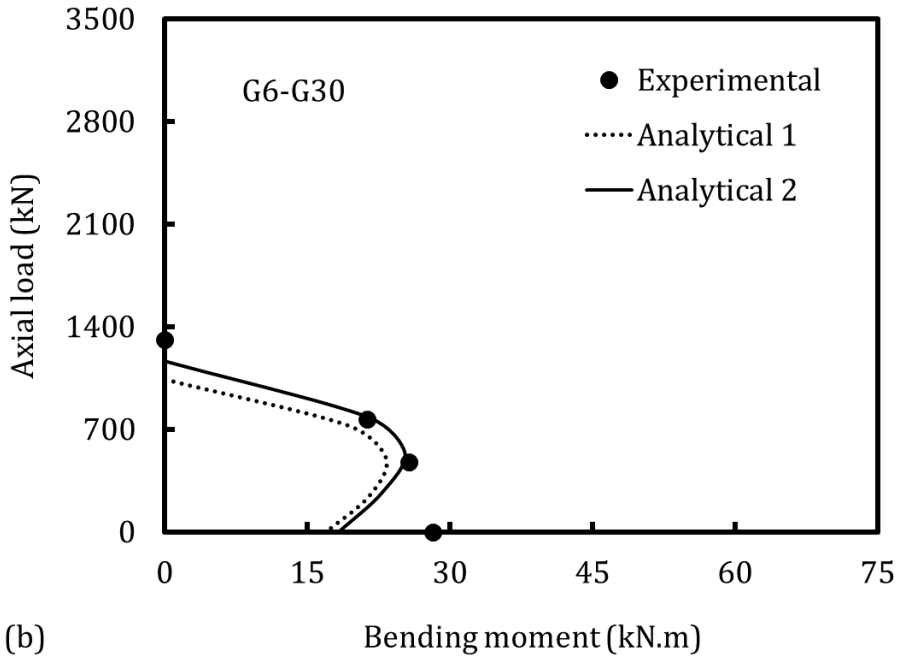

(b)

Figure 8.1. Experimental and analytical first peak $P_n - M_n$ diagrams: (a) G6-G60; and (b) G6-G30

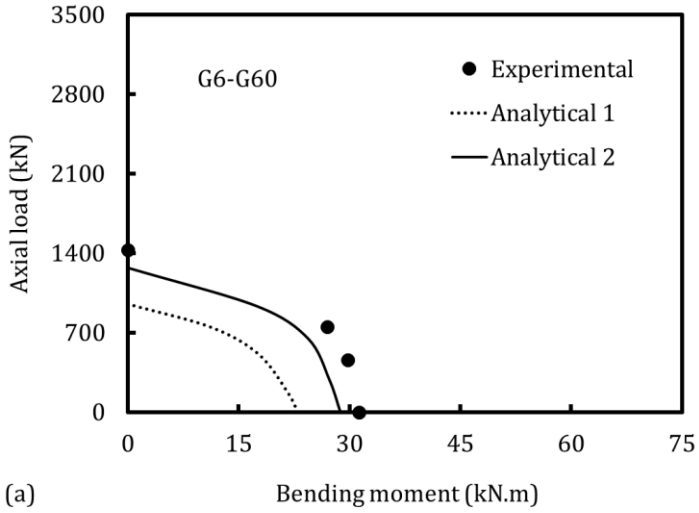

(a)

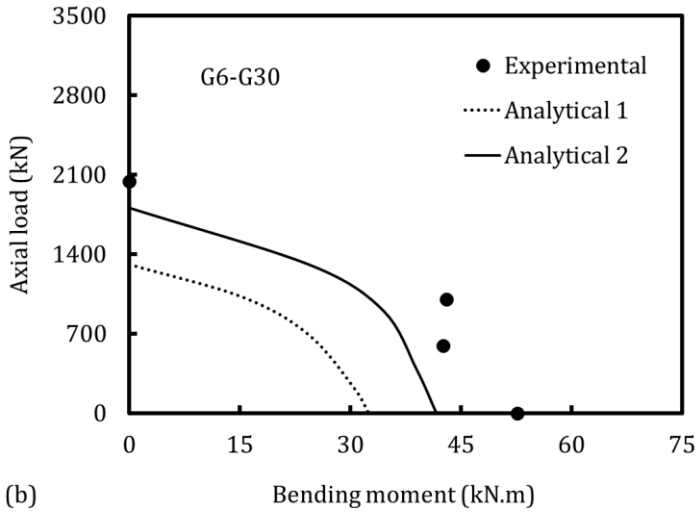

(b)

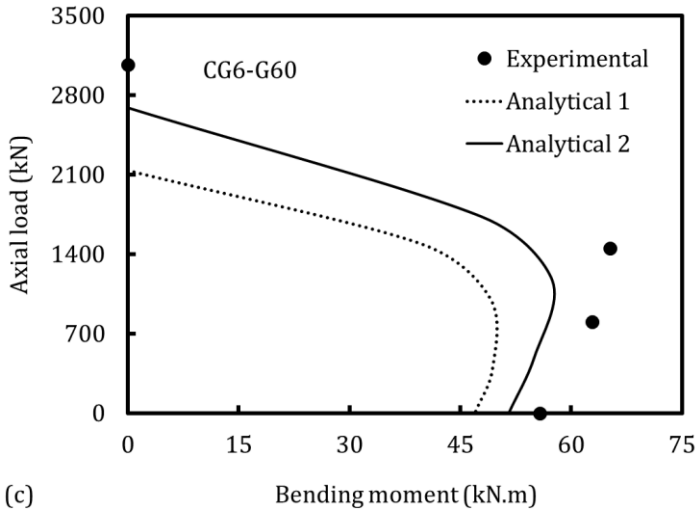

(c)

Figure 8.2. Experimental and analytical second peak $P_n - M_n$ diagrams: (a) G6-G60; (b) G6-G30; and (c) CG6-G60

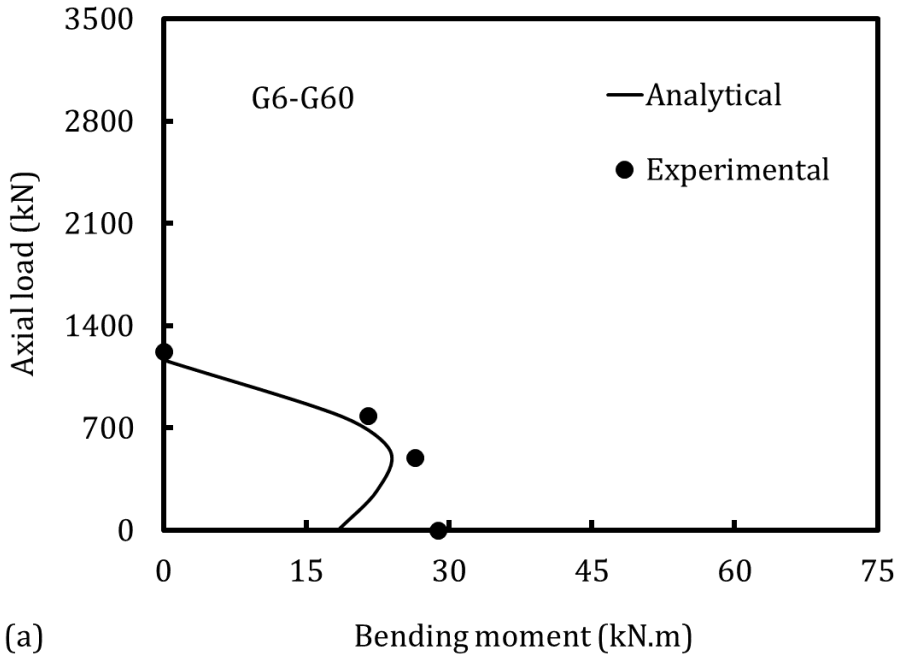

(a)

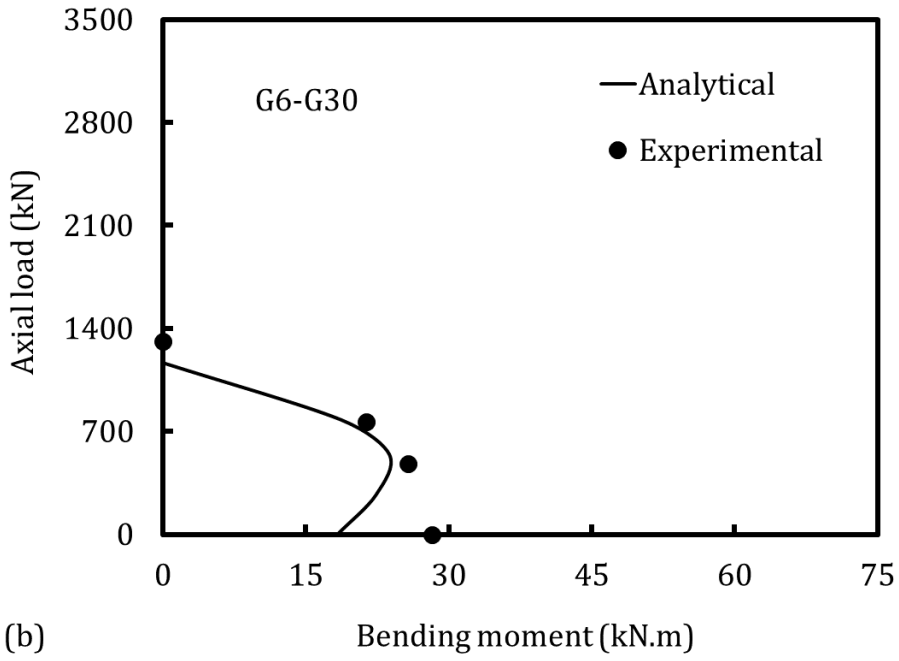

(b)

Figure 8.3. Experimental and analytical first peak $P_n - M_n$ diagrams: (a) G6-G60; and (b) G6-G30

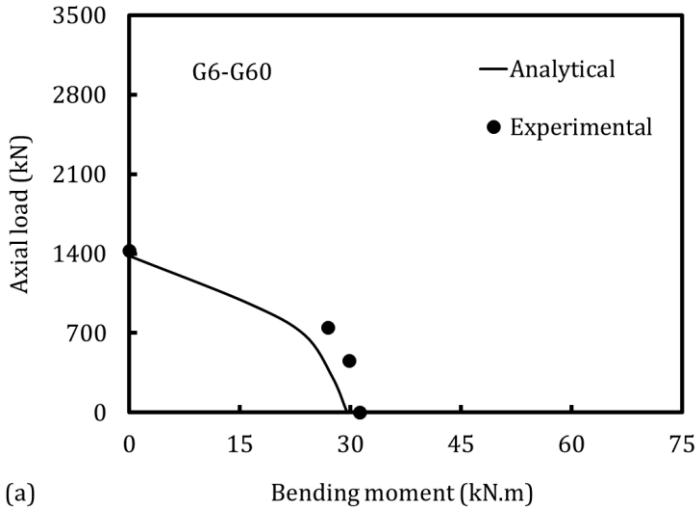

(a)

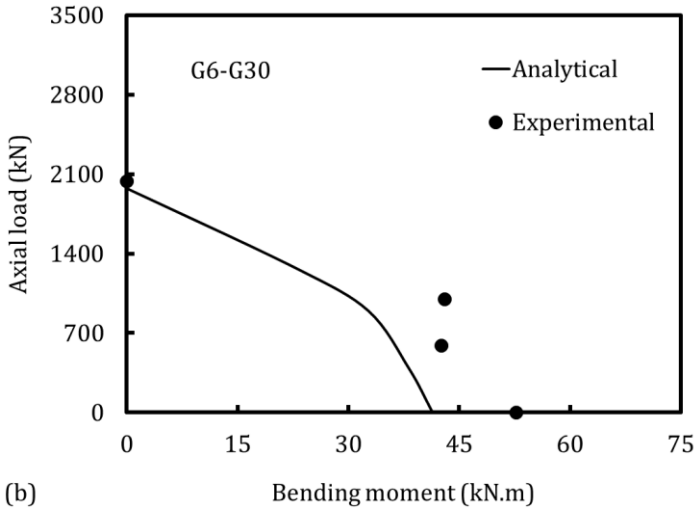

(b)

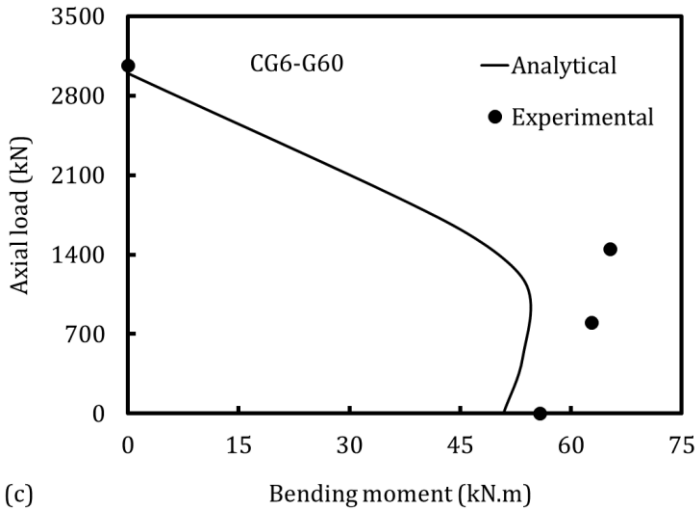

(c)

Figure 8.4. Experimental and analytical second peak $P_n - M_n$ diagrams: (a) G6-G60; (b) G6-G30; and (c) CG6-G60

8.2.1.3 Stress-block vs numerical integration

Figure 8.5 and Figure 8.6 show the comparisons between the experimental and two different analytical results. A considerable difference cannot be observed between the two analytical results. It can also be observed that both of the analytical results have good agreements with the experimental results.

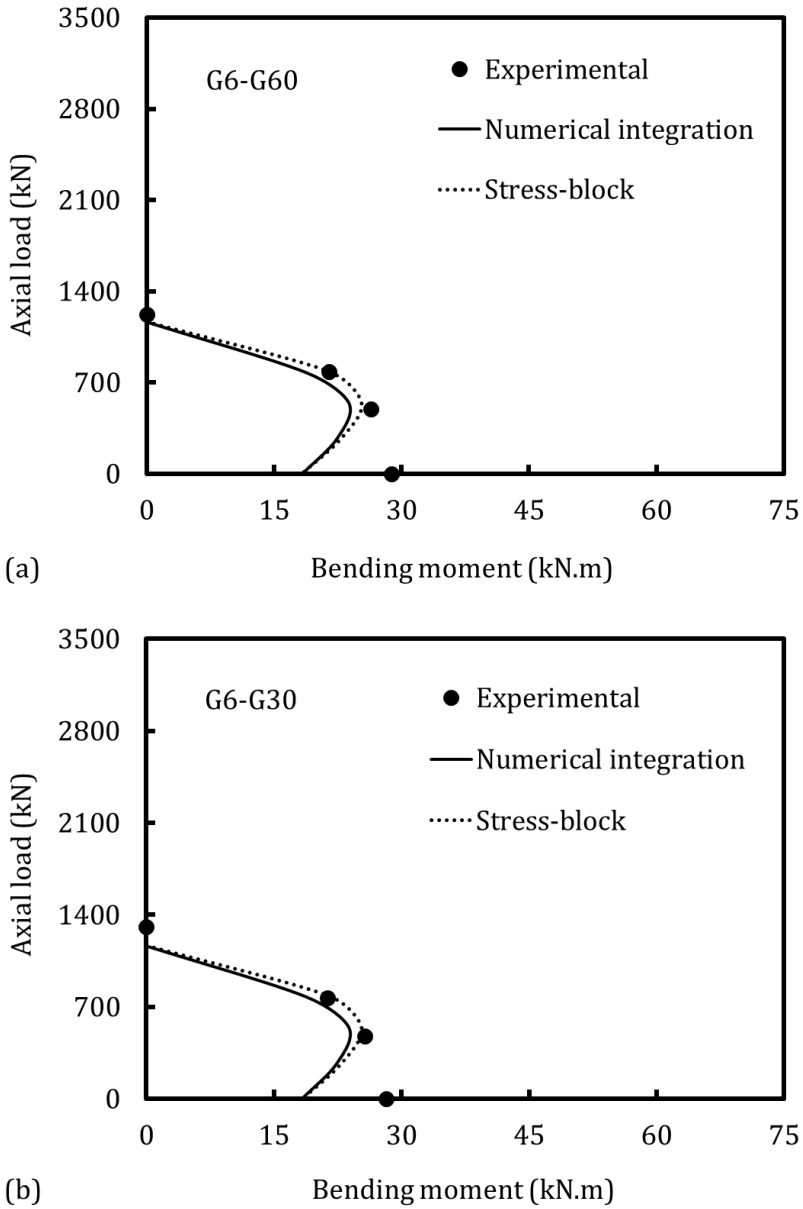

Figure 8.5. Experimental and analytical first peak $P_n - M_n$ diagrams: (a) G6-G60; and (b) G6-G30

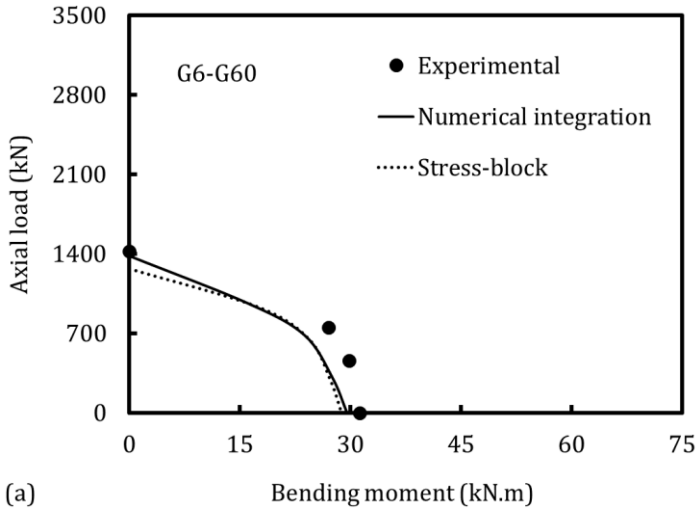

(a)

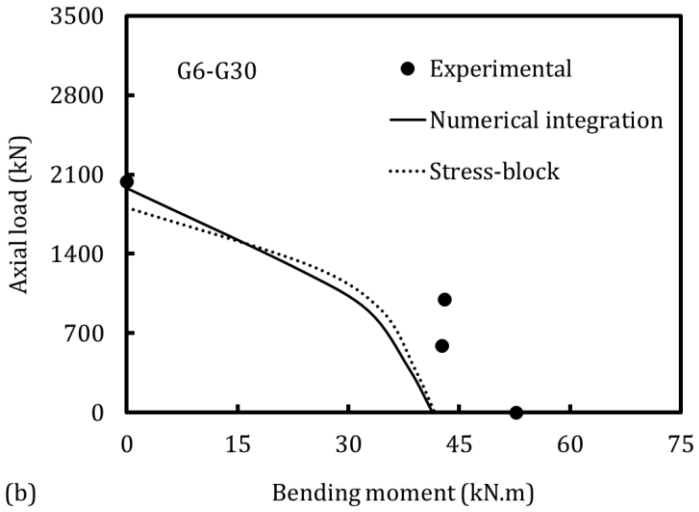

(b)

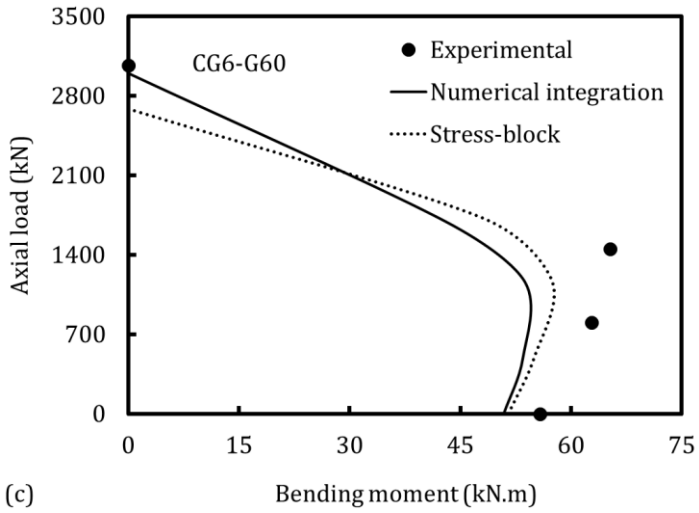

(c)

Figure 8.6. Experimental and analytical second peak $P_n - M_n$ diagrams: (a) G6-G60; (b) G6-G30; and (c) CG6-G60

8.2.2 Axial load-axial deformation behaviour

Figure 8.7 shows comparisons between the experimental and analytical axial load-axial deformation behaviour of the tested column specimens under concentric loads. The analytical axial load-axial deformation curve of the column specimens consisted of the superposition of the axial load-axial deformation of the different components (longitudinal bars, confined concrete core and unconfined concrete cover) of the specimens. A reasonable agreement can be observed between the experimental and analytical axial load-axial deformation behaviours particularly at the ascending part until the first peak load. This is because the behaviour of the load-deformation curve of the different components of the column specimens at the ascending part was relatively linear until the first peak load. The estimated value of n in Chapter 7 (Analytical study) governed the transition curve between the first and second ascending parts of the axial load-axial deformation behaviour reasonably close to the experimental results. Also, it can be seen that the second peak load of the axial load-axial deformation behaviour of the experimental results have close agreement with the analytical results. This close agreement essentially means that the developed analytical model calculated confined concrete strength and the corresponding axial strain in reasonable agreement the experimental results.

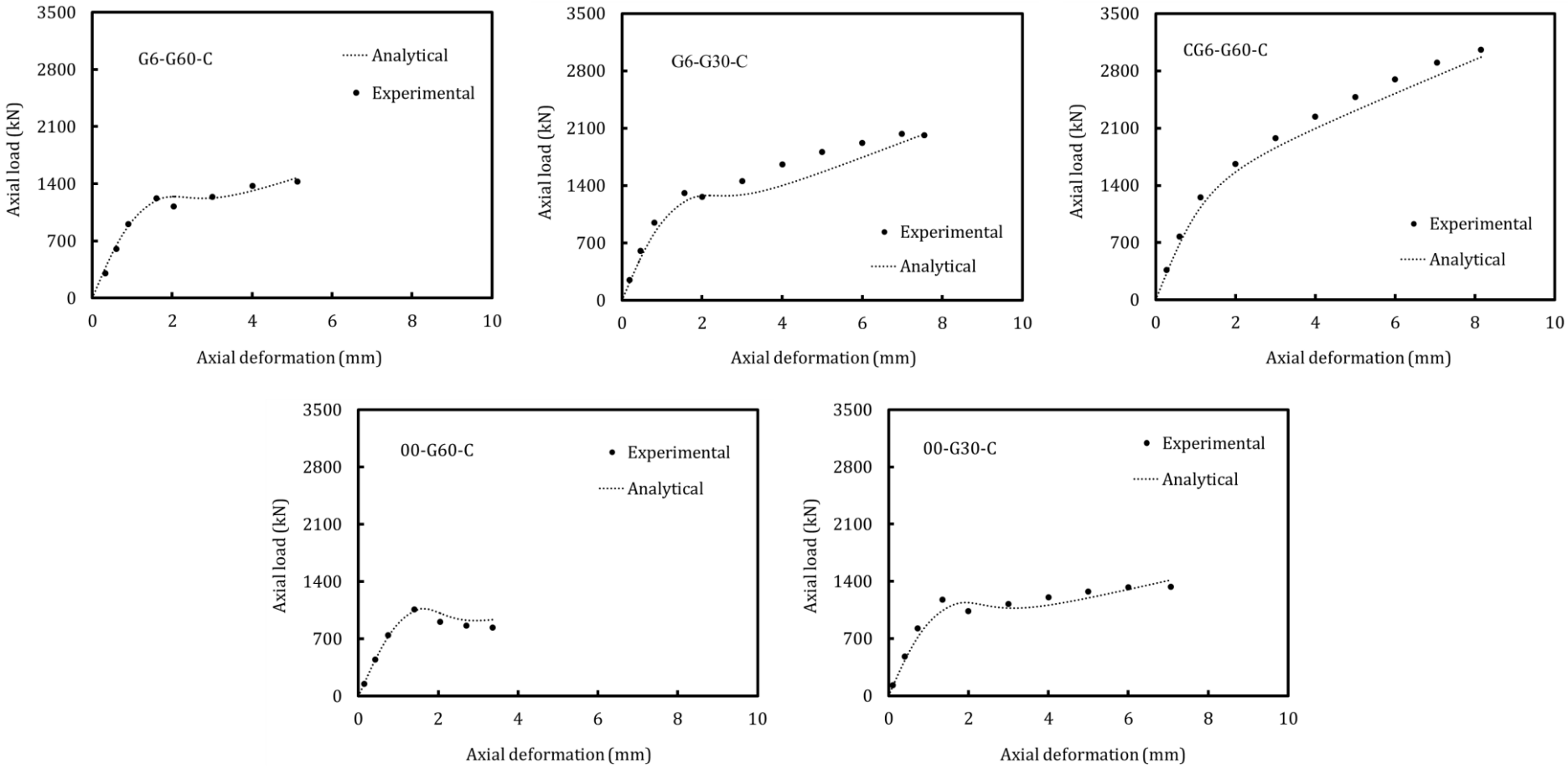

Figure 8.7. Comparison between experimental and analytical axial load-axial deformation behaviour of the tested columns

8.2.3 Moment-curvature behaviour

Figure 8.8 show the experimental and analytical moment-curvature ($M-\kappa$) curves for the tested specimens under 25 mm and 50 mm eccentricities. In general, a reasonable agreement can be observed between the experimental and analytical results especially in the specimens with 60 mm pitch GFRP helices. This is because the assumption of full composite action between concrete core and cover was achieved due to a reasonably large spacing between the transverse reinforcement. However, this assumption was not completely achieved in the specimens with 30 mm pitch of GFRP helices because small spacing of transverse reinforcement led to reducing the composite action between concrete core and cover[68, 70]. It is clear in Figure 8.8 that the analytical second peak bending moments and corresponding curvatures were lower than the experimental results. This indicates that the predicted confined concrete strains (ε_{cc}) using Equation 7.13 in Chapter 7 (Analytical study) were slightly smaller than the experimental ε_{cc}.

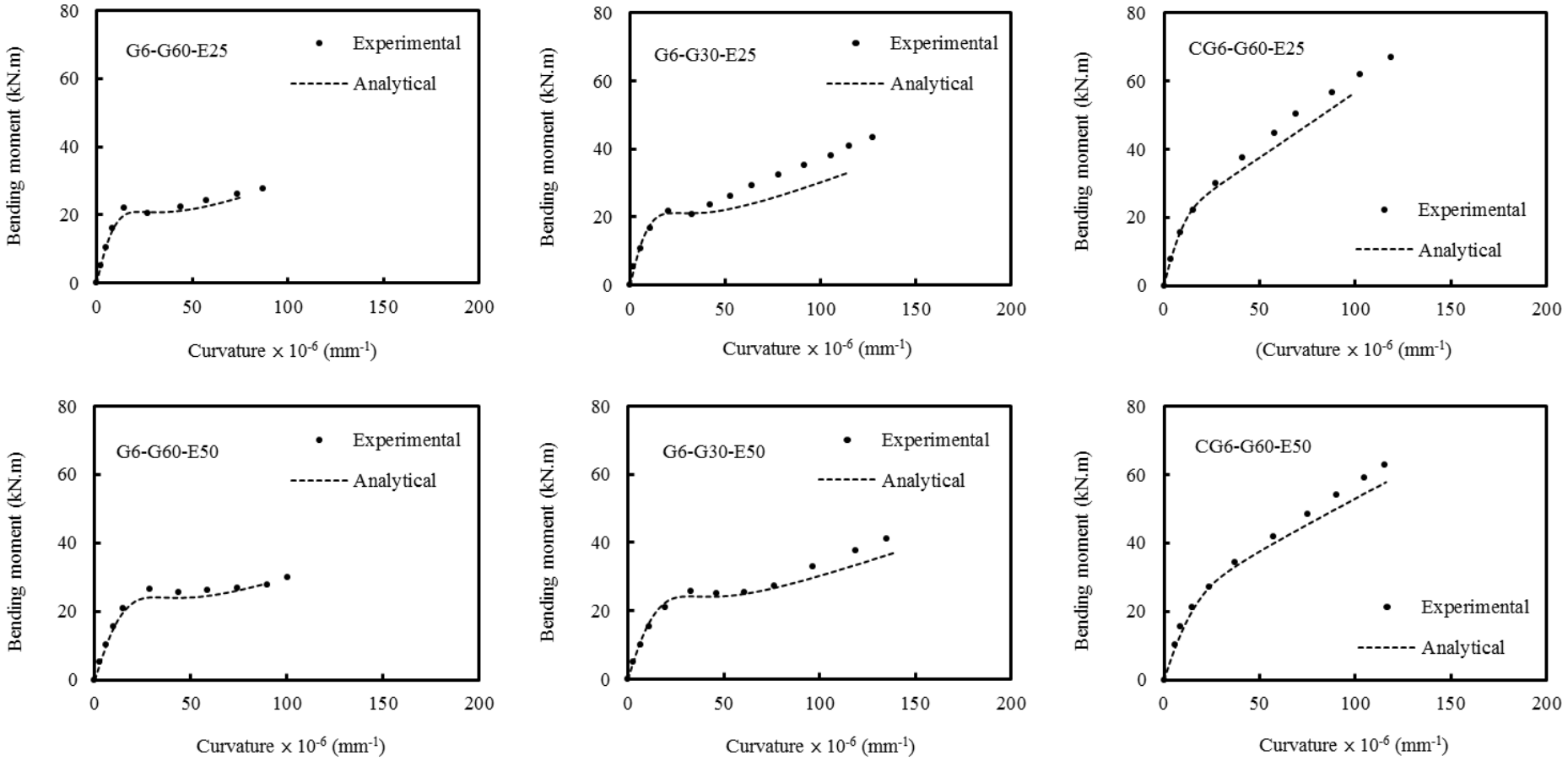

Figure 8.8. Comparison between experimental and analytical moment-curvature behaviour of the tested specimens

8.3 Parametric study

In order to investigate the effects of different parameters such as longitudinal GFRP reinforcement ratio, confinement ratio and slenderness ratio on the first and the second peak $P_n - M_n$ diagrams of GFRP-RC columns, a parametric study was conducted. Specimens in the first group (G6-G60) were employed as reference for the parametric study. The peak $P_n - M_n$ diagrams that presented in this section are normalized as:

$$P^* = \frac{P_n}{f'_{co}\ A_g} \quad \text{and} \quad M^* = \frac{M_n}{f'_{co}\ A_g\ h}$$

where $P_n^*\ and\ M_n^*$ are the normalized nominal axial loads and bending moments, respectively. In addition, any comparison between unconfined and confined cross-sections has been made in this section are based on the ultimate state condition. The first peak $P^* - M^*$ diagram represents the ultimate condition for unconfined concrete cross-sections and the second peak $P^* - M^*$ diagram represents the ultimate condition for confined concrete cross-sections.

8.3.1 Longitudinal reinforcement ratio

The effect of longitudinal reinforcement ratio (ρ_f) on the first and the second peak $P^* - M^*$ diagrams was investigated using the analytical models presented in Chapter 7 (Analytical study). The ρ_f ranged between 1% to 4% after AS[124]. Figure 8.9 shows the effects of changing ρ_f on the peak $P^* - M^*$ diagrams. Increasing ρ_f led to increasing the strength capacity of the specimens in the first and the second peak $P^* - M^*$ diagrams. The strength improvements due to increasing ρ_f were more pronounced in the second peak $P^* - M^*$ diagrams. This is because the strain distribution (compression and tension) in the cross-sections in the second peak loads (confined cross-section) was much greater than in the first peak loads (unconfined cross-section). It was observed that reducing ρ_f resulted in a great tensile strain in the tension side of the GFRP-RC cross-sections with increasing load-eccentricity, particularly in the flexural loading conditions. It can be noticed that insufficient ρ_f sometimes leads to a brittle tensile failure of the FRP bars before the peak $P^* - M^*$ diagrams reach to the pure bending condition, as this phenomenon was also observed in Choo et al.[53]. Choo et al.[56], therefore, proposed a set of equations to limit the minimum ρ_f for rectangular cross-sections to prevent brittle tensile failure of FRP bars in the tension side under pure bending loads. In addition, an extensive study was carried out in Chapter 5 to limit the minimum ρ_f for different cross-sectional geometry and different arrangements of FRP bars for FRP-RC members.

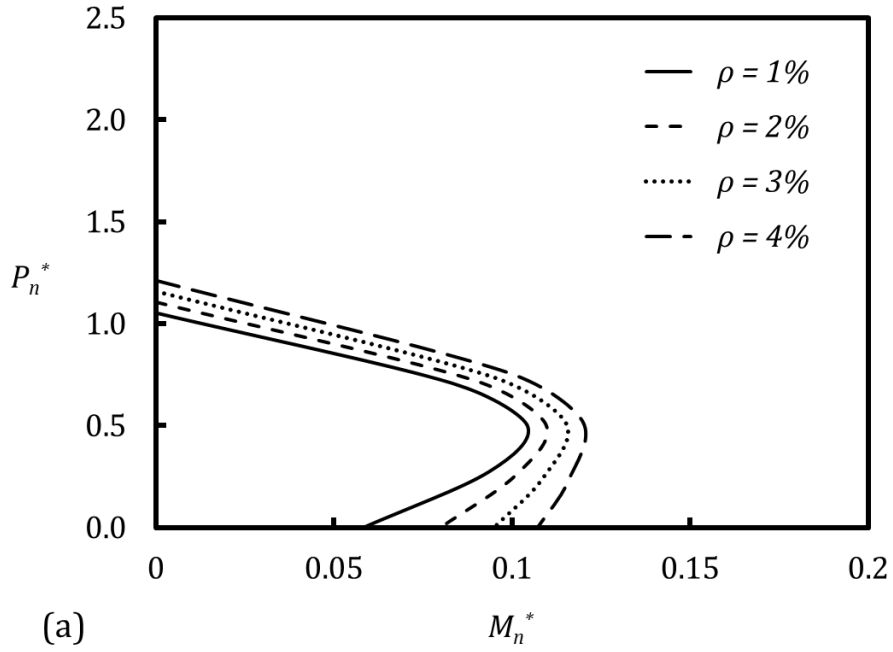

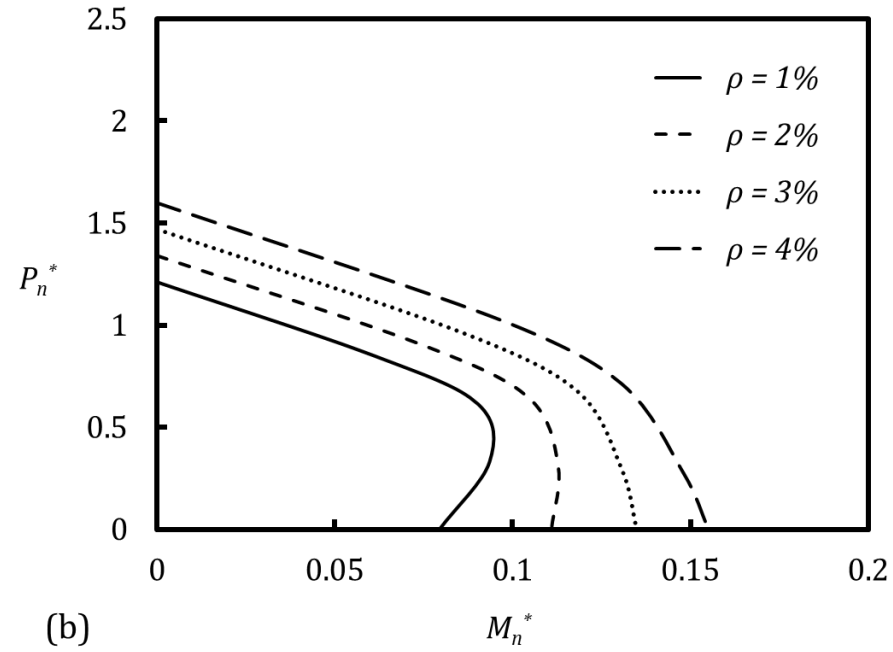

Figure 8.9. Effect of ρ_f on the peak $P^* - M^*$ diagrams: (a) first peak $P^* - M^*$ diagram; and (b) second peak $P^* - M^*$ diagram

8.3.2 Confinement ratio

It is clear that confinement ratio (f_l/f'_{co}) does not affect the first peak $P^* - M^*$ diagram, as the concrete cross-section considered unconfined concrete. Figure 8.10 shows the effects of four different f_l/f'_{co} (0.1-0.4) on the second peak $P^* - M^*$ diagram. The improvements in the second peak $P^* - M^*$ diagram of the GFRP-RC columns due to increasing f_l/f'_{co} were because of two reasons: (1) increasing the concrete strength; and (2) considerable increase in the concrete strain. Increasing concrete strain increases compression force in the concrete as well as the tensile forces in the FRP bars.

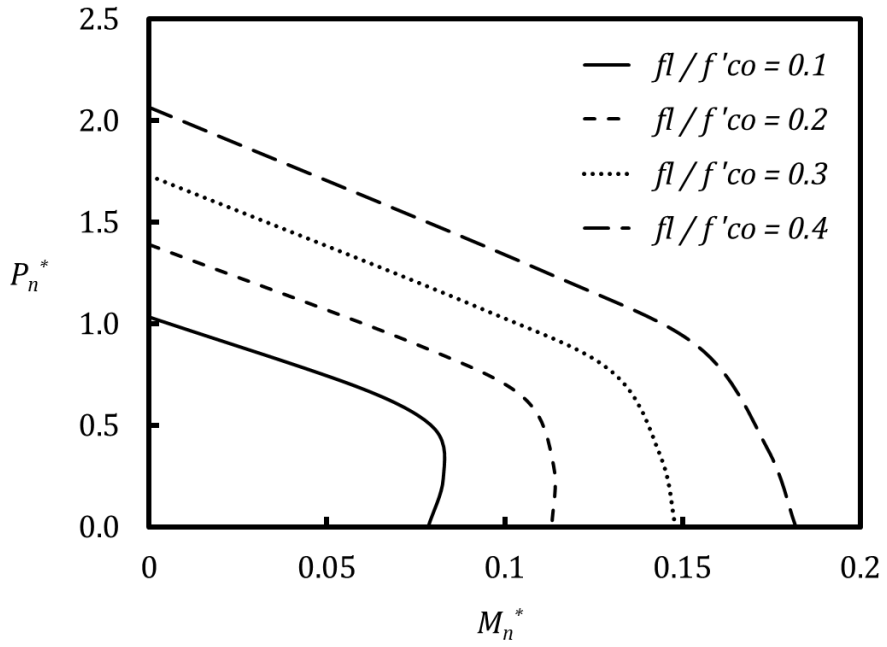

Figure 8.10. Effect of f_l/f'_{co} on second peak $P^* - M^*$ diagram

It is evident that providing confinement for concrete can enhance the strength and strain of the concrete. However, insufficient confinement may not be able to effectively confine the concrete core due to the weakness of the confining material to the non-uniform deformation of concrete[89, 157]. Mirmiran et al.[157] introduced the Modified Confinement Ratio (MCR) to limit minimum f_l/f'_{co} for externally bonded FRP. Based on MCR, no enhancement can be expected if $f_l/f'_{co} < 0.15$ for circular cross-sections. Also, Lam and Teng[89] limit the $f_l/f'_{co} \geq 0.07$ for effective confinement by the FRP jackets. Internal confinement by FRP helices or ties, however, needs greater f_l/f'_{co} to be strong enough for the non-uniform deformation of concrete as well as to substitute the loss of strength due to concrete cover spalling. Providing insufficient f_l/f'_{co} may not allow the specimens to obtain a second peak $P^* - M^*$ diagram comparable to the first peak one.

Figure 8.11 shows the comparison between the first and the second peak $P^* - M^*$ diagrams for reference GFRP-RC specimens with three different f_l/f'_{co}. It can be observed that $f_l/f'_{co} = 0.1$ cannot provide enough confinement for concrete core to reach the second peak to the first peak $P^* - M^*$ diagram. With the $f_l/f'_{co} = 0.15$, the second peak $P^* - M^*$ diagram improved and partially exceeded the first peak $P^* - M^*$ diagram. However, $f_l/f'_{co} = 0.2$ provides a greater second peak $P^* - M^*$ diagram for different load eccentricities than the first peak $P^* - M^*$ diagram.

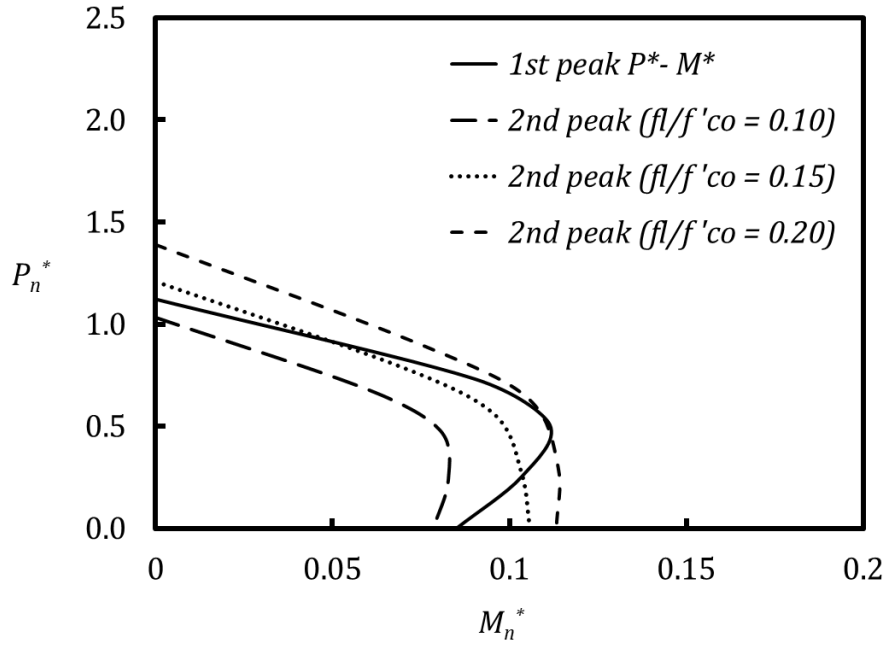

Figure 8.11. Comparison between first and second peak $P^* - M^*$ diagrams with three different f_l/f'_{co}

8.3.3 Slenderness ratio

The slenderness ratio (kL/r) of a RC column is defined as the ratio of effective length (kL) to radius of gyration (r). Figure 8.12 shows the effect of kL/r on the peak $P^* - M^*$ diagrams for a typical FRP-RC specimen, where $P_n e_i$ is the first order bending moment due to initial eccentricity (e_i) at the ends of the specimen and $P_n \delta$ is the second order bending moment due to maximum lateral deformation (δ) along the height of the column. With increasing kL/r, δ becomes larger and causes a considerable decrease in the peak $P^* - M^*$ diagram. A maximum limit, therefore, for kL/r is introduced in ACI[40] and AS 3600-2009[124] based on 5% strength reduction.

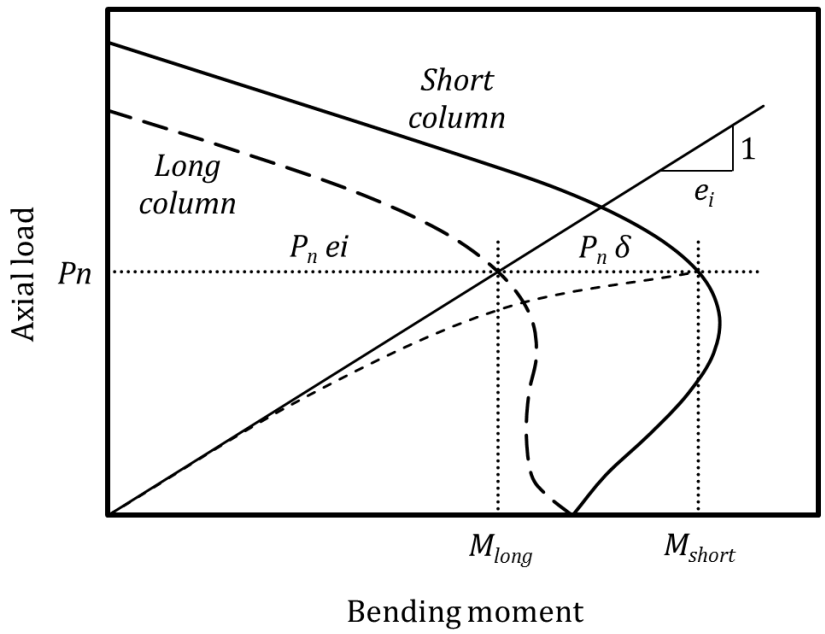

Figure 8.12. Typical peak $P^* - M^*$ diagram for short and long FRP-RC columns

Considering to the specimens in Group G6-G60, which are pin-ended columns and bend in a single curvature, the δ is at the mid-height of the columns. The deformed shape can be assumed to be a half-sine wave as explained in Bazant et al.[156] and Jiang and Teng[143] and shown in Figure 8.13. Hence, the δ can be calculated as:

$$\delta = (L/\pi)^2 \, \kappa_{mid} \tag{8.1}$$

$$\kappa_{mid} = \varepsilon_{cu}/c \tag{8.2}$$

where $L =$ the height of the columns and $\kappa_{mid} =$ the curvature at mid-height of the columns.

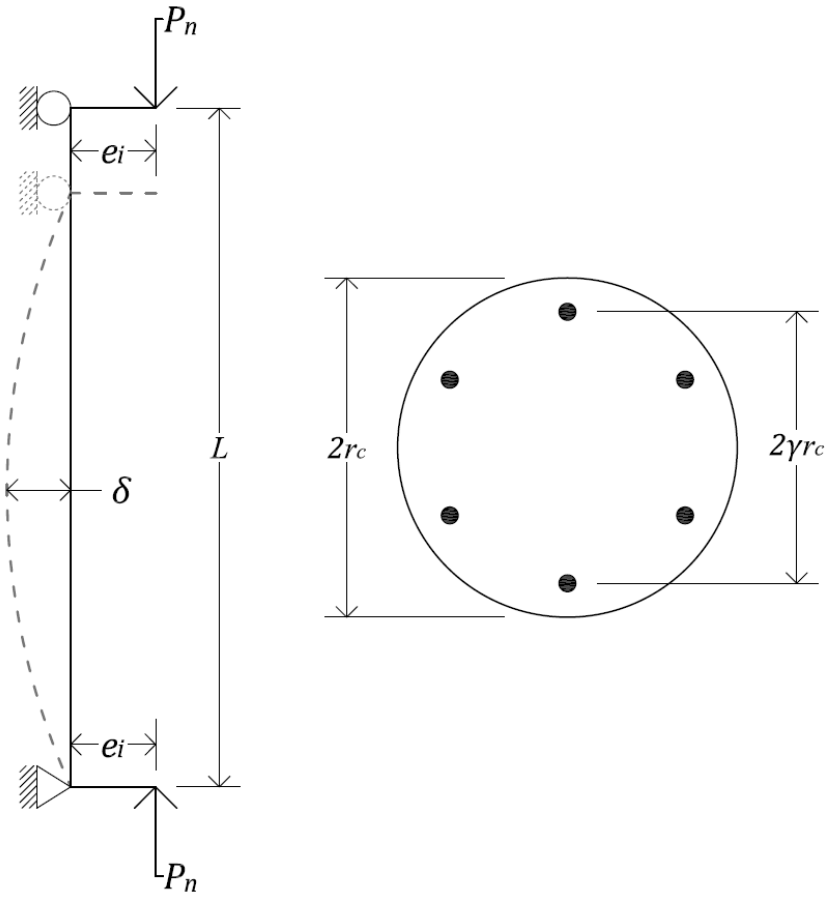

Figure 8.13. Typical deformation of pin-ended single curvature column

Figure 8.14(a, b) shows the effect of kL/r on the first and the second peak $P^* - M^*$ diagrams of the specimens in Group G6-G60. It is evident that the effect of kL/r was more pronounced in the second peak $P^* - M^*$ diagram because of greater secondary bending moments corresponding to the second peak loads.

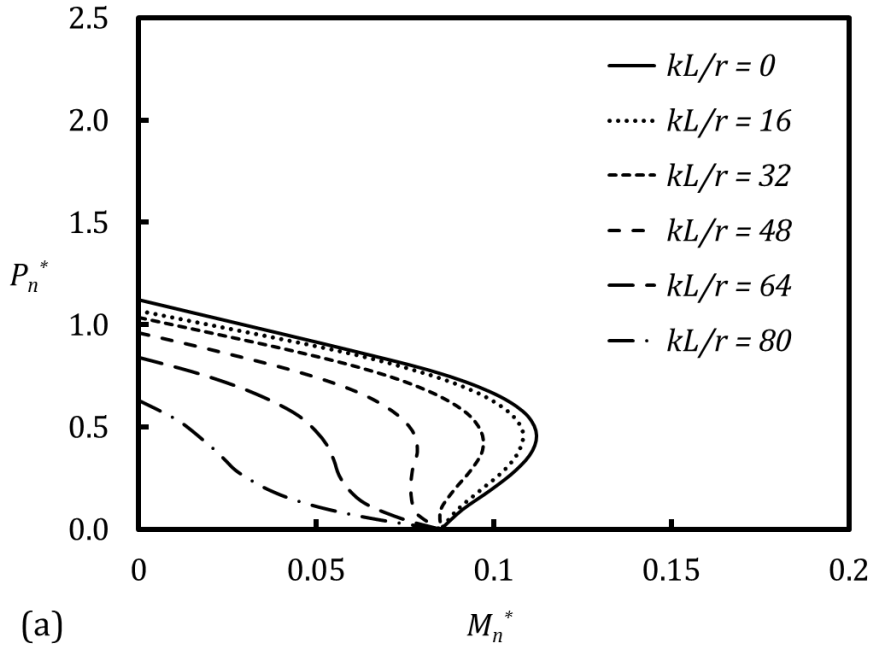

(a)

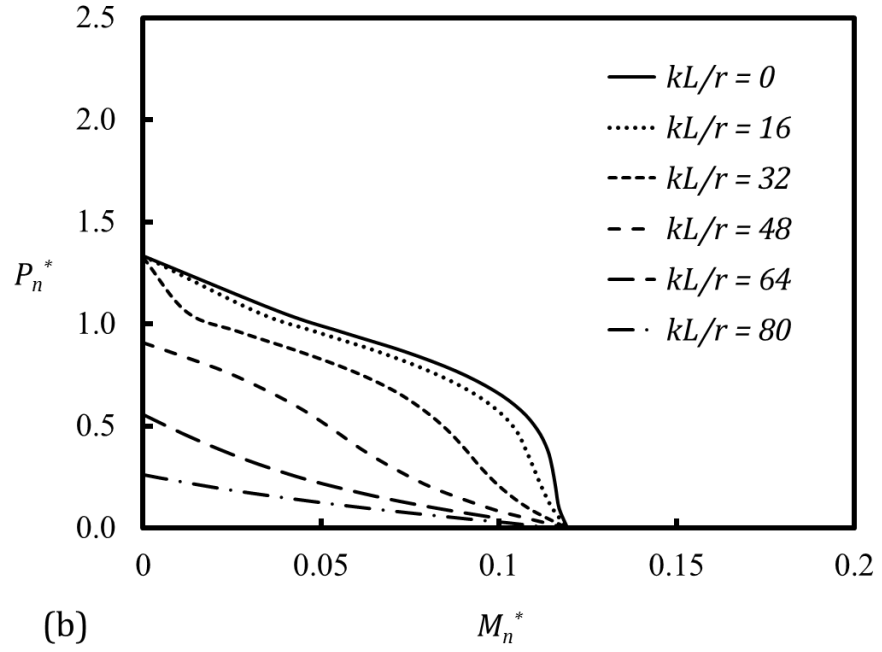

(b)

Figure 8.14. Effect of kL/r on the peak $P^* - M^*$ diagrams: (a) first peak $P^* - M^*$ diagram; and (b) second peak $P^* - M^*$ diagram

The parameters affecting kL/r for the specimens in Group G6-G60 can be investigated by assuming $M_{long} \leq 0.95M_{short}$ at the load eccentricity ratio(e_i/r_c) of 0.4 after Mirmiran et al.[55], where r_c is equal to $h/2$ for the first peak $P^* - M^*$ diagram and equal to $d_c/2$ for the second peak $P^* - M^*$ diagram. From Figure 8.12,

$$M_{long} = M_{short} - P_n\,\delta \tag{8.3}$$

Solving Equation 8.3 and considering $M_{long} = 0.95M_{short}$, $M_{short}/P_n = e_i$ and $e_i = 0.4\,r_c$,

$$\delta = 0.02\,r_c \tag{8.4}$$

By substituting Equations 8.1 and 8.2 in Equation 8.4 and considering $kL/r = 8L/r_c$ for circular columns bend in a single curvature, the maximum limit for kL/r can be expressed as:

$$\frac{kL}{r} = \frac{\pi}{5}\sqrt{\frac{2(1+\gamma)}{\varepsilon_{cu} - \varepsilon_{fmax}}} \tag{8.5}$$

where $\gamma =$ the ratio of distance between FRP bars in the tension side to FRP bars in the compression side to $2r_c$ as shown in Figure 8.13, and ε_{cu} and ε_{fmax} are the ultimate concrete compressive strain in the extreme compression fibre and maximum tensile strain in the first layer of the GFRP bars in the tension side, respectively. The maximum limit of kL/r calculated using Equation 8.5 for the reference GFRP-RC specimens was 18.7 which is smaller than 22 for steel-RC columns. This is because steel has a greater elastic modulus which results in a smaller absolute value for ε_{fmax} in Equation 8.5 and results in a greater kL/r. The maximum limit of kL/r for the reference GFRP-RC columns was greater than the 17.2 reported in Mirmiran et al.[55] for GFRP-RC columns. This is because the reinforcement ratio (ρ_f) and elastic

modulus (E_f) of the GFRP bars in this study were greater than the column specimen in Mirmiran et al.[55]. The greater ρ_f and E_f lead to a reduction in the absolute value of ε_{fmax} in Equation 8.5 and result in a greater kL/r. Equation 8.5 can also explain the reason of a greater effect of kL/r in the second peak $P^* - M^*$ diagram. This is because in confined concrete cross-section, ε_{cu} and absolute value of ε_{fmax} increase relatively with increasing f_l/f'_{co} and result in reducing the maximum limit of kL/r. Consequently, it can be observed the maximum limit of kL/r reduces from 18.7 (corresponding to the first peak load) to 13.6 (corresponding to the second peak load) for the reference GFRP-RC specimens.

It is evident From Figure 8.14 that with small kL/r $(kL/r = 16 \text{ and } 32)$ the strength of the columns under concentric load did not reduce considerably at the second peak $P^* - M^*$ diagram. Therefore, Figure 8.15 was drawn based on 5% strength reduction under concentric loads to show the effects of kL/r on the first and the second peak $P^* - M^*$ diagrams. The maximum limit of kL/r for the 5% strength reductions under concentric loads were 18.2 and 33.4 corresponding to the first and the second peak $P^* - M^*$ diagrams. It can be observed that with a small eccentricity, the strength of the columns at the second peak $P^* - M^*$ diagram considerably decreases. Also, the strength reductions under load eccentricity ratio (e_i/r_c) of 0.4 were about 4.7% and 26.7% corresponding to the first and the second peak $P^* - M^*$ diagrams, respectively. Finally, it can be concluded that at the ultimate limit state and under eccentric loads, the effects of kL/r are more pronounced on the strength reductions of confined cross-sections than unconfined cross-sections because of greater lateral deformation and secondary bending moments.

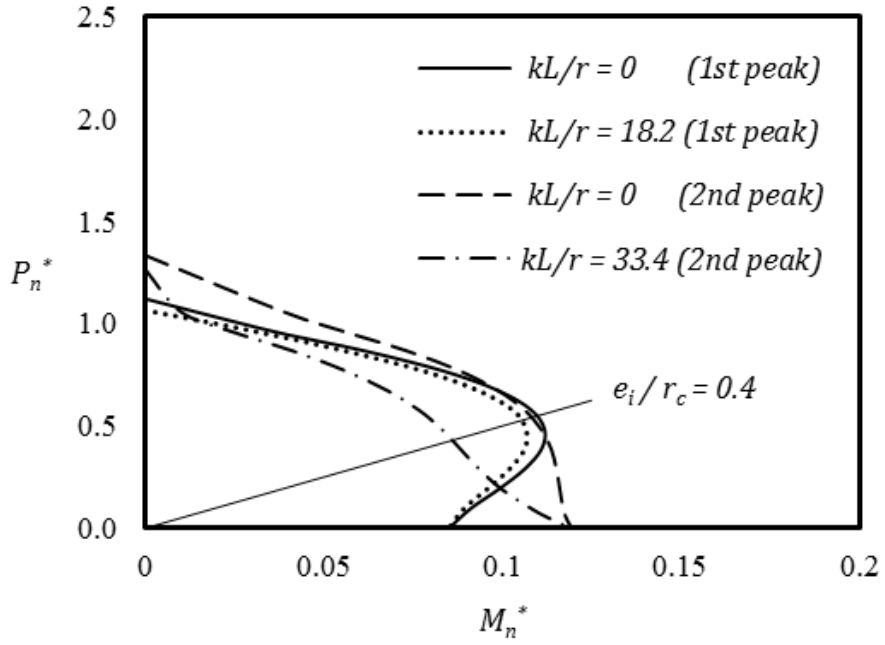

Figure 8.15. First and second peak $P^* - M^*$ diagrams for short and long columns with 5% strength reduction under concentric load

8.4 Summary

A comparison was carried out between the experimental and analytical results. In general, it can be concluded that the presented analytical calculation results in Chapter 7 (Analytical study) have a good agreement with the experimental results in Chapter 6 (Experimental study). It can also be noticed that the effect of slenderness ratio is more obvious on the confined concrete cross-section because of large lateral deformation and second order bending moment.

Conclusions that can be drawn based on the experimental and analytical studies carried out in this study are summarised in the next chapter. Also, recommendations are proposed for further studied about FRP-RC columns.

9 CONCLUSIONS AND RECOMMENDATIONS

The objective of this study was to investigate the behaviour and performance of reinforced concrete columns with GFRP bars and GFRP helices. A total of 18 circular concrete columns, divided onto five groups were cast and tested. The effect of different parameters on the behaviour of RC-specimens were investigated. These parameters include reinforcing materials (steel and GFRP), loading conditions (concentric, eccentric and flexural), different ratios of longitudinal and transverse GFRP reinforcement and wrapping the specimens with CFRP sheets.

A design guideline was proposed for the GFRP-RC columns under different loading conditions for each of the first (unconfined concrete cross-section) and the second (confined concrete core) peak loads. A parametric study was also carried out to propose an equation for the curve-shape parameter (n) for the stress-strain relationship of confined concrete. The proposed equation can estimate n which ensure that the ascending part of the stress-strain curve of confined concrete is the same as the ascending part of the stress-strain curve of unconfined concrete. The analytical axial load-axial deformation curve of the specimens was drawn based on the superposition of the axial load-axial deformation of the different components (longitudinal bars, confined concrete core and unconfined concrete cover) of the specimens. A numerical integration method was also adopted to analyse the GFRP-RC cross-sections and draw the bending moment and curvature relationship.

9.1 Conclusions

Based on the analytical and experimental investigations carried out in this study, the following conclusions can be drawn:

1. Replacing the steel bars and helices with the same amount of GFRP bars and helices led to reductions in the axial load carrying capacity and bending moment of the specimens under different loading conditions. Also, increase in the applied initial load eccentricity at the ends of the column specimens caused a reduction in the performance of the column specimens in terms of axial load carrying capacity and ductility.
2. The contribution of the longitudinal steel bars to the load carrying capacity of the column specimens under concentric load was about two times of the contribution of the longitudinal GFRP bars. However, the ductility of the GFRP-RC column specimens was slightly greater than the ductility of the reference steel-RC column specimens under different loading conditions.
3. Reducing the spacing of the GFRP helices or confining the specimens with CFRP sheets improved the performance of the specimens in terms of the second peak axial load-bending moment diagrams. However, the smaller pitch of the helices did not considerably change the first peak axial load-bending moment diagrams.
4. GFRP-RC specimens can achieve two peak axial loads. The first peak axial load represents the maximum load carrying capacity of the whole cross-section without confinement effects. The second peak axial load represents the maximum load carrying capacity of the confined concrete core alone.

5. Longitudinal GFRP bars improved the first and the second peak loads, the ductility and the confined concrete strength of the GFRP-RC columns.
6. The ratio of the hoop rupture strain to the ultimate tensile strain of the GFRP helices were 0.333 and 0.25 for the GFRP-RC columns with and without longitudinal GFRP bars, respectively, in this study. However, more experimental studies are needed to ascertain a representative value of the ratio of the hoop rupture strain to the ultimate tensile strain of GFRP helices.
7. The load carrying capacity and bending moment of the GFRP-RC specimens can be calculated by the same principles used for the conventional steel-RC specimens. Also, ignoring the contribution of the GFRP bars in compression may result in a large discrepancy between the experimental and analytical results.
8. The developed analytical model predicted the axial load-bending moment of the specimens reasonably close to the experimental results. However, the experimental bending moment of the GFRP-RC beam specimens was greater than the calculated results. This may be because the shear span of the beam specimens was smaller than two times the effective depth of the concrete cross-section.
9. The analytical procedures and the numerical integration presented in this study showed a reasonable agreement with the experimental results. However, the calculation steps and the height of the strips need to be considered carefully.
10. A parametric study was carried out to propose an equation for the curve-shape parameter (n) for the stress-strain relationship of confined concrete. The proposed equation can estimate n which ensures that the ascending part of the

stress-strain curve of confined concrete is the same as the ascending part of the stress-strain curve of unconfined concrete.

11. The analytical axial load-axial deformation behaviour of the GFRP-RC column specimens was drawn by the superimposing of the load-deformation behaviour of the different components (longitudinal GFRP bars, confined concrete core and unconfined concrete cover) of the columns. The analytical and experimental axial load-axial deformation curves agree reasonably well.
12. The assumption that stress-strain behaviour of confined concrete under concentric load can be used for concrete in the compression side for columns under eccentric load can be considered acceptable for circular cross-section columns. Also, the full composite action assumption between GFRP bars, concrete core and concrete cover for the analytical calculation showed reasonable agreement with the experimental results.
13. The parametric study showed that insufficient longitudinal reinforcement ratio sometimes leads to a brittle tensile failure of the FRP bars before the peak axial load-bending moment diagrams reach to the pure flexural strength. Therefore, minimum longitudinal reinforcement ratio should be provided to prevent brittle tensile failure of the FRP bars.
14. Internal confinement by FRP helices or ties should be strong enough for the non-uniform deformation of concrete as well as to substitute the loss of strength due to the spalling of concrete cover. A confinement ratio of 0.2 can ensure improvements in the second peak axial-load bending moment diagram.
15. The effect of slenderness ratio is more obvious on the confined concrete cross-section because of large lateral deformation and second order bending moment.

Also, the slenderness limit should be reduced for FRP-RC specimens because of lower modulus of elasticity of FRP bars.

16. The parametric study showed that unconfined concrete strength and longitudinal reinforcement ratio led to increasing the bending moments and reducing the corresponding curvatures. However, confinement ratio could increase the bending moments and corresponding curvatures.
17. The experimental and analytical investigations presented in this study indicated that GFRP bars can be used as longitudinal reinforcements to improve the performance of RC specimens in terms of axial load carrying capacity and bending moment. Also, the GFRP helices considerably confined the concrete core to sustain loads, especially after the first peak load.

9.2 Recommendations for future studies

Based on the investigations on the GFRP-RC specimens carried out in this study, the following future research areas can be recommended:

1. Similar studies on FRP-RC columns with different types of FRP bars and different cross-sections (square or rectangular) can be continued to demonstrate and establish a general design-guideline for FRP-RC members.
2. The slenderness effect on FRP-RC columns can also investigated by testing different slenderness ratios and different types of FRP bars. Also, the analytical models presented in Chapter 7 can be implemented for analysing the specimens.
3. Effect of concrete strength can also be investigated on the behaviour and performance of concrete specimens reinforced with FRP bars.

REFERENCES

1. Sheikh, M. N. and Légeron, F., "Performance based seismic assessment of bridges designed according to Canadian Highway Bridge Design Code," *Canadian Journal of Civil Engineering*, Vol. 41, No. 9, 2014, pp. 777-787.
2. Hollaway, L. C., "The evolution of and the way forward for advanced polymer composites in the civil infrastructure," *Construction and Building Materials*, Vol. 17, No. 6-7, 2003, pp. 365-378.
3. NACE (National Association of Corrosion Engineers) International, "Corrosion costs and preventive strategies in the United States," *FHWA-RD-01-156*, ⟨www.nace.org⟩, (Dec. 20, 2013).
4. Manning, D. G., "Corrosion performance of epoxy-coated reinforcing steel: North American experience," *Construction and Building Materials*, Vol. 10, No. 5 SPEC. ISS., 1996, pp. 349-365.
5. Castro, H.; Rodriguez, C.; Belzunce, F. J.; and Canteli, A. F., "Mechanical properties and corrosion behaviour of stainless steel reinforcing bars," *Journal of Materials Processing Technology*, Vol. 143-144, No. 1, 2003, pp. 134-137.
6. Chess, P. M. and Broomfield, J. P., *Cathodic protection of steel in concrete*, E & FN Spon, London and New York, 2003.
7. Bellezze, T.; Malavolta, M.; Quaranta, A.; Ruffini, N.; and Roventi, G., "Corrosion behaviour in concrete of three differently galvanized steel bars," *Cement and Concrete Composites*, Vol. 28, No. 3, 2006, pp. 246-255.
8. Sagüés, A. A.; Lee, J. B.; Chang, X.; Pickering, H.; Nystrom, E.; Carpenter, W.; Kranc, S.; Simmons, T.; Boucher, B.; and Hierholzer, S., "Corrosion of

epoxy coated rebar in Florida bridges," *Final Report to Florida DOT WPI*, University of South Florida, Tampa, Florida, 1994.

9. Xi, Y.; Abu-Hejleh, N.; Asiz, A.; and Suwito, A., "Performance evaluation of various corrosion protection systems of bridges in Colorado," *Final Report No. CDOT-DTD-R-2004-1*, Colorado Department of Transportation, Denver, Colorado, 2004.
10. Bank, L. C., *Composites for construction: Structural design with FRP materials*, John Wiley & Sons, Hoboken, New Jersey, 2006.
11. Nanni, A., "Flexural behavior and design of RC members using FRP reinforcement," *Journal of structural engineering New York, N.Y.*, Vol. 119, No. 11, 1993, pp. 3344-3359.
12. Benmokrane, B.; Chaallal, O.; and Masmoudi, R., "Flexural response of concrete beams reinforced with FRP reinforcing bars," *ACI Structural Journal*, Vol. 93, No. 1, 1996, pp. 46-55.
13. ACI Committee 440, "Guide for the design and construction of concrete reinforced with FRP bars (ACI 440.1R-15)," American Concrete Institute, Farmington Hills, MI, 2015.
14. Sonobe, Y.; Fukuyama, H.; Okamoto, T.; Kani, N.; Kimura, K.; Kobayashi, K.; Masuda, Y.; Matsuzaki, Y.; Mochizuki, S.; Nagasaka, T.; Shimizu, A.; Tanano, H.; Tanigaki, M.; and Teshigawara, M., "Design guidelines of FRP reinforced concrete building structures," *Journal of Composites for Construction*, Vol. 1, No. 3, 1997, pp. 90-114.

15. CAN/CSA S806-12, "Design and construction of building structures with fibre reinforced polymers (CAN/CSA S806-12)," Canadian Standards Association, Rexdale, ON, Canada, 2012.

16. ISIS Canada, "Reinforcing Concrete Structures with Fibre Reinforced Polymers," ⟨http://www.isiscanada.com⟩, 2007.

17. GangaRao, H. V. S.; Taly, N.; and Vijay, P. V., *Reinforced concrete design with FRP composites*, Taylor & Fracis Group, London and New York, 2006.

18. Bakis, C. E.; Bank, L. C.; Brown, V. L.; Cosenza, E.; Davalos, J. F.; Lesko, J. J.; Machida, A.; Rizkalla, S. H.; and Triantafillou, T. C., "Fiber-reinforced polymer composites for construction - State-of-the-art review," *Journal of Composites for Construction*, Vol. 6, No. 2, 2002, pp. 73-87.

19. Crawford, J. E.; Malvar, L. J.; Wesevich, J. W.; Valancius, J.; and Reynolds, A. D., "Retrofit of reinforced concrete structures to resist blast effects," *ACI Structural Journal*, Vol. 94, No. 4, 1997, pp. 371-377.

20. Wight, J. K. and MacGregor, J. G., *Reinforced concrete mechanics and design*, Pearson Education, Inc., Upper Saddle River, New Jersey, United States of America, 2012.

21. Almusallam, T. H. and Alsayed, S. H., "Stress-strain relationship of normal, high-strength and lightweight concrete," *Magazine of Concrete Research*, Vol. 47, No. 170, 1995, pp. 39-44.

22. Popovics, S., "A numerical approach to the complete stress-strain curve of concrete," *Cemement and Concroncrete Research*, Vol. 3, No. 5, 1973, pp. 583-599.

23. Ford, J. S.; Chang, D. C.; and Breen, J. E., "Behavior of concrete columns under controlled lateral deformation," *Journal of the American Concrete Institute*, Vol. 78, No. 1, 1981, pp. 3-20.

24. Carreira, D. J. and Chu, K.-H., "Stress-strain relationship for plain concrete in compression," *Journal of the American Concrete Institute*, Vol. 82, No. 6, 1985, pp. 797-804.

25. Hsu, L. S. and Hsu, C. T. T., "Complete stress-strain behaviour of high-strength concrete under compression," *Magazine of Concrete Research*, Vol. 46, No. 169, 1994, pp. 301-312.

26. Wee, T. H.; Chin, M. S.; and Mansur, M. A., "Stress-strain relationship of high-strength concrete in compression," *Journal of Materials in Civil Engineering*, Vol. 8, No. 2, 1996, pp. 70-76.

27. Légeron, F., "Seismic behavior of structures made with normal and high-performance concrete," PhD thesis, University of Sherbrooke, Sherbrooke, Canada, 1998.

28. Yang, K. H.; Mun, J. H.; Cho, M. S.; and Kang, T. H. K., "Stress-strain model for various unconfined concretes in compression," *ACI Structural Journal*, Vol. 111, No. 4, 2014, pp. 819-826.

29. Wang, P.; Shah, S.; and Naaman, A., "Stress-strain curves of normal and lightweight concrete in compression," *ACI Journal Proceedings*, Vol. 75, No. 11, 1978, pp. 603-611.

30. Tasnimi, A. A., "Mathematical model for complete stress-strain curve prediction of normal, light-weight and high-strength concretes," *Magazine of Concrete Research*, Vol. 56, No. 1, 2004, pp. 23-34.

31. Benmokrane, B.; Chaallal, O.; and Masmoudi, R., "Glass fibre reinforced plastic (GFRP) rebars for concrete structures," *Construction and Building Materials*, Vol. 9, No. 6, 1995, pp. 353-364.

32. Robert, M. and Benmokrane, B., "Physical, mechanical, and durability characterization of preloaded GFRP reinforcing bars," *Journal of Composites for Construction*, Vol. 14, No. 4, 2010, pp. 368-375.

33. Chaallal, O. and Benmokrane, B., "Physical and mechanical performance of an innovative glass-fiber-reinforced plastic rod for concrete and grouted anchorages," *Canadian Journal of Civil Engineering*, Vol. 20, No. 2, 1993, pp. 254-268.

34. Wu, W.-P., "Thermomechanical properties of fiber reinforced plastic (FRP) bars," PhD Thesis, West Virginia University, Morgantown, United States, 1990.

35. Kocaoz, S.; Samaranayake, V. A.; and Nanni, A., "Tensile characterization of glass FRP bars," *Composites Part B: Engineering*, Vol. 36, No. 2, 2005, pp. 127-134.

36. Carvelli, V.; Fava, G.; and Pisani, M. A., "Anchor system for tension testing of large diameter GFRP bars," *Journal of Composites for Construction*, Vol. 13, No. 5, 2009, pp. 344-349.

37. Deitz, D.; Harik, I.; and Gesund, H., "Physical properties of glass fiber reinforced polymer rebars in compression," *Journal of Composites for Construction*, Vol. 7, No. 4, 2003, pp. 363-366.

38. Kobayashi, K. and Fujisaki, T., "Compressive Behavior of FRP Reinforcement in non-Prestressed Concrete Members," *Proceeding of The 2nd International*

RILEM Symposium (FRPRCS-2) on Non-Metallic (FRP) Reinforcement for Concrete Structures, University of Ghent, Belgium, 1995, pp. 267-274.

39. ACI Committee 440, "Guide for the design and construction of concrete reinforced with FRP bars (ACI 440.1R-06)," American Concrete Institute, Farmington Hills, MI, 2006.
40. ACI Committee 318, "Building code requirements for structural concrete (ACI 318-14)," American Concrete Institute, Farmington Hills, MI, 2014.
41. Castro, P. F.; Howie, I.; and Karbhari, V., "Concrete columns reinforced with FRP rods," *International Journal of Materials and Product Technology*, Vol. 10, No. 3-6, 1995, pp. 338-343.
42. Alsayed, S.; Al-Salloum, Y.; Almusallam, T.; and Amjad, M., "Concrete columns reinforced by glass fiber reinforced polymer rods," *ACI Special Publication*, Vol. 188, 1999, pp. 103-112.
43. Lotfy, E. M., "Behavior of reinforced concrete short columns with Fiber Reinforced polymers bars," *International Journal of Civil and Structural Engineering*, Vol. 1, No. 3, 2010, pp. 545-557.
44. De Luca, A.; Matta, F.; and Nanni, A., "Behavior of full-scale glass fiber-reinforced polymer reinforced concrete columns under axial load," *ACI Structural Journal*, Vol. 107, No. 5, 2010, pp. 589-596.
45. Tobbi, H.; Farghaly, A. S.; and Benmokrane, B., "Concrete columns reinforced longitudinally and transversally with glass fiber-reinforced polymer bars," *ACI Structural Journal*, Vol. 109, No. 4, 2012, pp. 551-558.

46. Pantelides, C. P.; Gibbons, M. E.; and Reaveley, L. D., "Axial load behavior of concrete columns confined with GFRP spirals," *Journal of Composites for Construction*, Vol. 17, No. 3, 2013, pp. 305-313.

47. Afifi, M. Z.; Mohamed, H. M.; and Benmokrane, B., "Axial capacity of circular concrete columns reinforced with GFRP bars and spirals," *Journal of Composites for Construction*, Vol. 18, No. 1, 2014, pp. 04013017.

48. Afifi, M. Z.; Mohamed, H. M.; and Benmokrane, B., "Strength and axial behavior of circular concrete columns reinforced with CFRP bars and spirals," *Journal of Composites for Construction*, Vol. 18, No. 2, 2014, pp. 04013035.

49. Mohamed, H. M.; Afifi, M. Z.; and Benmokrane, B., "Performance evaluation of concrete columns reinforced longitudinally with FRP bars and confined with FRP hoops and spirals under axial load," *Journal of Bridge Engineering*, Vol. 19, No. 7, 2014, pp. 04014020.

50. Tobbi, H.; Farghaly, A. S.; and Benmokrane, B., "Behavior of concentrically loaded fiber-reinforced polymer reinforced concrete columns with varying reinforcement types and ratios," *ACI Structural Journal*, Vol. 111, No. 2, 2014, pp. 375-385.

51. Kawaguchi, N., "Ultimate strength and deformation characteristics of concrete members reinforced with AFRP rods under combined axial tension or compression and bending," *ACI Special Publication*, Vol. 138, 1993, pp. 671-684.

52. Amer, A.; Arockiasamy, M.; and Shahawy, M., "Ultimate strength of eccentrically loaded concrete columns reinforced with CFRP bars," *Proceeding of the 2nd International Conference on Advanced Composite Materials in*

Bridges and Strucures, ACMBS-II, Canadian Society for Civil Engineering, Montereal, Canada, 1996, pp. 209-216.

53. Choo, C. C.; Harik, I. E.; and Gesund, H., "Strength of rectangular concrete columns reinforced with fiber-reinforced polymer bars," *ACI Structural Journal*, Vol. 103, No. 3, 2006, pp. 452-459.

54. Mirmiran, A., "Length effects on FRP-reinforced concrete columns," *Proceeding of The 2nd International Conference on Composites in Infrastructure*, University of Arizona, Tucson, USA, 1998, pp. 518-532.

55. Mirmiran, A.; Yuan, W.; and Chen, X., "Design for slenderness in concrete columns internally reinforced with fiber-reinforced polymer bars," *ACI Structural Journal*, Vol. 98, No. 1, 2001, pp. 116-125.

56. Choo, C. C.; Harik, I. E.; and Gesund, H., "Minimum reinforcement ratio for fiber-reinforced polymer reinforced concrete rectangular columns," *ACI Structural Journal*, Vol. 103, No. 3, 2006, pp. 460-466.

57. Newhook, J.; Ghali, A.; and Tadros, G., "Concrete flexural members reinforced with fiber reinforced polymer: Design for cracking and deformability," *Canadian Journal of Civil Engineering*, Vol. 29, No. 1, 2002, pp. 125-134.

58. Masmoudi, R.; Thériault, M.; and Benmokrane, B., "Flexural behavior of concrete beams reinforced with deformed fiber reinforced plastic reinforcing rods," *ACI Structural Journal*, Vol. 95, No. 6, 1998, pp. 665-676.

59. El-Salakawy, E.; Kassem, C.; and Benmokrane, B., "Flexural behaviour of concrete beams reinforced with carbon FRP composite bars," *4th Structural Specialty Conference of the Canadian Society for Civil Engineering*, Canadian Society for Civil Engineering, Montreal, Canada, 2002, pp. 2025-2033.

60. Kassem, C.; Farghaly, A. S.; and Benmokrane, B., "Evaluation of flexural behavior and serviceability performance of concrete beams reinforced with FRP bars," *Journal of Composites for Construction*, Vol. 15, No. 5, 2011, pp. 682-695.

61. Kalpana, V. G. and Subramanian, K., "Behavior of concrete beams reinforced with GFRP BARS," *Journal of Reinforced Plastics and Composites*, Vol. 30, No. 23, 2011, pp. 1915-1922.

62. El-Nemr, A.; Ahmed, E. A.; and Benmokrane, B., "Flexural behavior and serviceability of normal- And high-strength concrete beams reinforced with glass fiber-reinforced polymer bars," *ACI Structural Journal*, Vol. 110, No. 6, 2013, pp. 1077-1087.

63. Toutanji, H. and Deng, Y., "Deflection and crack-width prediction of concrete beams reinforced with glass FRP rods," *Construction and Building Materials*, Vol. 17, No. 1, 2003, pp. 69-74.

64. Thériault, M. and Benmokrane, B., "Effects of FRP reinforcement ratio and concrete strength on flexural behavior of concrete beams," *Journal of Composites for Construction*, Vol. 2, No. 1, 1998, pp. 7-15.

65. Alsayed, S. H., "Flexural behaviour of concrete beams reinforced with GFRP bars," *Cement and Concrete Composites*, Vol. 20, No. 1, 1998, pp. 1-11.

66. Toutanji, H. A. and Saafi, M., "Flexural behavior of concrete beams reinforced with glass fiber-reinforced polymer (GFRP) bars," *ACI Structural Journal*, Vol. 97, No. 5, 2000, pp. 712-719.

67. Jaejer, L.; Mufti, A.; and Tadros, G., "The concept of the overall performance factor in rectangular-section reinforced concrete beams," *Proceedings of the*

3rd International Symposium on Non-Metallic (FRP) Reinforcement for Concrete Structures, 1997, pp. 551-558.

68. Razvi, S. R. and Saatcioglu, M., "Strength and deformability of confined high-strength concrete columns," *ACI Structural Journal*, Vol. 91, No. 6, 1994, pp. 678-687.

69. Mander, J. B.; Priestley, M. J. N.; and Park, R., "Observed Stress-Strain Behavior of Confined Concrete," *Journal of structural engineering New York, N.Y.*, Vol. 114, No. 8, 1988, pp. 1827-1849.

70. Pessiki, S. and Pieroni, A., "Axial load behavior of large scale spirally reinforced high-strength concrete columns," *ACI Structural Journal*, Vol. 94, No. 3, 1997, pp. 304-313.

71. Sheikh, S. A. and Toklucu, M. T., "Reinforced Concrete Columns Confined by Circular Spirals and Hoops," *ACI Structural Journal*, Vol. 90, No. 5, 1993, pp. 542-553.

72. Liu, J.; Foster, S. J.; and Attard, M. M., "Strength of Tied High-Strength Concrete Columns Loaded in Concentric Compression," *ACI Structural Journal*, Vol. 97, No. 1, 2000, pp. 149-156.

73. Bing, L.; Park, R.; and Tanaka, H., "Stress-Strain Behavior of High-Strength Concrete Confined by Ultra-High-and Normal-Strength Transverse Reinforcements," *ACI Structural Journal*, Vol. 98, No. 3, 2001, pp. 395-406.

74. Zahn, F. A., "Design of Reinforced Concrete Bridge Columns for Strength and Ductility," Ph.D. dissertation, University of Canterbury, Christchurch, New Zealand, 1985.

75. Razvi, S. R. and Saatcioglu, M., "Circular High-Strength Concrete Columns under Concentric Compression," *ACI Structural Journal*, Vol. 96, No. 5, 1999, pp. 817-825.

76. ACI Committee 318, "Building code requirements for structural concrete (ACI 318-89)," American Concrete Institute, Farmington Hills, MI, 1989.

77. Richart, F. E.; Brandtzaeg, A.; and Brown, R. L., "The Failure of Plain and Spirally Reinforced Concrete in Compression," *Engineering Experiment Station. Bulletin no. 190*, University of Illinois, Urbana, Illinois, 1929.

78. Ahmad, S. and Shah, S., "Stress-Strain Curves of Concrete Confined by Spiral Reinforcement," *ACI Journal Proceedings*, Vol. 79, No. 6, 1982, pp. 484-490.

79. Sargin, M.; Ghosh, S.; and Handa, V., "Effects of lateral reinforcement upon the strength and deformation properties of concrete," *Magazine of Concrete Research*, Vol. 23, No. 75 & 76, 1971, pp. 99-110.

80. Martinez, S.; Nilson, A. H.; and Slate, F. O., "Spirally Reinforced High-Strength Concrete Columns," *ACI Journal Proceedings*, Vol. 81, No. 5, 1984, pp. 431-442.

81. Fafitis, A. and Shah, S. P., "Predictions of Ultimate Behavior of Confined Columns Subjected To Large Deformations," *Journal of the American Concrete Institute*, Vol. 82, No. 4, 1985, pp. 423-433.

82. Mander, J. B.; Priestley, M. J. N.; and Park, R., "Theoretical Stress-Strain Model for Confined Concrete," *Journal of structural engineering New York, N.Y.*, Vol. 114, No. 8, 1988, pp. 1804-1826.

83. Saatcioglu, M. and Razvi, S. R., "Strength and Ductility of Confined Concrete," *Journal of structural engineering New York, N.Y.*, Vol. 118, No. 6, 1992, pp. 1590-1607.

84. El-dash, K. M. and Ahmad, S. H., "Model for Stress-Strain Relationship of Spirally Confined Normal and High-Strength Concrete Columns," *Magazine of Concrete Research*, Vol. 47, No. 171, 1995, pp. 177-184.

85. Assa, B.; Nishiyama, M.; and Watanabe, F., "New Approach for Modeling Confined Concrete. I: Circular Columns," *Journal of Structural Engineering*, Vol. 127, No. 7, 2001, pp. 743-750.

86. Karim, H.; Sheikh, M. N.; and Hadi, M. N. S., "Confinement of Circular Concrete Columns: A Review," *Proceeding of The 1st International Engineering Conference on Developments in Civil & Computer Engineering Applications (IEC2014)*, Ishik University, Erbil, KRG, Iraq, 2014, pp. 28-36.

87. Ozbakkaloglu, T. and Lim, J. C., "Axial compressive behavior of FRP-confined concrete: Experimental test database and a new design-oriented model," *Composites Part B: Engineering*, Vol. 55, 2013, pp. 607-634.

88. Pessiki, S.; Harries, K. A.; Kestner, J. T.; Sause, R.; and Ricles, J. M., "Axial behavior of reinforced concrete columns confined with FRP jackets," *Journal of Composites for Construction*, Vol. 5, No. 4, 2001, pp. 237-245.

89. Lam, L. and Teng, J. G., "Design-oriented stress-strain model for FRP-confined concrete," *Construction and Building Materials*, Vol. 17, No. 6-7, 2003, pp. 471-489.

90. De Lorenzis, L. and Tepfers, R., "Comparative study of models on confinement of concrete cylinders with fiber-reinforced polymer composites," *Journal of Composites for Construction*, Vol. 7, No. 3, 2003, pp. 219-237.

91. Ozbakkaloglu, T. and Oehlers, D. J., "Manufacture and testing of a novel FRP tube confinement system," *Engineering Structures*, Vol. 30, No. 9, 2008, pp. 2448-2459.

92. Ozbakkaloglu, T.; Lim, J. C.; and Vincent, T., "FRP-confined concrete in circular sections: Review and assessment of stress-strain models," *Engineering Structures*, Vol. 49, 2013, pp. 1068-1088.

93. Carey, S. A. and Harries, K. A., "Axial behavior and modeling of confined small-, medium-, and large-scale circular sections with carbon fiber-reinforced polymer jackets," *ACI Structural Journal*, Vol. 102, No. 4, 2005, pp. 596-604.

94. ACI Committee 440, "Guide for the design and construction of externally bonded FRP systems for strengthening concrete structures (ACI 440.2R-08)," American Concrete Institute, Framington, MI, 2008.

95. Lim, J. C. and Ozbakkaloglu, T., "Confinement Model for FRP-Confined High-Strength Concrete," *Journal of Composites for Construction*, Vol. 18, No. 4, 2013, pp. 04013058.

96. Karbhari, V. M. and Gao, Y., "Composite jacketed concrete under uniaxial compression - Verification of simple design equations," *Journal of Materials in Civil Engineering*, Vol. 9, No. 4, 1997, pp. 185-193.

97. Lin, H. J. and Chen, C. T., "Strength of concrete cylinder confined by composite materials," *Journal of Reinforced Plastics and Composites*, Vol. 20, No. 18, 2001, pp. 1577-1600.

98. Li, J. and Hadi, M. N. S., "Behaviour of externally confined high-strength concrete columns under eccentric loading," *Composite Structures*, Vol. 62, No. 2, 2003, pp. 145-153.

99. Hadi, M. N. S. and Li, J., "External reinforcement of high strength concrete columns," *Composite Structures*, Vol. 65, No. 3-4, 2004, pp. 279-287.

100. Lam, L. and Teng, J. G., "Ultimate condition of fiber reinforced polymer-confined concrete," *Journal of Composites for Construction*, Vol. 8, No. 6, 2004, pp. 539-548.

101. Hadi, M. N. S., "Comparative study of eccentrically loaded FRP wrapped columns," *Composite Structures*, Vol. 74, No. 2, 2006, pp. 127-135.

102. Hadi, M. N. S., "The behaviour of FRP wrapped HSC columns under different eccentric loads," *Composite Structures*, Vol. 78, No. 4, 2007, pp. 560-566.

103. Hadi, M. N. S., "Behaviour of FRP strengthened concrete columns under eccentric compression loading," *Composite Structures*, Vol. 77, No. 1, 2007, pp. 92-96.

104. Xiao, Y. and Wu, H., "Compressive behavior of concrete confined by carbon fiber composite jackets," *Journal of Materials in Civil Engineering*, Vol. 12, No. 2, 2000, pp. 139-146.

105. Matthys, S.; Toutanji, H.; and Taerwe, L., "Stress-strain behavior of large-scale circular columns confined with FRP composites," *Journal of Structural Engineering*, Vol. 132, No. 1, 2006, pp. 123-133.

106. Youssef, M. N.; Feng, M. Q.; and Mosallam, A. S., "Stress-strain model for concrete confined by FRP composites," *Composites Part B: Engineering*, Vol. 38, No. 5-6, 2007, pp. 614-628.

107. Hognestad, E., "Study of combined bending and axial load in reinforced concrete members," *Engineering Experiment Station. Bulletin no. 399*, University of Illinois, Urbana, Illinois, 1951.

108. Samaan, M.; Mirmiran, A.; and Shahawy, M., "Model of concrete confined by fiber composites," *Journal of Structural Engineering*, Vol. 124, No. 9, 1998, pp. 1025-1031.

109. Moran, D. A. and Pantelides, C. P., "Stress-strain model for fiber-reinforced polymer-confined concrete," *Journal of Composites for Construction*, Vol. 6, No. 4, 2002, pp. 233-240.

110. Fahmy, M. F. M. and Wu, Z., "Evaluating and proposing models of circular concrete columns confined with different FRP composites," *Composites Part B: Engineering*, Vol. 41, No. 3, 2010, pp. 199-213.

111. Richard, R. M. and Abbott, B. J., "Versatile elastic-plastic stress-strain formula," *Journal of the Engineering Mechanics Division*, Vol. 101, No. 4, 1975, pp. 511-515.

112. Toutanji, H. A., "Stress-strain characteristics of concrete columns externally confined with advanced fiber composite sheets," *ACI Materials Journal*, Vol. 96, No. 3, 1999, pp. 397-404.

113. Saafi, M.; Toutanji, H. A.; and Li, Z., "Behavior of concrete columns confined with fiber reinforced polymer tubes," *ACI Materials Journal*, Vol. 96, No. 4, 1999, pp. 500-509.

114. Spoelstra, M. R. and Monti, G., "FRP-confined concrete model," *Journal of Composites for Construction*, Vol. 3, No. 3, 1999, pp. 143-150.

115. Thériault, M. and Neale, K. W., "Design equations for axially loaded reinforced concrete columns strengthened with fibre reinforced polymer wraps," *Canadian Journal of Civil Engineering*, Vol. 27, No. 5, 2000, pp. 1011-1020.

116. Lam, L. and Teng, J. G., "Strength models for fiber-reinforced plastic-confined concrete," *Journal of Structural Engineering*, Vol. 128, No. 5, 2002, pp. 612-623.

117. Shehata, I. A. E. M.; Carneiro, L. A. V.; and Shehata, L. C. D., "Strength of short concrete columns confined with CFRP sheets," *Materials and Structures*, Vol. 34, No. 245, 2002, pp. 50-58.

118. Saiidi, M. S.; Sureshkumar, K.; and Pulido, C., "Simple carbon-fiber-reinforced-plastic-confined concrete model for moment-curvature analysis," *Journal of Composites for Construction*, Vol. 9, No. 1, 2005, pp. 101-104.

119. Matthys, S.; Toutanji, H.; Audenaert, K.; and Taerwe, L., "Axial load behavior of large-scale columns confined with fiber-reinforced polymer composites," *ACI Structural Journal*, Vol. 102, No. 2, 2005, pp. 258-267.

120. Wu, Y. F. and Wang, L. M., "Unified strength model for square and circular concrete columns confined by external jacket," *Journal of Structural Engineering*, Vol. 135, No. 3, 2009, pp. 253-261.

121. Wu, H. L.; Wang, Y. F.; Yu, L.; and Li, X. R., "Experimental and computational studies on high-strength concrete circular columns confined by aramid fiber-reinforced polymer sheets," *Journal of Composites for Construction*, Vol. 13, No. 2, 2009, pp. 125-134.

122. Benzaid, R.; Mesbah, H.; and Nasr Eddine, C., "FRP-confined concrete cylinders: Axial compression experiments and strength model," *Journal of Reinforced Plastics and Composites*, Vol. 29, No. 16, 2010, pp. 2469-2488.
123. CAN/CSA S6-06, "Canadian highway bridge design code (CAN/CSA S6-06)," Canadian Standards Association, Rexdale, ON, Canada, 2006.
124. AS 3600-2009, "Concrete structures (AS 3600-2009)," Australian Standard, NSW, Sydney, 2009.
125. Němeček, J. and Bittnar, Z., "Experimental investigation and numerical simulation of post-peak behavior and size effect of reinforced concrete columns," *Materials and Structures*, Vol. 37, No. 3, 2004, pp. 161-169.
126. Thériault, M.; Neale, K. W.; and Claude, S., "Fiber-reinforced polymer-confined circular concrete columns: Investigation of size and slenderness effects," *Journal of Composites for Construction*, Vol. 8, No. 4, 2004, pp. 323-331.
127. Silva, M. A. G. and Rodriguez, C. C., "Size and relative stiffness effects on compressive failure of concrete columns wrapped with glass FRP," *Journal of Materials in Civil Engineering*, Vol. 18, No. 3, 2006, pp. 334-342.
128. Marques, S. P. C.; Codá Dos Santos Cavalcanti Marques, D.; Lins Da Silva, J.; and Cavalcante, M. A. A., "Model for analysis of short columns of concrete confined by fiber-reinforced polymer," *Journal of Composites for Construction*, Vol. 8, No. 4, 2004, pp. 332-340.
129. AS 1012.9-1999, "Determination of the compressive strength of concrete specimens (AS 1012.9-1999)," Australian Standard, Sydney, NSW, 1999.

130. AS 1391-2007, "Metallic materials - Tensile testing at ambient temperature (AS 1391-2007)," Australian Standard, Sydney, NSW, 2007.
131. V-Rod Australia, "Composite reinforcing rods technical data sheet.," Largs Bay SA, Australia, 2012.
132. ISO 10406-1:2015, "Fibre-reinforced polymer (FRP) reinforcement of concrete - Test methods - Part 1: FRP bars and grids (ISO 10406-1:2015)," International Standard, Switzerland, 2015.
133. ASTM D7205/D7205M−11, "Standard test method for tensile properties of fiber reinforced polymer matrix composite bars (ASTM D7205/D7205M−11)," American Society for Testing and Materials, West Conshohocken, PA, 2011.
134. ASTM D7565/D7565M-10, "Standard test method for determining tensile properties of fiber reinforced polymer matrix composites used for strengthening of civil structures (ASTM D7565/D7565M-10)," American Society for Testing and Materials, West Conshohocken, PA, 2010.
135. Foster, S. J. and Attard, M. M., "Experimental tests on eccentrically loaded high-strength concrete columns," *ACI Structural Journal*, Vol. 94, No. 3, 1997, pp. 295-303.
136. Neville, A. M., *Properties of concrete: Fourth and final edition standards updated to 2002*, Longman, London, U.K, 2005.
137. Yong, Y.-K.; Nour, M. G.; and Nawy, E. G., "Behavior of laterally confined high-strength concrete under axial loads," *Journal of Structural Engineering*, Vol. 114, No. 2, 1988, pp. 332-351.

138. Cusson, D. and Paultre, P., "High-strength concrete columns confined by rectangular ties," *Journal of structural engineering New York, N.Y.*, Vol. 120, No. 3, 1994, pp. 783-804.

139. Saatcioglu, M. and Razvi, S. R., "High-strength concrete columns with square sections under concentric compression," *Journal of Structural Engineering*, Vol. 124, No. 12, 1998, pp. 1438-1447.

140. Jiang, T. and Teng, J. G., "Theoretical model for slender FRP-confined circular RC columns," *Construction and Building Materials*, Vol. 32, 2012, pp. 66-76.

141. Saadatmanesh, H.; Ehsani, M. R.; and Li, M. W., "Strength and ductility of concrete columns externally reinforced with fiber composite straps," *ACI Structural Journal*, Vol. 91, No. 4, 1994, pp. 434-447.

142. Yuan, X. F.; Xia, S. H.; Lam, L.; and Smith, S. T., "Analysis and behaviour of FRP-confined short concrete columns subjected to eccentric loading," *Journal of Zhejiang University: Science A*, Vol. 9, No. 1, 2008, pp. 38-49.

143. Jiang, T. and Teng, J. G., "Behavior and design of slender FRP-confined circular RC columns," *Journal of Composites for Construction*, Vol. 17, No. 4, 2013, pp. 443-453.

144. Bisby, L.; Take, W.; and Caspary, A., "Quantifying strain variation in FRP confined concrete using digital image correlation: Proof-of-concept and initial results," *The First Asia-Pacific Conference on FRP in Structures (APFIS 2007)*, University of Hong Kong, Hong Kong, China, 2007, pp.

145. Bisby, L. and Ranger, M., "Axial-flexural interaction in circular FRP-confined reinforced concrete columns," *Construction and Building Materials*, Vol. 24, No. 9, 2010, pp. 1672-1681.

146. Hadi, M. N. S.; Pham, T. M.; and Lei, X., "New method of strengthening reinforced concrete square columns by circularizing and wrapping with fiber-reinforced polymer or steel straps," *Journal of Composites for Construction*, Vol. 17, No. 2, 2013, pp. 229-238.

147. Ahmed, E. A.; El-Sayed, A. K.; El-Salakawy, E.; and Benmokrane, B., "Bend strength of FRP stirrups: Comparison and evaluation of testing methods," *Journal of Composites for Construction*, Vol. 14, No. 1, 2010, pp. 3-10.

148. Lee, J. Y.; Yi, C. K.; Jeong, H. S.; Kim, S. W.; and Kim, J. K., "Compressive response of concrete confined with steel spirals and FRP composites," *Journal of Composite Materials*, Vol. 44, No. 4, 2010, pp. 481-504.

149. Hu, H. and Seracino, R., "Analytical model for FRP-and-steel-confined circular concrete columns in compression," *Journal of Composites for Construction*, Vol. 18, No. 3, 2014, pp. A4013012.

150. Shirmohammadi, F.; Esmaeily, A.; and Kiaeipour, Z., "Stress-strain model for circular concrete columns confined by FRP and conventional lateral steel," *Engineering Structures*, Vol. 84, 2015, pp. 395-405.

151. MATLAB and Statistics Toolbox Release 2013b, The MathWorks, Inc., Natick, Massachusetts, United States.

152. Mohamed, H. M. and Masmoudi, R., "Flexural strength and behavior of steel and FRP-reinforced concrete-filled FRP tube beams," *Engineering Structures*, Vol. 32, No. 11, 2010, pp. 3789-3800.

153. Zadeh, H. J. and Nanni, A., "Design of RC columns using glass FRP reinforcement," *Journal of Composites for Construction*, Vol. 17, No. 3, 2013, pp. 294-304.

154. Yazici, V. and Hadi, M. N. S., "Axial load-bending moment diagrams of carbon FRP wrapped hollow core reinforced concrete columns," *Journal of Composites for Construction*, Vol. 13, No. 4, 2009, pp. 262-268.

155. Sheikh, M. N.; Tsang, H. H.; McCarthy, T. J.; and Lam, N. T. K., "Yield curvature for seismic design of circular reinforced concrete columns," *Magazine of Concrete Research*, Vol. 62, No. 10, 2010, pp. 741-748.

156. Bazant, Z. P.; Cedolin, L.; and Tabbara, M. R., "New method of analysis for slender columns," *ACI Structural Journal*, Vol. 88, No. 4, 1991, pp. 391-401.

157. Mirmiran, A.; Shahawy, M.; Samaan, M.; El Echary, H.; Mastrapa, J. C.; and Pico, O., "Effect of column parameters on FRP-confined concrete," *Journal of Composites for Construction*, Vol. 2, No. 4, 1998, pp. 175-185.

APPENDIX A: SOLVED EXAMPLES

A.1 EXAMPLE NO. 1 IN CHOO ET AL.[56]

Determine the minimum reinforcement ratio $(\rho_{f\min})$ required to prevent brittle-tension failure in a rectangular concrete column reinforced with GFRP reinforcing bars.

Given:

$f_c' =$ 48.5 MPa

$\varepsilon_{cu} =$ 0.003

$E_f =$ 44830 MPa

$\varepsilon_f =$ 0.014

$\gamma =$ 0.8

$P =$ 0

Result:

$\rho_{f\min} =$ 1.5%

Solution using presented equations:

$\alpha_1 =$ 0.85

From Equation 5.5, $\beta_1 =$ 0.7

From Equation 5.28, $\rho_{f\min} =$ 1.58%

A.2 EXAMPLE 9.2 IN ISIS CANADA 2007[16]

Determine deformability factor for a simply-supported one-way slab with 150 mm thickness. The concrete properties are $f_c' =$ 30 MPa and $E_c =$ 24650 MPa. The GFRP reinforcing bars are #16 bars at 100 mm spacing with diameter = 15.9 mm, Area = 198 mm^2, $\rho_f =$ 1.85%, $f_{fu} =$ 680 MPa and $E_f =$ 48200 MPa. The concrete cover for reinforcement is 35 mm, $\varepsilon_{cs} =$ 0.001, $\varepsilon_{co} =$ 0.002 and $\varepsilon_{cu} =$ 0.0035.

Result:

$DF =$ 5.7

Solution using presented equations:

From Equation 5.42, $a_s =$ 0.45

From Equation 5.41, $\varepsilon_{fs} = -0.00322$

From Equation 5.37, $n_s =$ 0.65

From Equation 5.51, $a_u =$ 0.80

From Equation 5.50, $\varepsilon_{fu} = -0.00763$

From Equation 5.46, $n_u =$ 0.59

From Equation 5.57, $DF =$ 5.7

Solution using simplified equation:

From Equation 5.63, $DF =$ 4.94

Because $\varepsilon_{cu} =$ 0.0035, so calculated DF using Equation 5.63 should be increased by 15%,

Hence, $DF =$ 4.94 x 1.15 = 5.68

APPENDIX B: MATLAB CODES

B.1 MATLAB CODE FOR CALCULATING CURVE-SHAPE PARAMETER

```
clc; clear all; close all;
p=0;
for i=1:14;
fo=(i+1)*10;
for j=1:12;
E2=(9*j-8)*100;
for k=1:10;
E1=(3*k+17)*1000;
fco=(E1/4730)^2;
eco=0.0005*fco^0.4;
Esec=fco/eco;
r=E1/(E1-Esec);
fc=fco*r*0.5/(r-1+0.5^r);
a=(E1-E2)/(2*fc/eco-E2);
b=(E1-E2)/(2*fo/eco);
go=1;
for l=1:9901;
if go==1;
n=(l+99)/1000;
c=(1+b^n)^(1/n);
d=abs(a-c);
```

```
if d<0.05;
p=p+1;
Fo(p)=fo;
X(p)=0.001*(E1-E2)/(fo^0.45);
Y(p)=n;
go=2;
end
end
end
end
end
end
end
```

B.2 MATLAB CODE FOR CALCULATING MOMENT-CURVATURE FOR GFRP-RC COLUMNS

```
clc; clear all; close all;
d=[171.15, 136.825, 136.825, 68.175, 68.175, 33.85];
fco=31.45;
E1=8470*fco^0.333;
eco=0.0016*exp(240*fco/E1);
r=(fco/10)^0.67;
B1=0.2*exp(0.73*r);
B2=0.41*exp(0.77*r);
fcco=55.5;
```

```
ecc=0.0066;
E2=(fcco-fco)/ecc;
x=0.001*(E1-E2)/fco^0.45
n=0.4*exp(0.35*x);
Af=126.677;
Ef=66000;
t=0.5;
ei=25;
l=0;
for ecu=0:0.0002:ecc;
l=l+1;
go=1;
for c=50:0.5:205;
if go==1;
i=0;
for N=1:1:c/t;
i=i+1;
bt=2*(102.5^2-(102.5-(N-0.5)*t)^2)^0.5;
ec=(1-(N-0.5)*t/c)*ecu;
if N<=45;
bc(i)=0;
bu(i)=bt;
fcc(i)=0;
if ec<=eco;
```

```
fc(i)=fco*(B1+1)*(ec/eco)/(B1+(ec/eco)^(B1+1));
else
fc(i)= fco*(B2+1)*(ec/eco)/(B2+(ec/eco)^(B2+1));
end
Pc(i)=0.5*(bu(i)*fc(i)+bc(i)*fcc(i))/1000;
Mc(i)=Pc(i)*(102.5-(0.5*N-0.25))/1000;
end
if N>45 && N<=365;
bc(i)=2*(80^2-(102.5-(N-0.5)*t)^2)^0.5;
bu(i)=bt-bc(i);
fcc(i)=(E1-E2)*ec/(1+(( E1-E2)*ec/fco)^n)^(1/n)+E2*ec
if ec<=eco;
fc(i)=fco*(B1+1)*(ec/eco)/(B1+(ec/eco)^(B1+1));
else
fc(i)= fco*(B2+1)*(ec/eco)/(B2+(ec/eco)^(B2+1));
end
Pc(i)=0.5*(bu(i)*fc(i)+bc(i)*fcc(i))/1000;
Mc(i)=Pc(i)*(102.5-(0.5*N-0.25))/1000;
end
if N>365;
bc(i)=0;
bu(i)=bt;
fcc(i)=0;
if ec<=eco;
```

```
fc(i)=fco*(B1+1)*(ec/eco)/(B1+(ec/eco)^(B1+1));
else
fc(i)= fco*(B2+1)*(ec/eco)/(B2+(ec/eco)^(B2+1));
end
Pc(i)=0.5*(bu(i)*fc(i)+bc(i)*fcc(i))/1000;
Mc(i)=Pc(i)*(102.5-(0.5*N-0.25))/1000;
end
end
for j=1:1:6;
ef(j)=(c-d(j))*ecu/c;
Pf(j)=ef(j)*Ef*Af/1000;
Mf(j)=Pf(j)*(102.5-d(j))/1000;
end
P=sum(Pc)+sum(Pf);
M=sum(Mc)+sum(Mf);
e=1000*M/P;
k=ecu/c;
def=k*(800/pi)^2;
error=100*abs(ei+def-e)/(ei+def);
if error<1;
go=2;
PP(l)=P;
MM(l)=M;
kk(l)=k*10^6;
```

```
end
end
end
end
plot(kk,MM);
```

B.3 MATLAB CODE FOR CALCULATING MOMENT-CURVATURE FOR GFRP-RC COLUMNS CONFINED WITH CFRP SHEETS

```
clc; clear all; close all;
d=[171.15, 136.825, 136.825, 68.175, 68.175, 33.85];
fco=31.45;
E1=8470*fco^0.333;
eco=0.0016*exp(240*fco/E1);
fcco=75.8;
ecc=0.012;
E2=(fcco-fco)/ecc;
x=0.001*(E1-E2)/fo^0.45;
n=0.4*exp(0.35*x);
Af=126.677;
Ef=66000;
t=0.5;
ei=25;
l=0;
for ecu=0:0.0002:ecc;
```

```
l=l+1;
go=1;
for c=50:t:205;
if go==1;
i=0;
for N=1:1:c/t;
i=i+1;
bt(i)=2*(102.5^2-(102.5-(N-0.5)*t)^2)^0.5;
ec=(1-(N-0.5)*t/c)*ecu;
fcc(i)=(E1-E2)*ec/(1+((E1-E2)*ec/fco)^n)^(1/n)+E2*ec;
Pc(i)=bt(i)*fcc(i)*t/1000;
Mc(i)=Pc(i)*(102.5-(N-0.5)*t)/1000;
end
end
for j=1:1:6;
ef(j)=(c-d(j))*ecu/c;
Pf(j)=ef(j)*Ef*Af/1000;
Mf(j)=Pf(j)*(102.5-d(j))/1000;
end
P=sum(Pc)+sum(Pf);
M=sum(Mc)+sum(Mf);
e=1000*M/P;
k=ecu/c;
def=k*(800/pi)^2;
```

```
error=100*abs(ei+def-e)/(ei+def);

if error<1;

go=2;

PP(l)=P;

MM(l)=M;

kk(l)=k*10^6;

end

end

end

plot(kk,MM);
```